INTERNATIONAL DOCTORAL
SCHOOL OF THE USC

Alfonso
Fernández Blanco

PhD Thesis

Advanced biomaterials for drug release and tissue engineering: applications in bioactive meniscus prosthesis and thymus organoids

Santiago de Compostela, 2024

Doctoral Programme in Drug Research and Development

ESCOLA DE DOUTORAMENTO
INTERNACIONAL DA USC

DOCTORAL THESIS

ADVANCED BIOMATERIALS FOR DRUG RELEASE AND TISSUE ENGINEERING: APPLICATIONS IN BIOACTIVE MENISCUS PROSTHESIS AND THYMUS ORGANOIDS

Alfonso Fernández Blanco

Directors: María Josefa Alonso Fernández & José Crecente Campo

Tutor: María Josefa Alonso Fernández

DOCTORAL PROGRAM IN DRUG RESEARCH AND DEVELOPMENT

SANTIAGO DE COMPOSTELA

2024

Conflict of interest

The doctoral candidate declares no conflicts of interest related to his thesis.

Santiago de Compostela. **December 10, 2024**.

Sgd.: **Alfonso Fernández Blanco**

A Rodrigo Blanco

A Atanasio Blanco

A Juli Arenas

A mis padres

«*Somewhere, something incredible is waiting to be known*»

(En algún lugar, algo increíble está esperando a ser descubierto)

Carl Sagan

«*Two ways. Gradually, then suddenly*»

(De dos maneras. Gradualmente, luego de repente)

Ernest Hemingway

«*If a man knows not to which port he sails, no wind is favorable*»

(Si un hombre no sabe a qué puerto navega, ningún viento le es favorable)

Seneca

«*At some point, everything's gonna go south […]. Now, you can either accept that or you can get to work. That's all it is. You just begin. You do the math. You solve one problem, and you solve the next one and then the next. And if you solve enough problems, you get to come home*»

(En algún momento, todo va a complicarse [...]. Bien, puedes aceptarlo o ponerte a trabajar. Eso es todo. Simplemente empiezas. Haces los cálculos. Resuelves un problema, luego el siguiente y después otro. Y si resuelves suficientes problemas, podrás volver a casa)

The Martian

ACKNOWLEDGEMENTS

ACKNOWLEDGEMENTS

Escribía Haruki Murakami en "Kafka en la orilla": "*Y cuando la tormenta haya pasado, no comprenderás cómo lograste cruzarla. Ni siquiera estarás seguro de que la tormenta haya cesado de verdad. Pero una cosa sí es cierta. Cuando salgas de la tormenta no serás la misma persona que entró en ella. De eso trataba la tormenta"*. Me gusta extrapolar esa frase a muchos acontecimientos de mi vida. Pero creo que hace especial justicia a esta tesis doctoral. Me alegra sentir, y poder confirmar mientras escribo estos párrafos, que la persona que entró en esta tesis no es la misma que sale. Estos años han forjado cualidades que valoraba mucho y que se han afilado ante las situaciones complicadas que se han ido presentando: tesón, constancia, perseverancia, dedicación, determinación, pasión e ingenio. Y, sobre todo, humildad y agradecimiento. Las fases buenas y las no tan buenas me han ayudado a darme cuenta de que todo lo que he avanzado estos años, no hubiera podido avanzarlo solo.

Primero de todo, agradecer a mis directores de tesis María José Alonso y José Crecente. María José, depositaste toda tu confianza en mi desde el primer momento y ese es el regalo más preciado que se le puede hacer a una persona. Me has dado seguridad cuando la he necesitado y me has empujado hacia delante cuando he querido avanzar. Una persona no corre sin saber andar primero. Me has enseñado todo lo que sé y también me has dado libertad para explorar cuanto he querido o necesitado. Lo que has hecho por mí estos años lo recordaré siempre. Has sido guía, mentora y siempre vas a ser mi referente.
José, aún recuerdo nuestra primera reunión informal en el pasillo de la planta 5 un septiembre de 2020, con mascarillas de por medio. Me has dado calma y un apoyo incalculable. Has ido más allá del laboratorio con tus consejos y recomendaciones. No he podido tener mejor co-director de tesis.

Muchas gracias a Gustavo Lou, por ser mi primer supervisor. También has sido amigo desde el primer momento. Ojalá el tiempo nos vuelva a juntar en momento y lugar. Extiendo este agradecimiento a María y a Isabel.

Muchas gracias a la Universidad de Santiago de Compostela y al CiMUS por darme los medios para desarrollar esta tesis. Muchas gracias a la Xunta de Galicia por sus contratos de formación predoctoral que han financiado mi tesis doctoral.

Thanks to the MEFISTO Project and all the collaborators involved. Special thanks to Fernando Torres, Alba Pensado, Aldo Ummarino, Pietro Conte, Giuseppe Anzillotti, and Elizaveta Kon from HUNIMED for all the help with the experiments in cells and animals. To Riccardo Levato, Paulina Nuñez, Mylene de Ruijter, and Jos Malda from UMCU for the bioreactor testing. To the Israeli Active Implants team, Eran Ganz, Dan Anavi, and Maoz Shemesh. To Kirsten Leufgen and Peter Ulrich, thank you for coordinating. To Matteo Santini, thank you for the critical insights regarding my polymer science and for sharing runs in Naples along the beautiful Mediterranean Sea while observing Pompeii in the distance. Finally, thank you to Evelyne Hasler for being the glue that kept everything together, your patience, and your leadership.

Muchas gracias a todos mis compañeros de laboratorio en Santiago de Compostela. A los antiguos, actuales y futuros. En especial muchas gracias a Ana López, Germán Berrecoso, Laura Piñeiro, Catarina Afonso y Shuubash Antiya por acogerme cuando llegué. Me hicisteis

sentir en casa desde el principio. Muchas gracias a Anna Abbadessa por nadar en el MEFISTO junto a mi y por los consejos. Muchas gracias a Cristina Iglesias, Lucía Sanjurjo, Julia Baena, Alberto Jiménez, Elisa Batisttini, Elena Ibeas, María González, Jorge Ruz, Paloma Rial, Virna Martín, Marta Martínez y Eva González. A Philipp Lapuhs y Darío Blanco por embarcarse en esta aventura a la vez que yo. A Giorgio Buttitta por ser amigo en todo momento, en la cercanía y en la distancia. Por demostrar que da igual el tiempo que pase, cuando el vínculo es fuerte, no se rompe. A Tamara Gómez por ser guía temporal y luego anfitriona en Boston. Has sido siempre un ejemplo para mí. A Adriana Martínez por dedicarme su tiempo cuando más dudas tenía y por ayudarme a aclarar el qué viene después de esta tesis.

Muchas gracias a Loli, Marcos, Noemí y a todo el laboratorio de la planta 2.

Muchas gracias a Puri Domínguez y a Balby Fernández. El consejo de sabios que se forma en los despachos me ha dado luz cuando escaseaba. Por supuesto, muchas gracias a Belén Cuesta, por estar siempre, aunque no estuviese ni yo. Gracias por el cariño y por el cuidado. No hay ningún Lab Manager que te vaya a poder sustituir, nunca.

Muchas gracias a Inés Rubio. Has sido mi primera alumna, pero he aprendido mucho más de lo que creo que te he podido enseñar. Con tus presentaciones de TFM y TFG te puedo asegurar que estaba yo más nervioso que tú. Me alegra haber podido ver cómo aprendías y mejorabas cada día hasta convertirte en la magnífica científica que eres hoy. Estoy muy orgulloso de ti.

Muchas gracias a Mireya López. No tengo hermanos, pero debes de ser lo más parecido a tener una hermana mayor. Me has cuidado, me has aconsejado, me has recomendado y me has empujado a ser cada vez mejor. Me has hecho sentir en casa. Me hablaste de Boston con tanto cariño que sabía que tenía que probarlo. Espero que dentro de no mucho volvamos a coincidir en la misma ciudad. Extiendo este agradecimiento a Alex.

Muchas gracias a Sabela Caamaño. Eres brillante y eres una persona extraordinaria. Llegarás a dónde quieras.

Muchas gracias a mis amigos de siempre: Pablo Santos, Laura Díez, Inés López, Alba García, Francisco Córdoba, Jorge García, Jorge Onrubia, Diego García, Alicia López, Diego Camacho, Javier Portomeñe, Guillermo Amilivia, Iván Carvajal, Juanjo Vidal, David Álvarez, Samuel García, Mario Castro, Cristina Cuervo, Pablo Martín, Pablo Marín, Víctor Antón, Alejandro Santos, Cristina Cuervo y Marina Ballesteros. Los años nos han llevado por caminos muy distintos, pero siempre es un placer volver a casa y teneros. Hacéis que todo sea más fácil.

Now, it is my turn to acknowledge the people of my stay overseas. First, thank you, Dave Mooney, for allowing me to fulfill my earliest dream: joining Harvard University. You believed in me, you gave me freedom, you gave me support, and you gave me a place I want to come back to. You are a true mentor and an outstanding leader.

Thank you to the rest of the Mooney Lab, and special thanks to the people I've worked closer to Andrew Khalil, Junzhe (Robin) Lou, Bryan Nerger, and Grace Bingham. Also, thanks to the rest of the SEAS Cambridge lunch committee: Giovanni Bovone, Nuria Lafuente, Leila

Krajnovic, Duncan Morgan, Gabrielle Nasello, Mason Dacus, Emily Roloson, Matt Pezone, and Shawn Kang.

Thank you to Rudolf Jaenisch for allowing me to attend MIT and use its facilities. And thank you to Tenzin Lungjangwa, Kristin Andrykovich, and Baboucarr Lowe for improving my days there. Tenzin, it has been a true privilege to work alongside you.

Muchas gracias a mis compañeros de Willow St: Matteo, Mateo y Erik ha sido increíble poder vivir con vosotros. Y ha sido aún más increíble haber encontrado un hogar tan lejos de casa.

Muchas gracias a la sucursal española en Boston. Ainhoa Genua y Sean McKay, solo tengo buenos recuerdos cuando hemos estado juntos. He disfrutado muchísimo conociéndoos y llamándoos amigos. Sois un ejemplo de que, si algo se cuida, crece y florece. Eduardo Bilbao, mi compañero de carreras largas los domingos y de series entre semana. Entrenar juntos era mucho más fácil. Iñigo Azkárate, seguir manteniendo esta amistad aún en la distancia es algo que valoro muchísimo. Llegaremos donde tengamos que llegar y volveremos a coincidir. A Irene Vicente y a Artistofanis Rontogiannis. A los recién estrenados roommates: Enya Miguel, Álvaro Martínez y Juan Rodrigo Mercau. Enya, eres una persona que ojalá todo el mundo pueda tener en su vida, es una pena que solo existas tú. Álvaro, gracias por confiar y por escuchar. JuanRo, qué pena que llegases tarde para haber podido disfrutar más meses. Eres una persona inmensamente dedicada y un gran, gran amigo.

Muchas gracias a Michael Setzke y a toda la familia Setzke. Michael, it is unbelievable that we can keep this friendship as intense and vivid as the first day we met back in Vermont. We have been all over the place, the US, Europe… We keep sharing memories and good moments. Uncertain and challenging times are upon us, but we keep moving. We always move. We always find a way to keep doing what we love. You are one of a kind. You are a brother to me.

Muchas gracias a Fabiola Álvarez Gallego. Llegaste a mi vida y nunca te has ido. Has transformado todo y te has unido a este nuevo viaje. Me haces feliz cada día, aprendo de ti cada día, y te admiro cada día. Me das razones para ser mejor, y lo soy gracias al prisma con el que me miran tus ojos. Eres un lugar al que siempre quiero llegar, un lugar del que nunca quiero irme. Eres mi mejor amiga, mi presente y mi futuro. No puedo esperar a seguir creciendo juntos y descubriendo a dónde nos llevará nuestro camino.

Por último, y por ello más importante, muchas gracias a mi familia. Muchas gracias a los que se han ido: Atanasio, Juli y Mari. Me cuidáis desde donde estáis. Muchas gracias a los que aún están: Ismael. Muchas gracias a los que acaban de llegar: Rodrigo. Cuanta alegría has traído. Muchas gracias a mis tíos: José y Marian; y a mis primas: María y Patricia. Sois mi hogar y mi apoyo.

Muchas gracias a Nora, por el apoyo incondicional. Por la amistad. Por la compañía. Por cuidar. Por esperar sin saber la fecha de vuelta. Por llenar cuando yo no he estado.

Muchas gracias a mi padre Luis y a mi madre Carmen. Nada de esto tendría sentido sin vosotros. Nada de esto sería posible sin vosotros. Me habéis acompañado en todos los pasos, dándome confianza, apoyo y amor. Habéis creído en mí siempre, fuisteis los primeros. Nunca

me habéis puesto ningún límite, ni habéis dejado que yo mismo me los ponga. Me habéis inculcado principios y valores, así como la voluntad para perseguirlos, respetarlos y mantenerlos. Me habéis enseñado a volar y me habéis dado libertad para hacerlo. Para que tomase el rumbo que más feliz me hiciese, siempre sabiendo que os tengo detrás. Unas frases nunca van a hacer justicia a lo que me habéis dado, ni a lo que me dais cada día. Nunca va a ser suficiente para describir lo que significáis para mí. Quizás la mejor forma de haceros justicia sea diciendo que ojalá todo el mundo pudiera tener unos padres como vosotros, que aprendo cada día lo que es el respeto y la familia. Que ojalá algún día pueda ser la mitad de buen padre que sois vosotros, porque será más de lo que cualquier persona pueda pedir. Esto es para vosotros. Esto es por nosotros.

Unos últimos agradecimientos. Al Alfonso de hace 10 años y al Alfonso de dentro de 10 años. Al Alfonso de hace 10 años. Gracias por soñar en grande y por creer que puedes hacer lo que te propongas. Gracias por no escuchar a la gente que decía que hay cosas que no se pueden conseguir. Gracias por creerte que puedes y gracias por mantener seguras tus ilusiones en una vitrina separada del resto de cosas. Has hecho que cuando se presenten las oportunidades tengamos la valentía de ir a por ellas. Al Alfonso de dentro de 10 años. Gracias por darme algo que perseguir. Estarás orgulloso.

Cierro estos agradecimientos con una cita de "Ulises" de Lord Alfred Tennyson: "*Aunque mucho se ha gastado, mucho queda aún; y si bien no tenemos ahora aquella fuerza que en los viejos tiempos movía tierra y cielo, somos lo que somos: corazones heroicos de parejo temple, debilitados por el tiempo y el destino, pero fuertes en voluntad para esforzarse, buscar, encontrar y nunca rendirse*".

TABLE OF CONTENTS

TABLE OF CONTENTS

ABSTRACT / RESUMEN

ABSTRACT

Knee osteoarthritis (OA) is a degenerative joint disease with rising global prevalence, characterized by the progressive breakdown of cartilage and bone. While meniscectomy provides temporary relief, it compromises patients' long-term quality of life because of OA onset. New therapies have been developed to prevent the onset of this condition. An emerging approach following total meniscectomy involves replacing the meniscus with a non-biodegradable prosthesis. This solution helps preserve the patient's natural articular cartilage, thereby reducing the likelihood of osteoarthritis development. However, patients often require prolonged use of anti-inflammatory drugs to manage pain and facilitate prosthesis integration. Conventional administration methods for these drugs pose significant challenges, including adverse side effects from long-term oral intake and discomfort or pain from intra-articular injections.

The objective was to develop a technology for localized and sustained release of a combination of anti-inflammatory drugs within the knee joint cavity. The first step of this work involved the design of a biodegradable bilayer polymer coating containing dexamethasone (DEX) and celecoxib (CLX), enabling the sequential release of two anti-inflammatory drugs with distinct release kinetics. DEX was selected to mitigate acute inflammation with a release timeframe of 1-4 weeks, while celecoxib (CLX) was chosen to address chronic inflammation with a release period of 6-9 months. The drug-releasing polymer coatings were evaluated *in vitro* and showed a low cytotoxicity profile and an efficient reduction of representative cytokines such as TNF-α, CCL2, and PGE2.

The second part of the thesis focused on optimizing the adhesion of the drug-releasing polymer coatings to the PCU meniscus prostheses. Various surface modification strategies were evaluated, including femtosecond-pulse laser treatment, plasma treatment, polydopamine (PDA) coatings, and the incorporation of an ethyl cyanoacrylate (ECA) adhesive layer. Among these approaches, the ECA adhesive layer showed the most promising results, significantly enhancing adhesion and showing the most favorable mechanical properties (storage modulus (G'), loss modulus (G''), elastic modulus (E), and tan δ). When evaluated in a representative *ex vivo* model using a bioreactor simulating gait with shear and compression forces, this strategy preserved the coating's integrity during mechanical stress and maintained consistent drug release kinetics. The optimized system was successfully adapted for anatomically relevant meniscus prostheses and tested *in vivo* in a pilot study in a sheep model. The functionalized prostheses reduced OA progression compared to the uncoated prostheses while showing secure fixation without delamination of the coating system.

As an independent part of the thesis work, the final section focused on the use of hydrogels for the understanding of thymus development and the exploration of the therapeutic potential of T cells in treating cancers and autoimmune disorders. Hydrogels, known for their versatility and adaptability, have become indispensable in various biomedical applications such as 3D cell culture. This study focused on how mechanical properties of extracellular matrix (ECM)-mimicking hydrogels influence thymus organoid development. Thymus organoids, composed of thymic epithelial progenitor cells (TEPCs) and neural crest cells (NCCs), were incorporated into ionically crosslinked alginate hydrogels containing Matrigel® with tunable mechanical properties. The results showed that matrix viscoelasticity played a pivotal role in guiding cell reorganization, forming tissue-like structures, and promoting the expression of key

developmental markers. These findings provide a foundation for designing advanced biomaterials to support thymus organogenesis, offering valuable insights for regenerative medicine, immunotherapy, and engineered immune system models.

RESUMEN

La osteoartritis (OA) de rodilla es una enfermedad articular degenerativa con una prevalencia global en aumento, caracterizada por la degradación progresiva del cartílago y el hueso. Aunque la meniscectomía proporciona alivio temporal, compromete la calidad de vida a largo plazo de los pacientes debido al desarrollo de la OA. Se han desarrollado nuevas terapias para prevenir la aparición de esta condición. Una estrategia emergente tras una meniscectomía total consiste en reemplazar el menisco con una prótesis no biodegradable. Esta solución ayuda a preservar el cartílago articular natural del paciente, reduciendo así la probabilidad de desarrollar osteoartritis. Sin embargo, los pacientes a menudo requieren el uso prolongado de medicamentos antiinflamatorios para manejar el dolor y facilitar la integración de la prótesis. Los métodos convencionales de administración de estos fármacos presentan desafíos importantes, incluidos efectos secundarios adversos por la administración oral prolongada y molestias o dolor asociados con inyecciones intraarticulares.

El objetivo de este trabajo fue desarrollar una tecnología para la liberación localizada y sostenida de una combinación de fármacos antiinflamatorios dentro de la cavidad articular de la rodilla. El primer paso de este estudio implicó el diseño de un recubrimiento polimérico biodegradable de dos capas que contiene dexametasona (DEX) y celecoxib (CLX), permitiendo la liberación secuencial de dos fármacos antiinflamatorios con cinéticas de liberación distintas. Se seleccionó DEX para mitigar la inflamación aguda, con un periodo de liberación de 1 a 4 semanas, mientras que CLX se eligió para tratar la inflamación crónica, con un periodo de liberación de 6 a 9 meses. Los recubrimientos poliméricos con liberación de fármacos se evaluaron in vitro y mostraron un perfil de baja citotoxicidad y una reducción eficiente de citocinas representativas como TNF-α, CCL2 y PGE2.

La segunda parte de la tesis se centró en optimizar la adhesión de los recubrimientos poliméricos liberadores de fármacos a las prótesis meniscales de PCU. Se evaluaron diversas estrategias de modificación superficial, incluidas el tratamiento con láser de pulsos femtosegundos, tratamiento con plasma, recubrimientos de polidopamina (PDA) y la incorporación de una capa adhesiva de etil cianoacrilato (ECA). Entre estos enfoques, la capa adhesiva de ECA mostró los resultados más prometedores, mejorando significativamente la adhesión y mostrando las propiedades mecánicas más favorables (módulo de almacenamiento (G'), módulo de pérdida (G''), módulo elástico (E) y tan δ). Cuando se evaluó en un modelo representativo ex vivo utilizando un biorreactor que simulaba el movimiento de la marcha con fuerzas de cizalladura y compresión, esta estrategia preservó la integridad del recubrimiento durante el estrés mecánico y mantuvo cinéticas consistentes de liberación de fármacos. El sistema optimizado se adaptó con éxito para prótesis meniscales anatómicamente relevantes y se probó in vivo en un estudio piloto en un modelo ovino. Las prótesis funcionalizadas redujeron la progresión de la OA en comparación con las prótesis no recubiertas, mientras mostraron una fijación segura sin delaminación del sistema de recubrimiento.

Como una parte independiente del trabajo de la tesis, la sección final se centró en el uso de hidrogeles para comprender el desarrollo del timo y explorar el potencial terapéutico de los linfocitos T en el tratamiento de cánceres y trastornos autoinmunes. Los hidrogeles, conocidos por su versatilidad y adaptabilidad, se han vuelto indispensables en diversas aplicaciones biomédicas, como el cultivo celular en 3D. Este estudio se centró en cómo las propiedades mecánicas de hidrogeles que imitan la matriz extracelular (ECM) influyen en el desarrollo de

organoides tímicos. Los organoides tímicos, compuestos por células progenitoras epiteliales tímicas (TEPCs) y células de la cresta neural (NCCs), se incorporaron en hidrogeles de alginato reticulados iónicamente que contenían Matrigel® con propiedades mecánicas ajustables. Los resultados mostraron que la viscoelasticidad de la matriz desempeñó un papel crucial en guiar la reorganización celular, formar estructuras similares a tejidos y promover la expresión de marcadores clave del desarrollo. Estos hallazgos proporcionan una base para el diseño de biomateriales avanzados que apoyen la organogénesis del timo, ofreciendo valiosas perspectivas para la medicina regenerativa, la inmunoterapia y los modelos de sistemas inmunitarios diseñados.

RESUMO *IN EXTENSO*

1 RESUMO IN EXTENSO

1.1 INTRODUCIÓN

O desenvolvemento de implantes médicos implica unha extensa investigación nas propiedades dos materiais, como a biomecánica e a biocompatibilidade, para garantir que cumpran eficazmente as súas funcións previstas, se integren sen problemas cos tecidos do corpo, minimicen o risco de resposta inmune e reduzan a probabilidade de complicacións. Como resultado, os implantes médicos continúan evolucionando, incorporando materiais e tecnoloxías avanzadas para mellorar o rendemento, a lonxevidade e a seguridade dos pacientes. Actualmente, utilízanse dous tipos de implantes: os implantes biodegradables, deseñados para descompoñerse gradualmente e ser absorbidos polo corpo, eliminando a necesidade de ser retirados cirurxicamente unha vez cumpriron a súa función; e os implantes non biodegradables, destinados a permanecer no corpo de maneira permanente ou durante períodos prolongados para proporcionar funcionalidade a longo prazo [1].

Neste contexto, as películas de polímeros emerxeron como recubrimentos prometedores para dispositivos médicos debido á súa capacidade para mellorar tanto a funcionalidade como a biocompatibilidade. Os biopolímeros empregados para a funcionalización de implantes deben posuír propiedades clave como biodegradabilidade, resistencia mecánica, flexibilidade e biocompatibilidade [2–4], reportáronse diversas técnicas para a síntese de recubrimentos poliméricos, incluíndo recubrimento por inmersión, pulverización, recubrimento por xiro e deposición química en fase vapor (CVD) [5,6]. Estes recubrimentos poliméricos compren múltiples funcións, como reducir a corrosión, a fricción e o desgaste, e previr a formación de biofilms.

Unha área de investigación significativa neste campo céntrase no desenvolvemento de películas poliméricas para a liberación controlada de axentes terapéuticos dende dispositivos médicos. Este enfoque permite que os implantes exhiban propiedades bioactivas, interactuando activamente cos tecidos circundantes. Porén, un desafío crítico no desenvolvemento de implantes radica na súa interacción co sistema inmune, que pode desencadear reaccións biolóxicas complexas, como inflamación e encapsulación fibrosa [7–9]. Unha das estratexias para abordar este desafío implica a creación de películas protectoras que liberen fármacos antiinflamatorios. A pesar dos avances nesta área, os efectos a longo prazo da liberación localizada de fármacos na compatibilidade tisular e a optimización das cinéticas de liberación seguen sendo pouco explorados.

As tecnoloxías emerxentes, como os hidroxeles recargables, ofrecen unha fonte de inspiración valiosa para o deseño de recubrimentos poliméricos que poidan ser reabastecidos con fármacos antiinflamatorios adicionais despois da implantación, unha vez liberada a dose inicial [10]. Ademais, persisten desafíos fundamentais e necesidades clínicas non cubertas, particularmente na consecución dun control preciso sobre a liberación de múltiples fármacos dende un único sistema. O equilibrio entre a dosificación precisa e as cinéticas de liberación variadas adoita requirir métodos de proba e erro e unha extensa criba para optimizar as taxas de liberación de diferentes moléculas, destacando a necesidade de solucións innovadoras [11].

1.2 RECUBRIMENTOS POLIMÉRICOS PARA A LIBERACIÓN SOSTIDA DE FÁRMACOS ANTIINFLAMATORIOS DENDE UN IMPLANTE DE MENISCO

Os implantes ou andamiaxes de menisco que promoven a rexeneración representan unha alternativa prometedora para evitar o desenvolvemento de osteoartrite (OA) despois dunha meniscectomía. Nos pacientes de maior idade, a autorrexeneración do menisco está limitada pola propia bioloxía do menisco e o proceso de envellecemento [12]. En consecuencia, podería empregarse unha prótese non biodegradable como substituto artificial do menisco. Nos pacientes que se someteron a unha meniscectomía total e nos que se incorporou a prótese de menisco non biodegradable NUsurface®, será necesario o uso de fármacos antiinflamatorios para o manexo da inflamación post-cirúrxica e a longo prazo. Isto proporcionará alivio sintomático da dor e asegurará a integración da prótese cos tecidos nativos circundantes na cavidade do xeonllo, xestionando a resposta do corpo estraño (FBR) [13,14].

Os inhibidores de COX-2, como o celecoxib (CLX), e os corticosteroides, como a dexametasona (DEX), son amplamente utilizados para o manexo da inflamación e a dor. O CLX, administrado oralmente, é eficaz para aliviar a dor e a inflamación crónica, pero o seu uso prolongado pode causar efectos secundarios sistémicos significativos, especialmente nos sistemas gastrointestinal, renal, cardíaco e hematolóxico [15,16]. Aínda que a aplicación tópica presenta menos efectos secundarios, a súa eficacia no alivio da dor adoita ser limitada [17]. CLX demostrou resultados superiores na mellora da función do xeonllo en pacientes con OA e na protección contra a dexeneración da cartilaxe, o que suxire o seu potencial como fármaco modificador da osteoartrite (DMOAD) [18–22]. Do mesmo xeito, a DEX, comunmente empregada mediante inxección intraarticular (IA) para a dor severa de xeonllo, mostrou ser prometedora como corticosteroide condroprotector en doses baixas.

Neste contexto, o noso obxectivo foi desenvolver un sistema de liberación innovador para a administración localizada e sostida de CLX, co propósito de manexar a dor e controlar a inflamación a longo prazo cunha liberación dirixida ao longo de 6 a 9 meses, e de DEX, para abordar a inflamación excesiva post-cirúrxica cunha liberación rápida durante 1 a 4 semanas. Este enfoque busca superar as limitacións das inxeccións IA e as terapias sistémicas actuais, ofrecendo unha solución máis eficaz e dirixida para o manexo da OA [20].

Nunha fase inicial de selección, avaliouse unha variedade de combinacións de polímeros e fármacos para optimizar as cinéticas de liberación, considerando factores como o tipo e a concentración do polímero, a dose do fármaco, a solubilidade, a interacción coa matriz polimérica e a cristalinidade. Entre os polímeros probados, seleccionouse unha mestura de PLLA/PCL (80/70 (m/m)) para a liberación de CLX. A inclusión de PCL na matriz de PLLA acelerou a liberación de CLX, logrando unha liberación case completa ao cabo dun ano. Ademais, a capacidade da mestura para incorporar unha maior concentración de CLX (30 mg/mL) en comparación con outras combinacións posicionouna como unha forte candidata para facilitar a integración da prótese de menisco, que require doses máis altas de CLX e cinéticas de liberación máis rápidas [23,24]. Para a liberación de DEX, os polímeros LMW-PLGA e PLA-PEG identificáronse como os candidatos máis axeitados, proporcionando perfís de liberación controlada máis alá dunha semana ou liberación sostida dentro da primeira semana, respectivamente.

Aínda que inicialmente se explorou o método de deposición con disolvente para a síntese de películas poliméricas debido á súa simplicidade, baixo custo e rápida preparación [25,26], finalmente optouse pola técnica de recubrimento por inmersión. Este método, adecuado para a xeometría complexa dos implantes, permitiu unha estratificación precisa e unha liberación consistente de fármacos, facéndoo ideal para a fabricación dos recubrimentos bicapa [27,28].

O estudo comparativo de liberación destacou diferenzas nas cinéticas de liberación entre os dous prototipos (Figura 1). A degradación e o inchazo máis rápidos de LMW-PLGA no Prototipo PLGA facilitaron unha liberación máis rápida de CLX desde a matriz subxacente de PLLA/PCL, en comparación coa liberación máis lenta e sostida observada co Prototipo PLA-PEG. Esta discrepancia atribuíuse á perda máis rápida de tortuosidade na capa de PLGA, que permitiu un acceso directo do tampón á capa de CLX nunha fase máis temperá.

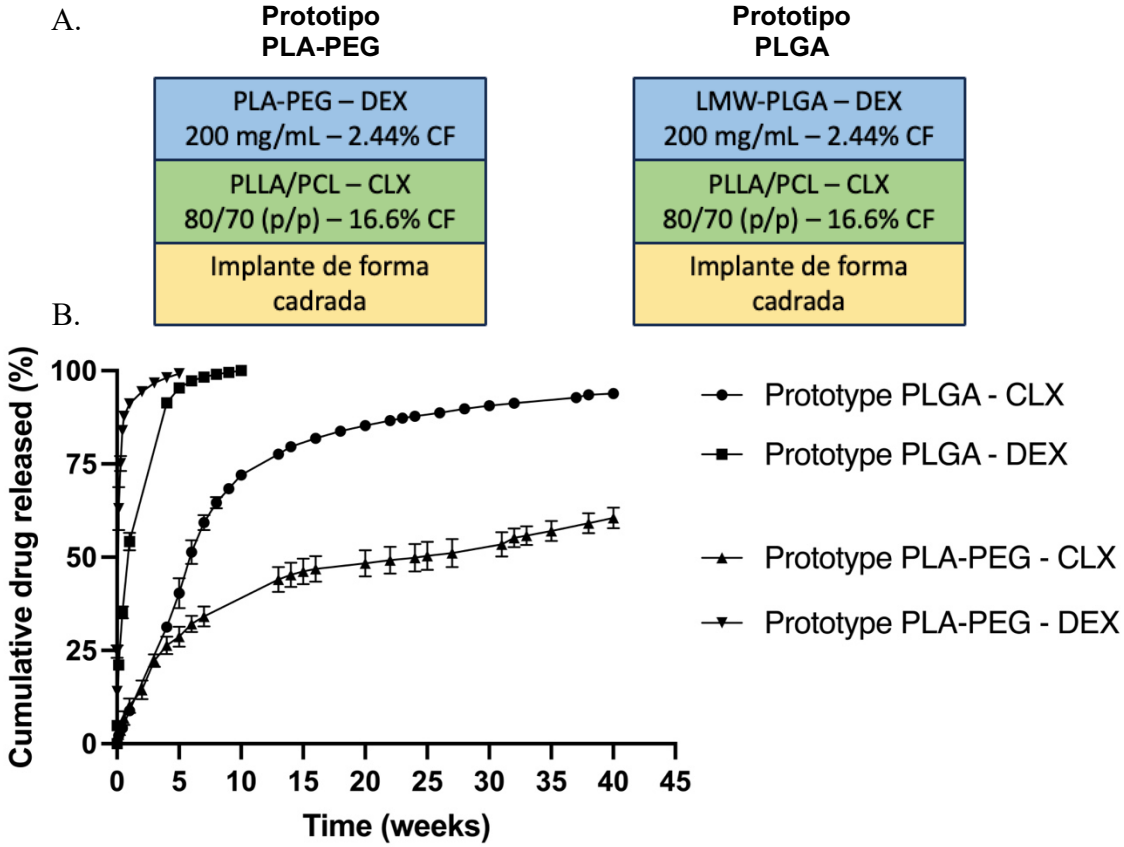

Figura 1. Representación esquemática dos dous prototipos finais de recubrimentos poliméricos bicapa (A). Liberación secuencial de DEX e CLX desde os recubrimentos poliméricos bicapa, compostos por unha primeira capa de polímero de PLLA/PCL, preparada a 150 mg/mL cunha proporción de 80/70 (w/w) e unha carga de CLX do 16,6%; e unha segunda capa de polímero de PLA-PEG ou LMW-PLGA, ambas preparadas a 200 mg/mL cunha carga de DEX do 2,44% (B).

Abreviacións: CF: Carga do fármaco. CLX: Celecoxib. DEX: Dexametasona. PLA-PEG: Copolímero di-bloque de ácido poli(áctico)-poli(etileno glicol). PLGA: Ácido poli(áctico-co-glicólico). PLLA: Poli(L-lactida). PCL: Poli(caprolactona). LMW: Baixo peso molecular (Low molecular weight). Os valores representan a media ± desviación estándar (n=3).

A redución do pH no medio de liberación observada no sistema *in vitro* indicou a degradación do polímero, coa acidificación do medio como resultado deste proceso. Este ambiente ácido, á súa vez, afectou a degradación adicional do recubrimento polimérico restante

mediante autocatalización, acelerando a taxa global de degradación. A pesar desta limitación, estudos previos demostraron que os perfís de degradación de PLGA *in vitro* e *in vivo* son comparables en termos de redución de peso molecular [29]. Esta semellanza pode deberse ás complexas interaccións entre polímeros e tecidos, incluíndo unha posible implicación enzimática no proceso de degradación.

Demostrouse que tanto o prototipo PLGA como o prototipo PLA-PEG exhibiron unha excelente biocompatibilidade cos macrófagos primarios humanos (HMDMs), sen impacto na viabilidade celular en ningún dos momentos avaliados. Dado que o medio de liberación incluía tanto os fármacos como os subprodutos da degradación do polímero, estes resultados indican que os subprodutos da degradación hidrolítica dos poliésteres non comprometeron a supervivencia celular, en consonancia con estudos previos e destacando a natureza non tóxica e biocompatible dos prototipos desenvolvidos [30].

É importante destacar que a eficacia antiinflamatoria dos fármacos liberados foi validada utilizando macrófagos HMDMs. Os resultados de ELISA demostraron que tanto DEX como CLX mantiveron a súa capacidade para regular a secreción de citoquinas (TNFα, CCL2 e PGE2) despois de ser encapsulados e posteriormente liberados dos recubrimentos poliméricos (Figura 2).

A.

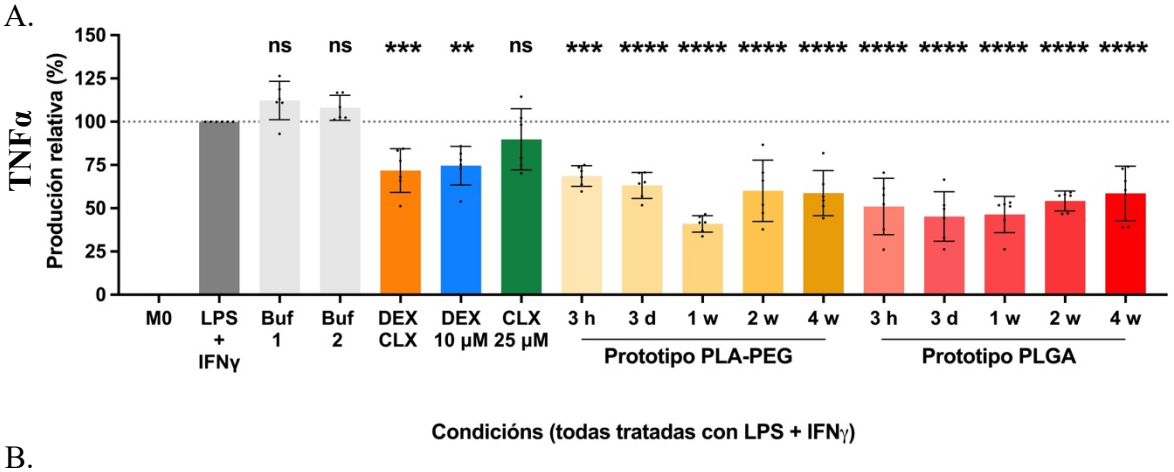

B.

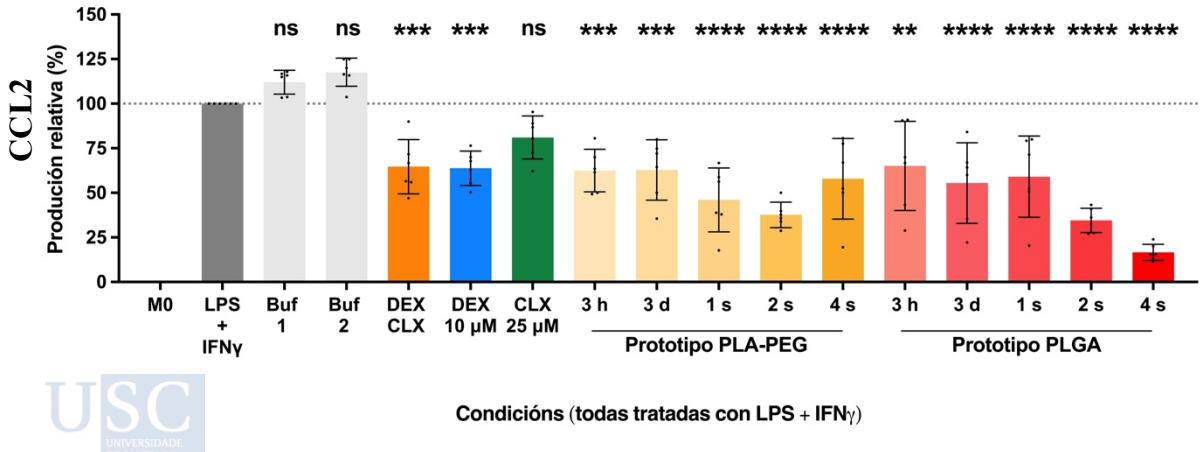

C.

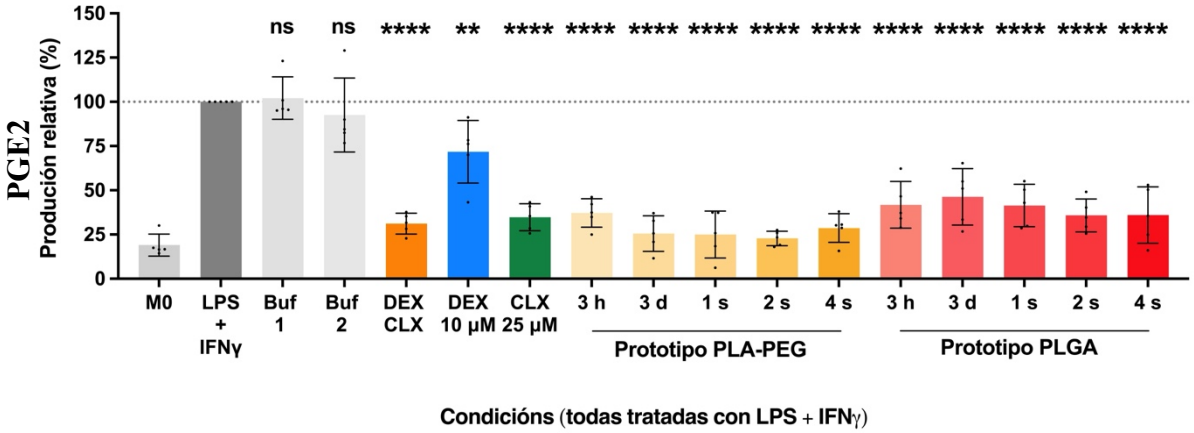

Figura 2. Secreción de TNFα (A), CCL2 (B) e PGE2 (C) por macrófagos primarios humanos expostos a medios nos que os prototipos PLA-PEG e PLGA, ambos cargados con CLX e DEX, foron incubados durante períodos específicos de tempo. A análise realizouse mediante ELISA.

Abreviacións: M0: Macrófagos non activados. Neg: Negativo. Pos: Positivo. Buf: Buffer. PLA-PEG: Ácido poli(áctico)-poli(etileno glicol) copolímero di-bloque. h: Hora. d: Días. w: Semanas. PLGA: Ácido poli(áctico-co-glicólico). LPS: Lipopolisacárido. IFN: Interferón. TNF: Factor de necrose tumoral. CCL2: Ligando da quimiocina do motivo C-C 2 ou proteína quimioatractante de monocitos-1 (MCP-1). PGE2: Prostaglandina E2. Unha comparación significativa foi realizada usando unha ANOVA unidireccional ordinaria seguida de probas de comparación múltiple de Tukey entre LPS + IFNy e o resto dos grupos. Os valores de $p < 0,05$ consideráronse estatisticamente significativos (*). Tamén, (**) se o valor de $p < 0,01$, (***) se $p < 0,001$ e (****) se $p < 0,0001$. ns: Non significativa. As columnas representan a media ± desviación estándar ($n \geq 5$).

DEX suprimiu de forma efectiva a secreción de TNFα e CCL2 nos primeiros puntos temporais, mentres que CLX reduciu principalmente os niveis de PGE2, en consonancia co seu papel como inhibidor da vía inflamatoria COX-2 [31]. Estes achados confirman os efectos antiinflamatorios sinérxicos de ambos fármacos, cun rol distinto de cada un na modulación da inflamación.

En resumo, o desenvolvemento de recubrimentos poliméricos bicapa con liberación de fármacos antiinflamatorios representa unha estratexia prometedora para mellorar a integración de próteses de menisco e abordar a inflamación durante a recuperación post-cirúrxica mediante perfís de liberación de fármacos adaptados.

1.3 Optimización da adhesión dos recubrimentos poliméricos para liberacion de antiinflamatorios en prótesis de menisco para el escenario *in vivo*

As próteses de menisco recubertas con polímeros de liberación de fármacos deben soportar forzas mecánicas substanciais dentro da cavidade do xeonllo, o que require unha boa adhesión entre o recubrimento polimérico e a prótese de policarbonato uretano (PCU) para evitar a delaminación. Para lograr isto, as técnicas de modificación da superficie son esenciais para mellorar a unión dos recubrimentos poliméricos con fármacos e garantir a súa durabilidade en condicións fisiolóxicas. Porén, aínda que o PCU é biocompatible e duradeiro, a súa natureza hidrofóbica, sensibilidade aos disolventes orgánicos e a necesidade de preservar a súa forma xeométrica de cuña presentan desafíos significativos [32,33]. Estes factores fan que métodos tradicionais de modificación, como o arenado [34], sexan menos efectivos e subliñan a necesidade de enfoques innovadores para mellorar as interaccións superficiais e manter a integridade do recubrimento.

Este capítulo avaliou catro estratexias de modificación superficial para mellorar a adhesión entre os recubrimentos poliméricos e a prótese de menisco mediante análises macroscópicas e microscópicas. Entre estas, investigouse o tratamento con láser de pulsos femtosegundo (**fs**) pola súa capacidade para controlar con precisión a rugosidade e a estrutura superficial a escala macro, micro e nano, atributos especialmente beneficiosos para aplicacións biomédicas [35]. Os láseres de pulsos fs son recoñecidos por minimizar os efectos térmicos ao mesmo tempo que xeran xeometrías superficiais complexas que promoven a actividade celular [36]. O tratamento con láser permitiu axustar finamente parámetros como a enerxía aplicada, a área superficial modificada, a xeometría do patrón, a separación dos buratos e o tempo de exposición, ofrecendo unha ferramenta versátil para personalizar as propiedades da superficie. A modificación en forma de patrón de grade mellorou a interacción entre o recubrimento e a prótese en comparación cos patróns de buratos (Figura 3).

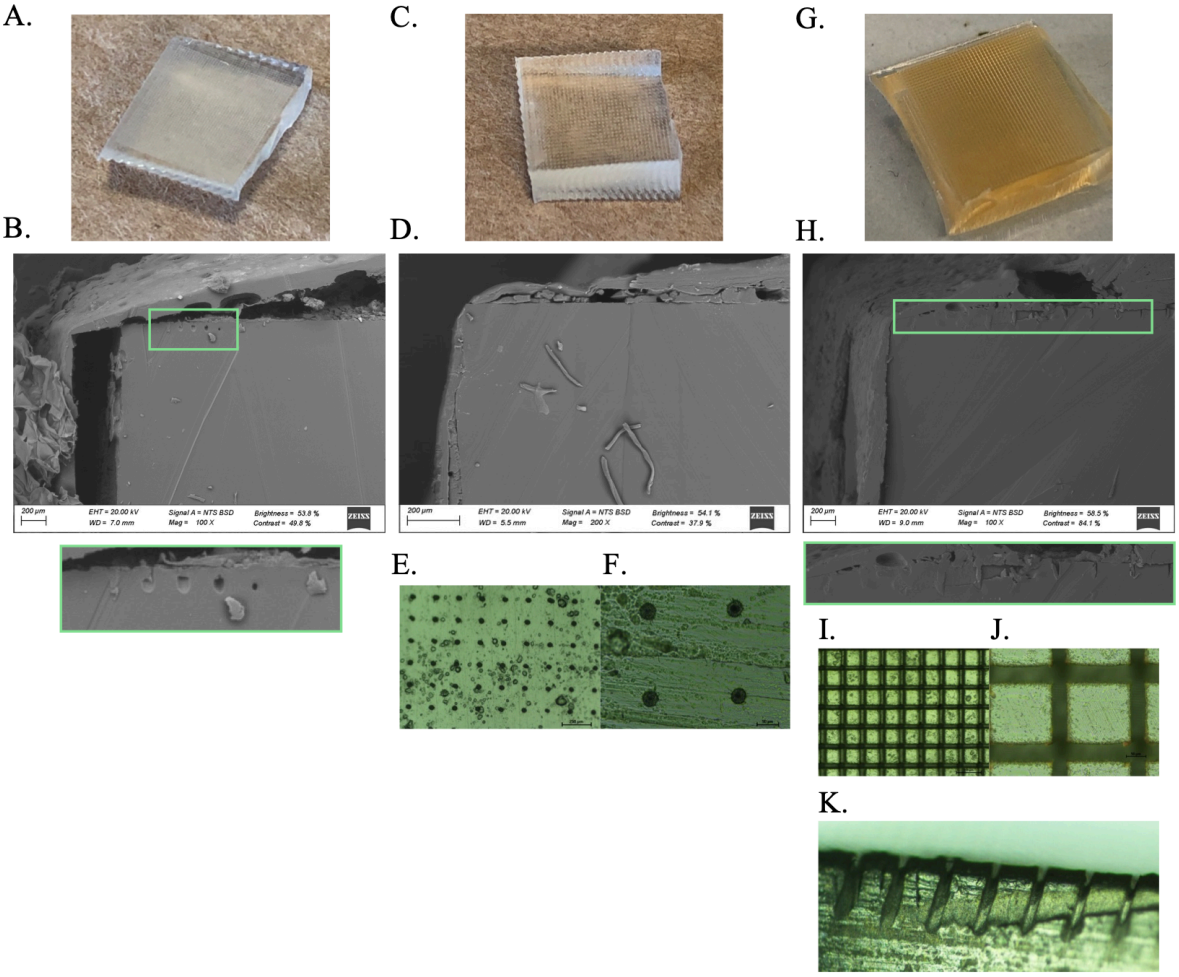

Figura 3. Aspecto macroscópico da prótese de PCU modificada fisicamente con láser de pulsos fs con diferentes patróns: alta densidade de poros (A), baixa densidade de poros (C) e grade (D). Imaxes de FESEM do corte sagital mostrando a interacción do recubrimento polimérico bicapa coas próteses de PCU modificadas fisicamente con diferentes patróns: alta densidade de poros (B), baixa densidade de poros (D) e grade (H). Imaxes de microscopía óptica da superficie da prótese de PCU modificada fisicamente utilizando un microscopio metrolóxico Nikon MM-400 con 5x (E e I) e 20x (F e J). Imaxe de microscopía óptica do lateral da prótese de PCU modificada fisicamente utilizando un microscopio metrolóxico Nikon MM-400 con 20x (K).

Abreviacións: FESEM: Microscopía electrónica de varrido por emisión de campo. µm: Micrómetros. EHT: Tensión alta de electróns. WD: Distancia de traballo. Mag: Ampliación.

Porén, o tratamento con láser tamén provocou cambios visibles de cor, o que indicou posibles alteracións nas propiedades mecánicas e na estrutura da prótese debido aos efectos térmicos. Este cambio de cor, probablemente causado pola carbonización debida a un exceso de calor, suxire unha descomposición do material e a formación dun residuo rico en carbono [37]. En consecuencia, este método foi considerado inadecuado para mellorar a adhesión do recubrimento e abandonouse en favor de enfoques máis fiables.

Posteriormente, avaliouse a modificación química da prótese de PCU mediante tratamento con plasma de osíxeno como unha estratexia para mellorar a adhesión. Este enfoque preservou as propiedades fundamentais da prótese de PCU, mantendo a súa integridade estrutural [38,39]. O tratamento con plasma de osíxeno conleva a introdución de grupos carboxilo (-COOH) e hidroxilo (-OH) na superficie da prótese, mellorando a súa hidrofilicidade e mollabilidade [40,41]. É de supoñer que estes grupos funcionais forman enlaces de hidróxeno cos grupos éster (COO) do recubrimento polimérico, proporcionando colectivamente a forza suficiente para mellorar a adhesión en condicións secas [42].

O procedemento foi optimizado cun tempo de procesamento de 6 minutos a 52W. Este enfoque garante unha adhesión eficiente en condicións secas, baseándose nos enlaces de hidróxeno, sen prolongar innecesariamente o tempo de tratamento nin aumentar a potencia do campo electromagnético, minimizando así a posible degradación do material. Porén, cando se probou en condicións húmidas, a eficacia destes enlaces era limitada, xerando incerteza sobre a súa funcionalidade no microambiente hidrofílico da cavidade do xeonllo, onde as moléculas de auga poden substituír as interaccións entre o polímero e a superficie. Ademais, as modificacións superficiais inducidas polo tratamento con plasma son temporais, o que require que a prótese sexa procesada e recuberta de forma inmediata para garantir que a mellora na adhesión persista [43].

Outra modificación química da prótese de PCU avaliada foi o recubrimento con polidopamina (PDA). A formación do recubrimento de PDA baséase na autopolimerización da dopamina [44]. Este proceso foi monitorizado mediante DLS, revelando un crecemento consistente do tamaño das partículas ata 24 horas, confirmando unha polimerización progresiva (Figura 4). A transición visual da reacción de incoloro a marrón escuro indicou, ademais, a oxidación da dopamina e a formación uniforme de PDA. Aínda que os recubrimentos resultantes de PDA melloraron a hidrofilicidade e ofreceron un método versátil e non invasivo adecuado para xeometrías variadas da prótese, o proceso requiría un tempo de preparación prolongado, incluíndo un pretratamento con plasma de osíxeno e 24 horas de polimerización.

Para abordar os desafíos relacionados coa adhesión dos recubrimentos poliméricos liberadores de fármacos, introduciuse unha capa de sacrificio de PLA-PEG despois do recubrimento de PDA. Supúxose que o dominio hidrofílico de PEG interactuaba coa superficie de PDA, mentres que o dominio hidrofóbico de PLA facilitaba a unión cos recubrimentos poliméricos. Este enfoque mellorou significativamente a adhesión en condicións secas, con avaliacións macroscópicas que mostraron fibras de interacción visibles que resistían a delaminación (Figura 5). Con todo, en condicións húmidas, a adhesión debilitouse debido a que as moléculas de auga interrompían os enlaces de hidróxeno entre a prótese e os recubrimentos. A pesar do seu potencial, este método foi finalmente considerado inadecuado debido ás súas limitacións en ambientes acuosos. Estes resultados subliñaron a necesidade de estratexias alternativas para lograr unha adhesión robusta tanto en condicións secas como húmidas.

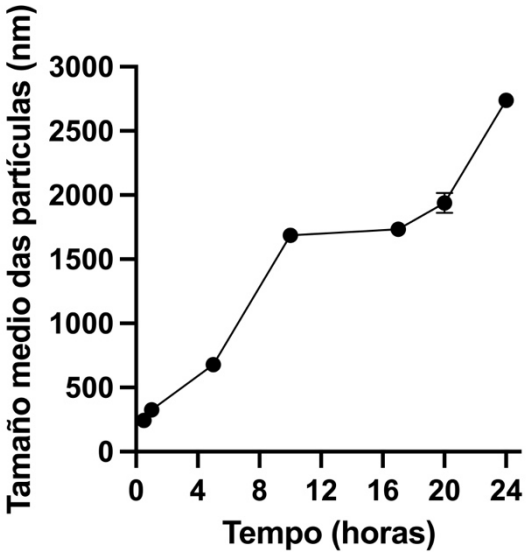

Figura 4. Tamaño medio das partículas dos gránulos de PDA medido mediante DLS, abordando indirectamente a polimerización de PDA.

Os valores representan a media ± desviación estándar (n=3).

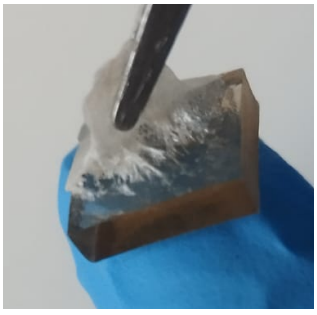

Figura 5. Avaliación macroscópica da prótese recuberta con polímero que incorpora a película de PDA e a capa sacrificial de PLA-PEG mediante proba de *scratch*.

Finalmente, avaliouse a modificación química da prótese de PCU mediante etil-2-cianoacrilato (ECA). O ECA está certificado baixo os estándares USP Clase VI e ISO-10993, o que o fai axeitado para aplicacións médicas, como adhesivos cirúrxicos e recubrimentos de dispositivos biomédicos [45–47], e xa foi descrito como un material capaz de adherir polímeros a poliuretano [48].

O ECA disolveuse en acetona [49] e foi optimizado nunha solución ao 40% (w/v), mantendo as propiedades adhesivas ao mesmo tempo que reducía significativamente a viscosidade, facéndoo adecuado para o recubrimento por inmersión da prótese de menisco. O ECA mostrou unha mellor estabilidade da adhesión en condicións húmidas debido a que polimeriza en presenza de humidade [50], superando as limitacións observadas cos tratamentos de PDA e plasma. As cinéticas de liberación permaneceron inalteradas para DEX, pero aceleráronse lixeiramente para CLX, probablemente debido á reestruturación do polímero causada por interaccións químicas entre o grupo ciano do ECA e o PLLA/PCL.

A.

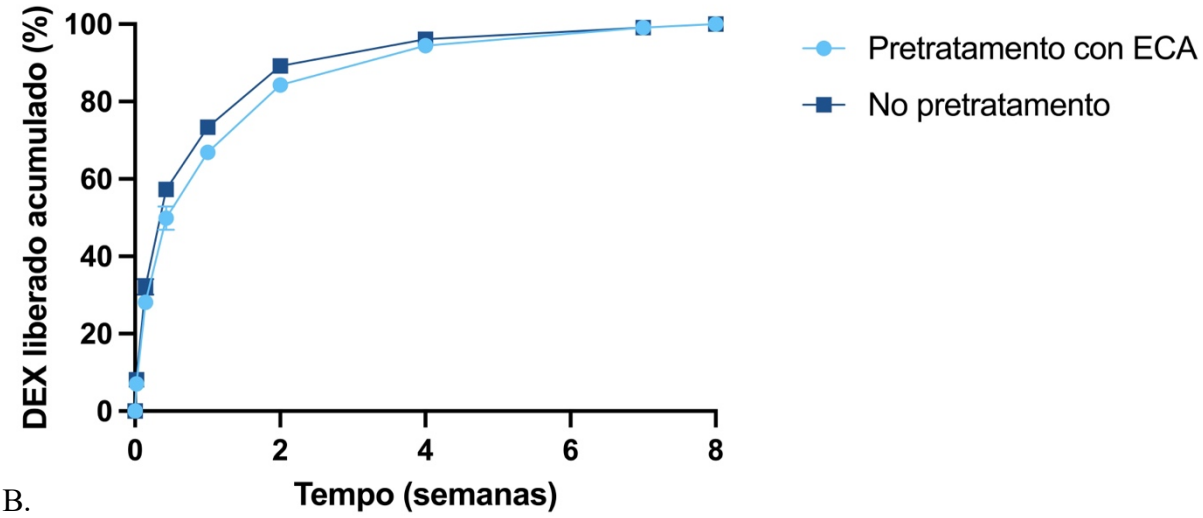

B.

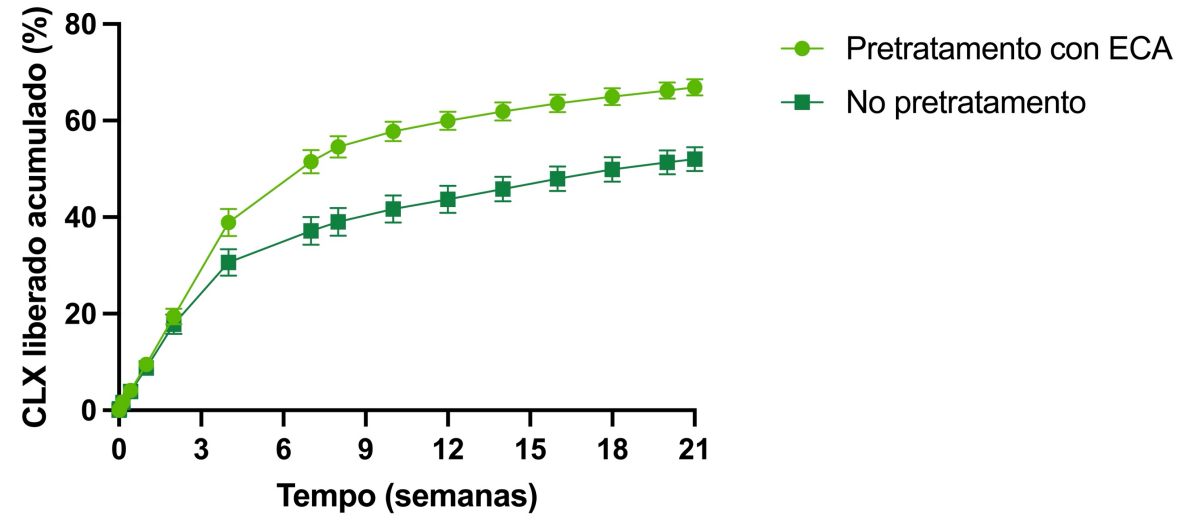

Figura 6. Liberación acumulada secuencial de DEX e CLX desde recubrimentos poliméricos bicapa compostos por unha primeira capa de polímero de PLLA/PCL, preparada a 150 mg/mL cunha proporción de 80/70 (w/w) e unha carga de CLX do 16,6%, e unha segunda capa de polímero de LMW-PLGA, preparada a 200 mg/mL cunha carga de DEX do 2,44%, sintetizados sobre unha capa adhesiva de ECA que recubre a prótese de PCU ou sobre a prótese de PCU sen tratar.

Abreviacións: CLX: Celecoxib. DEX: Dexametasona. PLA-PEG: Copolímero di-bloque de ácido poli(áctico)-poli(etileno glicol). PLGA: Ácido poli(áctico-co-glicólico). PLLA: Poli(L-lactida). PCL: Poli(caprolactona). ECA: Etil-2-cianoacrilato.
Os valores representan a media ± desviación estándar (n=3).

As avaliacións mecánicas mediante Análise Dinámica Mecánica (DMA) utilizando un sistema de tres puntos de flexión (TPB) foron realizadas para avaliar cuantitativamente o módulo e as propiedades mecánicas da prótese de PCU modificada, garantindo que se asemellen estreitamente ás necesidades mecánicas dos meniscos naturais. As propiedades mecánicas das próteses recubertas con ECA foron superiores en comparación con outras modificacións. A capa adhesiva de ECA incrementou significativamente o módulo de almacenamento (G'), indicando unha maior rixidez e un comportamento similar a un sólido, crítico para proporcionar soporte mecánico no ambiente de carga do xeonllo (Figura 7A). Ademais, o módulo elástico (E) das próteses recubertas con ECA foi substancialmente maior que noutros prototipos,

reflectindo unha mellora na rixidez e estabilidade, esenciais para a durabilidade na cavidade do xeonllo (Figura 7B). A pesar destas melloras, os valores de tan δ permaneceron baixos e comparables ás próteses sen recubrir, indicando que o tratamento con ECA preservou o equilibrio entre os comportamentos elásticos e viscosos, asegurando unha óptima recuperación de enerxía durante o movemento (Figura 7C).

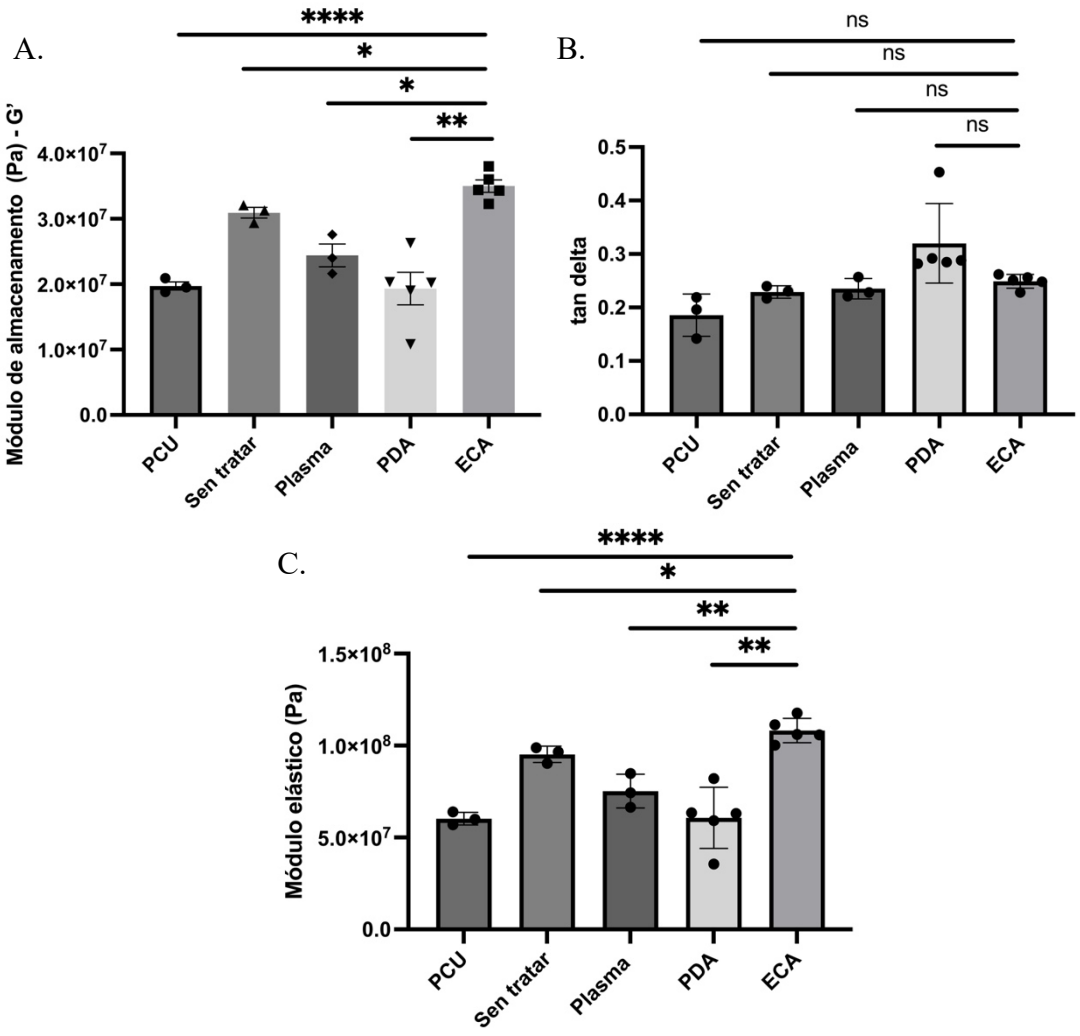

Figura 7. Módulos de almacenamento (A), tan delta (B), e módulos elásticos (E) medidos mediante DMA.

Abreviacións: PCU: Policarbonato uretano (sen recubrimento). PDA: Polidopamina. ECA: Etil-2-cianoacrilato. Delta: δ. Realizouse unha comparación significativa mediante a proba t de Welch non pareada entre o grupo ECA e o resto dos grupos. Os valores de $p < 0,05$ consideráronse estatisticamente significativos (*). Ademais, (**) se o valor de $p < 0,01$, (***) se $p < 0,001$ e (****) se $p < 0,0001$. Cando se mostra ns, non se observaron diferenzas significativas. As columnas representan a media ± desviación estándar ($n \geq 3$).

En xeral, as próteses recubertas con ECA superaron as próteses non tratadas ou tratadas con PDA ou plasma, establecendo a modificación con ECA como a candidata máis prometedora para as próteses de menisco no esixente ambiente mecánico do xeonllo.

Para probar as próteses de menisco de PCU recubertas *in vivo* escolléronse as ovellas como modelo, debido á súa semellanza anatómica co menisco humano [51–53]. Para adaptarse ás

características xeométricas da prótese de menisco de ovella, optimizouse o proceso de recubrimento por inmersión. A orientación da prótese foi axustada de horizontal a vertical, e a concentración da capa de PLLA/PCL modificouse de 80/70 (m/m) cunha carga de CLX do 16,67% a 53/47 (m/m) cunha carga de CLX do 16,6%. Estes axustes preservaron as propiedades mecánicas da prótese, evitaron a alteración estrutural durante o curado e mantiveron as cinéticas de liberación relativamente inalteradas, asegurando a súa compatibilidade coas condicións *in vivo*.

A configuración final, que utilizou a capa adhesiva de ECA, a nova orientación da prótese durante o proceso de recubrimento por inmersión e a redución da concentración do polímero na capa liberadora de CLX, foi avaliada nun biorreactor que simulaba a marcha e as dúas forzas predominantes que actúan sobre o menisco durante o movemento: compresión e cizalla [54,55]. O estrés mecánico acelerou a liberación de fármacos desde as próteses nun biorreactor en comparación cos controis non estimulados, liberándose o 67% de DEX e o 40% de CLX baixo estimulación fronte ao 59% e 25%, respectivamente, nos controis. A pesar destes cambios, os recubrimentos poliméricos permaneceron adheridos ás próteses de PCU sen delaminación, demostrando a durabilidade e a forte adhesión proporcionada pola capa adhesiva de ECA. Estes resultados confirman a estabilidade do recubrimento e a súa idoneidade para o esixente ambiente mecánico da cavidade do xeonllo.

Con respecto á esterilización antes da implantación *in vivo*, seleccionouse o óxido de etileno (ETO) como método debido á súa capacidade para preservar a estabilidade dos fármacos, manter as cinéticas de liberación e evitar danos estruturais nos recubrimentos poliméricos. Aínda que inicialmente se considerou a esterilización con plasma de peróxido de hidróxeno (H_2O_2), este método danou gravemente os recubrimentos poliméricos, especialmente a capa superior de PLGA, e presentou riscos debido ás altas temperaturas de operación e á exposición prolongada á luz UV, que poderían degradar o DEX [56,57]. A esterilización con ETO tamén demostrou non ter efectos adversos nas cinéticas de liberación ou na carga de fármaco, converténdose así no método máis adecuado para estudos *in vivo*.

Finalmente, as próteses de menisco recubertas con polímeros de liberación de fármacos optimizadas foron probadas *in vivo* en ovellas. As análises histolóxicas revelaron diferenzas entre os grupos (Figura 8). O grupo de meniscectomía mostrou os mellores resultados a curto prazo, con mínimos danos na cartilaxe, ausencia de formación de osteófitos e sen engrosamento significativo do óso subcondral. Porén, este grupo carecía dun dispositivo de descarga, como a prótese de menisco, o que podería levar a unha dexeneración progresiva das estruturas da cavidade do xeonllo a longo prazo. En contraste, o grupo de próteses sen recubrir mostrou os indicadores máis severos de OA, incluíndo unha fibrilación significativa da cartilaxe, extensa formación de fibrocartilaxe e notable engrosamento do óso subcondral. Estes resultados reflicten a falta dun mecanismo antiinflamatorio e unha pobre estabilidade de fixación, o que fixo necesario o sacrificio temperán deste grupo. As próteses recubertas pareceron ofrecer un mellor rendemento que as próteses sen recubrir en todas as avaliacións. A tinguidura con azul de toluidina revelou que as próteses recubertas minimizaron os danos na cartilaxe, con puntuacións próximas ás do grupo de meniscectomía. Ademais, as próteses recubertas reduciron a agrupación de condrocitos, a formación de fibrocartilaxe e a presenza de osteófitos en comparación coas próteses sen recubrir, suxerindo un efecto protector xerado pola liberación sostida de DEX e CLX. O engrosamento do óso subcondral tamén foi menos pronunciado no grupo recuberto, indicando un papel importante na mitigación da progresión da OA.

É importante destacar que as próteses recubertas mostraron potencial para mitigar a FBR, como se evidenciou pola redución na formación de fibrocartilaxe [58,59].

En resumo, aínda que as próteses recubertas non eliminaron completamente os marcadores da OA, demostraron claras vantaxes fronte ás próteses sen recubrir, incluíndo unha redución da inflamación sinovial e unha mellor preservación da cartilaxe. Estes resultados destacan o potencial das próteses recubertas como unha opción terapéutica a longo prazo, especialmente para abordar a inflamación e promover a saúde articular. Con todo, os resultados favorables a curto prazo do grupo de meniscectomía subliñan a necesidade de estudos con seguimento máis prolongado para confirmar a capacidade das próteses recubertas de atrasar a progresión da OA ao longo do tempo. Ademais, será crucial contar cun número maio de animais no estudo e estandarizar as técnicas de fixación para garantir resultados consistentes e comparacións máis fiables en futuras investigacións. Por tanto, este estudo debe considerarse como unha investigación piloto *in vivo*, proporcionando información valiosa sobre a capacidade dos recubrimentos poliméricos para soportar as forzas mecánicas na cavidade do xeonllo e identificando a técnica de fixación de prótese máis efectiva dentro da articulación.

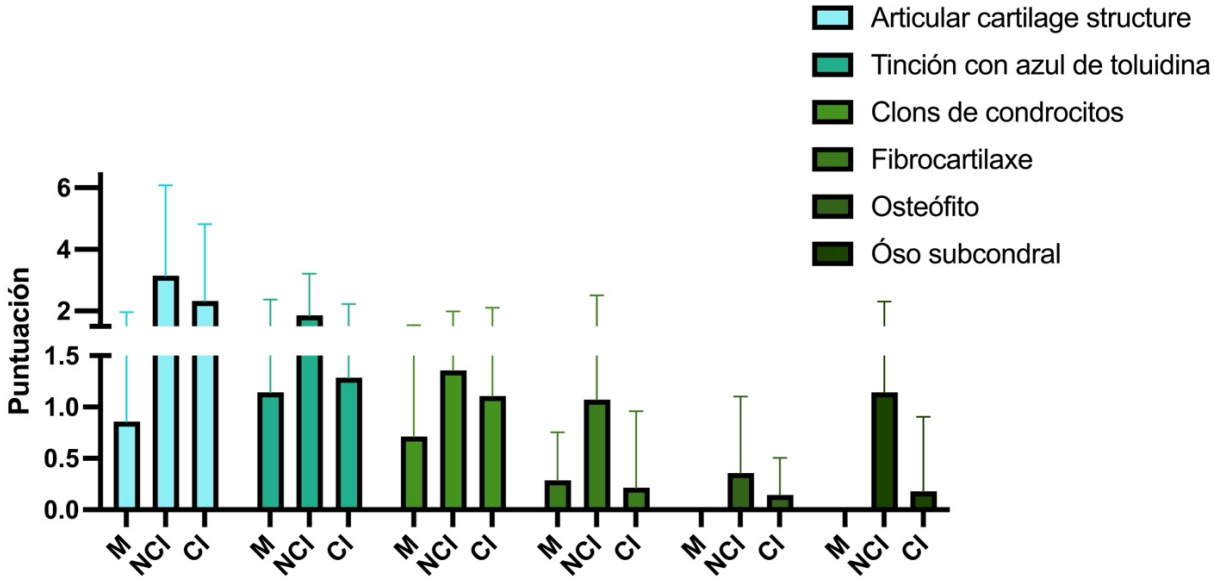

Figura 8. Media das puntuacións histolóxicas de todas as áreas analizadas (MFC, LFC, MTP, LTP, PAT e Troclea).

Abreviacións: M: Meniscectomía (sen prótese de menisco). NCI: Implante non recuberto (meniscectomía + prótese de menisco sen recubrir). CI: Implante recuberto (meniscectomía + prótese de menisco recuberta). MFC: Cóndilo femoral medial. LFC: Cóndilo femoral lateral. MTP: Plató tibial medial. LTP: Plató tibial lateral. PAT: Patela. Troclea: Ranura troclear. As columnas representan a media ± desviación estándar das puntuacións nas áreas analizadas (n ≥ 14). As ovellas analizadas foron meniscectomía (n = 1), implante non recuberto (n = 1) e implante recuberto (n = 2).

1.4 ENCAPSULACIÓN 3D DE ORGANOIDES DE TIMO EN IPNS QUE IMITAN A ECM PARA AVALIAR A MORFOXÉNESE IN VITRO

A formación do repertorio do receptor das células T (TCR) ocorre durante o desenvolvemento e a maduración destas células no timo a través de eventos rigorosamente regulados en zonas especializadas. Durante este proceso, sinais e tipos celulares distintos dirixen a diferenciación dos timocitos en células T completamente funcionais. A organización espacial e as propiedades

mecánicas do microambiente tímico, incluíndo a matriz extracelular (ECM) e a arquitectura dos tecidos, xogan un papel crucial [60].

Este capítulo explora como as propiedades mecánicas dos hidroxeles de alginato reticulados iónicamente, modificados para incorporar proteínas asociadas á ECM e formar redes poliméricas interpenetradas (IPNs), afectan o desenvolvemento de organoides tímicos. A resistencia dos hidroxeles á degradación celular permite unha axuste independente da viscoelasticidade, rixidez e densidade de ligandos. Ademais, a súa reticulación iónica pode adaptarse ás diferentes taxas de relaxación do estrés nos tecidos en desenvolvemento, mantendo a estabilidade en cultivo durante varias semanas [61].

Os organoides tímicos, compostos por células proxenitoras epiteliais do timo (TEPCs) e células da crista neural (NCCs) derivadas de células nai embrionarias humanas, foron encapsulados en catro formulacións de IPNs con propiedades mecánicas distintas. Os módulos oscilaron entre brandos ($E \approx 4.100$ Pa) e ríxidos ($E \approx 15.000$ Pa), mentres que a viscoelasticidade variou de máis elástica, con tempos de relaxación $\tau 70\%$ máis lentos, a máis viscoelástica, con tempos de relaxación $\tau 70\%$ máis rápidos.

Estes organoides cultiváronse e analizáronse durante unha semana para avaliar a reorganización celular en resposta aos estímulos mecánicos. Durante o desenvolvemento dos organoides tímicos, as NCCs superaban inicialmente en número ás TEPCs nunha proporción de 3:1, encapsulándoas progresivamente e dando forma á estrutura do organoide. A análise de circularidade revelou unha morfoloxía estable nos IPNs ríxidos, independentemente da viscoelasticidade, mentres que os IPNs brandos mostraron tendencias distintas: os IPNs brandos de relaxación lenta experimentaron unha diminución pronunciada na circularidade ata o día 3, estabilizándose no día 5, mentres que os IPNs brandos de relaxación rápida mostraron unha diminución gradual durante todo o período de observación. Estes achados subliñan os roles complementarios da rixidez e a viscoelasticidade na morfoloxía e organización espacial dos organoides. As NCCs formaron unha estrutura anular ao redor da parte central do organoide, encapsulando progresivamente as TEPCs co tempo (Figura 9), destacando a importancia das sinais mecánicas no desenvolvemento dos organoides e na morfoxénese dos tecidos [62,63].

A análise mediante inmunohistoquímica revelou que as propiedades mecánicas da ECM inflúen significativamente no desenvolvemento do tecido tímico, incluíndo a formación de estruturas semellantes a tecidos e a expresión de marcadores clave do desenvolvemento. Este achado resalta o papel fundamental da viscoelasticidade na creación de patróns estruturados semellantes a tecidos dentro dos organoides tímicos. No que respecta á formación de estruturas semellantes a tecidos, os IPNs brandos de relaxación rápida demostraron as estruturas máis avanzadas, coa presenza de lúmenes que indicaban unha progresión cara á organización madura dos tecidos (Figura 10). Pola contra, a ausencia de lúmenes noutras condicións indicou unha diferenciación limitada, destacando unha coordinación insuficiente entre os estímulos mecánicos e bioquímicos [64–66]. Os IPNs ríxidos de relaxación rápida apoiaron lixeiramente a formación de lúmenes e estruturas semellantes a tecidos, suxerindo que a rixidez complementa a viscoelasticidade na morfoxénese tímica. En contraste, os IPNs brandos de relaxación lenta mostraron unha complexidade limitada con menor formación de lúmenes, e os IPNs ríxidos de relaxación lenta careceron por completo de lúmenes e organización, subliñando a necesidade dun ambiente viscoelástico semellante á ECM para o correcto desenvolvemento do tecido

tímico, apoiando estudos previos que destacan o seu papel no desenvolvemento de tecidos e na instrución celular [67–69].

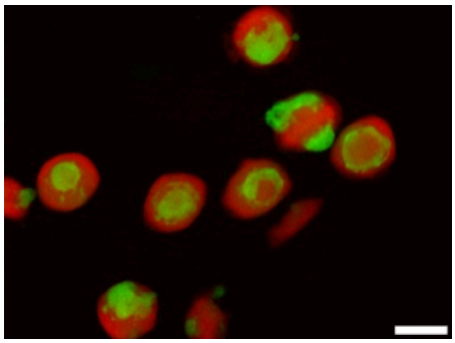

Figure 9. Organoides de timo fluorescentes encapsulados en IPNs brandos de relaxación rápida, imaxinados mediante microscopía de campo amplo.

Abreviacións: IPN: Rede polimérica interpenetrada. GFP representa as TEPCs. RFP representa as NCCs. As imaxes foron capturadas cunha ampliación de 4×, proporcionando unha visión xeral da distribución dos organoides dentro do campo. As barras de escala representan 500 µm.

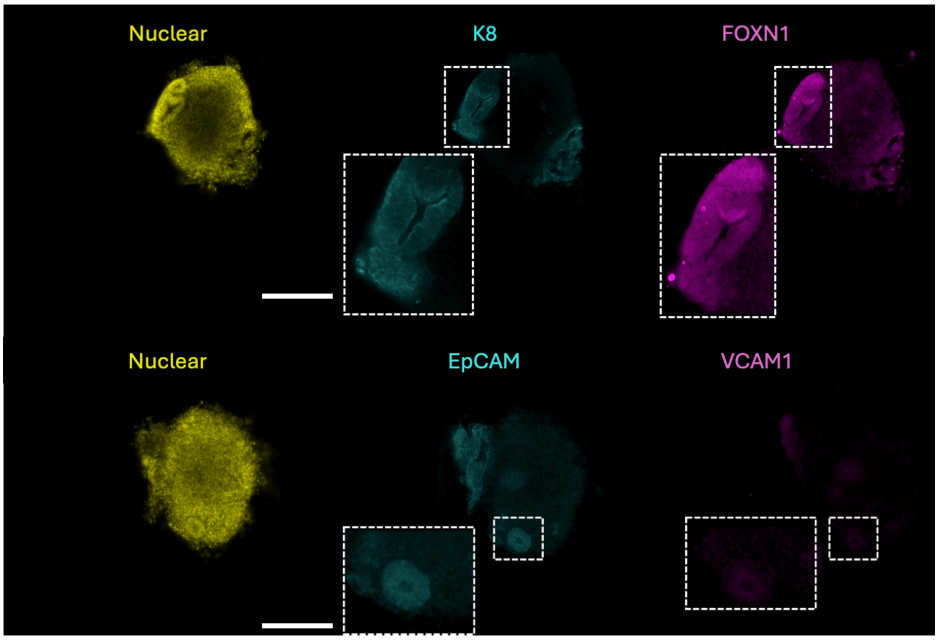

Figure 10. Imaxes fluorescentes representativas de organoides de timo encapsulados e diferenciados en IPNs brandos de relaxación rápida que imitan a ECM.

Abreviacións: K8: Queratina 8. FOXN1: Forkhead-box n1. EpCAM: Molécula de adhesión das células epiteliais. VCAM1: Molécula de adhesión das células vasculares-1. As imaxes de cada panel foron capturadas cunha ampliación de 20x. As imaxes nas caixas brancas punteadas presentan unha vista ampliada dunha parte do organoide, permitindo unha observación máis detallada da súa morfoloxía e características estruturais. As barras de escala representan 200 µm.

Por último, a análise dos marcadores de desenvolvemento do timo revelou diferenzas significativas na expresión a través dos IPNs con propiedades mecánicas variadas. Os IPNs brandos de relaxación rápida promoveron consistentemente os niveis máis altos de expresión de K8, FOXN1 e EpCAM, marcadores críticos para a organoxénese tímica. Observáronse diferenzas significativas na expresión de K8 entre os IPNs brandos de relaxación rápida e os IPNs ríxidos de relaxación lenta, mentres que outras condicións mostraron niveis comparables, destacando o papel dominante da viscoelasticidade na mellora da expresión de K8.

FOXN1, esencial para a morfoxénese do timo, presentou niveis significativamente máis altos nos IPNs brandos de relaxación rápida en comparación con todas as outras condicións, sendo os IPNs ríxidos de relaxación lenta os que mostraron a menor expresión. De forma similar, EpCAM, asociado coa organización epitelial, tamén se elevou significativamente nos IPNs brandos de relaxación rápida en comparación coas outras condicións, subliñando a súa capacidade superior para apoiar a diferenciación avanzada de tecidos. Pola contra, a expresión de VCAM1 foi uniformemente baixa en todas as condicións, sen diferenzas significativas, consistente co seu papel en etapas posteriores do desenvolvemento tímico [70,71].

Esta parte da tese destaca a viscoelasticidade como o principal motor da maduración dos organoides tímicos, mentres que a rixidez desempeña un papel secundario pero complementario. Enfatiza a importancia de optimizar as propiedades mecánicas dos IPNs que imitan a ECM para mellorar a organoxénese tímica.

INTRODUCTION

This introduction has been submitted to the journal *Regenerative Engineering and Translational Medicine* for the *Special Issue: Honoring Nicholas Peppas* as a scientific review and is currently under review for acceptance.

2 INTRODUCTION

The development of medical implants involves extensive research into materials properties such as biomechanics and biocompatibility to ensure that they perform their intended functions effectively and integrate seamlessly with the body's tissues, minimize the risk of immune response, and reduce the likelihood of complications. As a result, medical implants continue to evolve, incorporating advanced materials and technologies to enhance their performance, longevity, and patient safety. Two types of implants are currently being used: biodegradable implants, designed to gradually break down and be absorbed by the body, thus eliminating the need for surgical removal after they have served their purpose, and non-biodegradable implants, intended to remain in the body permanently or for extended periods, providing long-term functionality [1]. Some of the most used implants, materials, and required properties are summarized in Table 1.

In this context, polymer films have emerged as promising coatings for medical devices due to their ability to enhance both functionality and biocompatibility. While previous reviews have focused on specific polymers for particular implants, such as polyesters for bioceramic scaffolds [72], there is a need for a broader evaluation that spans different polymer coatings and their applications across various medical devices.

A significant area of research in this field is the development of polymer films for the controlled release of therapeutic agents from medical devices, enabling implants to exhibit bioactive properties and interact with surrounding tissues actively. Recently, many studies have explored specific devices—such as cardiovascular stents, balloons, or titanium implants [73,74] —or have focused on the release of different therapeutics from these coatings [75].

On the other hand, a critical issue to be confronted when developing implants is their interaction with the immune system, which often triggers complex biological reactions like inflammation and fibrous encapsulation [7–9]. An approach to deal with this issue has been the formation of protective films covering the implants and releasing anti-inflammatory drugs. Despite advances in this area, the long-term effects of localized drug release on tissue compatibility and the optimization of release kinetics remain underexplored. While Welch, Winkler, and Thissen [76] reviewed valuable insights into antifibrotic strategies for implants and prostheses, gaps persist in understanding how drug-releasing polymer coatings can more effectively mitigate this challenge.

Therefore, there is a need for a more in-depth evaluation of the broad application of polymer coatings across various implant and prosthesis compositions, synthesis methods, and functions. Specifically, this chapter addresses the gaps in knowledge regarding the synthesis strategies, the most promising tasks of these coatings, and their capacity to release anti-inflammatory agents to modulate the immune response and reduce adverse post-implantation effects.

This chapter will first describe the properties of polymers used as functional coatings, then examine the various types of medical implants and prostheses, their functional requirements, and current limitations. It will also present synthesis methods and applications of polymer coatings on specific implantable devices, emphasizing their contribution to improving prostheses' functionality and advancing implant technology. Finally, a comprehensive analysis

of their use in drug delivery, focusing on anti-inflammatory drugs, will be presented. This introduction will also discuss the evolution towards multi-drug release systems designed better to meet the complex biological demands of the body. Lastly, future directions in the field will be outlined.

2.1 KEY CHARACTERISTICS OF POLYMERS USED FOR FUNCTIONALIZATION OF IMPLANTS

Biopolymers used for functionalization of implants must exhibit key properties such as biodegradability, mechanical strength, flexibility, and biocompatibility [2–4]. Biodegradable polymers can fulfill their intended function and subsequently be eliminated from the body through excretion or resorption, eliminating the need for surgical removal [77]. When designing biodegradable biomaterials, several critical properties must be considered. These materials should minimize the risk of prolonged inflammatory responses and degrade at a rate that matches their intended purpose and is suitable for their specific application. Additionally, they should produce non-toxic degradation byproducts that the body can readily absorb or excrete while providing the necessary permeability and processability for their intended use [78].

The mechanical strength of polymers is critical because it determines the material's ability to withstand physiological forces and stresses without failing. For instance, orthopedic implants require sufficient mechanical integrity to support tissues and maintain their structure in the body. Thus, the polymer coatings synthesized over them will require similar mechanical properties to better adapt to their target location. Mechanical strength also influences the durability and longevity of medical devices. For example, very promising polymers such as collagen have been limited by their poor mechanical strength compared to their natural state in the body [79]. However, alternatives such as chemical, physical, or enzymatic crosslinkers have allowed their application in fields such as skin wound repair [80], corneal diseases [81], bone defects [82], or tendon damage [83], among others.

Regarding flexibility, it is a significant factor in biomedical polymers. When the degree of internal rotational freedom within a polymer is sufficiently high, the molecular chains can change their conformation, resulting in enhanced flexibility [84]. Flexibility enables these materials to closely replicate the mechanical behavior of organs and tissues, making them well-suited for use in implants, prosthetics and polymer coatings, and tissue engineering scaffolds. The ability of these polymers to adapt and conform to various shapes promotes seamless integration in the body, minimizing the risk of damage or rejection. This adaptability enhances patient outcomes and expands the potential applications of these polymers in regenerative medicine and other advanced medical technologies [85,86].

Finally, biocompatibility is crucial because it ensures that the material does not elicit an adverse immune response when in contact with body tissues. This property helps prevent inflammation, toxicity, or rejection by the body, enabling the polymer to function effectively within the biological environment. Biocompatible polymers are currently used safely in a wide range of medical devices, implants, and drug delivery systems, interacting closely with biological tissues without causing harm or disruption to physiological processes. For instance, polymeric materials in direct contact with human blood must effectively manage protein adsorption and blood cell adhesion. These interactions are critical as they can trigger the body's

defense mechanisms, potentially leading to complications such as clot formation or immune responses. Therefore, ensuring that these materials can handle these processes without adverse effects is essential for their safe and effective use in medical applications [87].

2.2 TECHNOLOGICAL APPROACHES FOR THE FUNCTIONALIZATION OF IMPLANTS WITH POLYMER COATINGS

As explained above, implants, from artificial joints to cardiovascular stents, are gaining importance as world populations tend to live longer (Table 1). However, the interaction between these foreign materials and the host's biological environment can pose challenges. These difficulties include the risk of infection, inflammation, and, finally, implant rejection. Revision surgeries cost millions and are detrimental to countries' public health [88,89]. These procedures usually occur because of improper implant functionality, wear, lack of integration, and infection. Moreover, the recurrence of revision surgeries significantly affects patients' quality of life [90–92]. Therefore, different processing methods and surface modification of implants have been developed to overcome this hurdle. Roughness modification (i.e., sandblasting [93,94], acid-etching [95,96], laser-based [97,98] processing), chemical modifications (i.e., anodization [99], plasma treatment [100–102]), organic coatings (i.e., polydopamine [103–105]), inorganic coatings (i.e., silver coating [106], hydroxyapatite [107,108]), grafting (i.e., graft polymerization [109]), and polymer coatings (i.e., polyester [110–114]).

Among these modifications, polymer coatings are essential because they provide a versatile and adaptable solution due to the vast array of commercially available and well-described polymers. By effectively modifying the surface properties of implants, polymer coatings can enhance implant performance and longevity, promote tissue integration and biocompatibility, minimize the risk of adverse reactions, wear, or infections, and provide controlled drug release, all of which contribute to the success and safety of implantable medical devices. This underscores the significance of polymer coatings in optimizing the performance of implants.

Table 1. Summary of the main types of implants, their composing materials, and the essential properties required for their effective performance.

Implant	Material	Needed properties	References
Dental	Metals and alloys (Titanium, Titanium alloys) Ceramics (Al_2O_3, silicon nitride) Polymers (PEEK)	Biocompatible Corrosion resistance Wear resistance High elastic modulus	[115]
Cardiovascular (Stent)	Metals and alloys (Stainless steel, nitinol, CoCr, Zn, Mg) Polymers (PLA, PLLA, PCL, PGA)	Biocompatible Bioresorbable (6 months – 2 years) No long-term inflammation Enable endothelial regeneration Maintain mechanical properties No restenosis	[116,117]
Neural (Cochlear)	Metals and alloys (Platinum, titanium) Polymer (PDMS) Ceramics	Biocompatible Maintain function of electrical components Flexibility and long-term stability No increased risk of bacterial infection No FBR	[118,119]
Orthopedic	Metals and alloys (Titanium, aluminum, stainless steel, Co-Cr-Mo) Polymers (PTFE, PMMA, PCU, PU, UHMWPe) Ceramics (Al_2O_3, ZrO_2)	Biocompatible Light weight Adaptable mechanical properties Corrosion resistance Wear resistance Reduce need of revision surgery Limited FBR	[120–122]

Abbreviations: Al_2O_3: Aluminum oxide (Alumina). PEEK: Polyetheretherketone. CoCr: Cobalt-Chromium. Zn: Zinc. Mg: Magnesium. PLA: Poly (lactic acid). PLLA: Poly (L-lactic acid). PCL: Poly (caprolactone). PGA: Poly (glycolic acid). PDMS: Polydimethylsiloxane. FBR: Foreign body reaction. Co-Cr-Mo: Cobalt-Chromium-Molybdenum. PTFE: Polytetrafluoroethylene. PMMA: Polymethyl methacrylate. PCU: Polycarbonate urethane. PU: Polyurethane. UHMWPe: Ultra-high-molecular-weight polyethylene. ZrO_2: Zirconium dioxide (Zirconia).

2.3 METHODOLOGY FOR THE COATING OF IMPLANTS

As previously outlined, various techniques for synthesizing polymer coatings have been reported, often without a specific focus on drug release or limited to particular implant materials [5,6]. In this section, we describe some of the most common methodologies for coating implants, irrespective of the implant's composition, focusing on approaches designed for controlled drug release. The preparation of polymer coatings on implants can be achieved through different methods, mainly utilizing liquid or gas-phase techniques (Figure 11):

2.3.1 Dip coating

Dip coating is a widely used technique known for its adaptability, affordability, simplicity, and ability to be scaled up [123]. The process involves immersing an implant into a polymer solution or suspension and then withdrawing it to form a polymeric coating. The versatility of this method stems from its ability to accommodate a range of variables, such as polymer concentration, solution volume, and viscosity. Consequently, this technique can coat various morphologies and complex shapes, as it does not depend on the object's geometry [124–127]. This technique has been used in commercially available products such as ZoMaxx (Abbott Vascular, USA) stent, which releases zotarolimus using phosphorylcholine coating to prevent restenosis of the metallic stent [128]. Limitations of this process include the processing time, the volume of material needed for the coating process, and the use of organic solvents [129–131].

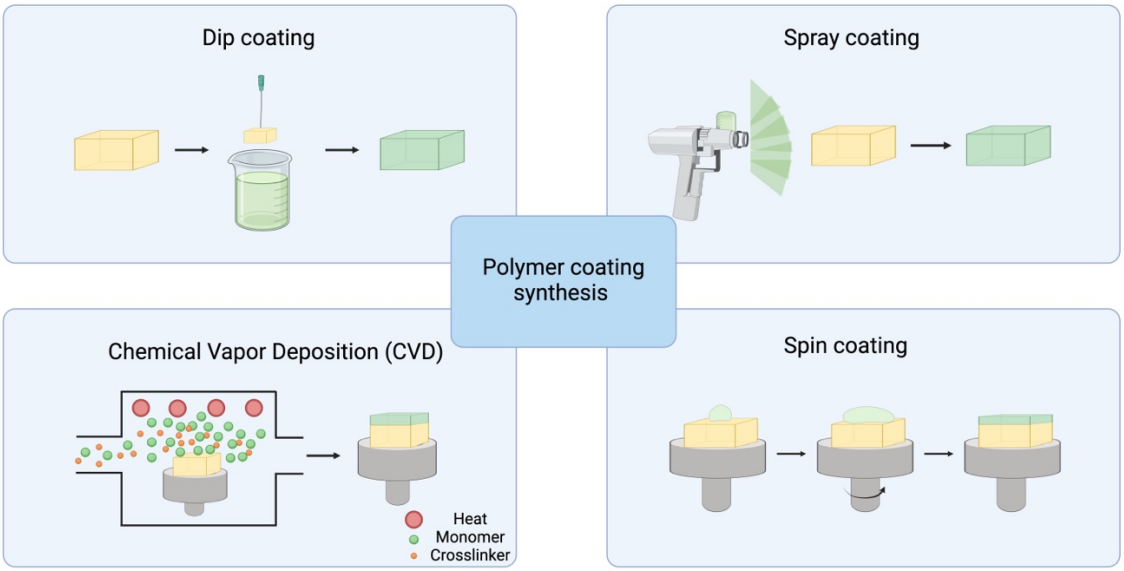

Figure 11. Representative methods for the synthesis of polymer coatings over implantable devices and prostheses.
Created with https://www.biorender.com/

2.3.2 Spray coating

Spray coating is known for its ease of use, scalability, and speed [132,133]. This technique creates films with a granular texture due to the pressurized atomization of the solution droplets [134]. One advantage of this method is that it can coat surfaces regardless of their shape. However, a significant drawback is that material waste is often not utilized during the coating process. To address this, variations like Ultrasonic Spray (US) have been developed to enhance material efficiency [135–137].

Additionally, films produced by spray coating are typically less durable and exhibit inferior mechanical properties [134]. Another limitation is the viscosity of the spraying solution; more viscous solutions can struggle to pass through the airbrush and atomize effectively. This challenge has led to the development of alternative spraying methods, such as airless systems,

to handle higher-viscosity solutions [133]. Spray coating has been used to create the polymer coating over CoCr stents, such as in XIENCE V (Abbott Vascular, US) stents, which release the immunosuppressive agent everolimus from PBMA and PVDF-HFP coating to prevent restenosis and improve long-term safety [128].

2.3.3 Chemical vapor deposition (CVD)

Chemical vapor deposition (CVD) polymerization consists of the delivery of monomers in a vapor-phase state to synthesize well-defined polymer films directly on the surface of substrates [138,139]. In this case, polymerization occurs without solvents in an all-dry process. The ability to provide uniform coating is a distinctive feature that sets CVD polymerization apart from solution methods of non-planar substrates, which may experience issues related to non-wetting, formation of aggregates, and surface tension effects [138,140,141]. This technique allows for modulation of the film thickness, enabling the control of tens of nanometers. It has been increasingly used in the field of drug delivery to tune the release kinetics of some drugs from a drug-loaded substrate coated by these films [142–145]. Among the drawbacks of this technique are its complexity and material requirements for film formation.

2.3.4 Spin coating

Spin coating is a deposition technique used to achieve homogeneous, uniform, and thin film, commonly used in the laboratory. The process involves dispensing a liquid solution onto the center of a spinning substrate and then rapidly spinning the substrate to spread the solution uniformly across its surface through the centrifugal force. This centrifugal force not only ensures an even distribution of the polymer solution but also aids in the rapid evaporation of the solvent. Spin-coated films are used in various biomedical applications, such as wound dressings, drug delivery, and biosensing [146]. Some drawbacks of this technique include challenges in scaling up production and limitations related to substrate geometry. Moreover, complex geometries pose difficulties in achieving effective coatings [147].

2.4 FUNCTIONALITY OF POLYMER COATINGS

2.4.1 Reduction of corrosion

Implants, especially metal-based prostheses, may suffer corrosion during their time implanted. Depending on their location, they may suffer structural damage because of the action of body fluids, in particular, pH variations, temperature, and electrolytes [148–152]. Polymer coatings should have good chemical inertness and stability to avoid degradation or corrosion by the surrounding environment (Figure 12A). Some polymers with good chemical resistance are epoxy PTFE [153] and PEEK [154], among others. Also, polyesters have been described as candidates for implant coating to protect these devices against biocorrosion [155].

2.4.2 Reduction of friction and wear

Based on the final purpose and location of the implant, the modulation of friction and wear can be a determining factor. Zones, where high mechanical stresses can be expected, would require the implant to succeed upon demanding conditions that can damage the device's integrity. This is the case with orthopedic implants, which are particularly important in joint replacements where the movement of the implant against the bone and other tissues should be as smooth as possible. Here, polymer coatings can be used to reduce friction and wear (Figure 12B). For example, titanium alloys, such as those used for hip and other joint replacements, present intrinsic properties such as high corrosion resistance. However, these implants are associated with wear, pitting, cracks, and failure, which could be avoided by limiting micromotion using polymer coatings. The presence of polymer coatings that limit micromotion would be beneficial in reducing these implants [156]. Reducing wear is particularly needed because wear debris can result in an undesired inflammatory reaction that compromises the action of the implant [157]. Among the properties that improve wear resistance appear mechanical properties such as high tensile strength, high Young's modulus, hardness, stiffness, plasticity to bear the mechanical load and prevent excessive wear (i.e., PAI, PI, and PEEK), and low friction coefficient to reduce energy loss and heat generation during sliding (i.e., UHMWPE, POM, PTFE, and PAI) [158,159].

2.4.3 Improvement of biocompatibility and anti-fouling

Human physiology tends to react against artificial objects implanted in the body. Consequently, biocompatible polymer coatings can be created to minimize the risk of immunological reactions or rejections to build a barrier between the surface implant material and surrounding tissues (Figure 12C). Among the polymers used to improve biocompatibility, polynucleotides [160–162], polysaccharides [163–165], polypeptides [166,167]) and synthetic polymers (such as PLA, PEG, and PVA) [168–171] stand up. The upgrade in biocompatibility can be based on the properties of the polymer itself or the modulation of the implant surroundings by releasing molecules. Hydrophobic surfaces are often associated with high protein adsorption and subsequent attraction of immune cells that react against the foreign object. If this degradation proves unsuccessful, fibroblasts will surround the implant and form a fibrous capsule, isolating it from the neighboring microenvironment. This phenomenon is known as the foreign body reaction (FBR) and results detrimental to the implanted device (Figure 3) [172–174]. Increasing the surface hydrophilicity of the implants using, for example, PEG [175] or PVA [176] enhances the overall performance of the implant by reducing non-specific protein adsorption responsible for immune rejection. The design of polymer coatings based on zwitterions, or with anti-coagulant and anti-inflammatory properties, has allowed for the modulation of inflammation, which significantly diminishes implant function [177–179].

Another point to consider is that most implants are intended to stay in place for extended periods. Even when the materials chosen for these prostheses exhibit good biocompatibility with host cells, they may also provide a suitable environment for bacterial adhesion and growth, leading to peri-implant infections. Implant-related infection has a huge socio-economic impact that supposes billions of expenses to healthcare systems worldwide [180,181]. These infections can occur anytime, but the first four weeks for dental implants are particularly critical

[180,182]. Biofilm formation on implant surfaces can severely compromise their function [183]. Recent advancements have focused on reducing bacterial adhesion and preventing biofilm formation through antibacterial modifications of implant surfaces, such as using chimeric peptides[184]. Some polymer coatings act as barriers to reduce the risk of infection associated with implants or even incorporate antimicrobial agents. Furthermore, the in-situ release of antimicrobials overcomes hurdles that can result from the systemic administration of antibiotics, such as systemic side effects and the growing multidrug resistance of bacteria [185–187]. Thus, polymer coatings can inhibit the growth of bacteria on the implant's surface and help prevent post-operative infections while keeping their antimicrobial effect localized.

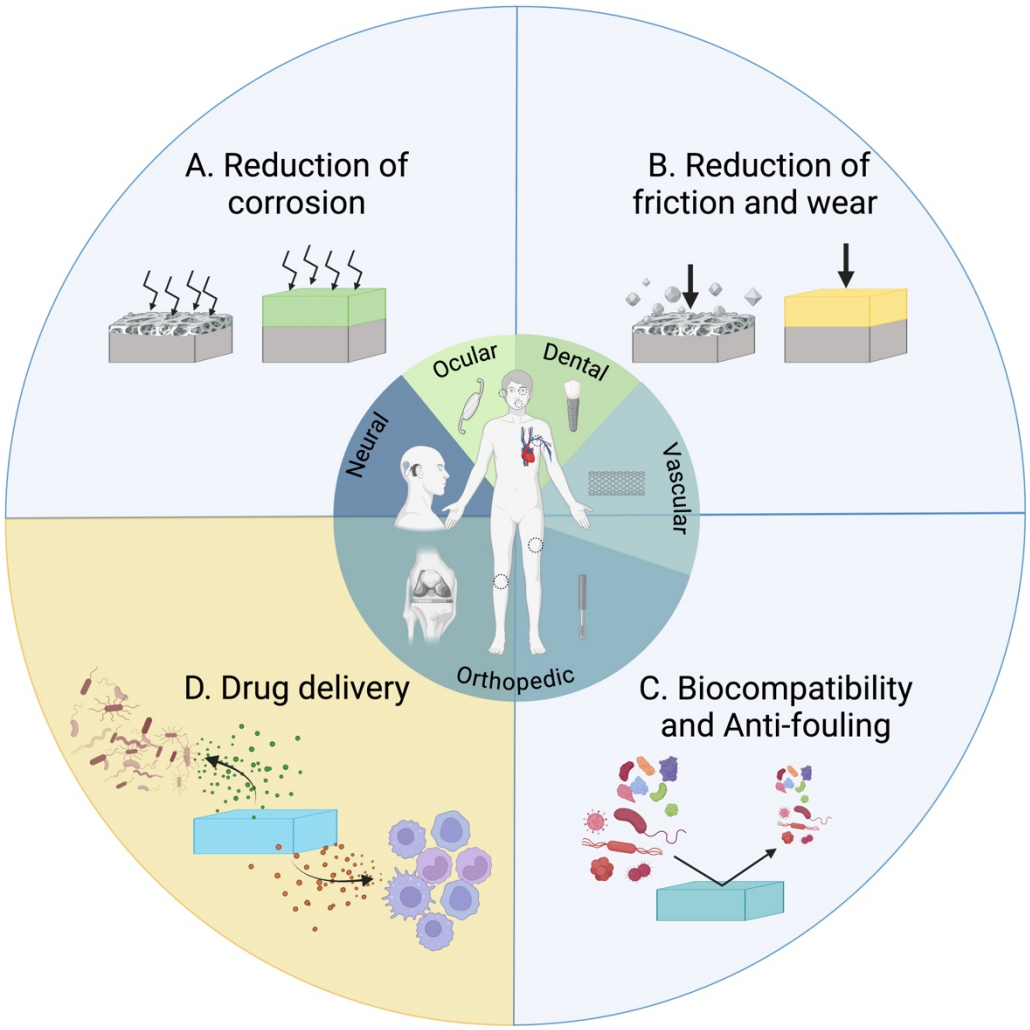

Figure 12. Main types of prostheses and implantable devices functionalized with polymer coatings, and the most characteristic functions of these polymer coatings: Reduction of corrosion (A), reduction of friction and wear (B), biocompatibility and anti-fouling (C), and drug delivery (D).
Created with https://www.biorender.com/

2.4.4 Drug delivery

The incorporation of drug delivery technologies in prostheses and implants is becoming increasingly important to achieve a site-specific effect of the delivered molecules. Controlled drug release may help manage pain, reduce the inflammatory response and fibrosis, promote

biocompatibility and cell adhesion, differentiation, and proliferation, and fight bacterial infections (Figure 12) [7,188–194]. Antibiotics, growth factors, anti-osteoporosis, anti-neoplastic, anti-thrombosis, and anti-inflammatory drugs are the most commonly used for these purposes [75]. Additionally, polymeric matrices can protect these molecules from enzymatic degradation within the body (Figure 2D). Furthermore, certain polymer coatings do not release drugs directly from their matrices; instead, they regulate the release of molecules from the implant surface as the polymer degrades [195].

The choice of polymer material and the coating design depend on the type of implant, its intended function, and the specific medical application. This selection is crucial in fields where precise sensing, drug dosing, and timing are essential. For example, porous drug-releasing polyurethane (PU) coatings over glucose sensors have been developed to mitigate local inflammation by the release of Dexamethasone (DEX) [196]. Also, Rifampicin (RIMP) loaded in PLGA films has been recently used to coat Ti dental implants to prevent peri-implant bacterial contamination [197]. Factors such as polymer type, drug formulation, and coating design significantly influence drug release rates, treatment duration, and the compatibility of the coating with both the implant and surrounding tissues. Thus, drug-eluting implants undergo rigorous evaluation by regulatory authorities such as the FDA to ensure they meet strict safety and efficacy standards before being approved for clinical use [198–200].

2.4.4.1 Delivery of anti-inflammatory drugs from polymer-coated prostheses

The release of anti-inflammatory drugs from implants is crucial, regardless of the implant type, location, or whether it is in soft or hard tissue [75]. The local administration of anti-inflammatory drugs at the site of action can avoid the two main limiting hurdles of oral administration: lack of adequate local concentrations and side effects due to long-term systemic administration.

The release of anti-inflammatory drugs is significant for mitigating foreign body reaction (FBR) and fibrosis, which can limit the survival and function of implantable devices. For example, in fields such as neural electrodes, FBR can severely affect implant performance, leading to complications like glial scar tissue formation and implant loosening due to macrophages' reaction to implant debris. To address this, the release of anti-inflammatory drugs has been explored to improve implant integration and reduce these inflammatory responses [75].

As illustrated in Figure 13, FBR progresses through multiple stages, occurring over a period ranging from minutes to months. Immediately after implantation, an acute inflammatory response is triggered by the adsorption of proteins onto the biomaterial's surface. In this initial phase, neutrophils rapidly migrate to the site, releasing factors and chemical signals that recruit monocytes. These monocytes then differentiate into M1 macrophages within the first few days post-implantation. If this acute response does not degrade the biomaterial, the process transitions into chronic inflammation. This second stage is marked by mononuclear cells, including lymphocytes and monocytes. Macrophages undergo a phenotypic switch from the pro-inflammatory M1 to the anti-inflammatory M2 phenotype, playing a crucial role in forming a fibroblast- and extracellular matrix (ECM)-rich capsule that encapsulates and isolates the implant. Additionally, macrophages may fuse into multinucleated foreign body giant cells (FBGCs). Ultimately, this process leads to a chronic fibrotic response, where the implant is

encapsulated in fibrous tissue and isolated from the surrounding environment. This encapsulation often results in the loss of implant function and increases the likelihood of revision surgery to remove the device. While the cellular processes of FBR are well understood, the main features and determinants of the foreign body reaction are not fully elucidated. Therefore, implants must be designed to accommodate some degree of FBR, ensuring its severity is manageable [174,201].

Many anti-inflammatory drugs have been investigated for their release from polymer-coated prostheses. Cyclosporin A (CsA), an immunosuppressant, has primarily been used in ocular applications. For example, spin-coated PLGA loaded with CsA has been applied to intraocular lenses (IOLs) to mitigate posterior capsular opacification (PCO). This coating has effectively modified IOLs by inhibiting cell proliferation, promoting cell death in vitro, and preventing PCO in vivo in rabbits [202]. Additionally, using ultrasonic spray technology, NSAIDs like Bromfenac have been loaded into PLGA to coat IOLs, providing intraocular anti-inflammatory effects. This method has successfully prevented PCO by inhibiting TGF-β2-induced cell migration and the epithelial-mesenchymal transition (EMT) of residual lens epithelial cells (LECs) via the ERK/GSK-3β/Snail signaling pathway while also demonstrating biocompatibility in vivo in a rabbit model [203].

Other NSAIDs, such as Aspirin, have been used to modify blood-contacting implants. For example, Chen et al. created a coating through thermal-initiated radical copolymerization of methacrylate esterified heparin (MA-heparin) with methyl methacrylate (MMA) and n-butyl acrylate (nBA). After this process, reactive oxygen species (ROS)-responsive polyoxalate containing vanillyl alcohol (PVAX) was anchored onto the coating via esterification, and Aspirin was dissolved in the MMA and nBA solution and encapsulated in the coating during copolymerization. This coating, which could be synthesized on surfaces of any size and geometry, effectively mitigates acute inflammation mediated by PVAX and addresses chronic inflammation with aspirin. In preclinical trials, this technology has shown promise in rabbits by being applied to PU-based indwelling needle cannulas and central venous catheters, where it demonstrated a significant reduction in inflammation and prevention of thrombosis. This indicates its potential for improving the performance and safety of blood-contacting medical devices [204].

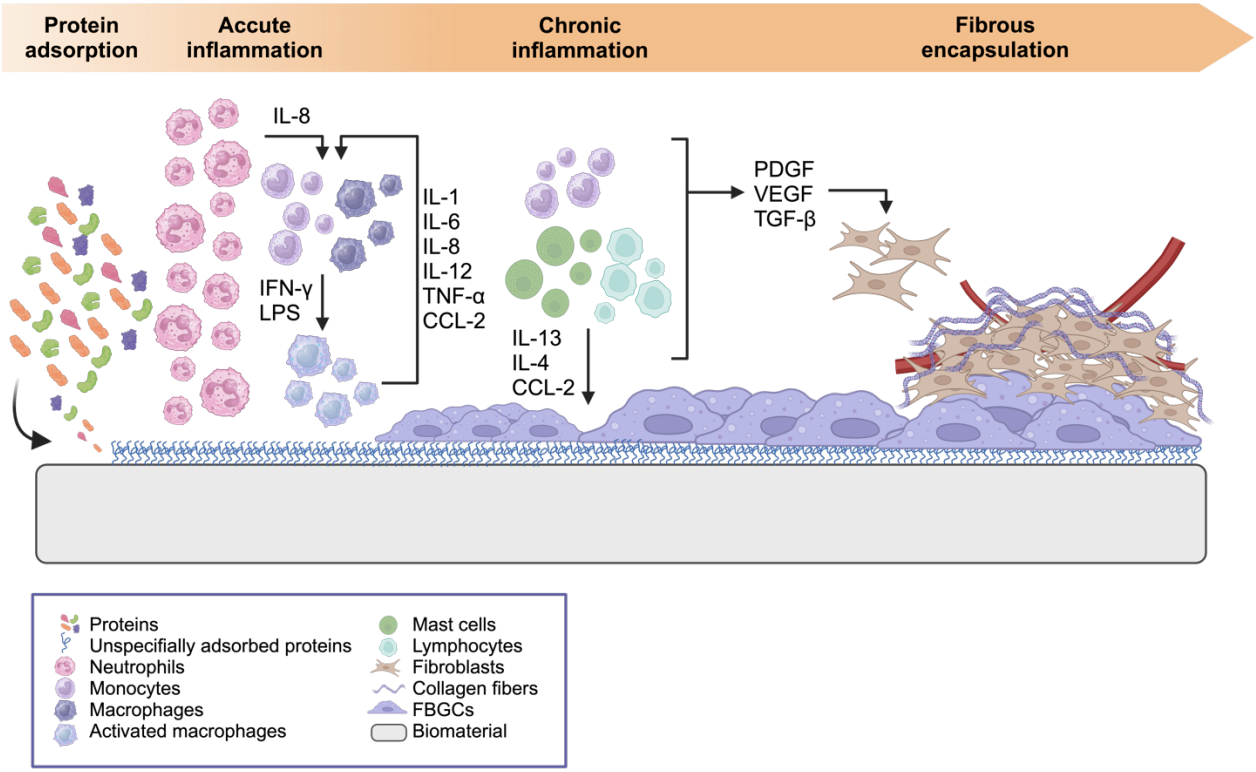

Figure 13. Schematic representation of the FBR upon implantation of a biomaterial in the body. **Abbreviations:** IL: Interleukin. IFN: Interferon. LPS: Lipopolysaccharide. TNF: Tumor necrosis factor. CCL: C-C motif chemokine ligand. PDGF: Platelet-derived growth factor. VEGF: Vascular endothelial growth factor. TGF: Transforming growth factor. Created with https://www.biorender.com/

DEX is considered the gold standard for reducing fibrous encapsulation and modulating inflammation following implantation. Recently, DEX has been incorporated into various polymer matrices for diverse biomedical applications. For instance, it has been explored in intracochlear applications using biodegradable implants made from PLGA or PEG-PLGA [205]. For bone regeneration, DEX has been incorporated into a hybrid layer composed of PEO, PCL, and a 3D-printed PG-NH-DEX scaffold, synthesized on a biodegradable Mg implant substrate. The osteogenic differentiation of these cells was promoted through the upregulation of mitogen-activated protein kinase phosphatase-1 (MKP-1), which stimulated the expression of RUNX2 and other osteogenic proteins [206].

In vascular applications, DEX has been applied to PDA-modified PLA stents using a membrane-mimicking copolymer, MA(PCLA), which serves a dual function by acting as both an antifouling and anti-inflammatory coating. This coating inhibits coagulation and inflammation during the early stages of implantation. Given the relationship between high concentrations of ROS and excessive inflammatory responses, a ROS-responsive molecular prodrug of thioketal-bearing DEX, known as PEI-Tk-DEX, was incorporated into the coating to promote self-regulation of inflammation and tissue healing under high ROS conditions. Its effectiveness in preventing intimal hyperplasia, enhancing endothelial coverage, and modulating inflammatory responses was demonstrated in vivo in rabbits following abdominal aortic stent implantation [207]. Additional examples of anti-inflammatory drug release from polymer coatings are summarized in Table 2.

Table 2. Relevant examples of recently developed polymer coatings over implants designed to release anti-inflammatory drugs.

Implant type	Material implant	Polymer coating	Polymer coating technology	Drug released and Function	Reference
Cochlear implant	Electrode (Silicone)	PLGA	Film casted by dip coating	DSP, Ara-C, NAD Reduce growth of connective tissue and increase neuroprotection	[208]
	Electrode (not specified)	HA crosslinked with BDDE	Hydrogel coating casted by extrusion coating	DEX Promote anti-inflammatory effects in the cochlea and protect against auditory hair cells (HCs) apoptosis	[209]
	Electrode (Silicone)	PLLA	PLLA layer synthesized by spray-coating over O_2 plasma and GOPS treated silicone	DEX (from silicone implant) and DCF (from PLLA coating) Reduce the formation of fibrous tissue isolating implant	[210,211]
Tissue engineering scaffold	Substrate independent	DEX-PEG-$(PDDA/PSS)_9$	PDDA and PSS layer-by-layer film coating	DEX Decreasing collagen deposition, promoting partial regeneration of skin appendages and mitigating post-implantation tissue fibrosis	[212]
Implantable device	Substrate independent i.e. PU glucose biosensor	PLGA/PVA	Composites of PLGA microspheres/PVA hydrogels coating synthesized by freeze-thaw cycles	DEX Control immunogenic response, negative tissue responses and guarantee device performance	[213,214]
Vascular stent	-	C-HA-Cys	Catechol HA and Cys hydrogel synthesized by spin-coating	Allicin Cross-linked network responsive to	[215]

				redox changes caused by inflammation and oxidative stress, smartly releasing allicin to improve biocompatibility, and to regulate atherosclerosis	
	PLA	Ox-HA and PEI	Layer-by-layer system of PEI-Tpl, EGCG and RIVA-Ox-HA nanogel	Thrombin-triggered RIVA (anticoagulant) release, and Tpl and EGCG (anti-inflammatory) Limit stent failure and restenosis	[216]
Non-biodegradable metallic implants	Ti-6Al-4V	PLGA	PLGA coating synthesized by drop coating	Asp Release from surface of the implant to immunoregulate macrophages, enhancing M2 and depressing M1 genes and proteins, improving osseointegration	[217]
	AlSl 316LVM	CMC, ß-CD	Multilayer bioactive system using CMC and DEX solubilized with ß-CD	DEX Promote anti-inflammatory activity and osteogenesis in orthopedic application	[218]
	Ti-SLA	CS	Drug-loaded chitosan microparticles coating PDA-modified Ti-SLA by Schiff-base reaction	Asp and Amo Modulate cell proliferation, decrease inflammation, and reduce bacterial activities	[219]
Biodegradable orthopedic implants	Zn	CMC/Gelatin	Organometallic hydrogel composite created by dip-coating	Asp and Zn^{2+} Modulation of inflammation, osteogenesis, and antibacterial performance	[220]
Patches for wound healing	Polymer	PCL/HAp, PGA and PLL	Multilayer polymer film by	Small molecule model drugs	[221]

		combinations of solvent casting and dip coating	Promote a model system to address wound healing by the release of the different drugs with different release kinetics

Abbreviations: PLGA: Poly(lactic-co-glycolic) acid. DSP: Dexamethasone sodium phosphate (DSP). Ara-C: Cytosine arabinoside hydrochloride. NAD: Nicotinamide adenine dinucleotide. HA: Hyaluronic acid. BDDE: 1, 4-butanediol diglycidyl ether. DEX: Dexamethasone. GOPS: (3-Glycidyloxypropyl) trimethoxysilane. DCF: Diclofenac. PEG: Poly(ethylene glycol). PDDA: Poly-diallyl dimethylammonium. PSS: poly-styrene sulfonate. PU: Polyurethane. PVA: Polyvinyl alcohol. C-HA: Catechol modification of hyaluronic acid. Cys: Cystamine. PLA: Poly(L-lactide). Ti-6Al-4V: Titanium alloy. Asp: Aspirin. Ox-HA: Oxidized hyaluronic acid. PEI: Polyethylenimine. RIVA: rivaroxaban. Tpl: Tempol. EGCG: epigallocatechin gallate. Hap: Hydroxyapatite. AlSl 316LVM: Medical grade stainless steel. CMC: carboxymethyl cellulose. ß-CD: ß-cyclodextrin. Ti-SLA: Sandblasted and acid-etched titanium. CS: Chitosan. PDA: Polydopamine. Amo: Amoxicillin. Zn: Zinc. PCL/HAp: Poly(caprolactone) reinforced with hydroxyapatite nanoparticles. PGA: Poly(glutamic acid). PLL: Poly-L-lysine.

Since the introduction of the first drug-eluting implant in 1937, advancements in polymer coating technology, like those described above, have reinforced the growing trend of developing smart systems for more precise and controlled drug release. These innovations highlight the need for stimuli-responsive or modulated drug-delivery systems that provide temporal release profiles to achieve optimal therapeutic effects [75]. In the context of anti-inflammatory activity, post-implantation inflammation, a complex and multi-factorial process, can sometimes lead to the isolation of the implant, rendering it ineffective and necessitating removal—resulting in significant socioeconomic costs.

Therefore, the development of systems capable of releasing multiple drugs to mitigate inflammation at both acute and chronic stages has become increasingly important. The localized and sustained release of drugs from polymer coatings on medical implants addresses inflammation at multiple levels while minimizing the side effects of long-term systemic drug administration. Delivery systems that can co-deliver different drugs with distinct kinetics would be particularly beneficial in managing the inflammatory microenvironment at various stages post-implantation. For example, a polyelectrolyte multilayer coating system has been designed for the fast delivery of heparin, combined with the long-term benefits of naproxen [222]. In applications such as osteoarthritis (OA) [223], our lab is exploring polymer coatings that could combine corticosteroids for rapid post-operative inflammation control with NSAIDs to manage pain and long-term inflammation, thereby enhancing the synergistic effects of individual drugs and improving overall therapeutic outcomes.

However, several considerations remain regarding the release of anti-inflammatory drugs from polymer coatings. For instance, in the context of preventing fibrotic encapsulation, it is crucial to determine the optimal duration of drug release to reduce or prevent fibrosis effectively [9]. Moreover, in this regard, a critical issue would be that the erosion of the polymer coating does not contribute to the inflammation process.

Lastly, in terms of pain management and the complications associated with long-term systemic administration of anti-inflammatory drugs, emerging technologies like re-loadable hydrogels offer valuable inspiration for designing polymer coatings that can be replenished with

additional anti-inflammatory drugs after implantation once the initial dose has been fully released [10]. These questions and outlooks underscore the need for continued exploration of polymer coatings for implants to enhance the quality of life for the growing number of individuals undergoing implantation surgeries worldwide.

2.5 Future Perspectives and Conclusions

In recent decades, significant advances in polymer chemistry and coating methodologies have driven the development of polymer coatings for drug delivery in implantable devices.

The functionalization of medical devices has become crucial in enhancing their performance, especially by developing polymer coatings. These coatings have significantly improved corrosion resistance and reduced friction and wear, both essential for ensuring durability and functionality. Additionally, creating antifouling and biocompatible surfaces has prevented the adhesion of undesirable proteins or cells, reducing the risk of bacterial infection and maintaining device functionality. Beyond structural improvements, polymer coatings have enabled the development of localized and controlled drug delivery systems, offering precise modulation of the surrounding biological environment. In particular, the release of anti-inflammatory and immunomodulatory drugs has become a cutting-edge strategy, effectively preventing complex and progressive responses such as foreign body reaction (FBR), enhancing device longevity and functionality, minimizing the need for revision surgeries, alleviating pain, and improving patient compliance. Designing polymer systems that release therapeutic agents, such as anti-inflammatory or immunomodulatory drugs, in a site- and time-specific manner can reduce complications and minimize the side effects associated with systemic drug administration.

Moreover, many fields would benefit from combining these technologies. For example, in knee osteoarthritis (OA), which is strongly influenced by inflammation and meniscus injury, considerable efforts have been directed toward either replacing injured menisci with meniscus orthopedic prostheses or scaffolds [224,225] or delivering anti-inflammatory drugs to prevent the onset of OA [226,227]. Thus, combining meniscus prostheses with surface functionalization using polymer coatings for inflammation management is expected to become a significant area of research [228,229]. To date, the only reported example is a silk/graphene oxide-based meniscus scaffold coated with tannic acid/Sr^{2+}, which has demonstrated the ability to protect cartilage and delay osteoarthritis progression due to its anti-inflammatory and anti-ROS properties [230].

Finally, the polymer coating field is moving towards developing advanced polymer systems that incorporate stimuli-responsive degradation by responding to changes in the tissue environment, such as pH variations or temperature fluctuations [231]. Furthermore, systems incorporating multiple polymers, such as layer-by-layer (LbL) coatings, enable precise control over the release of biomolecules and drugs with different functions to better address post-implantation needs, such as preventing bacterial infection, reducing inflammation, promoting tissue regeneration, or a combination of these outcomes [232–235]. Early efforts are also oriented to the design of hydrogels that enable drug reloading post-implantation [236]. This capability could significantly enhance the longevity and efficacy of implantable devices by allowing for on-demand refilling of drugs tailored to the patient's evolving needs while

minimizing invasive procedures or systemic drug administration. In addition, integrating computational biology, which can simulate biological responses without invasive procedures, and design of experiments (DoE), which optimizes formulation variables, could transform the approach to polymer coating design. These methodologies would enable precise predictions of biological responses across various tissue types and individual patients. This would enhance the development of smarter, more rational coatings tailored to specific clinical needs in the coming years. Together, these innovations promise to overcome current limitations and expand the potential of polymer-based drug delivery systems to tackle a wide range of medical conditions.

Looking forward, continued advances in polymer coatings with advanced drug delivery capabilities hold immense potential to transform implantable device technologies. By addressing challenges in drug release kinetics and immune modulation, these innovations could significantly improve the efficacy, safety, and affordability of medical treatments, ultimately enhancing the quality of life for patients undergoing implantation surgeries.

BACKGROUND, HYPOTHESIS, AND OBJECTIVES

3 BACKGROUND, HYPOTHESIS AND OBJECTIVES

3.1 BACKGROUND

Osteoarthritis (OA) is a complex, multifactorial, degenerative joint disease characterized by pain, stiffness, and a gradual loss of joint function, mainly due to the progressive degeneration of cartilage and bone [1]. The prevalence of knee osteoarthritis has increased significantly since the mid-20th century, and currently, it affects approximately one-tenth of the population over 55 [237,238]. For patients with limited tissue regeneration capacity, a novel approach has been the replacement of the meniscus with non-biodegradable prostheses, such as those made of PCU, designed to remain permanently in the body [239,240]. Although these prostheses help maintain the integrity of the articular cartilage and reduce the progression of osteoarthritis, they entail the long-term use of anti-inflammatory drugs to manage pain and facilitate prosthesis integration within the body. Conventional administration routes for these medications (topical, oral, and intra-articular) have significant drawbacks, such as the pain associated with intra-articular injections and the adverse effects of prolonged oral administration [241,242].

Separately, the second part of the thesis addresses the limitations of adoptive T cell transfer (ACT), a promising immunotherapy for cancer treatment. Although ACT has shown good results in hematological cancers such as leukemia and lymphoma, it faces several challenges when applied to solid tumors. These challenges include the limited availability of T cells, tumor antigen heterogeneity, antigen loss, and the hostile tumor microenvironment. These barriers reduce the effectiveness and longevity of patient-derived T cells, modified and re-administered to combat solid tumors [243,244]. To overcome these difficulties, generating T cells from stem cells by selection and maturation within thymus organoids represents an innovative strategy [9–11]. The field of *in vitro* morphogenesis and organogenesis has extensively explored ionically crosslinked alginate hydrogels for their impact on cell reorganization within spheroids, organoid differentiation, and their effects on stem cell behavior. These hydrogels offer a tunable mechanical environment to study how viscoelasticity and stiffness influence tissue development, making them a valuable tool in engineering different organoids [61,63,69,245].

While the first part of this thesis focuses on biomaterials for sustained drug delivery in orthopedic applications, the second part investigates the role of mechanical cues in biomaterial-based tissue engineering, with a focus on thymus organoids. Together, these studies aim to demonstrate the versatility and potential of advanced biomaterials in addressing complex medical challenges.

3.2 HYPOTHESIS

Regarding the first part of this thesis, the hypotheses are:

1. It is possible to design a drug delivery system that can be associated to the meniscus prostheses that allows for sustained, localized, and controlled release of anti-inflammatory agents. This system would limit the side effects of continuous drug administration and improve the patient's quality of life.

2. Polymeric coatings for meniscus prostheses can be created using biocompatible, biodegradable, and non-immunogenic materials. These coatings can be engineered to facilitate their function in the knee joint cavity, reduce the risk of rejection associated with orthopedic implants, and enable the delivery of multiple drugs with distinct release kinetics to address different stages of inflammation after surgery.

3. The polymeric coating could add clinical value to a commercially available prosthesis (NUsurface®) without interfering with its already demonstrated mechanical properties.

Regarding the second part, the hypotheses are:

1. The mechanical properties of the thymus change from embryonic development to postnatal involution.

2. Thymus organoids can be developed using characteristic embryonic development cells: thymic epithelial progenitor cells (TEPCs) and neural crest cells (NCCs).

3. Alginate-based hydrogels incorporating ECM proteins in the form of Matrigel® can mimic the native ECM, with different mechanical properties, and influence thymus organoid development.

4. Hydrogels with thymus-like mechanical properties can promote thymus organoid morphogenesis, displaying characteristic markers such as FOXN1 or K8.

3.3 OBJECTIVES

The objective of the first part of this thesis was to design and develop a functionalized meniscus prosthesis with a bilayer polymer coating capable of enabling the sustained and sequential release of two anti-inflammatory drugs within the knee joint cavity. Two drugs were selected to achieve this goal: dexamethasone, to address post-surgical pain and acute inflammation immediately after prosthesis implantation (with release over a few weeks), and celecoxib, to alleviate long-term inflammation (with release over several months). The following experimental objectives were defined to accomplish this:

1. Design, develop, and characterize a biodegradable polymer coating with the capacity to control the release of the selected drugs with tunable release kinetics.
2. Study the drug release kinetics *in vitro* of the coated prosthesis and the cytotoxicity and efficacy of the delivered drugs in terms of mitigating cytokine secretion in human primary macrophages.

The results corresponding to these objectives are presented in Chapter 1: "Polymer coatings for the sustained release of anti-inflammatory drugs from a meniscus implant".

3. Explore innovative approaches for optimizing the adhesion of the bilayer polymer coating to the prosthesis to prevent delamination under the mechanically demanding conditions of the knee cavity.
4. Characterize the mechanical properties of the polymer-coated prostheses.
5. Adapt the polymer coating to the anatomical shape of the meniscus prosthesis without compromising the implant's structural integrity and evaluate its performance in a simulated mechanical environment *ex vivo* using a bioreactor.
6. Evaluate the efficacy, *in situ* performance, and surgical procedure of the polymer-coated meniscus prosthesis *in vivo* in a sheep model.

The results corresponding to these objectives are presented in Chapter 2: "Optimizing the adhesion of the drug-releasing bilayer polymer coating to a meniscus prosthesis".

The objective of the second part of the thesis was to design and develop alginate-based hydrogels intended to mimic the mechanical properties of the thymus while evaluating the influence of viscoelasticity and stiffness on thymus organoid morphogenesis. This was achieved through the following experimental objectives:

1. Analyze the mechanical properties of the thymus during embryonic development and early postnatal stages to establish a reference for mimicking its native environment.
2. Generate thymus organoids using key cell types involved in thymus development, namely TEPCs and NCCs, to replicate native thymus structures *in vitro*.
3. Recreate these mechanical properties of native thymus using ionically crosslinked alginate-based hydrogels incorporating characteristic proteins (interpenetrating polymer networks, IPNs) that mimic the ECM.
4. Incorporate thymus organoids in IPNs with different mechanical properties.

The results corresponding to these objectives are presented in Chapter 3: “3D Encapsulation of thymic organoids in ECM-mimicking IPNs to evaluate morphogenesis in vitro”.

CHAPTER 1

Polymer coatings for the sustained release of anti-inflammatory drugs from a meniscus implant

4 POLYMER COATINGS FOR THE SUSTAINED RELEASE OF ANTI-INFLAMMATORY DRUGS FROM A MENISCUS IMPLANT

This section has been done in collaboration with Dr. Fernando Torres Andón, Dr. Alba Pensado López, and Dr. Paola Allavena (Humanitas Research Hospital, Italy).

4.1 ABSTRACT

Knee osteoarthritis (OA), a degenerative joint disease, is increasingly prevalent worldwide, often resulting from meniscal deterioration that leads to meniscus removal. Replacing the damaged meniscus with a non-biodegradable prosthesis offers an innovative solution to prevent OA progression, particularly for older patients. However, long-term use of anti-inflammatory drugs for pain relief can cause severe off-target side effects. Although intra-articular drug injections are an option, they often result in patient discomfort and potential cartilage damage.

In this work, we designed functional coatings for a meniscus polycarbonate urethane (PCU) prosthesis based on a drug-releasing bilayer system made of biodegradable polymers. This system provided a sustained release of two anti-inflammatory drugs - dexamethasone (DEX) and celecoxib (CLX) - with distinct release kinetics (1-4 weeks for DEX and 6-9 months for CLX). This release profile was defined with the intention of to modulating, respectively, post-surgical and chronic inflammation within the knee joint. Two bilayer prototypes successfully met the target release profiles, showing consistent biodegradation and reproducibility. Furthermore, the systems were sterile, biocompatible, and maintained the anti-inflammatory efficacy of the released drugs, effectively reducing pro-inflammatory cytokine secretion from human primary macrophages.

4.2 INTRODUCTION

Osteoarthritis (OA) is a multifactorial, degenerative, and chronic joint disease characterized by the progressive loss, thinning, and roughening of articular cartilage and bone remodeling due to insufficient inherent repair mechanisms and imbalance between synthesis and degradation processes. Consequently, OA patients suffer pain, inflammation, swelling, stiffness, and loss of function, which leads to joint disability and significant reduction in life quality [246]. The disease has a huge socioeconomic impact worldwide, being the most frequent form of arthritis and one of the leading causes of disability, with more than 650 million people aged over 40 affected worldwide in 2020 [247]. Among OA, knee OA is especially noteworthy, not just because it is more prevalent than other forms of the disease, but also due to its tendency to occur at younger ages, particularly in obese women. The prevalence of knee OA increases with advancing age and is further influenced by the population's growing average body weight and extended life expectancy [248].

The menisci are semi-circular wedge-shaped fibrocartilaginous, alymphatic, and aneural connective tissue located in the knee joint, between the femoral condyles and the tibial plateau, and surrounded by synovial fluid, a viscous liquid that provides lubrication and nutrients to the knee cartilage. The main functions of the meniscus are to provide a low-friction surface via its resilient wear resistance and stiffness, correct stabilization, load distribution, shock absorption, and lubrication [249–251]. The wear and tear of the meniscus compromise the proper function of the knee joint and can trigger the onset of knee OA. Upon meniscal tear, regeneration is limited because of the biological complexity of the meniscus. Three different zones can be distinguished in the menisci: the vascular and innervated peripheral zone (red region), the avascular and non-innervated internal zone (white region), and the intermediate zone (red-white region) [252]. The avascular zone results in a lack of blood supply and poor cellularity, and consequently, it has a low capacity to regenerate and self-heal [253,254]. Thus, the removal of an injured meniscus is a common procedure in the clinic. Meniscectomy can be partial or total, depending on the meniscus surface resected. The current preference is to preserve the meniscus as much as possible and avoid the need for total knee arthroplasty, a highly invasive end-stage procedure [255–258]. The resection of the meniscus provides pain relief and improves knee function in the short term. However, it has been reported that the risk of developing OA can increase in patients who had previously undergone meniscectomy, especially after total meniscectomy [259].

The use of meniscus implants or scaffolds that promote regeneration is a promising alternative to avoid the onset of OA after a meniscectomy [12]. For younger patients, partial substitution with biodegradable scaffolds or tissues may be a solution, as the regeneration of the meniscus could be expected [260]. Among the therapeutic options for these patients, autologous tissue transplant, meniscal degradable substitutes, and allograft transplantation have shown the best prognosis. For older patients, for whom self-regeneration of the meniscus is not only limited by the meniscus biology but also by aging biology [12], a non-biodegradable prosthesis could be used as an artificial meniscus substitute after total meniscectomy. To date, three implants have been approved for human use: Actifit® (polyurethane implant), CMI® (collagen meniscus implant), and NUsurface® (polycarbonate urethane (PCU) implant) [261]. The first two are biodegradable scaffolds specially designed for partial meniscectomy aiming for meniscus repair [252,262–264]. However, NUsurface® is a non-biodegradable prosthesis designed for meniscus replacement after total meniscectomy that has the potential to address

the treatment gap of those suffering from persistent knee pain who are too old for meniscus repair and too young for total knee arthroplasty [265]. For those patients who have undergone total meniscectomy, and have incorporated the NUsurface® prosthesis, the use of anti-inflammatory drugs will be necessary for the management of the post-surgical and long-term inflammation, providing symptomatic relief and ensuring the integration of the prosthesis into the surrounding native tissues in the knee cavity managing the foreign body reaction (FBR) [13,14]. The NUSurface® implant (Active Implants, Israel), which is approved for use in some European countries and Israel, and ongoing FDA clinical trials, has been the focus of this work [266].

Polymer coatings are crucial for enhancing the biocompatibility, performance, tissue integration, and longevity of medical implants, as well as for decreasing the probability of adverse reactions, wear, and infections. Biocompatible polymeric coatings can be used to establish a barrier between the surface of the implant material and the surrounding tissues. In addition, they can be used to harbor different types of drugs, even providing controlled drug release. Both, natural polymers (polynucleotides [160–162], polysaccharides [163–165], and polypeptides [166,167]) and synthetic biodegradable polymers [168,169] have been used to enhance biocompatibility, either due to their inherent properties or through the release of specific molecules. Polymer coatings, designed to release drugs and other therapeutic agents in a controlled manner, play a crucial role in enhancing the biocompatibility of medical implants.. The site-specific release of these molecules minimizes side effects and shields them from enzymatic breakdown in the body. Furthermore, certain polymeric coatings can regulate the release of molecules directly from the implant's surface, offering an alternative to drug release from matrices [195]. The selection of polymeric materials and coating characteristics for medical implants is driven by the type of implant, its intended use, and the specific medical requirements. The success of drug-releasing implants depends on the right choice of polymer, drug formulation, and coating design. Factors such as the rate of drug release, treatment duration, and biocompatibility are crucial. This is especially significant for coatings designed to regulate inflammatory processes near the implant site through the release of anti-inflammatory drugs [267,268].

COX-2 inhibitors and corticosteroids are two classes of anti-inflammatory drugs used for pain management. COX-2 inhibitors, such as Celecoxib (CLX), are typically administered orally to alleviate pain and control chronic inflammation. However, long-term oral use can lead to side effects affecting the gastrointestinal, renal, cardiac, and hematological systems [15,16]. Unfortunately, topical administration is less effective in relieving pain compared to systemic administration [17]. CLX, in particular, has been noted for its superior ability to alleviate pain and enhance physical function in knee osteoarthritis (OA) patients compared to traditional NSAIDs [18,19]. It has also shown potential in mitigating and protecting against cartilage deterioration associated with OA [20,21], positioning it as a potential disease-modifying osteoarthritis drug (DMOAD) [22]. To maximize its effects on knee outcomes, especially for implant integration that requires long-term treatment, it is crucial to ensure extended residence time. On the other hand, corticosteroids, such as dexamethasone (DEX), control inflammation by directly acting on nuclear receptors, thereby interrupting the inflammatory cascade at various levels (Figure 1.1). This, results in their immunosuppressive and anti-inflammatory properties. Corticosteroids are generally administered via intra-articular (IA) injection, which, while causing fewer systemic side effects and allowing more direct medication deposition inside the joint, is often associated with pain, discomfort, potential cartilage damage, and risk of infections

[17]. DEX has been widely used in clinical settings via IA injection to treat OA patients with severe knee pain. Its role as a chondroprotective corticosteroid when administered IA in low doses has been discussed, and its potential consideration as a DMOAD has been suggested. Therefore, the development of a novel delivery system that allows *in situ* administration of CLX to prolong its retention time in the knee cavity and also enables the direct deposition of low DEX doses into the knee cavity while avoiding the limitations associated with IA injections could address the challenges posed by current therapies [20].

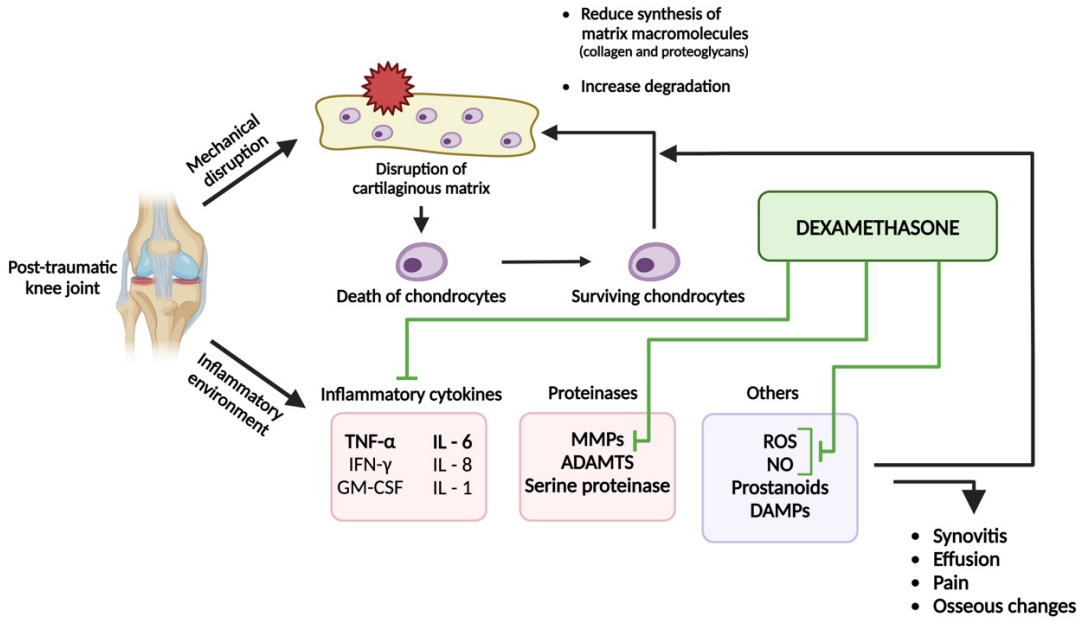

Figure 14.1. Schematic representation of the pathophysiological processes in a post-traumatic knee joint leading to osteoarthritis (OA) and effects of administration of Dexamethasone interrupting the inflammatory cascade at different levels.

Abbreviations: TNF: Tumor necrosis factor. IFN: Interferon. GM-CSF: Granulocyte-macrophage colony-stimulating factor. IL: Interleukin. MMP: Matrix metalloproteinase. ADAMTS: a disintegrin-like and metalloproteinase with thrombospondin motif. ROS: Reactive oxygen species. NO: Nitric Oxide. DAMP: Damage-associated molecular pattern. Created with https://www.biorender.com/

Within this context, the current challenge in the field of meniscus-related degenerative pathologies is to explore *in situ* therapies that involve sustained delivery of drugs to achieve a more direct and effective response, reduce systemic side effects, and avoid repeated administrations [269].

For this reason, our objective was to create a bilayer polymer coating over the polycarbonate urethane (PCU) implant prosthesis for the sustained release of anti-inflammatory drugs, aiming to replace the meniscus after complete meniscectomy. Here, using square-shaped implants (0.7 x 0.7 x 0.3 cm), we investigated optimal polymer options for the controlled release of DEX from an upper layer, aimed at managing excessive post-surgery inflammation with a targeted rapid release over 1 to 4 weeks. This approach seeks to enhance the efficacy of corticosteroids by reducing the rapid clearance typically associated with local administration and minimizing the pain and discomfort caused by repeated IA injections. Additionally, we screened various polymer combinations to facilitate the release of CLX from an underlying layer, focusing on pain management and long-term inflammation control, with a targeted sustained release over 6 to 9 months. The drug-releasing bilayer polymer coatings were quantitatively and microscopically evaluated to assess their biodegradability. To validate our

hypothesis regarding the anti-inflammatory effects of coating implants, we conducted *in vitro* studies to assess the toxicity, biocompatibility, activity, and efficiency of this technology using a relevant cellular model of human primary macrophages. Following this comprehensive screening, a bilayer polymer coating was selected for further optimization and adaptation to the specific morphology of the NUsurface® meniscus implant.

4.3 Materials and Methods

4.3.1 Materials

The drugs dexamethasone (DEX) and celecoxib (CLX) were supplied by Acofarma (Madrid, Spain) and Sigma-Aldrich (Missouri, USA), respectively. The polymers used Poly (lactic-co-glycolic acid) (PLGA), of two different lactic acid:glycolic acid (LA:GA) ratios (PLGA 50:50, and PLGA 85:15), poly(caprolactone) (PCL) of low (LMW-PCL) and high molecular weight (HMW-PCL), poly(L-lactide) (PLLA) of low (LMW-PLLA) and high molecular weight (HMW-PLLA), and poly(lactic acid)-poly(ethylene glycol) di-block copolymer (PLA-PEG) were purchased from Evonik Industries (Darmstadt, Germany). LMW-PLGA LA:GA ratio 50:50 was obtained from PolySciTech, a division of Akina (Indiana, USA). The polyethylene glycol (PEG) of low (PEG 400) and high molecular weight (PEG 1450) were purchased from BASF (Ludwigshafen am Rhein, Germany). Sodium azide (NaN_3) was purchased from Sigma-Aldrich (Missouri, USA). Acetone was obtained from Fisher chemicals (New Hampshire, USA). Dichloromethane (DCM and acetonitrile (ACN) were distributed by Scharlau (Barcelona, Spain). Phosphate saline buffer (PBS), Tween®80, trifluoracetic acid (TFA) and methanol (MeOH) were supplied by Scientific (Nottingham, England), Merck (Darmstadt, Germany), Sigma-Aldrich (Missouri, USA) and VWR Chemicals (Pennsylvania, USA), respectively. The square-shaped implants made of polycarbonate urethane (PCU) were kindly donated by Active Implants (Israel).

4.3.2 Drug solubility in release buffer

An excess of the drugs (DEX and CLX) was incubated in agitation (700 rpm) in 1 mL of PBS supplemented with concentrations of Tween®80 ranging from 0 to 1% (w/v) for 24 hours. Then, samples were centrifuged at 10,000 rpm for 20 minutes, the supernatant was diluted in MeOH:H_2O 65:35 (v/v), and the solutions were quantified by ultraperformance liquid chromatography (UPLC) with a TUV detector at 239 nm with a column Kinetex® 1.7 µm C18 100 Å, LC Column 50 x 2.1 mm acquired from Phenomenex (Torrance, CA, USA), maintaining the samples at 20 °C in a Waters Acquity H-Class UPLC system (Waters, Milford, USA).

4.3.3 Production of drug-releasing polymer films

To prepare the polymer-drug solutions, appropriate amounts of each drug, DEX or CLX, were dissolved in acetone and DCM, respectively [270–272]. In DEX-releasing polymers, PLGA (PLGA 50:50; intrinsic viscosity (IV) = 0.32-0.44 dL/g and PLGA 85:15; IV = 1.3-1.7 dL/g), LMW-PLGA (PLGA 50:50; MW = 8 kDa), and PLA-PEG (MW = 5.3 kDa) were dissolved to their final concentrations using acetone solutions of DEX of determined

concentrations. Polymer mixtures incorporating PEG required the addition of HMW-PEG or LMW-PEG to the core polymer at determined (v/v) ratios. Regarding CLX-loaded polymers, the polymers PCL, with intrinsic viscosities of 0.39 dL/g (~32 KDa; "LMW-PCL") and 0.9 dL/g (~73 KDa; "HMW-PCL") and PLLA, with IV of 1.0 dL/g (~74 KDa; "LMW-PLLA") and 2.9 dL/g (~210 KDa; "HMW-PLLA") as well as combinations of LMW-PCL (IV=0.39 dL/g ~32 kDa) and HMW-PLLA (IV=2.9 dL/g ~210 kDa) were dissolved to their final concentrations usingDCM solutions of CLX of determined concentrations. The polymers used were selected based on their hydrophobicity and degradation rates. All these procedures were carried out under ambient conditions.

These films were prepared by solvent casting. Seventy µL of polymer-drug solutions were then cast on square-shaped meniscus implants (made of PCU) of 0.7 x 0.7 x 0.3 cm. The organic solvent was allowed to evaporate for 1 hour at room temperature. The resulting drug-loaded polymer films were then vacuum-dried for at least 24 hours.

4.3.4 Production of bilayer drug-releasing polymer coatings

To prepare the polymer-drug solutions, appropriate amounts of each drug, DEX or CLX, were dissolved in acetone and DCM, respectively [270–272]. Polymers, LMW-PLGA (PLGA 50:50; MW = 6.9 kDa), and PLA-PEG (MW = 5.3 kDa) were dissolved at a concentration of 200 mg/mL in combination with a solution of DEX of 5 mg/mL. Regarding CLX-releasing polymers, pure HMW-PLLA combinations of PCL (IV=0.39 dL/g; MW ~32 kDa) and PLLA (IV=2.9 dL/g; MW ~210 kDa) were dissolved to their final concentrations using a solution of CLX of 30 mg/mL.

The square-shaped PCU implants (0.7 x 0.7 x 0.3 cm), held in place by a needle, were immersed in the polymer-CLX solution and immediately withdrawn, allowing 10 min for drying. The cycle was repeated a total of 3 times. After an additional 3 hours of drying, 5 new immersion cycles were performed, in this case in the polymer-DEX solution and with a drying time of 15 minutes between cycles. Finally, the organic solvent was allowed to evaporate for 72 hours.

4.3.5 Drug release evaluation

Drug release studies were performed in agitation (450 rpm) at 37 °C in PBS Tween®80 1% (w/v) to ensure sink conditions. The amount of drug (DEX and CLX) released was quantified by reverse phase ultra-performance liquid chromatography (UPLC) with a TUV detector at 239 nm using a column Kinetex® 1.7 µm C18 100 Å, LC Column 50 x 2.1 mm acquired from Phenomenex (Torrance, CA, USA), maintaining the samples at 20 °C in a Waters Acquity H-Class UPLC system (Waters, Milford, USA) [273]. The mobile phase consisted of A: deionized H_2O acidified with TFA 0.1% (v/v) and B: ACN acidified with TFA 0.1% (v/v) pumped with a flow rate of 0.1 mL/min. The injection volume was 5 µL, and the column oven temperature was set to 40°C. To control the UPLC/UV system as well as for data acquisition and processing, EMPOWER software was used. To quantify the amount of DEX and CLX, a calibration curve, ranging from 1 to 100 ppm was used. The curves had a correlation coefficient (R^2) of 1 for DEX, and 0.9999 for CLX (n=22). The validation procedure was carried out according to the ICH guidelines [274,275] . Limit of detection (LOD) and quantification (LOQ) were calculated directly from the calibration plots,as 3.3σ/S and 10σ/S, respectively, where σ

is the standard deviation of intercept and S is the slope of the calibration plot [276]. The values were LOD = 1.73, and LOQ = 5.25 for DEX, and LOD = 0.3, and LOQ = 0.92 for CLX.

4.3.6 Drug loading assay

PCU prostheses coated with drug-releasing polymers were immersed in 5 mL of a mixture of DCM/acetone 3/2 (v/v) for up to 24 hours to ensure polymer solution. Samples of 200 µL were then transferred to microtubes containing 800 µL methanol and centrifuged at 10,000 rpm for 20 min. 200 µL of supernatant were further diluted with 800 µL MeOH:H_2O 65:35 (v/v) and the concentration of drug was quantified by UPLC with a TUV detector at 239 nm using a column Kinetex® 1.7 µm C18 100 Å, LC Column 50 x 2.1 mm acquired from Phenomenex (Torrance, CA, USA), maintaining the samples at 20 °C in a Waters Acquity H-Class UPLC system (Waters, Milford, USA) [273]. The mobile phase consisted of A: deionized H_2O acidified with TFA 0.1% (v/v) and B: ACN acidified with TFA 0.1% (v/v) pumped with a flow rate of 0.1 mL/min. The gradient was from 25% to 60% of B in 6.5 min, and 6 min from 60% to 25% of B. The injection volume was 5 µL, and the column oven temperature was set to 40°C. To control the UPLC/UV system as well as for data acquisition and processing, EMPOWER software was used. To quantify the amount of DEX and CLX, a calibration curve, ranging from 1 to 100 ppm was used. The release buffer had no matrix effect on the quantification of the drugs. The curves had a correlation coefficient (R^2) of 1 for DEX, and 1 for CLX (n=8). The values were LOD = 0.383, and LOQ = 1.162 for DEX, and LOD = 0.187, and LOQ = 0.567 for CLX.

4.3.7 Characterization of the drug-releasing polymer films

4.3.7.1 Differential Scanning Calorimetry (DSC)

DSC measurements for polymers, drugs, and combinations of polymer and drug were recorded with a DSC Q1000 V9.9 (TA Instruments, New Castle, DE, USA) in standard aluminum sample pans. The samples were heated from 20°C to 400°C, depending on the sample analyzed, with a heating rate of 10°C/min in a nitrogen atmosphere. Data recording and processing of the first heating cycles were carried out with the software Advantage (TA Instruments, New Castle, DE, USA).

4.3.7.2 Powder X-ray diffraction (XRD)

Diffraction measurements of crystalline powder were carried out by an Empyrean diffractometer of the PANAlytical brand. The X-rays were obtained from a sealed tube with Cu anode (λ(Kα1) = 1.5406 Å) and were collimated prior to incidence on the sample with optics including a W/Si bilayer mirror. The radiation emitted by the sample was collected with a "PIXcel3D" type solid state detector. The samples were mounted at ambient on a flat base without signal (Si single crystal), to avoid the amorphous component different from that coming from the sample. Diffractograms were taken in an angular range of 2 to 40° with a step of 0.04 and a time per step of 8s. To perform the mathematical adjustments of the obtained diffractograms, the program HighScore Plus: Version 3.0d was used.

4.3.8 Degradation of bilayer drug-releasing polymer coatings

Drug-releasing polymer coated PCU implants were immersed in a volume of 10 mL of PBS (pH 7.4) supplemented with 1% (w/v) Tween®80. At defined time points, the coated squared-shaped PCU implants were removed from the release buffer for further analysis:

4.3.8.1 Field-emission scanning electron microscopy (FESEM)

Drug-releasing polymer coatings were sputter coated with a layer of iridium and imaged in a Zeiss UltraPlus analytical FESEM with a beam voltage of 3 kV and a magnification ranging from 500 to 10,000X for the analysis of the surface of the coatings. Also, Zeiss EVO analytical FESEM with a beam voltage of 20 kV and magnification ranging from 60X to 5,000X was used for the measure of the coating thickness and analyzing side profile upon degradation after sagittal cut.

4.3.8.2 pH measurements

pH was measured in the media where the polymer coated PCU implants were incubated over specific periods using a pH meter calibrated using standard buffer solutions of known pH values ranging from pH 2.0 to 10.0.

4.3.9 *In vitro* assessment of sterile conditions, biocompatibility, activity, and efficiency of the bilayer drug-releasing polymer-coated PCU implants

4.3.9.1 Drug release evaluation

Drug release studies to evaluate released drug activity *in vitro* were performed at 37 °C in PBS Tween®80 0.05% (w/v) supplemented with penicillin/streptomycin 1% (v/v). The amount of drug (DEX and CLX) released was quantified by UPLC using the same method as described in section *Drug loading assays (Section 1.4.6)*. The release buffer collected and quantified at each time point was subsequently lyophilized. Afterward, the powder was resuspended in sterilized miliQ water and evaluated *in vitro*.

4.3.9.2 *In vitro* control of endotoxin contamination

The chromogenic LAL-test (LO50650U, Lonza) was used, following the manufacturer's indications. Stored release buffers were diluted appropriately to achieve a concentration of DEX and CLX as close as possible to their demonstrated active concentration (10 μM for DEX and 25 μM for CLX) (Table 1.1). It is worth noting that regardless of the concentration of drugs quantified in the media after their release, a minimum dilution of 1:10 was implemented because of the toxic effects of Tween®80 0.05% (w/v) in cells above such dilution.

4.3.9.3 Monocyte isolation, differentiation, and treatment of human primary macrophages

Monocytes were isolated from the whole blood of six healthy donors (buffy coats) following the Ficoll and Percoll separation method, as previously described [277], and subsequently counted with Trypan Blue staining 0.04% using a counting chamber (Kova international, BVS100H). In order to obtain human monocyte-derived macrophages (HMDMs), monocytes were resuspended in RPMI supplemented with penicillin/streptomycin and glutamine, subsequently counted, and $1*10^6$ cells were plated in each well of 24-well plates to allow their attachment to the plate. After 30 minutes of incubation at 37°C, media was removed, and a new media containing human recombinant M-colony stimulating factor (hrM-CSF, Peptrotech, 300-25) supplemented with fetal bovine serum (FBS), penicillin/streptomycin and glutamine was added for differentiation towards macrophages after 5 days.

At day 5, macrophages were treated with appropriately diluted release buffers. Samples were added together with complete media for 24 hours. 1 hour later, LPS + IFNγ (100 ng/ml and 50 ng/ml, respectively) were added. Non-treated HMDMs were used as the negative control, while HMDMs treated only with LPS + IFNγ were used as the positive control. All other samples were treated with free drugs (DEX, CLX, and DEX+CLX) at appropriate concentrations (10 μM for DEX and 25 μM for CLX) for comparison with equivalent concentrations of the drugs in released buffer from Prototype PLA-PEG or Prototype PLGA drug-releasing bilayer polymer coatings at determined times.

4.3.9.4 Evaluation of biocompatibility and toxicity

To assess the biocompatibility and non-toxic profile of the drug-loaded polymer coatings toward primary human macrophages, an AlamarBlue™ cell viability assay was performed. After exposure of macrophages to conditions described in Table 1.1 for 24 hours (relative day 6), which corresponds to the release buffer containing the drugs and products of polymer degradation at different time points, supernatants were collected for cytokine quantification, while 1 ml of AlamarBlue™ HS Cell Viability Reagent 10% (Invitrogen, A50101) was added to the remaining cells in the bottom of each well of the 24-well plates, following the manufacturer's protocol. Plates were incubated for 3 hours at 37°C, protected from light. 100 μl from each well, in triplicate, were transferred to black 96-well plates, and fluorescence was measured at 560-590 nm using the Synergy H4 Microplate reader (BioTek).

Non-treated cells were used as controls and considered as 100% cell viability. Cell viability was calculated according to the equation: % Cell viability = (Sample Fluorescence / Control Fluorescence) × 100.

4.3.9.5 Assessment of anti-inflammatory activity and efficacy by measurement of cytokine secretion

After checking the absence of LPS contamination and non-toxic activity of the release buffer containing DEX and CLX at indicated time points, the anti-inflammatory activity of the drugs in the release buffer was compared with the free drugs at equivalent concentrations by ELISA assay. The anti-inflammatory activity was evaluated by quantifying the secretion of relevant inflammatory signals (TNF-α, CCL2, and PGE2) from primary human macrophages

treated with stimulated with LPS + IFNγ alone, in combination with free drugs or exposed to the release buffer for 24 hours.

ELISA assays were performed using the commercial kit DuoSet® ELISA Development Systems (Bio-Techne) for TNF-α (DY210) and the Prostaglandin E2 ELISA kit (Cayman) for PGE2 (004CA514010-96), following the manufacturer's instructions. ELISA assays for CCL2 were performed using a custom kit developed in the HUNIMED lab [277].

The amount of cytokine secretion (ng/ml) in macrophages treated with LPS + IFNγ (positive control) was normalized to 100%, and subsequently, values for the remaining samples were normalized and expressed as percentage (%) of control, according to the equation: % of Control = (ng/ml of Sample / ng/ml of Control) × 100.

Table 3.1. Concentrations of DEX and CLX released from Prototype PLA-PEG and Prototype PLGA bilayer polymer coatings at each timepoint and dilutions implemented for the *in vitro* validation of their sterility and anti-inflammatory activity and efficacy.

		CLX		DEX		
Prototype	Time point	ppm	μM	ppm	μM	Dilution
Prototype PLA-PEG	3 hours	27.27	71.50	193.63	493.38	1:50
	3 days	118.75	311.38	97.58	248.65	1:20
	1 week	58.13	152.44	22.95	58.49	1:10
	2 weeks	130.69	342.70	17.41	44.36	1:10
	4 weeks	134.31	352.17	1.81	4.60	1:15
Prototype PLGA	3 hours	7.14	18.74	16.40	41.80	1:10
	3 days	40.81	107.00	45.82	116.74	1:10
	1 week	60.53	158.73	48.45	123.46	1:10
	2 weeks	108.59	284.74	25.69	63.46	1:10
	4 weeks	115.87	303.84	10.49	26.75	1:12

Abbreviations: CLX: Celecoxib. DEX: Dexamethasone. PLA-PEG: poly(lactic acid)-poly(ethylene glycol) di-block copolymer. PLGA: Poly(lactic-co-glycolic) acid. ppm: parts per million (μg/mL). μM: Micromolar. Values represent the mean ± standard deviation (n=3).

4.4 RESULTS AND DISCUSSION

The aim of this chapter is to engineer a biodegradable bilayer polymer coating around a PCU meniscus prosthesis with the capacity to control the release of two anti-inflammatory drugs. More precisely, dexamethasone (DEX) is intended to be released for 1-4 weeks to alleviate the inflammation caused mainly by the surgery. Meanwhile, celecoxib (CLX) is intended to be released for 6-9 months to relieve the inflammation related to the prosthesis. Both drugs are intended to mediate the incorporation of the implant into the knee cavity, reducing adverse inflammatory reactions. After the synthesis of the bilayer coating, we aim to evaluate the effect and activity of both drugs *in vitro* and test the behavior of the prototypes in a bioreactor, simulating the knee environment.

To achieve this, we followed a specific work plan consisting of:

1) The screening of different biodegradable and biocompatible polymers for the independent release of DEX and CLX within the desired periods of time.
2) The development of drug-releasing bilayer polymer coatings results from the combination of the most promising prototypes selected for the independent release of the drugs. This development consisted of evaluating the capacity of the bilayer systems to release CLX and DEX in a required time frame, characterization of their physicochemical properties, and *in vitro* study of their degradation.
3) The *in vitro* evaluation of the sterility and biocompatibility of the drugs and polymer degradation products of the bilayer coated system and the anti-inflammatory activity of these drugs upon release was conducted using a relevant cell model (human primary macrophages).

4.4.1 Solubility of CLX and DEX in different release buffers. Definition of sink conditions.

In this study, PBS was supplemented with different concentrations of Tween®80 [278]. As shown in Table 1.2, increasing concentrations of Tween®80 resulted in increasing solubility of both drugs, making this effect especially remarkable for CLX solubility. Thus, as the drugs were intended to be in the release buffer for extended periods of time, and the amount of drug released from the polymer coatings was unknown, it was decided to use PBS supplemented with Tween®80 1% (w/v) for the drug release studies.

Table 1.4. Solubility of drugs CLX and DEX (ppm and μM) in PBS supplemented with different concentrations of Tween®80.

	CLX		DEX	
PBS Tween®80 (w/v)	ppm	μM	ppm	μM
1%	396.27 ± 19.37	1039.05 ± 41.47	196.75 ± 18.02	501.33 ± 37.49
0.5%	198.06 ± 11.39	519.34 ± 24.39	124.94 ± 12.14	318.35 ± 25.27
0.25%	98.08 ± 13.27	257.16 ± 28.42	89.90 ± 0.93	229.07 ± 1.94
0.1%	43.37 ± 15.19	113.73 ± 32.53	73.91 ± 4.14	188.33 ± 8.61
0.05%	26.17 ± 2.53	68.62 ± 5.41	68.39 ± 2.13	174.26 ± 4.44
0%	1.69 ± 0.71	4.44 ± 1.43	62.36 ± 2.18	158.89 ± 4.54

Abbreviations: CLX: Celecoxib. DEX: Dexamethasone. PBS: Phosphate buffered saline. ppm: parts per million (μg/mL). μM: Micromolar. Values represent the mean ± standard deviation (n=3).

4.4.2 Selection of the polymers for the independent release of CLX and DEX from polymer films

Polyesters were the polymers of choice to engineer the bilayer coating loaded with anti-inflammatory drugs. These polymers were selected because of their hydrophobicity, also considering the hydrophobic nature of the anti-inflammatory drugs, biocompatibility, biodegradability, tunable release profile, and favorable regulatory profile. The first goal of this section was to evaluate the influence of the polymer on the drug release and why other parameters, such as the preparation method, were kept constant. Despite the primary objective of these polymer films being to achieve the release of two different anti-inflammatory drugs

from the same meniscus prosthesis with different release kinetics, for simplicity of the first screening, the release of each drug from a polymeric matrix was first evaluated independently.

4.4.2.1 Evaluation and characterization of polymer films for CLX release

CLX was intended to be delivered following a long-term release profile (6 to 9 months)to aid in the modulation of chronic inflammation. Poly(caprolactone) (PCL) and poly(L-lactide) (PLLA) were chosen due to their slow degradation rate [279,280]. Moreover, looking for more precise modulation of the release kinetics and knowing the influence of the polymer MW on their degradation [281–285], an HMW and an LMW polymer were investigated. Thus, using these four polymers, CLX-loaded films were created by dissolving each polymer and CLX in a suitable solvent and then depositing the solution over a square-shaped PCU implant via solvent casting. After film curation, the film and the implant were immersed in PBS supplemented with Tween®80 1% (w/v), and the drug release was measured by UPLC (Figure 1.2). The drug release was halted when a plateau release phase was observed.

The release studies demonstrated that CLX was consistently released more rapidly from PCL films, irrespective of the MW or drug loading (DL). In contrast, PLLA films exhibited distinct release kinetics: higher CLX loading resulted in faster release rates, while HMW-PLLA showed a more sustained release compared to LMW-PLLA. This aligns with previous findings where higher MW polymers were associated with prolonged drug release [283].

Regarding MW, the differences in release kinetics can be explained by the structural effects of polymer chain length. As none of these polymers is expected to degrade within a few weeks, the release cannot be only controlled by degradation but also by other mechanisms such as diffusion [286]. Longer chains in HMW polymers create a denser matrix, restricting water penetration and making drug diffusion more challenging. Additionally, the slower degradation of HMW polymers further delays release. These effects are more pronounced in PLLA films due to the substantial MW difference between HMW-PLLA and LMW-PLLA (~140 kDa) compared to the smaller MW difference in PCL (~41 kDa). Consequently, PCL films exhibit more uniform release kinetics regardless of MW, while PLLA films demonstrate MW-dependent release behavior.

When the DL was increased from 5% to 20%, differences in CLX release kinetics from PLLA matrices were observed (Figures 1.2A and 1.2B). This is because higher DL results in a greater number of drug nuclei, both molecular and crystalline, being distributed within the polymer matrix. Upon water penetration, these drug nuclei become more readily accessible, facilitating a faster and more consistent dissolution process, which accelerates drug release. The plateau observed in the release profile can be explained by the interplay between drug diffusion and polymer degradation. During the initial weeks to months, the release is primarily driven by diffusion through water-filled pores, with dispersed drug contributing most significantly to the release process. However, a large percentage of the drug remains entrapped within the polymer matrix, inaccessible to the release medium. This entrapped drug cannot be released until polymer degradation occurs, which is a much slower process. Consequently, incomplete release of the drug is observed, as degradation does not progress significantly within the study timeframe. Thus, the release kinetics of PLLA reflect both the diffusion-driven release of dispersed drug and the delayed availability of drug trapped within the intact polymer matrix [287].

Although the release from HMW-PLLA 20% DL appeared to fit the desired release timeframe of approximately 6 to 9 months, it entered a plateau phase after 20 weeks, with less than 30% of total CLX released from the film (Figure 1.2B). Thus, HMW-PLLA showed a sustained but incomplete drug release profile, which was explained by an incomplete degradation of the polymer. This incomplete degradation might pose challenges in the long term, such as drug recrystallization [288]. Despite these limitations, HMW-PLLA 20% DL was preferable to 5% DL due to its higher drug loading. LMW-PLLA, regardless of DL, was unsuitable because its faster release kinetics resulted in a plateau phase within just 5 weeks—far earlier than desired. These findings highlight the need to balance sustained release with complete drug availability. Moving forward, an intermediate release profile was targeted to achieve full CLX release within the 6–9-month window.

A.

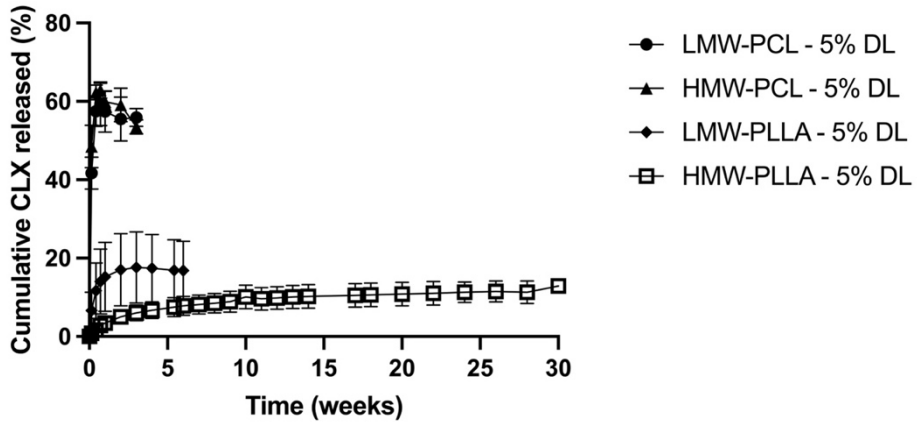

B.

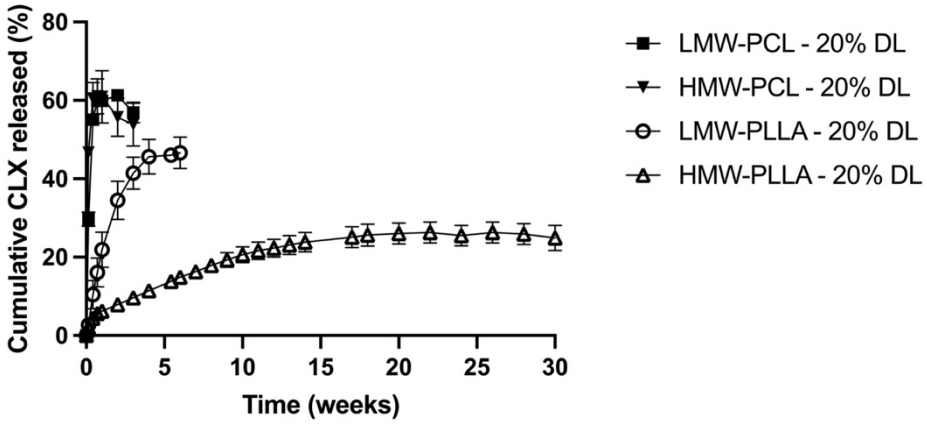

Figure 1.15. Release kinetics of CLX expressed as the total percentage of drug released (%) from polymer films composed of polymers PCL and PLLA, both HMW and LMW, at a concentration of 50 mg/mL, with CLX loadings of 5% (A) and 20% (B).

Abbreviations: CLX: Celecoxib. LMW: Low molecular weight. HMW: High molecular weight. DL: Drug loading. PLLA: poly(L-lactide) (PLLA). PCL: poly(caprolactone). Values represent the mean ± standard deviation (n=3).

As HMW-PLLA exhibited the most sustained release kinetics among PLLA formulations, and PCL release kinetics were independent of MW, all subsequent references to PLLA will denote HMW-PLLA, while PCL will denote LMW-PCL.

To achieve an intermediate release profile between LMW-PLLA 20% DL and HMW-PLLA 20% DL, Acetyl Tributyl Citrate (ATBC), a well-characterized plasticizer compatible with PLA [289–292], was incorporated into the HMW-PLLA matrix at varying concentrations to modify the release rate of CLX. The addition of a plasticizer like ATBC affects the polymer matrix by reducing intermolecular forces between polymer chains. This enhances water penetration, leading to faster drug diffusion and potentially accelerating drug release by lowering the polymer's glass transition temperature (Tg). Consequently, this allows for more precise control over the drug release profile.

It was observed that increasing ATBC concentration accelerated CLX release, with PLLA 20% DL - 20% ATBC exhibiting a release profile similar to LMW-PLLA 20% DL (Figure 1.2 and Figure 1.3), reaching a plateau at around week 6. However, despite this acceleration, the use of ATBC presented challenges, such as the occurrence of a plateau phase. Therefore, although the release kinetics approached the target release, further optimization was deemed necessary, and ATBC was not selected for continued use.

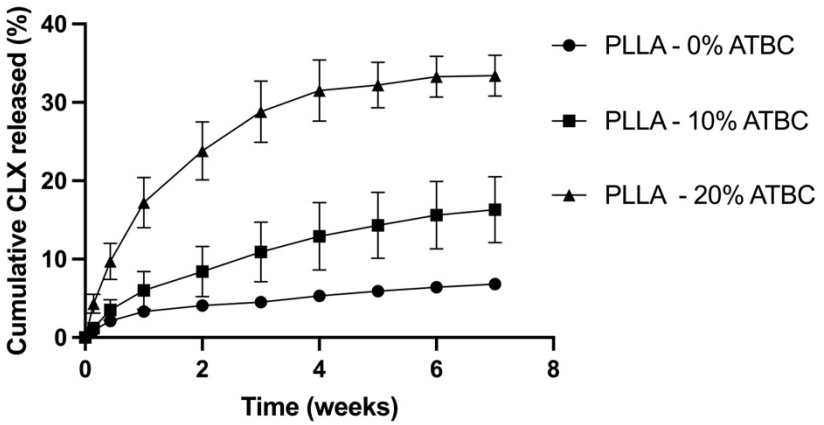

Figure 1.16. Release kinetics of CLX expressed as the total percentage of drug released (%) from polymer films composed of PLLA with added ATBC at a concentration of 50 mg/mL, with a CLX loading of 20%.

Abbreviations: CLX: Celecoxib. PLLA: poly(L-lactide). ATBC: Acetyl tributyl citrate. Values represent the mean ± standard deviation (n=3).

Based on previous observations where PLLA provided a very sustained release of CLX and PCL facilitated a faster release, polymer blends of PLLA and PCL were formulated to achieve intermediate CLX release kinetics between PLLA and PCL (Figure 1.4). These blends had already been described in the literature for their applications as implantable biomaterials [293,294]. The different ratios of the blends demonstrated that increasing PCL content accelerated CLX release. According to Can [23], an increased quantity of PCL in the blend leads to larger PCL domains. The incorporation of PCL domains into the PLLA potentially creates polymer-to-polymer interfaces that facilitate water access. As a result, there is an enhancement in the overall degradation rate, accompanied by an increased release of CLX through the diffusion of the drug near this interface [295].

Additionally, PCL has been shown to induce nucleation of PLLA at polymer interfaces, promoting the formation of crystalline domains in the semi-crystalline PLLA. This effect is driven by the limited miscibility of PLLA and PCL, which leads to the aggregation of PCL domains and a localized depression of Tg at the interfaces. These conditions enhance chain

mobility, facilitating nucleation and improving PLLA's mechanical properties, such as flexibility and toughness [24].

Specifically, the polymer blends with PLLA/PCL ratios of 70/80 (w/w) and 80/70 (w/w) showed promising results, releasing 40% of the loaded CLX after 3 months without reaching a plateau (Figure 1.4). This approach successfully addressed the initial objectives of accelerating CLX release to meet the 6-9 months target and avoiding the plateau phase observed in LMW-PLLA and PLLA with supplemented ATBC.

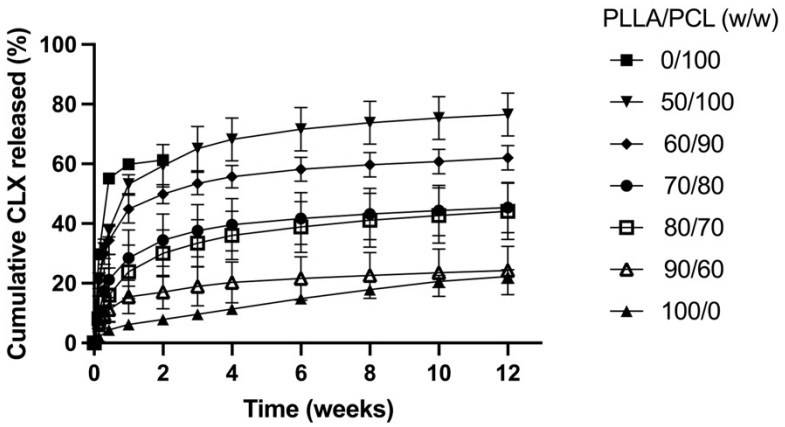

Figure 1.17. Release kinetics of CLX expressed as the total percentage of drug released (%) from PLLA/PCL blends prepared at 150 mg/mL at different (w/w) ratios (ranging from 0/100 to 100/0) with a CLX loading of 7.7%.

Abbreviations: CLX: Celecoxib. PLLA: poly(L-lactide). PCL: poly(caprolactone). (w/w): weight-to-weight ratio. Values represent the mean ± standard deviation (n=3).

Previous studies had explored the intraarticular (IA) administration of CLX, but there has been no consensus on dosing across different prototypes and animal models. Doses tested include 1-1.25 mg CLX/kg in mice [296], 0.46 mg CLX/kg/week over 5 weeks in rabbits [297], 0.0292 mg CLX/kg [298] or 1 mg/kg [299] in rats, and approximately 1 mg/kg in sheep [300]. Thus, highlighting the challenge in establishing a standardized dosing regimen for CLX in IA applications across different species and experimental conditions.

Building on previous findings, it can be assumed that higher doses of CLX could enhance therapeutic effects in both *in vitro* and *in vivo* models (e.g., reduced fibrous encapsulation, foreign body reactions, and modulation of signaling pathways). Thus, the concentration of CLX incorporated into the polymer blends was increased by 2.4 times, from 12.5 mg/mL to 30 mg/mL, raising the drug loading from 7.7% to 16.6%. Subsequent observations confirmed that CLX was released more rapidly with increasing amounts of PCL in the matrix, consistent with trends seen in prototypes with lower CLX loading. Among the different polymer-to-polymer ratios explored, the PLLA/PCL blend at an 80/70 (w/w) ratio was selected for its intermediate release kinetics (Figure 1.5).

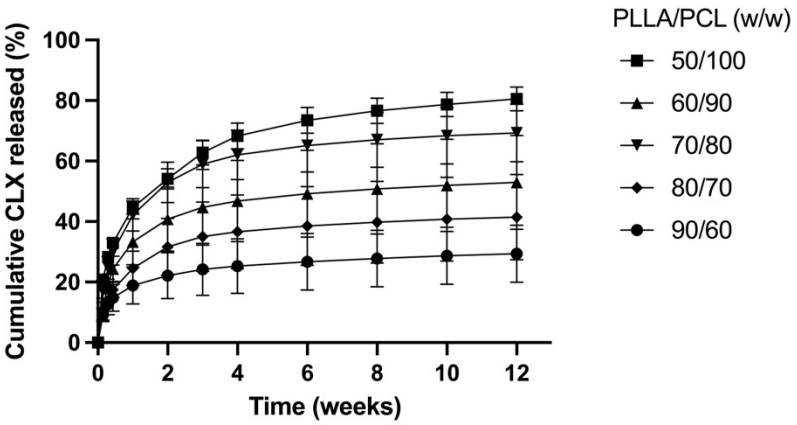

Figure 1.18. Release kinetics of CLX expressed as the total percentage of drug released (%) from PLLA/PCL blends prepared at 150 mg/mL at different (w/w) ratios (ranging from 50/100 to 90/60) with a CLX loading of 16.6%.

Abbreviations: CLX: Celecoxib. PLLA: poly(L-lactide). PCL: poly(caprolactone). (w/w): weight-to-weight ratio. Values represent the mean ± standard deviation (n=3).

Table 1.5. Tg, Tcc, Tm, and Xc values of the CLX-releasing prototypes analyzed by DSC and XRD.

Sample	Tg (ºC)	Tcc (ºC)	Tm (ºC)	Xc (%)
CLX	-	-	161	-
PLLA	64	98	179	5.07
PLLA - CLX	59	111	174	2.85
PCL	Not shown*	-	61	14.14
PCL - CLX	Not shown*	-	58	16.21
PLLA/PCL	62	98	180	14.87
PLLA/PCL - CLX	58	98	175	7.10

Abbreviations: CLX: Celecoxib. PLLA: poly(L-lactide). PCL: poly(caprolactone). Tg: Glass transition temperature. Tcc: Cold crystallization temperature. Tm: Melting temperature. Xc: Crystallinity.
*Value not observed in Figure 1.6A, obtained from [301].

Differential Scanning Calorimetry (DSC) characterization of drug-polymer solid dispersions is a recognized method for determining the apparent solubility and miscibility of components [302]. This technique provides insights into the thermal behavior of drug-polymer mixtures, including phase transitions like melting, crystallization, and glass transition temperatures. By analyzing these transitions, DSC can reveal the drug dispersion within the polymeric matrix and identify specific interactions between the drug and polymer [303]. DSC allows for the precise assessment of drug distribution within the polymer matrix. A homogeneous distribution typically indicates good miscibility and solubility, whereas the presence of multiple phases or distinct thermal events may suggest phase separation or poor miscibility.

Furthermore, DSC can detect subtle thermal events that indicate specific interactions between the drug and polymer molecules, such as hydrogen bonding or van der Waals forces. These interactions can affect the stability and release profile of the drug within the polymeric matrix [304,305]. Overall, DSC provides a detailed understanding of the physical state and compatibility of drug-polymer mixtures, aiding in the optimization of formulations for enhanced drug delivery and performance.

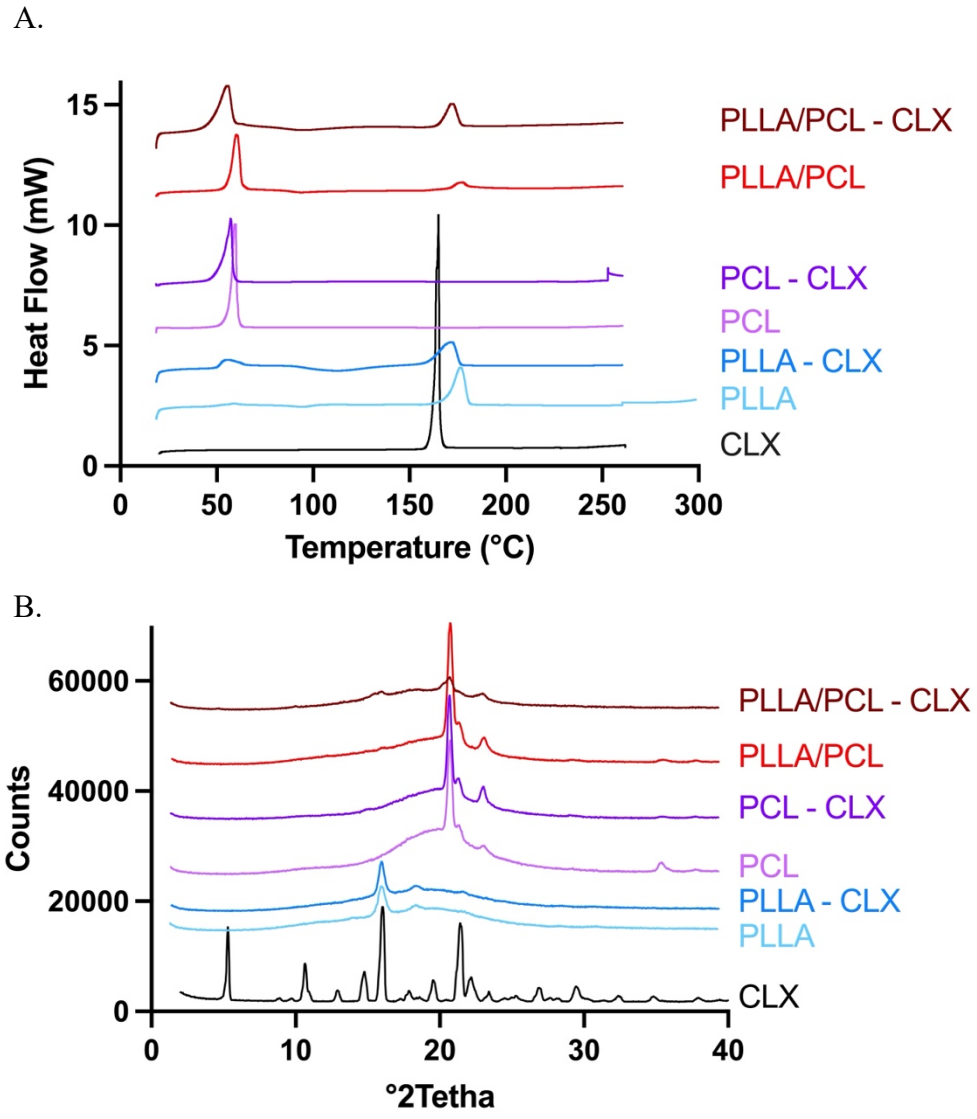

Figure 1.19. DSC thermograms (A) and XRD diffractograms (B) of the CLX-releasing prototypes.
Abbreviations: CLX: Celecoxib. PLLA: poly(L-lactide). PCL: poly(caprolactone). mW: milli Watts.

Thermogram Analysis of PLLA with loaded CLX

CLX interacts with PLLA chains, acting as a plasticizer by reducing intramolecular attraction and increasing polymer chain mobility [306–309]. This is evident in the thermograms, which show a reduction in Tg, cold crystallization temperature (Tcc), and melting temperature (Tm) values. The reduction in Tg can be attributed to the plasticizing effect of the CLX molecules, which enhance the mobility of the polymer chains [310]. These changes reflect enhanced chain mobility and interactions between CLX and PLLA [311]. Additionally, the lack of surface crystallites further supports that the release kinetics are controlled by molecular dispersion within the matrix. The plasticizing effect facilitates initial diffusion-driven release, but the high MW and dense PLLA structure limit water penetration, resulting in a sustained yet incomplete release profile because of slow PLLA degradation.

Thermogram Analysis of PCL with loaded CLX

The Tg of PCL, at -60°C, places its amorphous regions in a rubbery state at room temperature, while its semi-crystalline nature makes it rigid below the melting temperature (Tm) and liquid above it. After incorporating CLX, the PCL Tm (~58°C) becomes broader, shorter, and slightly shifts left, indicating interactions between CLX and PCL. The absence of CLX's Tm peak (~150°C) confirms its molecular dispersion in the PCL matrix, existing in an amorphous state [303] (Figure 1.6A, and Table 1.3). The consistently lower MW of PCL, with shorter polymer chains, facilitates drug-polymer interactions, explaining the molecular dispersion of CLX and its faster release from the PCL matrix compared to PLLA. MW is thus a key driver of the observed release kinetics (Figure 1.6A, and Table 1.3)

Thermogram Analysis of PLLA/PCL blend and PLLA/PCL blend with loaded CLX

DSC results revealed that, despite previous studies showing that these polymers are phase-separated when in a blend due to the separation during the evaporation of the solvent, coalescing in different domains, there is still interaction between them [23,312]. This is supported by the Tm of PCL and the Tm and Tg of PLLA in the blend. Thermograms showed an overlapping of these endothermic peaks, with slight variations in their original temperatures, indicating relatively good miscibility [313]. After CLX is incorporated into this blend, a reduction in the characteristic temperatures of the blend can be observed, indicating, once again, the interaction between the drug and the polymeric matrix (Figure 1.6A, and Table 1.3)

On the other hand, X-ray diffraction (XRD) is a common technique used for pharmaceutical and material analysis. This technique allows physicochemical characterization and structural features of materials and drugs, among other solid materials. Among the different XRD, powder XRD possesses the ability to produce a unique pattern regardless of the crystalline phase. This technique has been used for monitoring scaling-up, processing, manufacture, or formulation [314]. In this study, XRD has been selected as a complementary technique to DSC to determine how the drugs have been incorporated in the polymeric matrix and to look for explanations regarding the different release kinetics of the same drug from different polymeric matrices.

In the XRD analysis, pure CLX exhibited a crystalline diffraction pattern, while PCL and PLLA films without CLX showed a partially crystalline diffractogram. The PLLA/PCL films displayed characteristic peaks of both polymers [294,315,316]. Notably, when CLX was incorporated into the PLLA/PCL films, the absence of CLX's characteristic Bragg peaks suggested successful solubilization of the drug within the polymer matrix. This study further investigated the degree of crystallinity (Xc) to assess its impact on drug release. Since drug molecules are primarily located in the amorphous regions of a polymer, which are more permeable and accessible to water, it is generally assumed that polymers with lower crystallinity exhibit higher drug release rates [317,318]. However, our findings revealed that the Xc of the polymer-CLX combinations did not consistently align with the observed release kinetics. For instance, the PLLA matrix, despite having the lowest Xc, exhibited the slowest CLX release, while the PCL matrix, with the highest Xc, showed the fastest release (Table 1.3). These observations are in agreement with previous research, which indicated that the correlation between increased drug release rates and lower crystallinity is not consistently observed, with

some subclasses of samples showing an opposite trend [319,320]. These observations suggest that factors beyond crystallinity, such as crystallite size and porosity, may significantly influence drug release rates, as supported by previous studies [319] (Figure 1.6B).

In conclusion, the PLLA/PCL blend 80/70 (w/w) with 16.67% DL, along with pure PLLA with 20% DL, emerged as the most promising candidates for sustained CLX release over months (Figure 1.2B and 1.5). The PLLA formulation provided a very prolonged and low-rate release, with less than a quarter of the drug released after 6 months, while the PLLA/PCL blend achieved a faster release, with approximately 40% of the drug released after 3 months. These two formulations were, therefore, selected for further in-depth exploration. Moreover, using both thermograms and diffractograms, PLLA and PLLA/PCL blends were identified as suitable prototypes for CLX release due to their ability to incorporate CLX in a molecularly dispersed form, as evidenced by the absence of crystalline CLX peaks in XRD. Additionally, thermograms demonstrated interactions between CLX and the polymers, such as reductions in Tg, Tm, and Tcc, which indicate enhanced chain mobility and drug-polymer compatibility, crucial for sustained and diffusion-driven release.

4.4.2.2 Evaluation and characterization of polymer films for DEX release

To effectively address post-surgical acute inflammation, DEX was selected as the corticosteroid due to its potent anti-inflammatory properties and widespread clinical use. The objective was to achieve a rapid and consistent release of DEX over a 1 to 4-week period by incorporating it into a second polymeric layer. To achieve this goal we relied on polyesters again.

Firstly, PLGA was chosen for this purpose. PLGA-based systems typically exhibit a biphasic release profile, characterized by an initial burst release due to drug diffusion from the polymer film’s surface, followed by a sustained release phase driven by the polymer's autocatalytic hydrolysis into biodegradable monomers and oligomers [321,322]. The degradation rate of PLGA is significantly influenced by the ratio of lactic acid (LA) to glycolic acid (GA), with higher LA content resulting in slower degradation due to increased hydrophobicity and crystallinity, which reduce susceptibility to hydrolytic cleavage. GA enhances the polymer’s hydrophilicity and accelerates degradations, being the ratio LA:GA 50:50 the fastest degrading one [323].

First, the influence of LA:GA ratio was assessed. In Figure 1.7, two PLGA formulations with different LA to GA ratios were compared to determine the optimal candidate for DEX release. It was observed that DEX release was slow across all PLGA types, failing to meet the target release window of 1-4 weeks. However, PLGA 50:50 demonstrated an increase in DEX release after 4 weeks, resembling the typical biphasic release of PLGA, particularly in prototypes with lower drug loading. In contrast, PLGA 85:15 showed minimal DEX release throughout the study, regardless of drug loading. Thus, while PLGA 50:50 provided a better release profile for DEX, it was still not within the desired kinetics. Lower drug loading enhanced the release, but PLGA 85:15 was ultimately discarded due to its poor performance. Consequently, from now on, PLGA refers to PLGA 50:50.

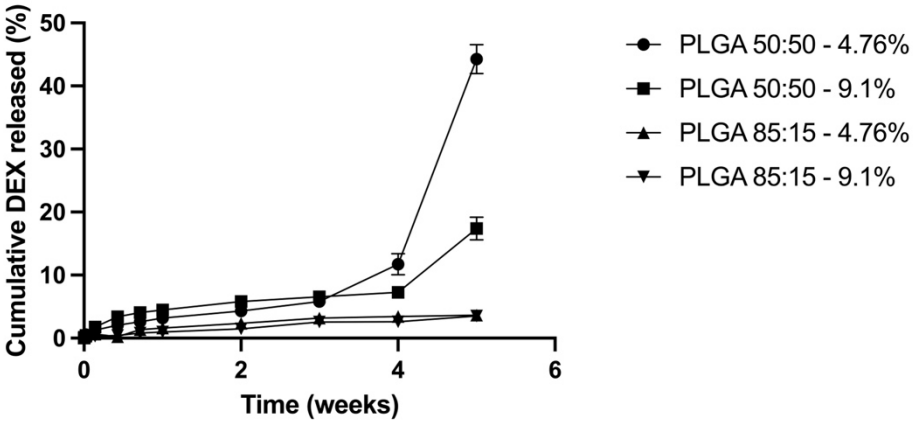

Figure 1.20. Release kinetics of DEX expressed as the total percentage of drug released (%) from PLGA films of different lactic acid to glycolic acid (LA:GA) ratios prepared at 100 mg/mL with DEX loadings of 4.76% and 9.1%.

Abbreviations: DEX: Dexamethasone. PLGA: Poly(lactic-co-glycolic) acid. Values represent the mean ± standard deviation (n=3).

It was determined that further testing of variables such as drug loading, polymer concentration, and polymer molecular weight (MW) was needed to optimize DEX release.

Drug loading was the first variable explored. To evaluate the potential impact of increased drug loading on DEX release kinetics, it was hypothesized that higher concentrations could influence the distribution and release behavior of DEX within the polymer matrix. Previous studies have shown that elevated drug loading can create a more extensive pore network during the release process, facilitating faster diffusion and modifying the physical properties of the polymer, such as swelling and erosion, which in turn can affect release kinetics [324,325].

In Figure 1.8, DEX exhibited a burst release within the first week of immersion in the release buffer, with the release profile fitting within the targeted 1-4 weeks timeframe. However, the release appeared not to be well-controlled, as only 40% of the total drug load was released by week 4, characteristic of the biphasic release pattern typical of PLGA matrices. This observation was consistent across the drug loadings tested. The observed release kinetics suggest that DEX may not have been fully dissolved in the polymer nor adequately interacting with it. As a result, DEX exposed on the surface of the polymer film was rapidly released upon contact with the release buffer, leading to an initial burst release followed by a slower, less controlled release phase. Similar to what has been previously described [326].

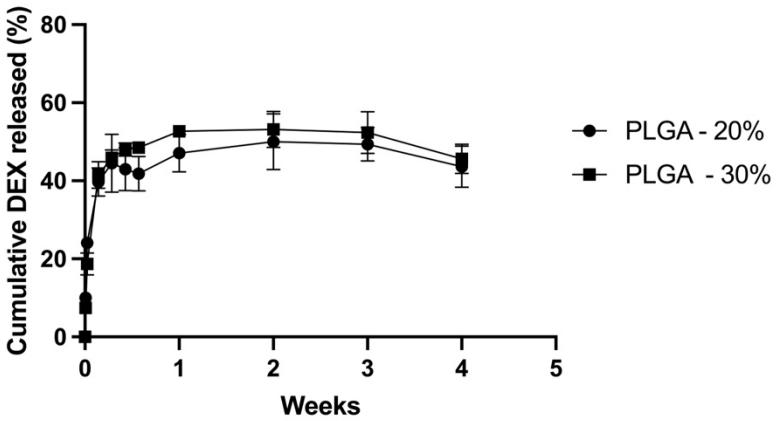

Figure 1.21. Release kinetics of DEX expressed as the total percentage of drug released (%) from PLGA prepared at 100 mg/mL with DEX loadings of 20% and 30%.

Abbreviations: DEX: Dexamethasone. PLGA: Poly(lactic-co-glycolic) acid. Values represent the mean ± standard deviation (n=3).

Then, to investigate the impact of the influence of PLGA concentration on DEX release kinetics, polymer concentrations ranging from 50 mg/mL to 90 mg/mL were evaluated while keeping the drug concentration constant at 5 mg/mL (Figure 1.9). It was observed that DEX was released more quickly from matrices with lower polymer concentrations. Although the release from PLGA at 50 mg/mL and 60 mg/mL was relatively rapid, it remained incomplete within the first two weeks, following an expected biphasic release pattern. Moreover, PLGA concentrations above 80 mg/mL presented a profile similar to polymer films in Figure 1.7, indicating that higher concentrations are a limiting factor in achieving the release of DEX from PLGA within the desired period of time. The target of achieving a complete and steady DEX release over 1-4 weeks was hindered by the biphasic nature of the release from the PLGA matrices studied, which does not support a consistent release profile within this timeframe.

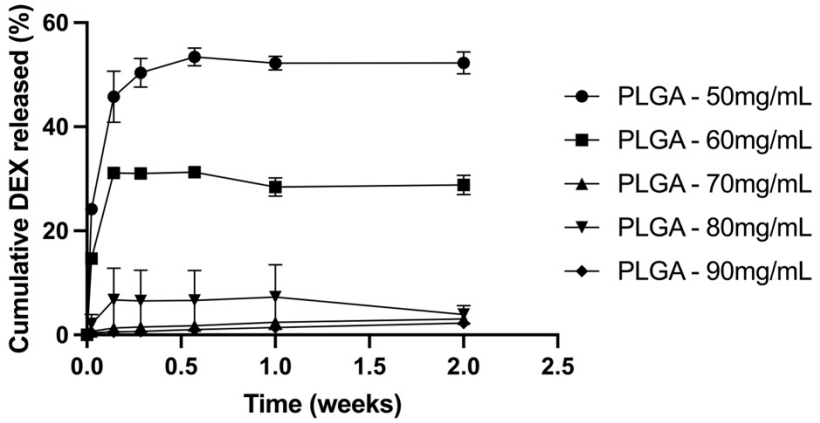

Figure 1.22. Release kinetics of DEX expressed as the total percentage of drug released (%) from PLGA prepared at different concentrations ranging from 50 to 90 mg/mL with varying drug loadings but keeping the drug concentration constant at 5 mg/mL.

Abbreviations: DEX: Dexamethasone. PLGA: Poly(lactic-co-glycolic) acid. mg: milligrams. mL: milliliters. Values represent the mean ± standard deviation (n=3).

To enhance the release kinetics of DEX, PEG, a water-miscible polymer known for its plasticizing properties and ability to solubilize DEX, was incorporated into PLGA films [327]. Furthermore, the incorporation of PEG is expected to improve the biocompatibility of the polymer coating. The addition of PEG, regardless of its MW, improved film homogeneity and transparency, suggesting better solubilization of DEX, particularly at a 70/30 (w/w) ratio. Despite these improvements, a burst release was still observed in PLGA/PEG films, particularly in those prepared at 70 mg/mL, which had not shown this behavior without PEG (Figure 1.10). The inclusion of PEG accelerated DEX release across all prototypes, with higher MW of PEG leading to faster release. However, the biphasic release profile persisted, with the initial burst occurring within the first week, followed by a second release phase around week 5. For PLGA at 100 mg/mL, the initial release was more sustained rather than a burst, yet the overall release remained very low, failing to fit within the desired 1-4 weeks timeframe. This way, while the incorporation of a hydrophilic domain like PEG facilitated greater access of the aqueous buffer to the polymeric matrix and accelerated drug release, the inherent properties of PLGA, such as

MW and LA ratio, made it challenging to achieve a steady, sustained release of DEX beyond one week.

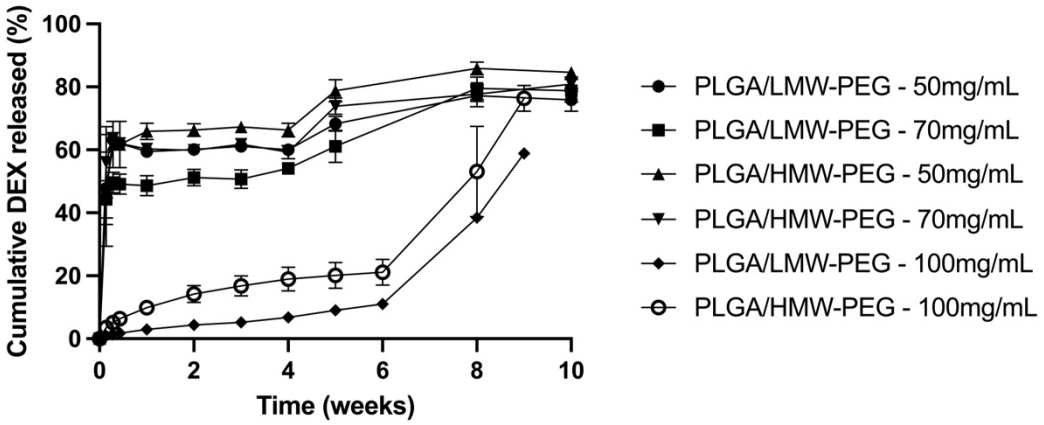

Figure 1.23. Release kinetics of DEX expressed as the total percentage of drug released (%) from PLGA/PEG blend films. PEG of both molecular weights were incorporated into the main PLGA matrix. Films were prepared at different concentrations ranging from 50 to 100 mg/mL with a PLGA/PEG ratio of 70/30 (w/w). with varying drug loadings but keeping the drug concentration constant at 5 mg/mL.

Abbreviations: DEX: Dexamethasone. PLGA: Poly(lactic-co-glycolic) acid. PEG: Poly(ethylene glycol). LMW: Low molecular weight. (w/w): weight to weight. mg: milligrams. mL: milliliters. Values represent the mean ± standard deviation (n=3).

Given the intrinsic limitations of PLGA, particularly its tendency to exhibit a biphasic release profile that may not align with the desired drug release kinetics, an alternative amphiphilic polymeric matrix, poly(lactic acid)-poly(ethylene glycol) di-block co-polymer (PLA-PEG), was explored. As previously reported [328,329], the use of di-block co-polymers may have an influence on the polymer-drug interaction and, consequently, drug release. This influence is based on the possible difference between using a di-block or a tri-block instead of the combination of the polymers composing these blocks separately. PLA-PEG is a di-block copolymer that has been widely documented in the literature for its applications in drug delivery and tissue engineering [330]. Figure 1.11 indicates that PLA-PEG indeed offered a more sustained release of DEX, maintaining the release over one week and extending it beyond the first week when the polymer concentration was increased to 200 mg/mL. Additionally, the release of DEX from this matrix was more complete compared to previous PLGA-based prototypes, suggesting a more efficient delivery system. This enhanced release profile is likely due to the PEG component, which may create channels within the polymer matrix that allow for easier access of the aqueous buffer to the drug, thus facilitating its release. Despite these promising results, the degradation time of the PLA-PEG matrix warrants careful consideration. While the PEG component is expected to accelerate the hydrolytic degradation of PLA, PLA itself degrades remarkably more slowly than PLGA, potentially requiring up to a year for complete degradation. This slower degradation of the PLA-PEG matrix in the upper layer of the bilayer system could impact the release of CLX from the bottom layer by increasing tortuosity, thereby hindering drug diffusion and altering the intended release profile.

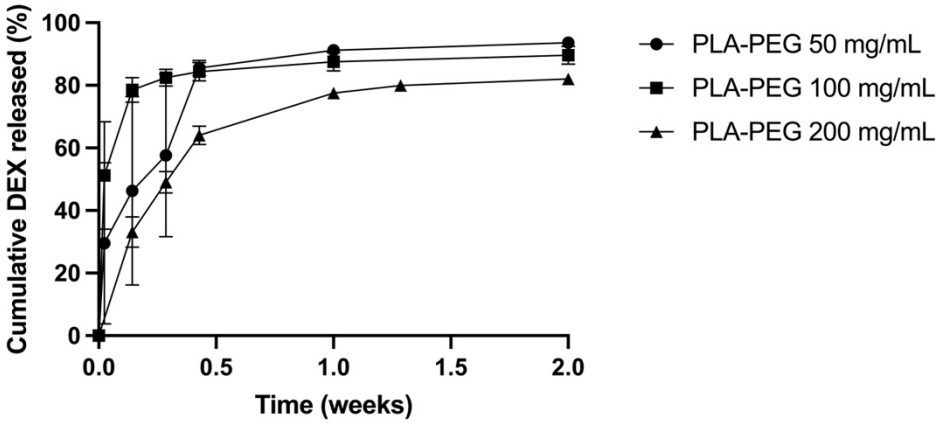

Figure 1.24. Release kinetics of DEX expressed as the total percentage of drug released (%) from PLA-PEG films prepared at different concentrations ranging from 50 to 200 mg/mL with varying drug loadings but keeping the drug concentration constant at 5 mg/mL.

Abbreviations: DEX: Dexamethasone. PLA-PEG: poly(lactic acid)-poly(ethylene glycol) di-block co-polymer. mg: milligrams. mL: milliliters. Values represent the mean ± standard deviation (n=3).

Finally, the influence of PLGA MW was evaluated. As previously discussed, the polymer MW was the final variable considered to impact DEX release from PLGA matrices. In all the studies described so far, PLGA with a MW of 24–38 kDa (HMW) was used, but to further investigate this variable, two additional PLGA variants with MW of 2 kDa (VLMW) and 8 kDa (LMW) were evaluated. Given the favorable results observed with PLA-PEG, these lower MW PLGA variants were mixed with PLA-PEG at various (w/w) ratios. The observations revealed that the PLA-PEG/ PLGA exhibited release profiles similar to pure PLA-PEG, regardless of the PLGA MW or mixture ratio (Figure 1.12). However, the PLA-PEG/LMW-PLGA mixture at a 50/50 (w/w) ratio achieved a sustained release of DEX for up to two weeks. This indicates that the incorporation of LMW-PLGA into the PLA-PEG matrix successfully prolonged the drug's release, with the effect becoming more pronounced as the proportion of LMW-PLGA in the mixture increased. This underscores the significance of MW in modulating release kinetics in these polymer matrices.

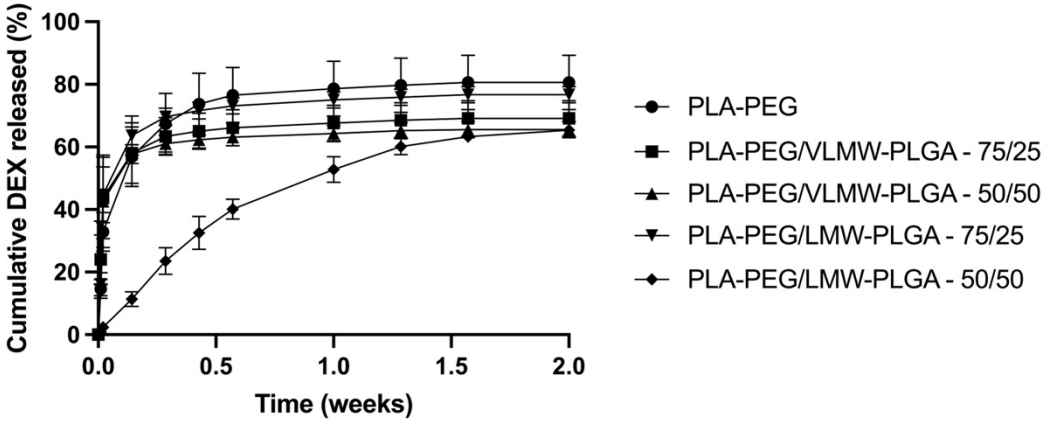

Figure 1.25. Release kinetics of DEX expressed as the total percentage of drug released (%) from pure PLA-PEG and PLA-PEG/PLGA blend films. PLGA of both molecular weights, VLMW and LMW, were incorporated to the PLA-PEG matrix with different PLA-PEG/PLGA ratios ranging from 50/50 to 75/25 (w/w). Films were prepared at 200 mg/mL with constant drug loadings of 2.44%.

Abbreviations: DEX: Dexamethasone. PLA-PEG: poly(lactic acid)-poly(ethylene glycol) di-block co-polymer. PLGA: Poly(lactic-co-glycolic) acid. VLMW: Very low molecular weight. LMW: Low molecular weight. Values represent the mean ± standard deviation (n=3).

To further explore this observation, various PLA-PEG/LMW-PLGA (w/w) ratios were tested to optimize the release kinetics of DEX, to achieve a release profile that fits within the desired 1-4 weeks period (Figure 1.13). This approach was motivated by earlier research suggesting that lower MW PLGA degrades more rapidly, leading to faster drug release [331]. The results demonstrated that higher ratios of LMW-PLGA led to a more sustained release of DEX within the first two weeks, a pattern also observed in pure LMW-PLGA matrices. Given that pure LMW-PLGA exhibited a release profile comparable to PLA-PEG/LMW-PLGA mixtures with a high concentration of LMW-PLGA, this polymer was identified as a viable alternative to PLA-PEG for achieving the targeted release kinetics. This selection also simplifies the formulation process by reducing the need for polymer blends while still meeting the therapeutic release goals. Therefore, LMW-PLGA was identified as a suitable alternative to PLA-PEG for achieving the desired DEX release kinetics, simplifying the formulation process while maintaining the target release kinetics.

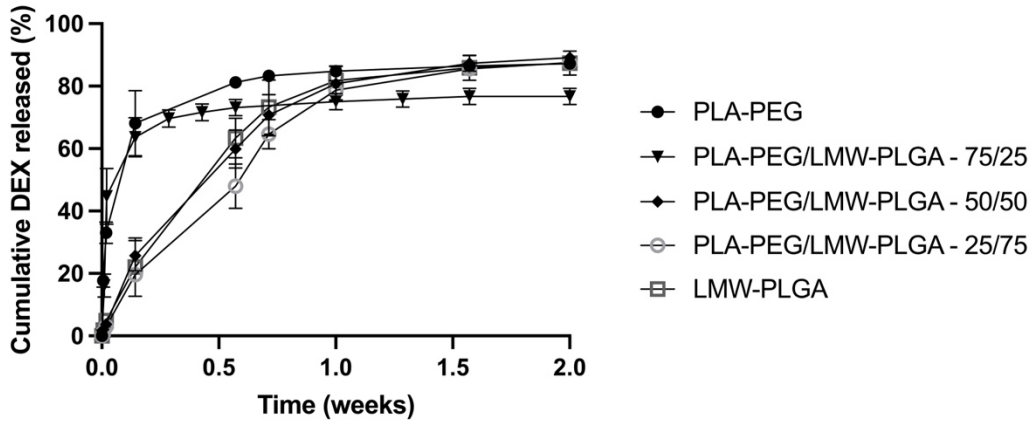

Figure 1.26. Release kinetics of DEX expressed as the total percentage of drug released (%) from pure PLA-PEG, pure LMW-PLGA, and PLA-PEG/PLGA blend films. LMW-PLGA was incorporated to the PLA-PEG matrix with different PLA-PEG/PLGA ratios ranging from 25/75 to 75/25 (w/w). Films were prepared at 200 mg/mL with constant drug loadings of 2.44%.

Abbreviations: DEX: Dexamethasone. PLA-PEG: poly(lactic acid)-poly(ethylene glycol) di-block co-polymer. PLGA: Poly(lactic-co-glycolic) acid. LMW: Low molecular weight. Values represent the mean ± standard deviation (n=3).

Thermogram Analysis of HMW-PLGA and LMW-PLGA with loaded DEX

PLGA is an amorphous polymer, and therefore, no Tm was expected [332]. This holds for both pure PLGA samples regardless of their MW. Both samples showed a slight bump at 44-48ºC, corresponding to Tg, and a degradation peak at approximately 360ºC for HMW-PLGA and 290ºC for LMW-PLGA. These differences in degradation temperatures were likely attributed to the variations in MW [333]. Moreover, the peak corresponding to Tm of DEX, at around 260ºC, completely disappears once the DEX is incorporated into the PLGA matrix. This means that the drug is correctly dissolved in the polymer (Figure 1.14A and Table 1.4)

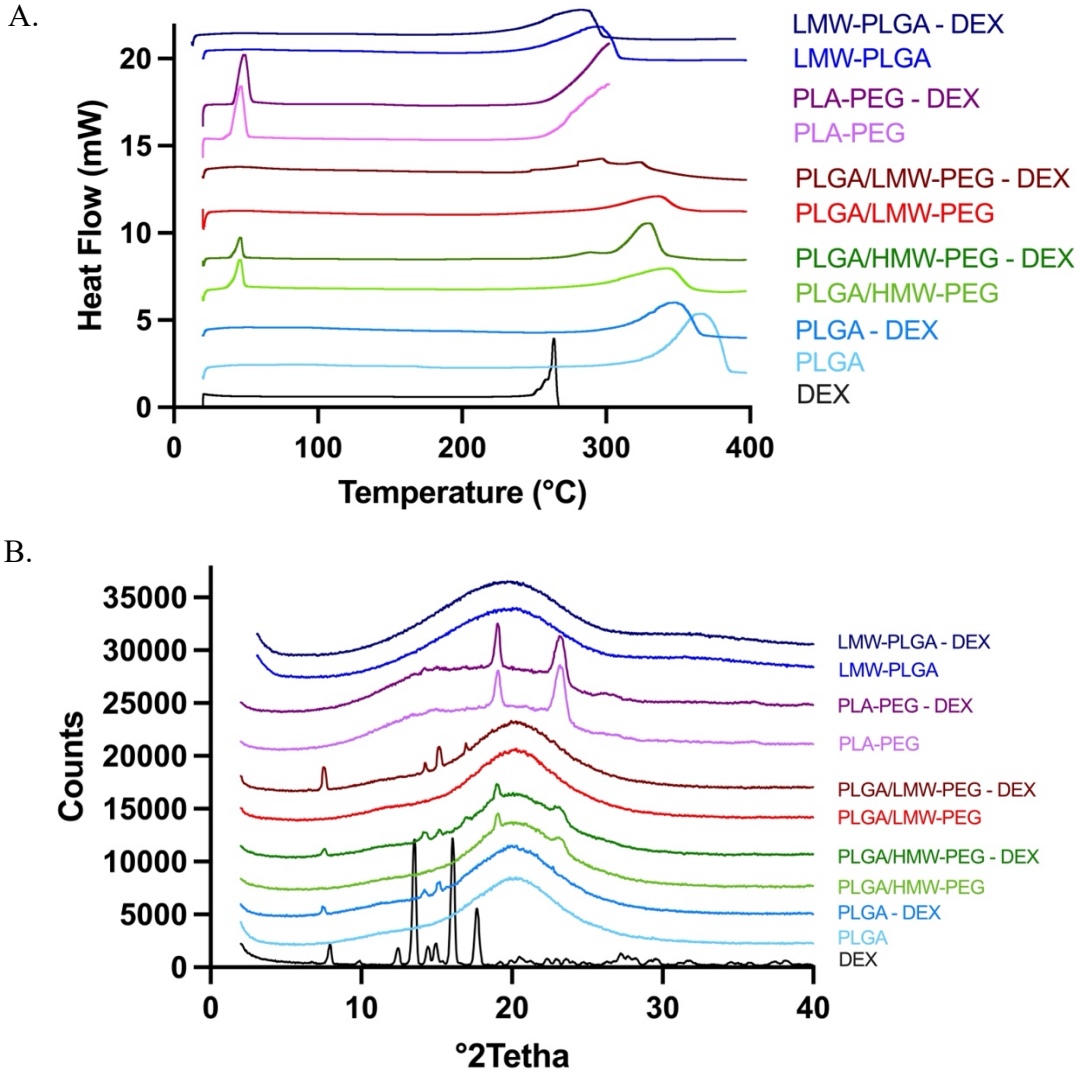

Figure 1.27. DSC thermograms (A) and XRD diffractograms (B) of the DEX-releasing prototypes.

Abbreviations: DEX: Dexamethasone. PLGA: Poly(lactic-co-glycolic) acid. PLA-PEG: poly(lactic acid)-poly(ethylene glycol) di-block co-polymer. HMW: Low molecular weight. LMW: Low molecular weight. mW: milli Watts.

Table 1.6. Tg, Tcc, Tm and Xc values of the DEX-releasing prototypes analyzed by DSC and XRD.

Sample	Tg (ºC)	Tm (ºC)	Xc (%)
DEX	-	260	-
PLGA	44-48	-	-
PLGA – DEX	44-48	-	1.89
PLGA/HMW-PEG	-	46	4.75
PLGA/HMW-PEG – DEX	-	48	6.39
PLGA/LMW-PEG	-	4*	-
PLGA/LMW-PEG – DEX	-	-	1.55
PLA-PEG	48	-	6.53
PLA-PEG - DEX	50	-	8.62
LMW-PLGA	44-48	-	-
LMW-PLGA - DEX	44-48	-	1.8

Abbreviations: DEX: Dexamethasone. PLGA: Poly(lactic-co-glycolic) acid. PLA-PEG: poly(lactic acid)-poly(ethylene glycol) di-block co-polymer. HMW: Low molecular weight. LMW: Low molecular weight. Tg: Glass transition temperature. Tcc: Cold crystallization temperature. Tm: Melting temperature. Xc: Crystallinity.
*Value not observed in Figure 1.14A, obtained from [334]. When "-" appeared in Tg or Tm, the peak corresponding to the temperature could not be observed. When "-" appeared in the Xc, the crystallinity could not be measured. It occurred with amorphous polymers.

Thermogram Analysis of PLGA/HMW-PEG and PLGA/LMW-PEG blends with loaded DEX

PEG, being semi-crystalline, generally lacks a well-defined Tg, which for lower MW PEGs ranges between -60°C and -50°C. The Tm of HMW-PEG increased from 46°C to 48°C after incorporating DEX, suggesting interactions between DEX and the PEG matrix that enhance crystallinity or create more ordered structures, requiring higher energy to disrupt. Differentiating the Tg of PLGA from the Tm of PEG was challenging due to overlapping thermal events, with the observed peak likely corresponding to the Tg of PLGA, the primary matrix component (70/30 w/w). The Tm of LMW-PEG (~4°C) was undetectable in the thermogram [334], consistent with findings that PEG's Tm rises with MW [335]. The peak at ~325°C indicates the polymer mixture's degradation temperature (Figure 1.14A and Table 1.4). These thermograms and diffractograms support the observed rapid release of DEX from PLGA/PEG blends due to the hydrophilic nature of PEG, which facilitates water penetration into the polymeric matrix. The increased crystallinity upon DEX incorporation may create more structured domains, but it also leads to greater accessibility of water to the amorphous regions of the matrix, where DEX is likely distributed, resulting in the observed faster release.

Thermogram Analysis of PLA-PEG with loaded DEX

PLA-PEG is composed of PLA and PEG5000. PLA is an amorphous polymer, and consequently, no Tm was expected to be observed [336]. The peak around 46ºC could correspond to either the Tg of PDLA or the Tm of PEG5000 (Mw = 5000 g/mol). However, given the high MW of this PEG and PLA being the major contributor to co-polymer, it is expected that this peak corresponds to the Tg of PLA. The incorporation of DEX into the matrix slightly shifts the peak to a higher temperature, indicating an interaction between DEX and the polymer matrix (Figure 1.14A and Table 1.4). Thus, this thermogram was unsuitable to justify the release kinetics observed from PLA-PEG matrices.

In the XRD analysis (Figure 1.14B), pure DEX exhibited a characteristic crystalline diffraction pattern. Still, this pattern was absent when DEX was incorporated into the polymer films, indicating that the drug was well-solubilized within the films. The semicrystalline pattern of PLA-PEG, consistent with its amphiphilic nature, likely contributes to the faster release of DEX compared to LMW-PLGA. This amphiphilicity generated by the long PEG domains facilitates the creation of hydrophilic channels within the matrix, enabling greater water penetration and enhancing the diffusion-driven release of DEX.

In contrast, PLGA-containing matrices showed amorphous diffractograms, typically associated with sustained release and justifying the biphasic release controlled first by diffusion and then by degradation. In particular, LMW-PLGA presented the most sustained release of DEX, highlighting the influence of the PLGA MW on achieving the desired release kinetics.

4.4.2.3 Summary of the best polymers for CLX and DEX release

A comprehensive screening of biodegradable and biocompatible synthetic polymers was conducted to identify the best candidates for the independent release of CLX and DEX.

For CLX, two prototypes providing the targeted release kinetics (6-9 months) were selected:

1) PLLA – 20% DL: A semicrystalline polymer known for its long degradation time. PLLA was chosen due to its ability to provide the longest release kinetics for CLX. However, a limitation is the relatively low concentration of CLX (12.5 mg/mL) it can incorporate [330,337–339].
2) PLLA/PCL blend 80/70 (w/w) - 16.6% DL: The inclusion of PCL in the PLLA matrix accelerated CLX release. Arguably, the incorporation of PCL domains into the PLLA potentially creates polymer-to-polymer interfaces that facilitate water access, disrupting the very robust structure of pure PLLA. This blend, presenting a higher concentration of polymer, allowed for a higher CLX concentration (30 mg/mL), making it a strong candidate for applications requiring faster release kinetics [23,24].

For DEX, two prototypes providing the targeted release kinetics (1-4 weeks) were identified:

1) PLA-PEG – 2.44% DL: It provided a controlled release of DEX for approximately 1 week, facilitated by the hydrophilic domain provided by PEG [340,341].
2) LMW-PLGA (MW = 8 kDa, 50:50 LA:GA ratio) – 2.44% DL: It provided a sustained release of DEX for more than 1 week [283,331,342].

4.4.3 Engineering a bilayer drug-releasing polymer coating for the sequential release of DEX and CLX

This section focuses on developing a system for the simultaneous release of DEX and CLX, which have distinct release kinetics, from a non-biodegradable, square-shaped PCU implant (~ 7 x 7 x 3 cm). To achieve this, a bilayer drug-releasing polymer coating was designed. This

system had a bottom CLX-releasing layer in close contact with the implant and a DEX-releasing layer deposited on top of the layer that releases CLX. The four polymer matrices that previously showed the most promising results in section 1.5.2.3 were combined and evaluated for this purpose.

Additionally, an alternative method was explored to effectively coat the entire implant. Solvent casting proved effective for creating a thin polymer film over one face of the implant, offering a simple, cost-effective, and quick preparation method [25,26]. We selected dip coating among standard techniques that allowed for the coating of the whole implant, such as spray coating, spin coating, grafting, and dip coating [6]. This method, widely used in tissue engineering and drug delivery, adapted well to different substrate shapes and allowed for the multiple coatings needed to achieve our bilayer drug-releasing polymer system [27,28]. Therefore, dip coating was chosen for further development.

After further evaluation, the goal was to select a single polymer matrix for the release of each drug for final implementation.

4.4.3.1 Influence of the organic solvent used in DEX-releasing top polymer layer synthesis on the CLX-releasing bottom polymer layer

The organic solvent acetone, used during the synthesis of the DEX-releasing layer, was evaluated for its potential effect on the drug release behavior of the underlying CLX-loaded layer. Thus, a volume of acetone was deposited on top of the CLX-loaded layer. The results indicated that the influence of acetone varied depending on the type of polymeric matrix employed (Figure 1.15). When acetone was applied to PLLA/PCL films, a slight acceleration in CLX release was noted, yet the overall release kinetics remained consistent. However, for pure PLLA, acetone significantly altered the release profile, accelerating CLX release from approximately 10% to over 60% by week 21.

DSC analysis revealed that acetone treatment significantly affected the thermal behavior of PLLA-CLX films, with the Tg around 60°C becoming less distinct, a consistent Tcc at ~95°C, and a broader Tm peak. These changes suggest reduced interaction between CLX and PLLA after acetone exposure, correlating with the accelerated CLX release observed in the release studies. Conversely, the PLLA/PCL-CLX thermogram showed minimal changes after acetone treatment, reflecting stronger CLX-polymer blend interactions that preserved the release kinetics. These findings align with the observed differences in acetone's impact on the drug release profiles of the two matrices (Figure 1.15).

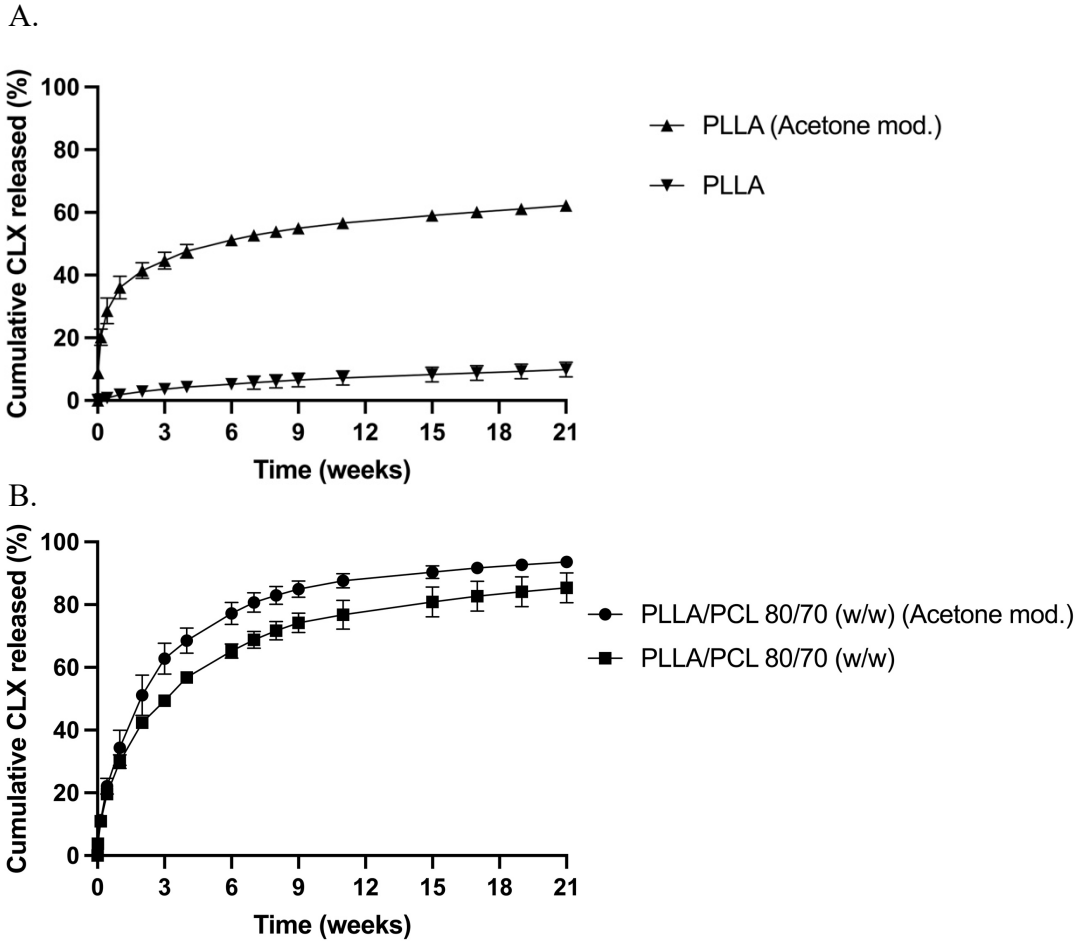

Figure 1.28. Release kinetics of CLX expressed as the total percentage of drug released (%) from unmodified or acetone-modified PLLA prepared at 50 mg/mL with a CLX loading of 20% (A) and unmodified or acetone-modified PLLA/PCL blends prepared at 150 mg/mL at 80/70 (w/w) with a CLX loading of 16.67% (B).

Abbreviations: CLX: Celecoxib. PLLA: poly(L-lactide). PCL: poly(caprolactone). (w/w): weight to weight ratio. mod.: modified. Values represent the mean ± standard deviation (n=3).

Furthermore, XRD analysis revealed an increase in the Xc for both PLLA and PLLA/PCL after the films were treated with acetone. Further confirming that the addition of acetone on top of the bottom polymer layer had an impact on the structure and properties of the CLX-releasing polymer layer. Nevertheless, similar to what was observed for untreated polymer films, higher Xc did not align with a slower release of CLX.

4.4.3.2 Evaluation of the release of CLX from the bottom layer of the bilayer drug-releasing polymer coating

The findings described above highlighted the need to carefully select the optimal CLX-releasing layer when developing a bilayer drug-releasing polymer coating. To streamline this process, the DEX-loaded layer was kept constant while the release of CLX from the two previously selected polymer matrices in section 1.5.2.3 was thoroughly evaluated.

Polymer coatings were developed using dip coating, in which CLX was dissolved in DCM and then used to dissolve either PLLA/PCL or pure PLLA to create the CLX-releasing layer.

PCU implants were immersed in the polymer-CLX solution at a constant rate, and the process was repeated three times for uniform coating. Subsequently, a DEX-releasing layer was formed by dissolving DEX in acetone and using this solution to dissolve PLA-PEG with five coating cycles.

The shift from solvent casting to dip-coating led to changes in expected drug release kinetics due to the increased amount of drug attached, the creation of multiple layers, and the coating of the entire implant surface. The incorporation of a DEX-releasing layer above the CLX-loaded layer resulted in a significant reduction in the release rate of CLX, regardless of the polymeric matrix. This effect contrasts with the accelerated release observed in acetone-modified CLX-loaded films (Figure 1.15). Moreover, the release profiles of CLX were comparable between PLLA and PLLA/PCL matrices in the presence of the DEX-releasing layer (Figure 1.16), suggesting that the addition of acetone and the subsequent polymeric layer effectively neutralized the release differences observed between the two polymers.

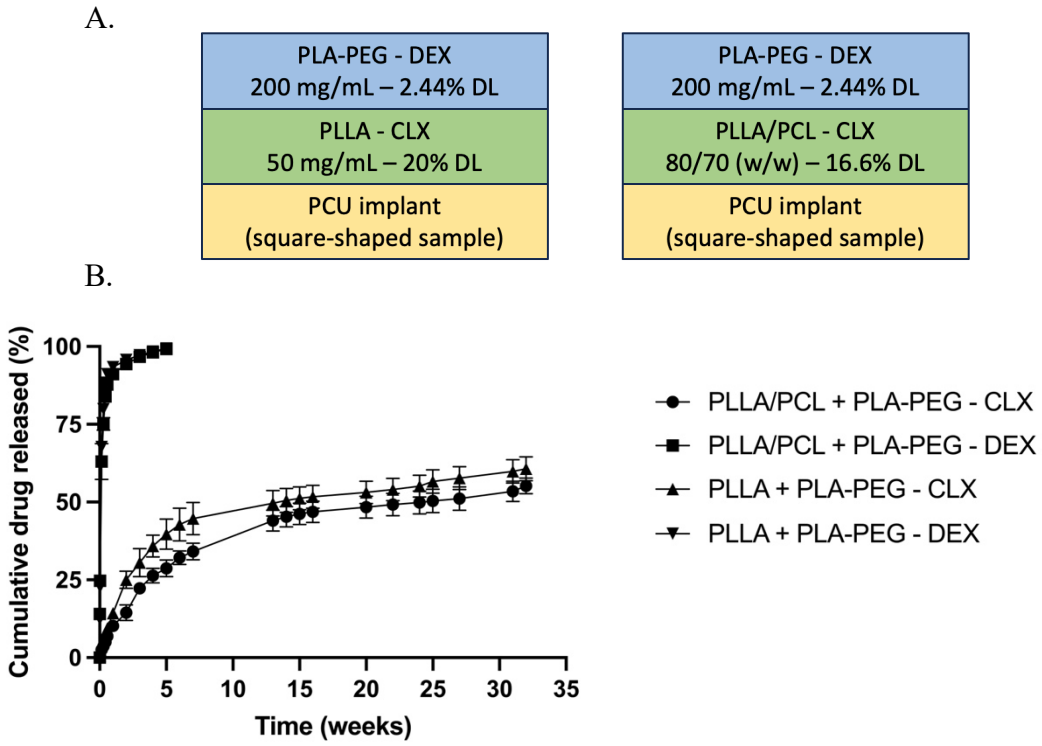

Figure 1.29. Schematic representation of the two bilayer polymer coatings (A). Sequential release of DEX and CLX from bilayer polymer coatings composed of a first polymer coating of either PLLA/PCL, prepared at 150 mg/mL at 80/70 (w/w) with CLX loading of 16.67%, or PLLA, prepared at 50 mg/mL with CLX loading of 20%; and a second polymer coating of PLA-PEG prepared at 200 mg/mL with DEX loading of 2.44% (B).

Abbreviations: PCU: Polycarbonate urethane. CLX: Celecoxib. DEX: Dexamethasone. PLA-PEG: poly(lactic acid)-poly(ethylene glycol) di-block co-polymer. PLLA: poly(L-lactide). PCL: poly(caprolactone). Values represent the mean ± standard deviation (n=3).

Previous studies have indicated that high doses of intraarticular CLX (up to 1000 µg/kg) are non-toxic in animal models such as sheep [300], horses [343], and rats [344,345]. Moreover, the safety and activity of the *in situ* forming depot BEPO™, a mixture of di- and tri-block copolymers based on PLGA and PEG, was recently evaluated in humans (NCT03541655) with a CLX dose of 175,000 µg (speculation based on published results [346]). From this point of view, we sought to prepare polymer coatings with CLX doses close to the therapeutic values.

Considering the dose sought and the release profiles obtained, PLLA/PCL showed the best properties for the release of CLX (Table 1.5 and Figure 1.16).

Table 1.7. Amount of DEX and CLX (µg/cm2) encapsulated in each of the bilayer polymer coatings analyzed.

Drug	PLLA + PLA-PEG	PLLA/PCL + PLA-PEG
DEX (µg/cm^2)	570.84 ± 116.61	431.21 ± 96.31
CLX (µg/cm^2)	2220.10 ± 645.87	3184.64 ± 105.01

Abbreviations: DEX: Dexamethasone. CLX: Celecoxib. PLA-PEG: poly(lactic acid)-poly(ethylene glycol) di-block co-polymer. PLLA: poly(L-lactide). PCL: poly(caprolactone). µg: micrograms. cm^2: square centimeters. Values represent the mean ± standard deviation (n=3).

Given these findings, including the remarkably higher drug loading and optimal release profile, and considering the expected improved mechanical properties after PCL incorporation, PLLA/PCL was selected as the optimal CLX-releasing prototype for further development [347].

4.4.3.3 Evaluation of the release of DEX from the top layer of the bilayer drug-releasing polymer coating

Here, the release profiles of DEX from the two polymer matrices selected in section 1.5.2.3, PLA-PEG and LMW-PLGA, were evaluated while maintaining a constant CLX-releasing layer composed of the previously selected PLLA/PCL blend (section 1).5.3.2). The PCU implants were coated using a dip-coating technique, where CLX was dissolved in DCM and incorporated into the PLLA/PCL matrix, followed by DEX dissolved in acetone and incorporated into either PLA-PEG or LMW-PLGA.

Notably, despite the consistent CLX layer, differences in the release kinetics of DEX and CLX were observed (Figure 1.17). The release of CLX was more accelerated when LMW-PLGA was used as the top layer, likely due to the faster degradation rate of PLGA compared to PLA-PEG. It was hypothesized that this faster degradation of the PLGA layer allowed for the earlier removal of the top layer, facilitating a quicker release of CLX from the underlying PLLA/PCL matrix. Conversely, the slower degradation of PLA-PEG created a more sustained barrier, leading to a slower release of CLX.

The DEX release profiles from both PLA-PEG and LMW-PLGA matrices were consistent with previous findings. PLA-PEG demonstrated a pronounced burst release during the first week, followed by a more gradual and sustained release phase. In contrast, LMW-PLGA exhibited a more prolonged and steady release over time. Despite these differences, both matrices achieved complete DEX release within the first few weeks, effectively fulfilling the objective of delivering the drug to manage acute post-surgical inflammation.

The primary difference between these prototypes is the polymer used for the DEX-releasing layer, which directly influenced the drug loading and release kinetics of both DEX and CLX (Table 1.6). Thus, prototypes are going to be referred to as Prototype PLA-PEG and Prototype PLGA. Given the observed release profiles and degradation characteristics, these prototypes offered valuable insights for the design of dual-drug delivery systems aimed at

addressing post-surgical inflammation and ensuring sustained therapeutic effects for chronic inflammation.

A.

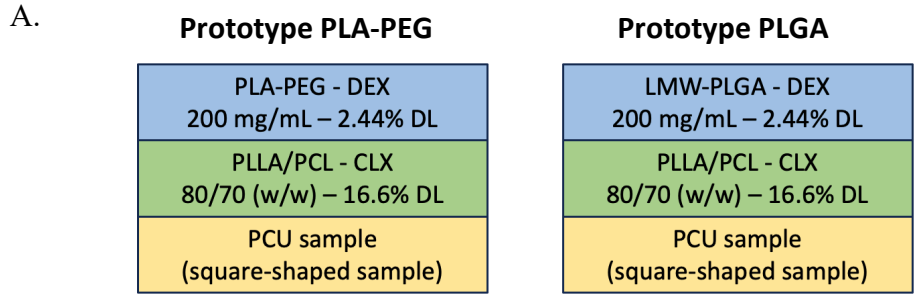

B.

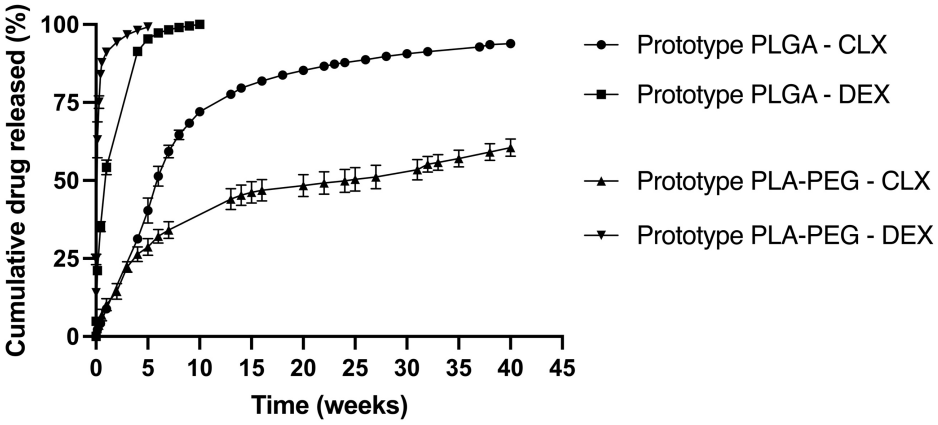

Figure 1.30. Schematic representation of the two final prototypes of bilayer polymer coatings (A). Sequential release of DEX and CLX from bilayer polymer coatings composed of a first polymer coating of PLLA/PCL, prepared at 150 mg/mL at 80/70 (w/w) with CLX loading of 16.6%; and a second polymer coating of either PLA-PEG or LMW-PLGA, both prepared at 200 mg/mL with DEX loading of 2.44% (B).

Abbreviations: PCU: Polycarbonate urethane. CLX: Celecoxib. DEX: Dexamethasone. PLA-PEG: poly(lactic acid)-poly(ethylene glycol) di-block co-polymer. PLGA: Poly(lactic-co-glycolic) acid. PLLA: poly(L-lactide). PCL: poly(caprolactone). LMW: Low molecular weight. Values represent the mean ± standard deviation (n=3).

Table 1.8. Amount of DEX and CLX (µg/cm^2) encapsulated in each of the bilayer polymer coatings analyzed.

Drug	Prototype PLA-PEG	Prototype PLGA
DEX (µg/cm^2)	431.21 ± 96.31	322.69 ± 15.68
CLX (µg/cm^2)	3184.64 ± 105.01	3505.21 ± 94.57

Abbreviations: DEX: Dexamethasone. CLX: Celecoxib. PLA-PEG: poly(lactic acid)-poly(ethylene glycol) di-block co-polymer. µg: micrograms. cm^2: square centimeters. Values represent the mean ± standard deviation (n=3).

4.4.3.4 Analysis of the biodegradation of Prototype PLA-PEG and Prototype PLGA

The selection of the final prototype could not be finalized based solely on release studies, as both achieved the desired release kinetics for DEX (1-4 weeks) and CLX (6-9 months). Consequently, both prototypes were evaluated focusing on their biodegradation over time when immersed in a release buffer. These biodegradation studies also aimed to explore the observed differences in CLX release when the top layer was changed from PLA-PEG to PLGA and validate the hypothesis regarding the slower degradation of PLA-PEG. The study involved

immersing the coated square implants in PBS supplemented with 1% (w/v) Tween80 and periodically removing them for pH measurements, microscopic analysis, and thickness evaluation.

Over time, prototype PLA-PEG exhibited a steady decrease in thickness, with a marked reduction between 4 and 6 months, corresponding to significant structural changes observed in FESEM images. These images showed polymer degradation, layer separation, and poor interaction between the coating and the implant, particularly after 6 months. The coating's integrity deteriorated to the point where thickness measurement was impossible after 1 year. In contrast, prototype PLGA initially showed an increase in thickness, likely due to swelling, followed by a constant decrease over the course of a year (Figure 1.18A, Figure 1.19 and Figure 1.20) [348,349].

Regarding pH changes, both prototypes demonstrated a decrease over time, reflecting the acidification of the buffer due to polymer degradation. Similar to what observed in thickness analysis, prototype PLA-PEG maintained a relatively stable pH until around 4 months, after which a sharp decline occurred between 4 and 6 months, stabilizing again up to 1 year. Prototype PLGA, however, showed a rapid pH drop by the second month, which then remained relatively stable through the year. Because of the long-term degradation of PLLA and PCL, these pH variations are attributed primarily to the degradation of the DEX-releasing layer, with differences reflecting the faster degradation of LMW-PLGA compared to PLA-PEG. Thus, it was observed that Prototype PLGA degrades more quickly than Prototype PLA-PEG, as evidenced by the faster pH decrease (Figure 1.18B).

This quicker degradation, combined with the swelling behavior of LMW-PLGA, likely explains why CLX is released more rapidly from Prototype PLGA despite both prototypes using the same PLLA/PCL matrix for CLX. Initially, both prototypes would allow similar buffer access to the CLX layer due to PEG-induced hydrophilic pores in PLA-PEG and PLGA swelling. However, as LMW-PLGA degrades faster, the top layer in Prototype PLGA would lose its tortuosity more quickly, allowing direct contact of the CLX layer with the release buffer and thereby accelerating CLX release.

It is worth noting that the thickness measurements in this study were influenced by the manual sagittal cuts during sample preparation and the specific angle and location on the square implant where FESEM images were captured. These factors introduced variability, making the values approximate rather than absolute. While the data indicates thickness trends, these measurements should not be considered universally representative of the entire implant. Instead, they provide insight into thickness variations, with caution advised when extrapolating these results, as they illustrate relative trends rather than serve as definitive quantitative metrics (Figure 1.19 and Figure 1.20).

pH proved to be a more reliable indicator of the degradation of the bilayer polymer coating. This measurement was unaffected by external variables, with the only potential influence being human-related variations during the coating's manufacturing process from replicate to replicate. This *in vitro* setup caused a significant reduction in the medium's pH within the container, which is believed to have further accelerated the degradation of the polymer. Therefore, the results obtained here cannot be directly applied to *in vivo* degradation, where pH levels are likely to remain stable. Nonetheless, previous studies have shown that the *in vitro* and *in vivo* degradation profiles of PLGA are comparable in terms of MW reduction [29]. This similarity

may arise from the complex nature of the *in vivo* degradation process, which includes interactions with tissues and possibly enzyme involvement in the degradation.

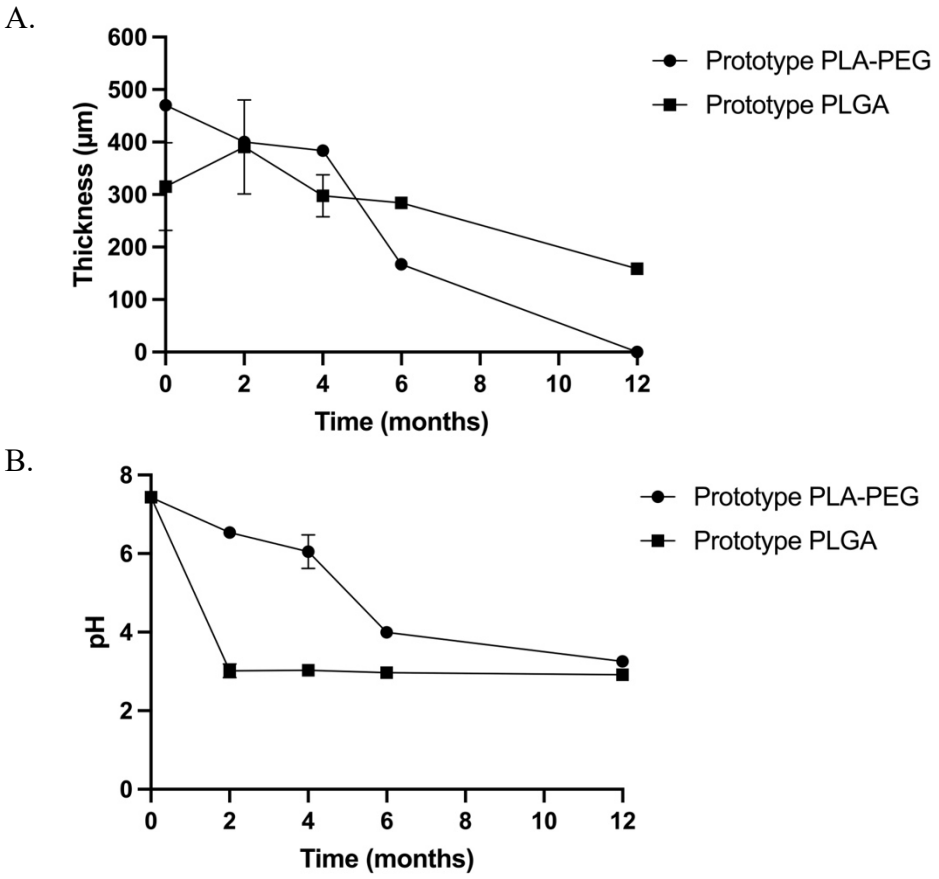

Figure 1.31. Changes in thickness (A) and pH (B) of Prototype PLA-PEG and Prototype PLGA with time.

Abbreviations: PLA-PEG: poly(lactic acid)-poly(ethylene glycol) di-block co-polymer. PLLA: poly(L-lactide). PCL: poly(caprolactone). PLGA: Poly(lactic-co-glycolic) acid. µm: micrometers. Values represent the mean ± standard deviation (n≥1).

Prototype PLA-PEG

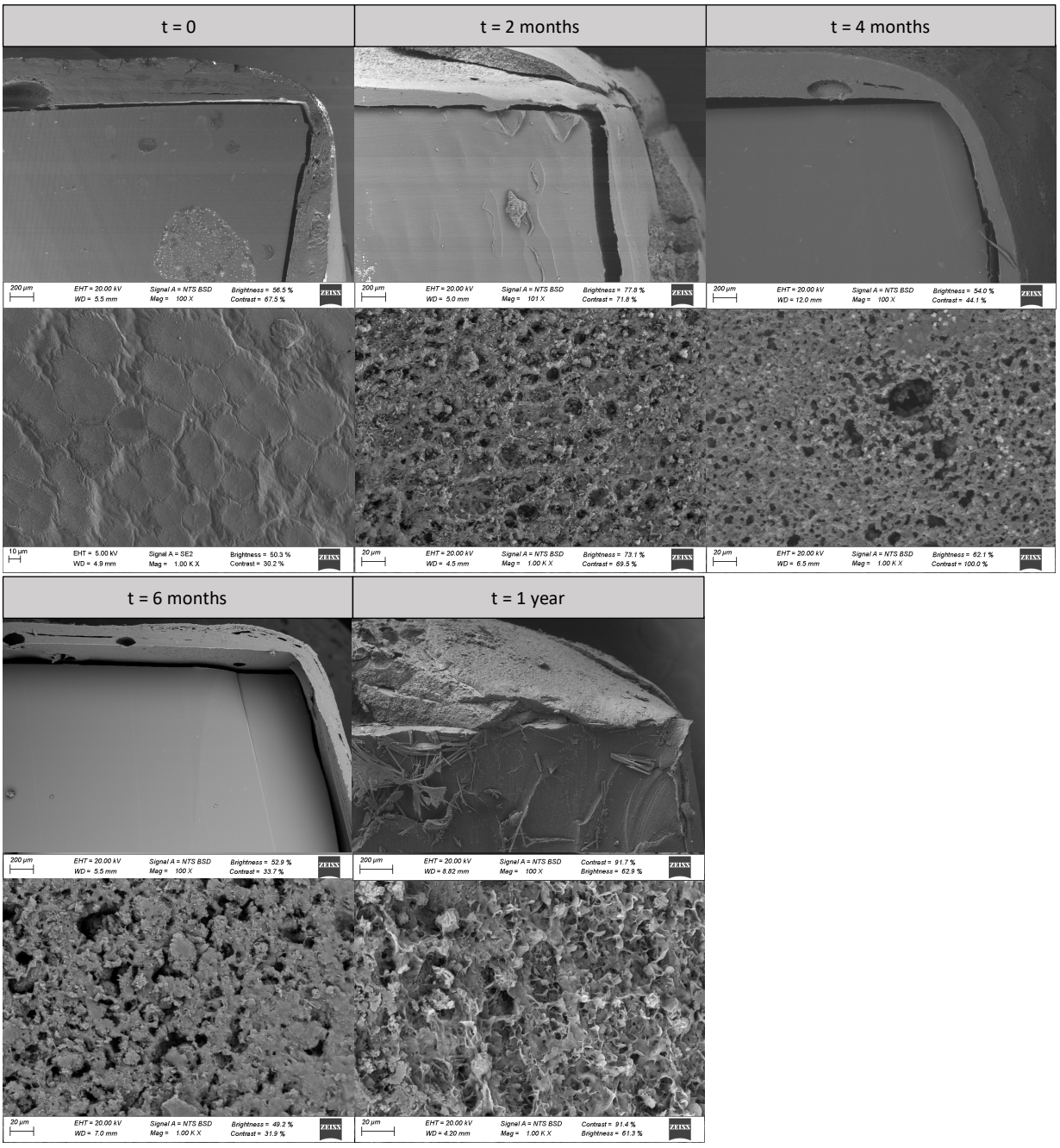

Figure 1.32. FESEM images of the Prototype PLA-PEG at different times of the biodegradation process. Images are divided into pairs per time point, a top image and a bottom image. The top images correspond with the sagittal cut of the bilayer polymer coating and the PCU implant and were obtained using Zeiss EVO analytical FESEM with a magnification of 100X. The thickness of the polymer coating was measured in these top images. The bottom images correspond with the view from above of the bilayer polymer coating sputter coated with iridium and were obtained using Zeiss UltraPlus analytical FESEM with a magnification of 1000X.

Abbreviations: FESEM: Field emission scanning electron microscopy. PLA-PEG: poly(lactic acid)-poly(ethylene glycol) di-block co-polymer. µm: micrometers. EHT: Electron high tension. WD: Working distance. Mag: Magnification.

Prototype PLGA

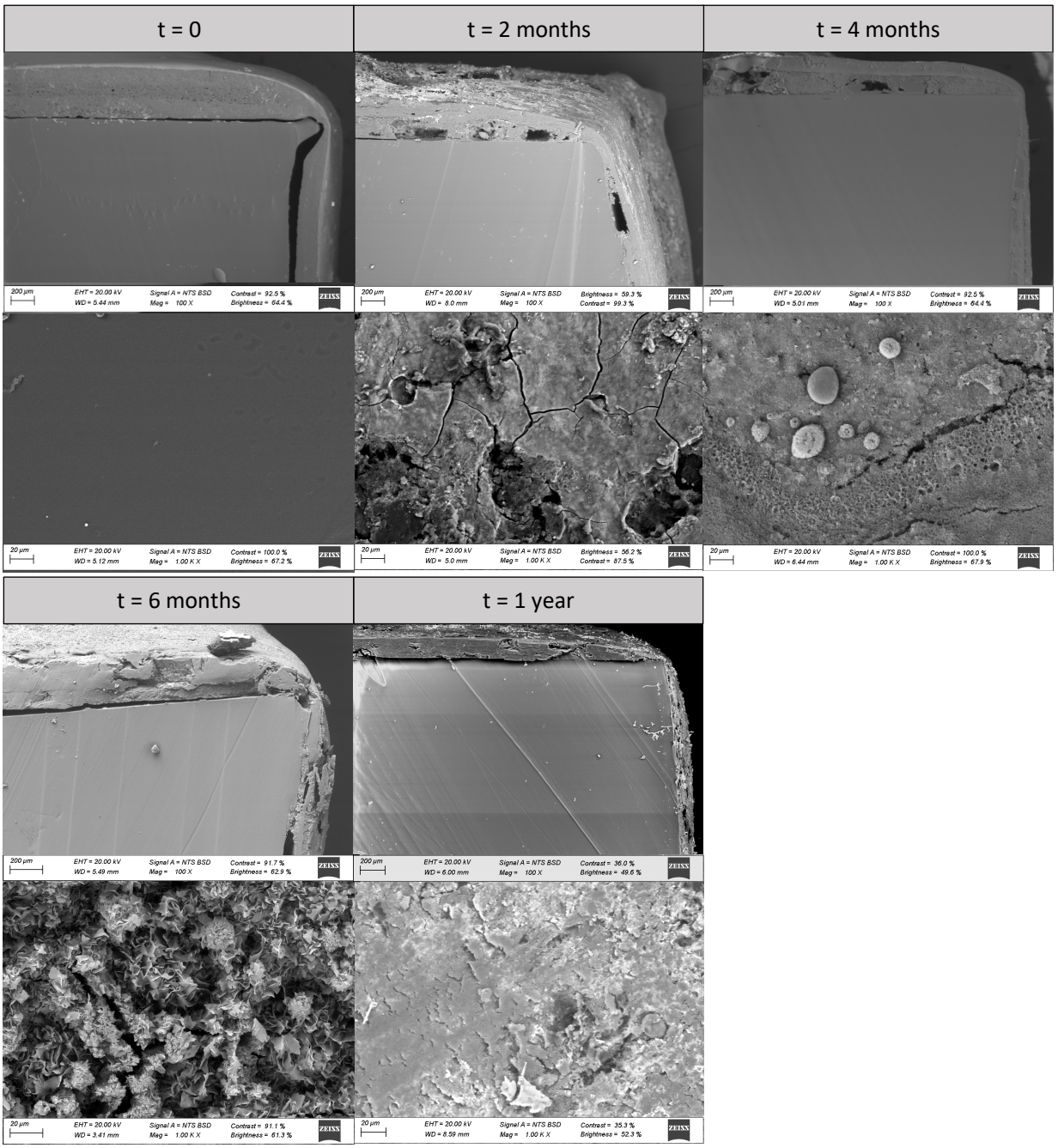

Figure 1.33. FESEM images of the Prototype PLA-PEG at different times of the biodegradation process. Images are divided into pairs per time point, a top image and a bottom image. The top images correspond with the sagittal cut of the bilayer polymer coating and the PCU implant and were obtained using Zeiss EVO analytical FESEM with a magnification of 100X. The thickness of the polymer coating was measured in these top images. The bottom images correspond with the view from above of the bilayer polymer coating sputter coated with iridium and were obtained using Zeiss UltraPlus analytical FESEM with a magnification of 1000X.

Abbreviations: FESEM: Field emission scanning electron microscopy. PLGA: Poly(lactic-co-glycolic) acid. µm: micrometers. EHT: Electron high tension. WD: Working distance. Mag: Magnification.

4.4.3.5 Evaluation of the reproducibility of Prototype PLA-PEG and Prototype PLGA

The consistency in the drug incorporation of finally selected prototypes named as Prototype PLGA and Prototype PLA-PEG was assessed to determine their reproducibility. The total amount of DEX and CLX per unit area (µg/cm²) of square-shaped PCU implants was quantified across different replicates. Prototype PLGA exhibited consistent drug loading for both DEX and CLX across all replicates, indicating a reproducible and well-optimized coating process in terms of the number of dipping cycles and solvent evaporation times. In contrast, Prototype PLA-PEG demonstrated variability in the loading of both DEX and CLX between replicates. This inconsistency suggested potential challenges in achieving uniform drug distribution within the polymer matrices of Prototype PLA-PEG, possibly due to the way the polymers deposit on the surface of the square-shaped PCU implants, variations in polymer-drug interactions, or sensitivity to the coating conditions. These findings indicated that Prototype PLGA offered reliable and reproducible drug incorporation, but Prototype PLA-PEG showed inconsistency in drug loading (Figure 1.21).

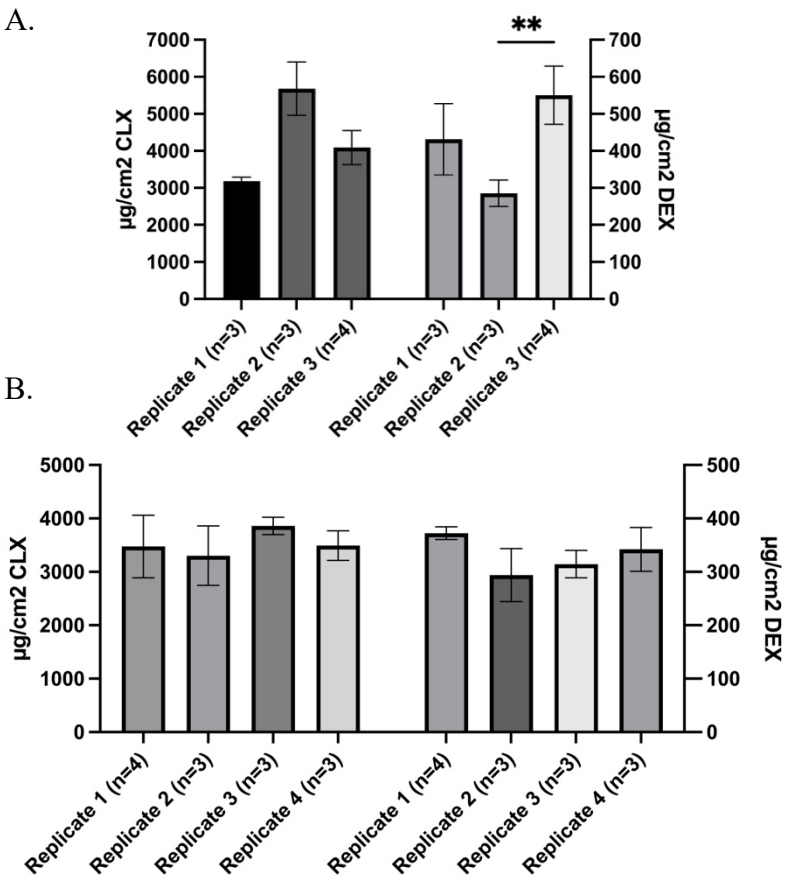

Figure 1.34. Drug loading of both CLX and DEX in Prototype PLA-PEG (A) and Prototype PLGA (B) across intra- and inter-day replicates.

Abbreviations: CLX: Celecoxib. DEX: Dexamethasone. µg: micrograms. cm²: square centimeters. A significant comparison was performed using a Brown-Forsythe and Welch one-way ANOVA followed by Tukey's multiple comparison tests between groups. *p*-values < 0.05 were considered statistically significant (*). Also, (**) if *p*-value < 0.01. When no asterisk is displayed, not significative differences (ns) were observed. Columns represent the mean ± standard deviation (n ≥ 3). Each replicate corresponds with an inter-day replicate.

4.4.4 *In vitro* assessment of sterility, biocompatibility, anti-inflammatory activity, and efficiency of the bilayer drug-releasing polymer-coated PCU implants

4.4.4.1 Evaluation of drug release from the bilayer drug-releasing polymer coating

Drug release studies for the *in vitro* experiments were performed using PBS supplemented with 0.05% (w/v) Tween®80 and 1% (v/v) penicillin/streptomycin. The adjustment to a lower concentration of Tween®80 was necessary due to its potential toxicity to human primary macrophages (HMDMs). The release profiles, presented in Figure 1.22A, depict the percentage of drug released, while the actual concentrations of CLX and DEX in the release medium from Prototype PLA-PEG and Prototype PLGA are shown in Figure 1.22B.

In vitro evaluations were conducted at five time points: 3 hours, 3 days, 1 week, 2 weeks, and 4 weeks post-immersion, strategically chosen to capture the distinct drug effects over time. The earliest point reflects the effect of DEX alone, intermediate points represent the combined effects of DEX and CLX, and later points focus on CLX. Previous studies by the HUNIMED team established minimum effective concentrations of 10 μM for DEX and 25 μM for CLX to elicit anti-inflammatory responses in human primary macrophages. The selected intervals ensure measurements exceed these effective concentrations for each drug individually and in combination. The minimum effective concentration is indicated by a dotted line in Figure 1.22B.

4.4.4.1 Sterility evaluation of the bilayer drug-releasing polymer coated implants

Testing the endotoxin contamination is a pre-requisite for any drug or device intended for medical applications, and according to FDA regulation, levels must remain below 0.5 EU/ml [350]. Furthermore, given the ability of endotoxins (LPS) to activate TLR4 and induce inflammation, a more stringent limit of 0.125 EU/mL was applied as the maximum permissible concentration of LPS before conducting *in vitro* testing of these prototypes. The chromogenic LAL test was employed for this analysis. Using the dilutions described in Table 1.1, the LAL test results indicated that all samples remained below the 0.125 EU/mL threshold. This confirms that the samples are free from endotoxin contamination, indicating that the synthesis of the bilayer polymer coating kept the sterility of the samples, making them suitable for subsequent *in vitro* biocompatibility and immunotoxicity experiments. The results of the chromogenic LAL test are not shown in this thesis.

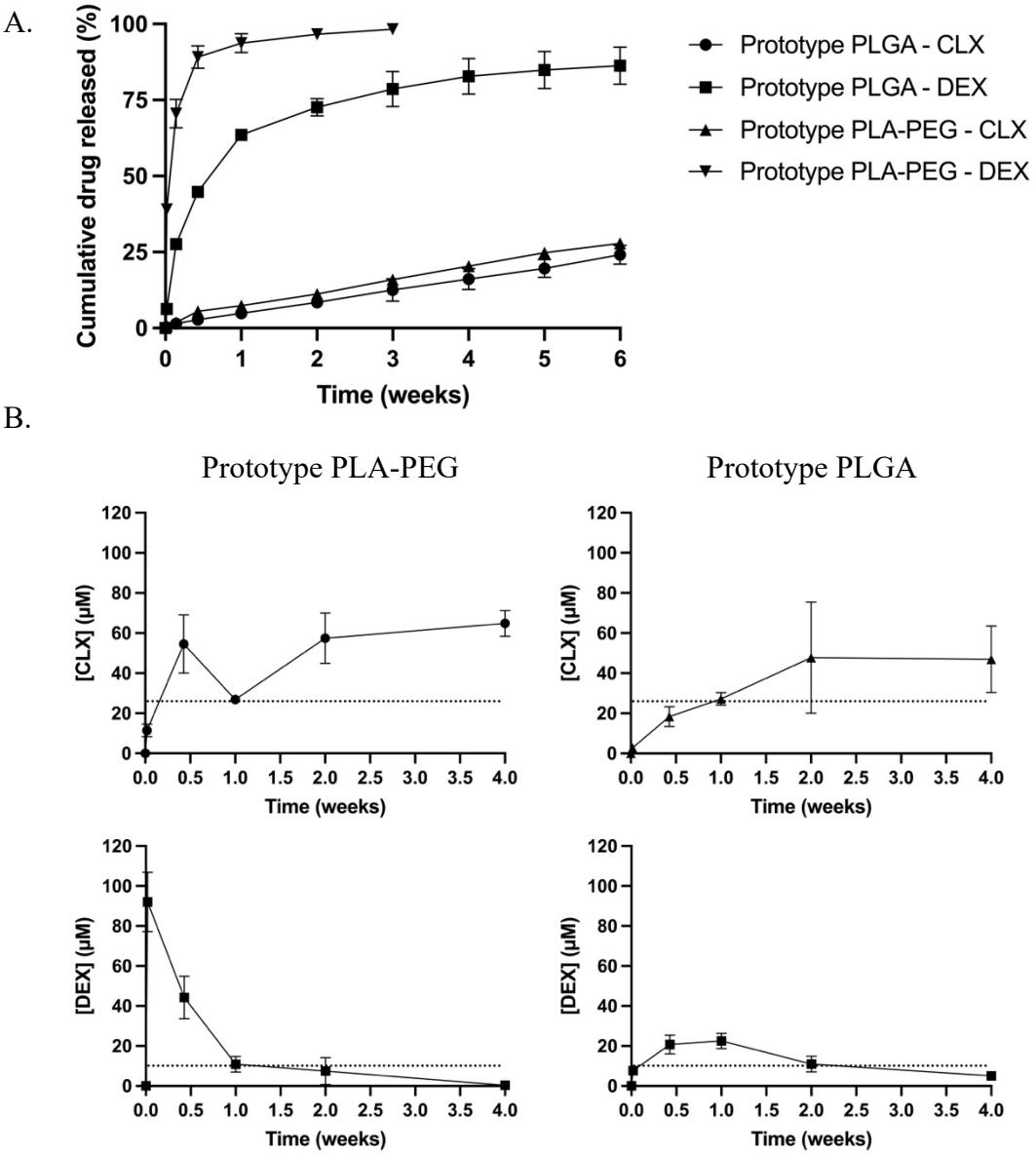

Figure 1.35. Sequential cumulative release of DEX and CLX from bilayer polymer coatings composed of a first polymer coating of PLLA/PCL, prepared at 150 mg/mL at 80/70 (w/w) with CLX loading of 16.6%; and a second polymer coating of either PLA-PEG (Prototype PLA-PEG) or LMW-PLGA (Prototype PLGA), both prepared at 200 mg/mL with DEX loading of 2.44% (A). Non-cumulative release of CLX and DEX (µM) from Prototype PLA-PEG and Prototype PLGA at 3 hours, 3 days, 1 week, 2 weeks, and 4 weeks.

Abbreviations: CLX: Celecoxib. DEX: Dexamethasone. PLA-PEG: poly(lactic acid)-poly(ethylene glycol) di-block co-polymer. PLGA: Poly(lactic-co-glycolic) acid. PLLA: poly(L-lactide). PCL: poly(caprolactone). µM: micromolar. Values represent the mean ± standard deviation (n=3).

4.4.4.2 Biocompatibility of the bilayer drug-releasing polymer coated implants

To evaluate the cytotoxicity of the drugs and polymer degradation products from the selected prototypes with HMDMs, an AlamarBlue™ cell viability assay was conducted. As illustrated in Figure 1.23, macrophages viability remained unaffected at all time points assessed. These findings suggest that the drugs released from both Prototype PLGA and Prototype PLA-PEG did not compromise macrophage survival, indicating a satisfactory biocompatibility

profile. Furthermore, since the entire release buffer from different time points was added to the macrophages, it could be inferred that not only the drugs but also the degradation byproducts of the polymer coatings were present in the media. This suggests that the byproducts resulting from the hydrolytic degradation of the polyesters did not negatively impact the biocompatibility of the system, in agreement with previous investigations [30].

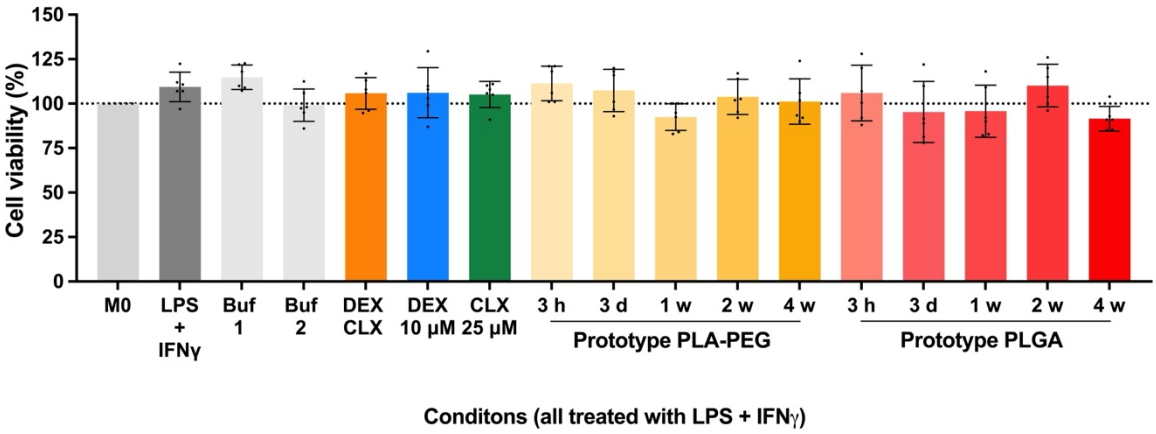

Figure 1.36. AlamarBlue™ cell viability assay to evaluate the biocompatibility of Prototype PLA-PEG and Prototype PLGA at indicated times.

Abbreviations: M0: Unactivated macrophages. Neg: Negative. Pos: Positive. Buf: Buffer. PLA-PEG: poly(lactic acid)-poly(ethylene glycol) di-block co-polymer. h: hour. d: days. w: weeks. PLGA: Poly(lactic-co-glycolic) acid. A significant comparison was performed using an ordinary one-way ANOVA followed by Tukey's multiple comparison tests between M0 and the rest of the groups. p-values < 0.05 were considered statistically significant (*). When no asterisk is displayed, not significative differences were observed. Columns represent the mean ± standard deviation (n = 6).

4.4.4.3 *In vitro* evaluation of the bioactivity of the drugs released from the bilayer polymer coated PCU implants

The immune system reacts to different signals by cytokine secretion (Figure 1.24). Cytokines are small proteins that play a role in cell communications and interactions. Depending on the source, primarily M1 macrophages or M2 macrophages, cytokines can be divided into pro-inflammatory and anti-inflammatory, respectively. Pro-inflammatory cytokines participate in the upregulation of inflammatory responses, while anti-inflammatory cytokines modulate the pro-inflammatory responses [351,352].

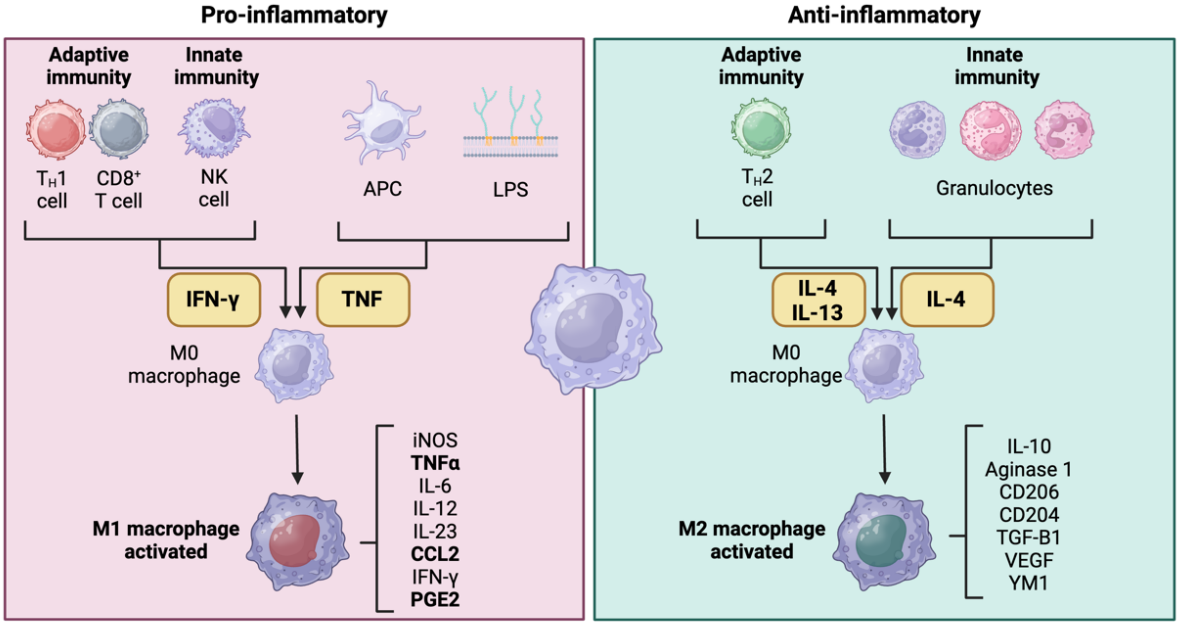

Figure 1.37. Summary of the activation of M0 to M1 and M2 and the cytokines secreted by them.

Abbreviations: M0: Unactivated macrophages. M1: Activated macrophages. M2: Activated macrophages. Th: T Helper. APC: Antigen-presenting cells. LPS: Lipopolysaccharide. IFN: Interferon. TNF: Tumor necrosis factor. Inducible nitric oxide synthase. IL: Interleukin. CCL2: C-C motif chemokine ligand 2 or Monocyte chemoattractant protein-1 (MCP-1). PGE2: Prostaglandin E2. TGF: Transforming growth factor. YM1: Chitinase-like protein. Created with https://www.biorender.com/

In order to evaluate the potential capacity of the released drugs to decrease inflammation, the release media in which the coated prostheses were incubated were added to *in vitro* cultures of activated macrophages (M1), and the secretion of representative cytokine was measured. The cytokines analyzed were TNF-α, a pro-inflammatory cytokine secreted by M1 macrophages and involved in acute inflammation [7,353,354]; CCL-2, involved in the regulation of monocytes and macrophages migration to the implantation site, as well as in the fusion of macrophages for the formation of foreign body giant cells (FBGCs) [355,356]; and PGE-2, a pro-inflammatory cytokine secreted by synovial lining macrophages and fibroblast-like synoviocytes and considered a relevant marker of joint inflammation, playing a role in vasodilation, vascular permeability and pain [357,358].

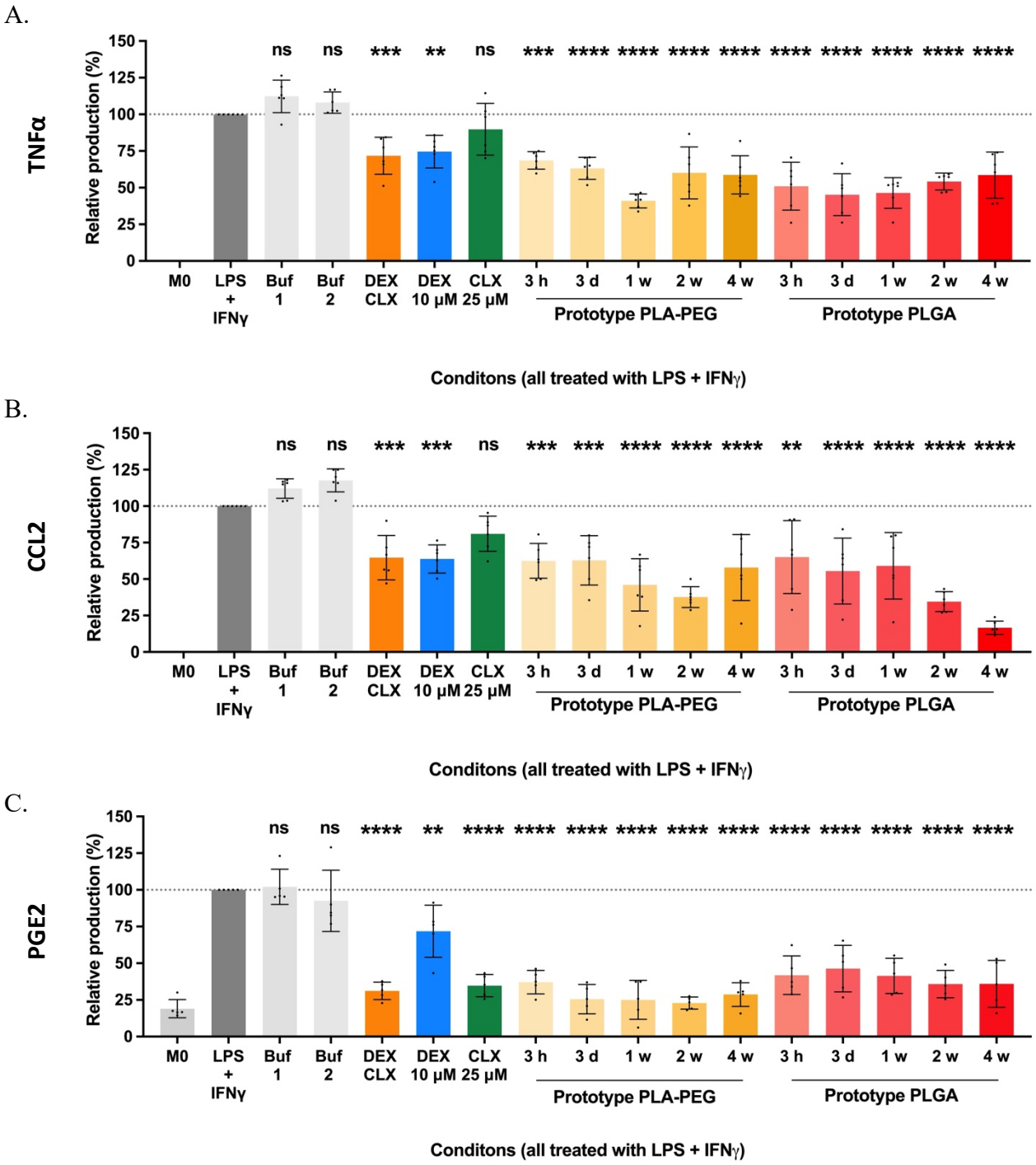

Figure 1.38. TNFα (A), CCL2 (B), and PGE2 (C) secretion by human primary macrophages exposed to media where Prototype PLA-PEG and Prototype PLGA, both loaded with CLX and DEX, were incubated for specific periods of time. Analysis was carried out by ELISA.

Abbreviations: M0: Unactivated macrophages. Neg: Negative. Pos: Positive. Buf: Buffer. PLA-PEG: poly(lactic acid)-poly(ethylene glycol) di-block co-polymer. h: hour. d: days. w: weeks. PLGA: Poly(lactic-co-glycolic) acid. LPS: Lipopolysaccharide. IFN: Interferon. TNF: Tumor necrosis factor. CCL2: C-C motif chemokine ligand 2 or Monocyte chemoattractant protein-1 (MCP-1). PGE2: Prostaglandin E2. A significant comparison was performed using an ordinary one-way ANOVA followed by Tukey's multiple comparison tests between LPSy and the rest of the groups. p-values < 0.05 were considered statistically significant (*). Also, (**) if *p*-value < 0.01, (***) if *p*-value < 0.001, (****) if *p*-value < 0.0001. ns: not significative. Columns represent the mean ± standard deviation (n ≥ 5).

The anti-inflammatory capacity of DEX and CLX released from the bilayer drug-releasing polymer coatings to regulate cytokine secretion was assessed by ELISA, using the free drugs as positive control. Encouragingly, comparable levels of anti-inflammatory activity were observed between the free drugs and the drugs released from the coatings across various temporal points. Selection of these time points was based on the predominant effect of DEX at early time points, and of CLX at later time points.

DEX and CLX released from the polymer coatings of Prototype PLA-PEG and Prototype PLGA at all time points were able to prevent the secretion of TNFα and CCL2 from human macrophages (Figure 1.25A and 1.25B). This supports the synergistic effect of both drugs to tackle inflammation but shows the bigger influence role of DEX. On the other hand, PGE2 secretion was mainly reduced with CLX, as well as with the released drugs with independence of the time point analyzed (Figure 1.25C). This could be expected as PGE2 is a product of the COX2 inflammatory pathway [31]. These findings demonstrate that drugs encapsulated within the coatings and subsequently released at distinct time points maintained their initial anti-inflammatory efficacy, regardless of the duration of entrapment within the coating or the time of their release.

4.5 CONCLUSIONS

In this chapter, we have successfully developed a bilayer polymer coating technology that enables the sequential release of DEX and CLX from a meniscus prosthesis to address post-implantation inflammation. Two prototypes, Prototype PLA-PEG, and Prototype PLGA, were selected from a large screening based on their capacity to provide the desired release kinetics, with DEX released over 1-4 weeks to control acute inflammation and CLX providing sustained anti-inflammatory effects over 6-9 months. Prototype PLGA exhibited faster degradation, resulting in a more sustained and controlled CLX release, while Prototype PLA-PEG showed slower degradation, increasing the tortuosity and delaying CLX release. Although Prototype PLA-PEG had a higher drug-loading capacity, Prototype PLGA provided more consistent and reproducible drug release profiles and demonstrated superior compatibility with the bilayer system. Both prototypes were biocompatible, non-toxic, and preserved the anti-inflammatory activity of the drugs.

Ultimately, Prototype PLGA was selected for further optimization due to its favorable degradation kinetics, which do not limit the interaction of the CLX layer with the release buffer. Its ability to achieve the desired release profile also supported its advancement to the polymer coating's optimization phase. During this next phase, the coating system was transferred from square-shaped PCU implants to actual meniscus prostheses for a representative animal model.

CHAPTER 2

Optimizing the adhesion of the drug-releasing bilayer polymer coating to a meniscus prosthesis

5 OPTIMIZING THE ADHESION OF THE DRUG-RELEASING BILAYER POLYMER COATING TO A MENISCUS PROSTHESIS

This work has been done in collaboration with Carmen Bao Varela, Ph.D (Universidade de Santiago de Compostela, Spain), Rebeca Bouza Padín, Ph.D. (Universidad de Coruña, Spain), Paulina Núñez Bernal, Ph.D and Riccardo Levato, Ph.D (University Medical Center Utrecht, The Netherlands), Giuseppe Anzillotti, M.D. and Elizaveta Kon, M.D (Humanitas Research Hospital, Italy), and Emmanuel Loeb, DVM (Patho-Logica, Israel).

5.1 ABSTRACT

As shown in Chapter 1, a bilayer drug-releasing polymer coating was engineered to release two anti-inflammatory drugs, celecoxib (CLX) and dexamethasone (DEX). The drug-releasing polymer-coated meniscus prostheses face substantial mechanical forces within the knee cavity, needing strong adhesion between the polymer coating and the polycarbonate urethane (PCU) prosthesis to prevent delamination. Therefore, optimizing the adhesion of the bilayer coating to the prosthesis was a critical step in this work.

This chapter presents a novel approach using an ethyl-2-cyanoacrylate (ECA) adhesive layer to enhance adhesion. This approach was compared to other adhesion-enhancing techniques, such as femtosecond-pulse laser physical modification, polydopamine (PDA) coating, and plasma treatment. The dynamic mechanical analysis (DMA) showed that the use of ECA to improve adhesion was successful in terms of the mechanical properties, such as storage modulus (G'), loss modulus (G''), and elastic modulus (E) as well as in terms of maintaining an optimal viscoelastic balance (tan δ). To adapt the coating to the sheep meniscus prosthesis, the concentration of the CLX-releasing PLLA/PCL layer was adjusted, and the dip-coating technique was adjusted. An *ex vivo* bioreactor study simulating knee joint forces revealed that mechanical stimulation altered the polymer coating distribution and accelerated drug release without significant damage to the coating. Ethylene oxide (ETO) sterilization was chosen to preserve the integrity of both the drugs and the polymer. Finally, preliminary *in vivo* evaluations *in sheep* demonstrated that the ECA-coated prostheses outperformed the uncoated versions, showing great promise for long-term meniscus substitution.

5.2 INTRODUCTION

The knee joint is subject to intense and constant mechanical stress due to its load-bearing role in the body. It undergoes continuous compression, tension, and shear forces, especially during walking, running, and jumping. This stress is particularly pronounced in the synovial cavity, where joint movement and pressure fluctuations occur continuously during movement. Synovial fluid, which lubricates the joint, is in constant motion, and the surrounding articular cartilage undergoes significant deformation to absorb shock [359]. These factors combine to create a highly dynamic and challenging environment for our meniscus prosthesis and the drug-releasing polymer coatings.

As these forces are directly transferred to the meniscus prosthesis, it is critical that the prosthesis and the drug-releasing polymer films developed in Chapter 1 maintain a solid and durable attachment. Poor adhesion between the prosthesis surface and the coating could result in film delamination, which could severely compromise its functionality. This delamination would expose the underlying prosthetic surface, limiting the anti-inflammatory effects of the polymer coating and leading to further issues, such as polymer films sticking out and damaging articular cartilage. Moreover, in Chapter 1, field emission scanning electron microscopy (FESEM) images of sagittal cuts of the coated prostheses revealed suboptimal interaction between the prosthesis surface and the applied coatings. This observation highlights the need to improve adhesion between the polymer film and the prosthesis to prevent film detachment. To address this, various surface modification techniques can be employed. Current methods for surface modification have demonstrated significant potential in enhancing the interface between materials, particularly in biomedical applications [360,361]. However, polycarbonate urethane (PCU) composing the meniscus prosthesis, while biocompatible and durable, presents unique challenges due to its hydrophobicity, sensitivity to organic solvents, and the need to maintain geometrical wedge shape [32,33]. This makes traditional modification techniques, such as sand-blasting [34], less effective, necessitating novel approaches to enhance surface interactions.

Moreover, the promising *in vitro* results demonstrating the anti-inflammatory activity of the drugs released from the prosthesis needed to be evaluated in environments like the actual conditions expected in the knee cavity, which are influenced by gait. Bioreactors have been used in the orthopedic field to simulate these conditions while avoiding or reducing the need for *in vivo* tests to validate the technologies [362,363]. Furthermore, animal experiments must be comparable to and transferable across species to facilitate the translation of findings from animal models to humans. Various animal models, including goats, sheep, dogs, and pigs, have been utilized in orthopedic research to evaluate meniscus shape and function restoration. Among these, sheep have been historically the most widely used due to their anatomical similarities to the human meniscus, making them an ideal model for meniscal research. Sheep provide the closest match in size, structure, and biomechanical properties, making them highly relevant for preclinical testing [364–366].

In response to these challenges, in this chapter, four distinct surface modification strategies were explored to enhance the adhesion of drug-releasing polymer films on PCU prostheses: physical modification using femtosecond (fs)-pulse laser, oxygen plasma treatment, polydopamine (PDA) coatings, and ethyl cyanoacrylate (ECA) as an adhesive. Laser-based

modifications have been widely described to modify the topology and surface of prostheses to improve properties such as cell adhesion [367,368]. Oxygen plasma treatment is a widely used technique in material science to introduce functional groups that promote better coating adhesion [369]. Similarly, PDA, inspired by the adhesive properties of mussel proteins, has emerged as an effective bio-coating that enhances material surfaces for medical applications [370]. Finally, ECA, a fast-curing adhesive, is known for creating robust bonds and improving the interaction between coatings and polymer surfaces, making it a viable candidate for enhancing the attachment strength of drug-polymer layers [371].

This study assessed the indicated surface modification techniques, macroscopically and microscopically, to evaluate the adhesion between the polymer coatings and the meniscus prosthesis. This assessment led us to identify the most promising approaches in terms of modulus and engineering properties, ensuring they closely mimicked the mechanical needs of natural menisci. Additionally, the polymer coating synthesis method was optimized to fit the sheep meniscus prosthesis while ensuring that the release kinetics of the drug remained consistent. Finally, the selected adhesion method and optimized coating were tested in simulated synovial fluid using a bioreactor simulating gait, followed by an explorative three-month *in vivo* evaluation in sheep to confirm its performance under physiological conditions.

5.3 Materials and Methods

5.3.1 Materials

The drugs dexamethasone (DEX) and celecoxib (CLX) were supplied by Acofarma (Madrid, Sapin) and Sigma-Aldrich (Missouri, USA), respectively. The polymers used PLGA, PLLA, and PCL were acquired from Evonik Industries (Darmstadt, Germany). Dopamine hydrochloride (HCl), sodium azide (NaN_3), Tris-hydrochloride (Tris-HCl), and bovine serum albumin (BSA) were purchased from Sigma-Aldrich (Missouri, USA). Medical grade ethyl cyanoacrylate (ECA, Loctite 4061), hyaluronic acid (HA) (M_W = 1.3MDa), and acetone were obtained from Henkel (Düsseldorf, Germany), Bloomage Biotechnology Corporation Limited (Beijing, China) and Fisher chemicals (New Hampshire, USA), respectively. Dichloromethane (DCM), acetonitrile (ACN), chlorohydric acid (HCl), and sodium hydroxide (NaOH) were distributed by Scharlau (Barcelona, Spain). Phosphate saline buffer (PBS), Tween 80® (T80), trifluoracetic acid (TFA), Sodium azide (NaN_3), and methanol (MeOH) were supplied by Scientific (Nottingham, England), Merck (Darmstadt, Germany), Sigma-Aldrich (Missouri, USA) and VWR Chemicals (Pennsylvania, USA), respectively. Acetone was obtained from Fisher Chemicals (New Hampshire, USA). The sheep meniscus prostheses and the polycarbonate urethane (PCU) samples were facilitated by Active Prosthesis (Israel).

5.3.2 Production of bilayer drug-releasing polymer coatings

To prepare the polymer-drug solutions, appropriate amounts of each drug, DEX or CLX, were dissolved in acetone and DCM, respectively [270–272]. LMW-PLGA (PLGA 50:50; MW = 6.9 kDa) was dissolved to their final concentration using a solution of DEX of 5 mg/mL. Regarding CLX-releasing polymers, combinations of PCL (IV=0.39 dL/g; MW ~32 kDa) and

PLLA (IV=2.9 dL/g; MW ~210 kDa) were dissolved to their final concentrations using a solution of CLX of 30 mg/mL. The meniscus prostheses, held in place by a needle, were immersed in the polymer-CLX solution and immediately withdrawn, allowing 10 min for drying. The cycle was repeated a total of 3 times. After an additional 3 hours of drying, 5 new immersion cycles were performed, in this case in the polymer-DEX solution and with a drying time of 15 minutes between cycles. Finally, the organic solvent was allowed to evaporate for 72 hours. Also, when polymer films were crafted, films were prepared by solvent casting. 70 µL of polymer-drug solutions were then cast on square-shaped meniscus prostheses (made of PCU) of 0.7 x 0.7 x 0.3 cm. The organic solvent was allowed to evaporate for 1 hour at room temperature. The resulting drug-loaded polymer films were then vacuum-dried for at least 24 hours.

5.3.3 Drug release evaluation

Drug release studies were performed in agitation (450 rpm) at 37 °C in 10 mL of PBS Tween®80 1% (w/v) to ensure sink conditions. The amount of drug (DEX and CLX) released was quantified by reverse-phase ultra-performance liquid chromatography (UPLC) with a TUV detector at 239 nm using a column Kinetex® 1.7 µm C18 100 Å, LC Column 50 x 2.1 mm acquired from Phenomenex (Torrance, CA, USA), maintaining the samples at 20 °C in a Waters Acquity H-Class UPLC system (Waters, Milford, USA) [273]. The mobile phase consisted of A: deionized H_2O acidified with TFA 0.1% (v/v) and B: ACN acidified with TFA 0.1% (v/v) pumped with a flow rate of 0.1 mL/min. The injection volume was 5 µL, and the column oven temperature was set to 40°C. To control the UPLC/UV system as well as for data acquisition and processing, EMPOWER software was used. To quantify the amount of DEX and CLX, a calibration curve, ranging from 1 to 100 ppm was used. The curves had a correlation coefficient (R^2) of 1 for DEX, and 0.9999 for CLX (n=22). The validation procedure was carried out according to the ICH guidelines [273–276]. The limit of detection (LOD) and quantification (LOQ) were calculated directly from the calibration plots. LOD and LOQ were calculated as 3.3σ/S and 10σ/S, respectively, where σ is the standard deviation of the intercept and S is the slope of the calibration plot [276]. The values were LOD = 1.73, and LOQ = 5.25 for DEX, LOD = 0.3, and LOQ = 0.92 for CLX.

5.3.4 Drug loading determination

PCU prostheses coated with drug-releasing polymers were immersed in a mixture of DCM/acetone 3/2 (v/v) for up to 24 hours to ensure polymer dissolution. Samples, typically 200 µL, were then transferred to Eppendorf tubes containing 800 µL methanol and centrifuged at 10,000 rpm for 20 min. 200 µL of supernatant were further diluted with 800 µL MeOH:H_2O 65:35 (v/v) and the concentration of drug was quantified by UPLC with a TUV detector at 239 nm using a column Kinetex® 1.7 µm C18 100 Å, LC Column 50 x 2.1 mm acquired from Phenomenex (Torrance, CA, USA), maintaining the samples at 20 °C in a Waters Acquity H-Class UPLC system (Waters, Milford, USA) [273]. The mobile phase consisted of A: deionized H_2O acidified with TFA 0.1% (v/v) and B: ACN acidified with TFA 0.1% (v/v) pumped with a flow rate of 0.1 mL/min. The gradient was from 25% to 60% of B in 6.5 min, and 6 min from 60% to 25% of B. The injection volume was 5 µL, and the column oven temperature was set to 40°C. To control the UPLC/UV system as well as for data acquisition and processing,

EMPOWER software was used. To quantify the amount of DEX and CLX, a calibration curve, ranging from 1 to 100 ppm was used. The release buffer had no matrix effect on the quantification of the drugs. The curves had a correlation coefficient (R^2) of 1 for DEX, and 1 for CLX (n=8). The values were LOD = 0.383, and LOQ = 1.162 for DEX, and LOD = 0.187, and LOQ = 0.567 for CLX.

5.3.5 Field-emission scanning electron microscopy (FESEM)

Drug-releasing polymer coatings were sputter coated with a layer of iridium and imaged in a Zeiss UltraPlus analytical FESEM with a beam voltage of 3 kV and a magnification ranging from 500 to 1,000X for the analysis of the surface of the coatings. Also, Zeiss EVO analytical FESEM with a beam voltage of 20 kV and magnification ranging from 60X to 5,000X was used to measure the coating thickness and analyze the side profile upon degradation after the sagittal cut.

5.3.6 Functionalization of the prosthesis surface

The surfaces of the prostheses were physically and chemically modified to investigate their effect on the interaction between the prosthesis and the polymeric layers of the coating.

5.3.6.1 Physical modification: Treatment with femtosecond-pulse laser

A femtosecond (fs) pulse laser was used to irradiate the prostheses with a titanium-sapphire (Ti:Za) laser emitting at 800 nm, with a pulse duration of 60 fs and a fixed repetition rate of 1 kHz. Thus, grids and holes aiming to improve interaction were created on the surface of the PCU prostheses.

5.3.6.2 Chemical modification: Oxygen plasma treatment

Plasma treatment was performed with a Diener Electronic Atto-BLS plasma surface treatment machine (Ebhausen, Germany). The chamber's O2 influx was set at 1 bar. PCU prostheses were processed for 7 minutes at different powers in a controlled O_2 atmosphere (0.4 bar).

5.3.6.3 Chemical modification: Polydopamine (PDA) coating

Polymerization parameters were optimized for a 7-minute pre-treatment of the PCU prostheses with oxygen plasma and direct immersion in an aqueous solution of 2 mg/mL of dopamine in Tris-HCl buffer 10 mM at pH 8.5 for 24h under mild shaking.

5.3.6.4 Chemical modification: Ethyl-2-cyanoacrylate (ECA) adhesive layer

The instant adhesive ECA Loctite®4061 was dissolved in acetone at a previously optimized concentration of 40% (w/v). Subsequently, prostheses were submerged in the ECA

dissolution immediately before their functionalization through the procedure of the double-layer drug-releasing polymer coatings.

5.3.7 Dynamic light scattering (DLS)

PDA polymerization was stopped at different time points by the addition of HCl 4M to acidify the solution samples, reducing the pH to 2. The mean particle size (Z-average) and polydispersity index (PDI) of the non-diluted samples were characterized by DLS. These properties were analysed using a Zetasizer® Pro (Malvern Panalytical Ltd.; Malvern, UK). Each analysis was conducted in triplicate at 25ºC with a backscatter angle of detection.

5.3.8 Macroscopic evaluation

Macroscopic evaluation included a bending test, consisting of manually bending the prostheses to assess their flexibility and the adhesion of the coatings, and a scratch test, using tweezers to separate the drug-releasing polymer films deposited on the surface of the prostheses. Both tests were conducted under dry and wet conditions. For the wet conditions, the functionalized prostheses were immersed in the aqueous buffer for at least 24 hours before performing the tests. In all cases, this evaluation was qualitative, meaning that the effort required to detach the drug-polymer films was subjectively assessed.

5.3.9 Dynamic mechanical analysis (DMA)

PCU prostheses of 1.8 x 0.8 x 0.3 cm were placed on a DMA 7 analyzer (PerkinElmer, USA) to carry out the dynamic mechanical measurements by a three-point bending test. This analysis was conducted within a temperature range of -80ºC to 100ºC and a heating rate of 2 ºC/min in an inert gas medium with a flow rate of 40 mL/min. The test continued until fracture or maximum deflection occurred, allowing for the determination of the storage modulus storage modulus (G'), loss modulus (G''), elastic modulus (E), and tan delta (tan δ) of the prosthesis. Data obtained at 37ºC were evaluated using GraphPad Prism 9 software (GraphPad Software Inc., San Diego, USA). The statistical analysis of Welch's t-test was utilized to compare the experimental groups to the ECA prototype, which is considered the most promising one.

5.3.10 Simulated synovial fluid (SSF) preparation

SSF was prepared to simulate the protein concentration, salts, viscosity, and molecular interactions expected in an osteoarthritic knee. Based on the literature [372–381], 20 g/L of BSA, 1.5 g/L of HMW HA, azide 0.01% (w/v), and sterile PBS were used. The required amounts of these components were mixed under mild magnetic stirring until complete dissolution was achieved. Afterward, the pH of the solution was adjusted to 7.4 with NaOH 1N (VWR Chemicals). Additionally, Tween 80 0.05% (v/v) was added to increase drug solubility.

5.3.11 Solubility of DEX and CLX in SSF

An excess of the drugs (DEX and CLX) was incubated in agitation (700rpm) for 24 hours in 1 mL of SSF supplemented with concentrations of Tween® 80 ranging from 0 to 1% (v/v). Then, samples were centrifuged, and the concentration of the drug in the supernatant was quantified by ultraperformance liquid chromatography (UPLC). The solubility of DEX and CLX in each simulated synovial fluid (SSF) is not shown in this thesis.

5.3.12 *Ex vivo* simulation: Bioreactor test

The bioreactor test was performed at the University Medical Center Utrecht (Utrecht, Netherlands) to evaluate the stability of the bilayer drug-releasing polymer coating over PCU prosthesis under dynamic mechanical stimulation. A custom-made bioreactor system (LifeTec BV., The Netherlands) was employed. This system combines compression and shearing motions to mimic the human gait better, thus simulating the conditions our meniscus prostheses would experience in the knee cavity. Briefly, cylindrical PCU prostheses (total area 2.31 cm^2, radius 3.75 mm and 6 mm height) were fixed within custom 3D printed polylactic acid (PLA) holders (n=6). Samples were then subjected to a human gait-mimicking protocol for 2 hours of loading per day at a frequency of 1 Hz, using flat-ended stainless-steel pistons controlled by a linear rotary actuator (SMAC LAR300-050-72-2F). The loading pattern consisted of a sequence of 250 µm axial compression motion combined with a sliding movement of 3 mm to each side in a predefined timing. Daily loading was performed for 21 days at 37ºC, with the samples submerged in 8mL of an SSF. Control samples were cultured statically in the same medium volume inside a 50mL Falcon tube. On days 3, 7, 10, 14, 17, and 21, the medium of all samples was collected for analysis, stored at -20ºC, and replenished with fresh medium. On days 3, 7, 14, and 21, one sample per condition (mechanically stimulated and static) was collected for macroscopic and microscopic evaluation, and the last 3 samples were collected on day 21 (Figure 2.1).

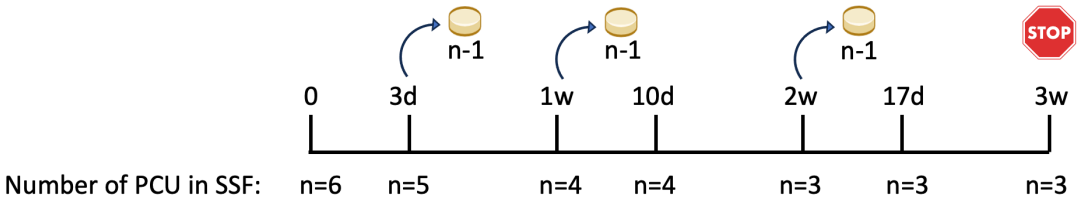

Figure 2.39. Design of experiment scheme of the bioreactor test.

Abbreviations: PCU: Polycarbonate urethane. SSF: Simulated synovial fluid. Created with https://www.biorender.com/

5.3.13 *In vivo* evaluation: Sheep surgical procedure

All surgical procedures were performed under aseptic conditions. The skin was prepared aseptically, and an Ioban film was applied following standard draping with disposable drapes. A medial incision to the stifle joint was made with the knee flexed at approximately 90° of flexion. To enhance access to the medial meniscus, a 2-4 mm thick bone block, including the proximal origin of the medial collateral ligament (MCL), was detached from the femoral condyle surface using an oscillating saw to perform a 30° osteotomy. An osteotome was then

used to expose the joint and the medial meniscus further. Before complete detachment of the bone fragment, a hole was pre-drilled through the fragment and femoral condyle to facilitate fixation with a cortical screw later in the procedure. The cranial insertion of the MCL and its deep fibers connecting the MCL to the medial meniscus was then detached, allowing access to the medial meniscus.

5.3.13.1 Meniscectomy procedure

Meniscectomy was initiated at the posterior root of the medial meniscus, with a peripheral incision using a scalpel, enabling anterior subluxation of the tibial plateau. This provided easier access for the progressive detachment of the meniscus-capsular fibers from posterior to anterior. The procedure was completed by detaching the anterior root from the inferior tibial surface, and any remnants of the medial meniscus were removed using a Luer bone rongeur to create sufficient space for prosthesis positioning.

5.3.13.2 Prosthesisation procedure

For the groups receiving the NUsurface prothesis, two tunnels were drilled through the tibia at the natural insertion points of the anterior and posterior meniscal roots to accommodate the prosthesis's anchoring extensions. The posterior tunnel was drilled first using a guiding pin and a specially designed drill guide, with the distal entry point positioned posterior to the extensor digitorum longus tendon. The anterior tunnel was drilled similarly, with the guiding wire placed distally to the extensor digitorum longus tendon and positioned at the native anterior meniscal root. The meniscal prosthesis was inserted into the joint and through the drilled tunnels using custom instruments and was secured to the tibia by screws and fixation fibers at the ends of its ligament-like anterior and posterior extensions. The MCL bone block was repositioned and fixated to the medial femoral condyle with a cortical screw, applied in full knee extension. Tensile force was applied to the anterior and posterior extensions to ensure firm fixation of the meniscal prosthesis to the tibial surface.

5.3.13.3 Post-surgical care and inflammatory induction

Following meniscectomy or prosthesisation, the joint was flushed with saline, and the incision was closed in layers using polydioxanone (PDS) suture material for fascia and 2-0 nylon with staples for skin closure. Postoperatively, an adhesive bandage was applied to cover the surgical site. In all groups, intra-articular inflammation was induced postoperatively by injecting lipopolysaccharide (LPS) (1 µg LPS from *E. coli* diluted in PBS) into the target knee [382]. The aim was to evaluate whether the bioactive prosthesis, loaded with DEX and CLX, could reduce intra-articular inflammation.

5.3.13.4 Postoperative monitoring

The clinical health of the sheep and the intra-articular inflammation were evaluated at various time points. Body weight was measured, and limping was assessed.

5.3.13.5 Final evaluation and sacrifice

At 3 months post-surgery, sheep were euthanized for final evaluation. X-rays were taken of the index knee before euthanasia with potassium chloride.

5.3.14 *In vivo* evaluation: Histology analysis

The samples were initially fixed in 70% ethanol and sent to Patho-Logica for further processing. The samples were transferred to 4% formaldehyde for an additional 48 hours of fixation. The tissues were then placed in Rapid-Cal decalcification solution for 28 days to ensure complete decalcification. Following decalcification, the tissues were trimmed, placed in embedding cassettes, and processed using standard procedures for paraffin embedding.

5.3.14.1 Slide preparation

Paraffin-embedded tissue sections, 4 microns thick, were cut and mounted onto glass slides. The slides were stained with Hematoxylin and Eosin (H&E) to assess general tissue morphology and with Toluidine Blue (TB) to evaluate cartilage characteristics.

5.3.14.2 Histological evaluation

All prepared slides were subjected to histological evaluation to assess tissue morphology and integrity.

5.3.14.3 Light microscopy and imaging

Microscopic images were captured using an Olympus BX60 microscope (serial No. 7D04032) equipped with an Olympus DP73 camera (serial No. OH05504). Images were taken at a magnification of 4x to document and analyze the histological findings.

5.3.14.4 Grading score system

a) Articular cartilage structure (Hematoxylin and Eosin, H&E):

0 Normal.
1 Undulating articular surface but no fibrillation.
2 Minimal/mild superficial fibrillation (61/10 of the articular cartilage thickness) involving < half of the plateau.
3 Minimal/mild superficial fibrillation (61/10 of the articular cartilage thickness) involving P half of the plateau.
4 Fibrillation/clefts/loss of articular cartilage involving superficial 1/3 of articular cartilage in < half of the plateau.
5 Fibrillation/clefts/loss of articular cartilage involving superficial 1/3 of articular cartilage in P half of the plateau.
6 Fibrillation/clefts/loss of articular cartilage involving superficial 1/3 to 2/3 of articular cartilage in < half of the plateau.

7 Fibrillation/clefts/loss of articular cartilage involving superficial 1/3 to 2/3 of articular cartilage in P half of the plateau.
8 Fibrillation/clefts/loss of articular cartilage involving >2/3 depth of articular cartilage in < half of the plateau.
9 Fibrillation/clefts/loss of articular cartilage involving >2/3 depth of articular cartilage in P half of the plateau.
10 Fibrillation/clefts/loss of articular cartilage to subchondral bone.

b) Toluidine blue staining intensity:

0 Normal.
1 Loss of staining in 6 superficial half of articular cartilage and involving < half of the plateau.
2 Loss of staining in 6 superficial half of articular cartilage and involving P half of the plateau.
3 Loss of staining in > half of articular cartilage thickness and involving < half of the plateau.
4 Loss of staining in > half of articular cartilage thickness and involving P half of the plateau.

c) Chondrocyte clones:

0 None.
1 1–5 clones.
2 6–10 clones.
3 11–15 clones.
4 >15 clones.

d) Fibrocartilage:

0 None.
1 Fibrous tissue/fibrocartilage covers or replaces <1/3 of articular cartilage of plateau.
2 Fibrous tissue/fibrocartilage covers or replaces 1/3 to 2/3 of articular cartilage of plateau.
3 Fibrous tissue/fibrocartilage covers or replaces >2/3 of articular cartilage of plateau.

e) Osteophyte:

0 None.
1 Axial or abaxial osteophyte present.
2 Axial and abaxial osteophytes present.

f) Subchondral bone:

0 Normal or decreased subchondral plate thickness.
1 Mild increase in subchondral bone thickness involving < half of plateau.
2 Mild increase in subchondral bone thickness involving P half of plateau.
3 Moderate increase in subchondral bone thickness involving < half of plateau.

4 Moderate increase in subchondral bone thickness involving P half of plateau.
5 Marked increase in subchondral bone thickness involving < half of plateau.
6 Marked increase in subchondral bone thickness involving P half of plateau.

5.4 RESULTS AND DISCUSSION

The aim of this chapter is to optimize the polymer coating for improved adhesion to the PCU prosthesis by investigating and comparing four distinct surface modification techniques. The chapter also focuses on adapting the polymer coating to the prosthesis's *in vivo* geometry, evaluating its performance in a bioreactor under simulated mechanical conditions, and conducting *in vivo* testing in a representative large-animal model. Achieving enhanced adhesion is critical to maintaining prosthesis stability under the high mechanical stresses experienced in the knee cavity. The surface modification techniques explored include physical modification using a laser, oxygen plasma treatment, PDA coatings, and ECA adhesives.

The study followed a structured approach, which involved:

1) The evaluation of surface modifications, both macroscopically and microscopically, to determine their effects on the adhesion between polymer coatings and the PCU meniscus prosthesis.
2) The quantitative analysis of the moduli and other mechanical properties of the modified surfaces ensures that they mimic the biomechanical requirements of natural menisci.
3) The optimization of the polymer coating synthesis method to ensure compatibility with the modified PCU surface while maintaining consistent drug release kinetics.
4) The ex vivo analysis of the functionalized prosthesis in the simulated synovial fluid to evaluate their performance in a dynamic environment.
5) The *in vivo* evaluation of the most promising prototype in the sheep model to assess performance under physiological conditions.

5.4.1 Physical modification of PCU prosthesis: Treatment with femtosecond-pulse laser

Previous studies have demonstrated that surface modification of materials with periodic micro- or sub-micrometer structures can enhance mechanical, biological, and optical properties [383]. Recent research has also emphasized the potential of nature-inspired surface patterns (like lotus leaves) to improve surface characteristics, particularly for biomedical applications [384]. Depending on the material, surface roughness modification has either increased or decreased wettability and cell adhesion [385–387]. Both macro and micro-scale topographies are essential in prosthesis stability and tissue integration. Macro-topographies (ranging from microns to millimeters) contribute to long-term fixation, while micro-topographies (on the micron scale) directly influence cell adhesion and proliferation. Thus, by increasing the available surface area, textured surfaces could create additional contact points, which may be advantageous when applying a polymer layer to a prosthesis. This increase in points capable of

surface interaction was hypothesized to improve the adhesion between the polymer coating and the prosthesis, mainly when applied to PCU prostheses.

Laser-based surface modification technologies offer precise control over the roughness and structure of materials at multiple scales, including macro-, micro-, and nanoscales, making them particularly useful for biomedical applications [35]. In this context, fs-pulse lasers have gained popularity due to their ability to minimize thermal effects while creating complex surface geometries that enhance cellular activity [36].

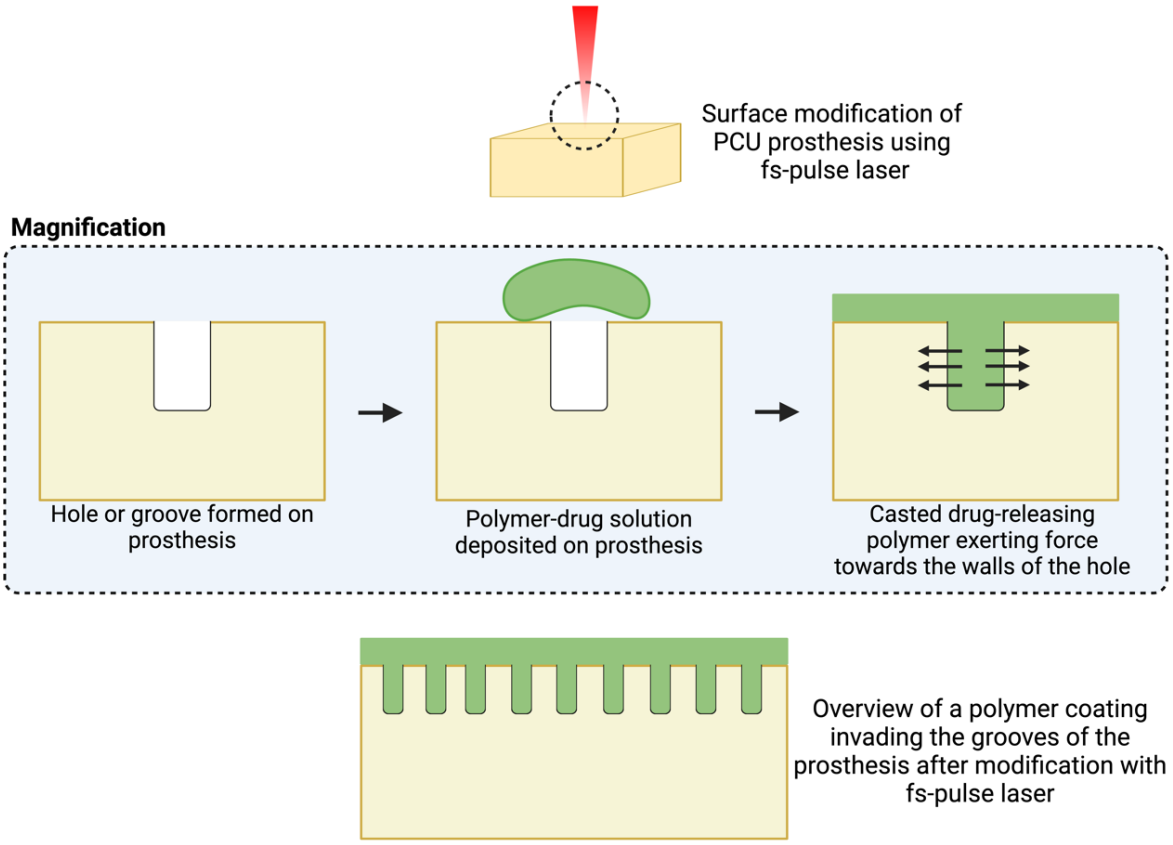

Figure 2.40. Schematic representation of how physical modification of PCU surface using fs-pulse laser is hypothesized to improve the adhesion of the polymer coating to the prosthesis.

Abbreviations: PCU: Polycarbonate urethane. fs: Femtosecond. Created with https://www.biorender.com/

In this study, surface modifications with different patterns—specifically dots and lines—were applied to PCU square-shaped prostheses using an fs-pulse laser (Figure 2.3). This approach aimed to modify roughness and increase surface area, providing more zones where the polymer coating could migrate during casting and potentially enhancing adhesion. The laser provided fine control over various parameters, such as energy input, the proportion of surface area modified, pattern geometry, hole separation, and exposure time (Table 2.1).

The first surface modification investigated aimed to create a high density of holes on the prosthesis surface (Figure 2.4A). However, FESEM imaging revealed inconsistent results. Sagittal cut images showed a substantial gap between the polymer coating and the prosthesis surface, indicating that the desired improvement in adhesion was not achieved. Furthermore,

while some holes were visible in sagittal cross-sections (Figure 2.4B, green square), confirming whether the polymer coating had effectively penetrated them was difficult.

The second surface modification aimed to create a lower density of holes on the prosthesis surface (Figure 2.4C). FESEM images showed that the holes were not visible from the lateral view of the sagittal cut, even at a magnification of 200x (Figure 2.4D). This could be attributed to the low density of holes, making it challenging to align the sagittal cut with their precise locations. As a result, it was impossible to confirm whether the polymer coating effectively penetrated these holes, increasing the number of contact points with the prosthesis surface. However, Figure 2.3D suggests that the overall adhesion to the hole-modified prosthesis was improved compared to prosthesis with a high density of holes.

The third surface modification involved the creation of a grid-shaped pattern on the PCU prosthesis, hypothesizing that the laser-engraved lines could retain a more significant amount of polymer coating compared to small holes, thereby improving adhesion (Figure 2.4G). FESEM images revealed that, in this case, the polymer efficiently penetrated the grooves (Figure 2.4H), demonstrating a significant improvement in the interaction between the coating and the prosthesis compared to other modifications. Thus, the initial hypothesis was further supported by the depth of the laser-engraved channels, which was approximately 65 µm (n=8). As shown in Figure 2.4K, deeper channels could accommodate more polymer, potentially leading to even better adhesion.

Table 2.9. Types of modifications and parameters used for the fs-pulse laser set-up.

Modification	Separation between centers (µm)	Laser energy (mJ)	Number of modifications per sample
High density of holes	200	57	2900
Low density of holes	200	57	1100
Grid	200	57 (Speed 1 mm/s)	87

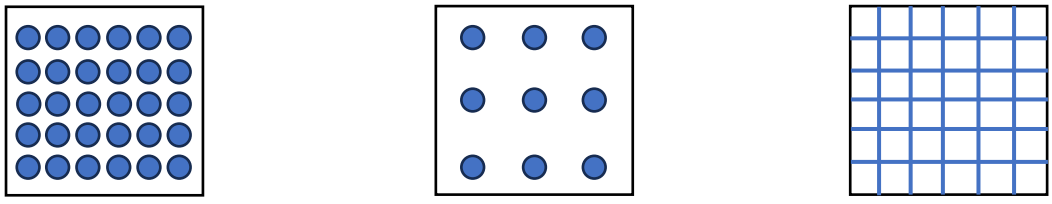

Figure 2.41. Theoretical patterning of the fs-modified PCU square-shaped prosthesis.

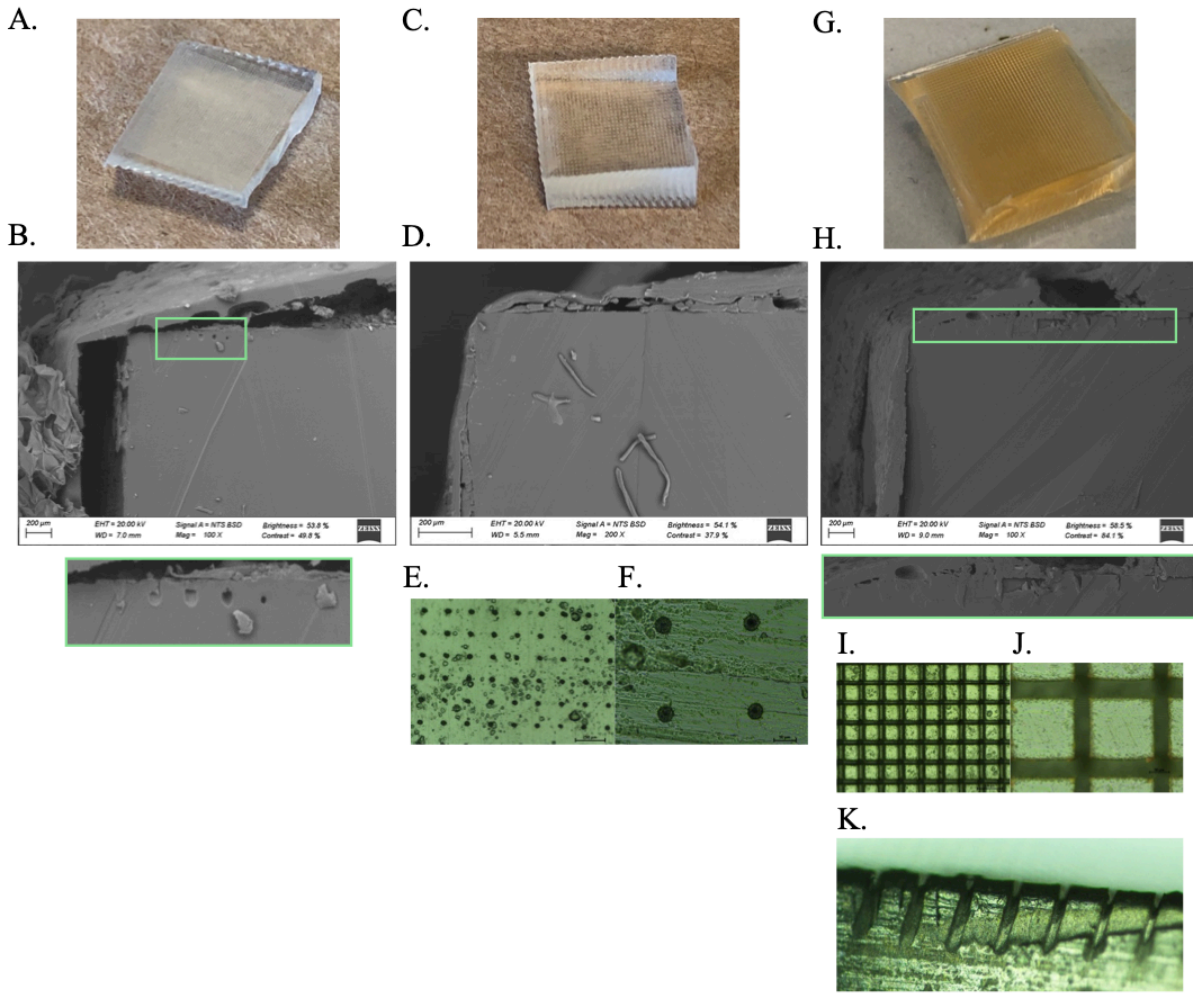

Figure 2.42. Macroscopic aspect of physically modified PCU prosthesis with fs-pulse laser with different patterns: high density of pores (A), low density of pores (C), and grid (D). FESEM images of sagittal cut showing the bilayer polymer coating interaction with physically modified PCU prostheses with different patterns: high density of pores (B), low density of pores (D), and grid (H). Optic microscopy images of the physically modified PCU prosthesis surface using a Nikon MM-400 Metrological Microscope 5x (E and I) and 20x (F and J). Optic microscopy image of the side of physically modified PCU prosthesis using Nikon MM-400 Metrological Microscope 20x (K).

Abbreviations: FESEM: Field emission scanning electron microscopy. µm: micrometers. EHT: Electron high tension. WD: Working distance. Mag: Magnification.

Among the evaluated patterns, low-density holes and grid shape emerged as the most promising, with the grid pattern demonstrating the most significant potential. In addition, evaluations of DEX and CLX release kinetics from unmodified and laser-modified prostheses showed no significant differences, indicating that the laser treatment primarily affected adhesion rather than the coating's functional performance.

Nevertheless, the formation of holes in the PCU prosthesis was discarded due to surface irregularities, which hindered the consistent creation of a uniform hole pattern without requiring frequent laser beam refocusing. The peripheral holes were smaller and shallower than those in the center, demonstrating poor reproducibility. Furthermore, despite promising results with the grid pattern, thermal effects from the laser treatment altered the color of the PCU prosthesis (Figure 2.3G), thus suggesting potential structural and mechanical changes. This color change,

likely caused by carbonization from excessive heat, indicated material decomposition and the formation of a carbon-rich residue. Lower laser energies (24 µJ, 17.5 µJ, and 10 µJ) were tested, but while they slightly reduced the color change, they did not fully resolve the thermal issue (data not shown). Thus, laser treatment was considered suboptimal for enhancing the interaction between the prosthesis and the bilayer polymer coating due to its detrimental impact on the prosthesis's physicochemical properties. Additionally, fs-laser patterning is costly and time-intensive, posing scalability challenges, especially for modifying the three-dimensional geometry of complex prostheses. Tests conducted on square PCU prostheses with smooth, uniform surfaces demonstrated that the process requires exact control to ensure consistent results, limiting its applicability for intricate implant geometries such as the meniscus prosthesis.

In conclusion, while the grid-pattern modification enhanced the interaction between the coating and the prosthesis, the laser treatment induced color changes that suggested alterations in the prosthesis's mechanical properties due to thermal effects. These findings indicated that the approach was unsuitable for improving coating adhesion and was ultimately discontinued.

5.4.2 Chemical modification of PCU prosthesis: Treatment with oxygen plasma

Plasma treatment was investigated to improve adhesion between the prosthesis surface and drug-releasing polymer films while preserving the bulk properties of the materials [38,39]. Plasma, an ionized gas with free electrons and ions, was produced using electromagnetic fields at low pressure to avoid compromising the structural and mechanical integrity of the prosthesis [388]. The energetic particles in the plasma interacted with the prosthesis surface, altering its chemical properties, particularly by functionalizing it with carboxyl (-COOH) and hydroxyl (-OH) groups, which increased surface hydrophilicity and wettability [40,41]. These modifications were expected to enhance adhesion by facilitating hydrogen bonding [42]. Though weak individually, the hydrogen bonds hypothesized to be formed between the ester (COO) groups in the polymer coating and the -OH or -COOH groups on the prosthesis surface were expected to provide sufficient cumulative strength to improve adhesion (Figure 2.5). The parameters for plasma treatment were optimized through macroscopic evaluation of adhesion under dry conditions, specifically by adjusting the power and processing time.

The first results indicated significant issues with the adhesion once the two polymer layers of the bilayer system (PLLA/PCL - CLX and PLGA - DEX) were deposited. Although the first polymer film was apparently well attached, the deposition of the second layer resulted in the delamination. This suggests that the mechanical stress generated during the solvent evaporation in the second layer (PLGA - DEX) created tension forces that promoted detachment, highlighting a critical challenge in the bilayer formation (Figure 2.6). It was hypothesized that the delamination was due to insufficient plasma treatment time. This was supported by the fact that a short 30-second treatment was used, regardless of the power applied (Table 2.2). Previous research on the same material (PCU) has suggested that longer plasma treatment times might improve surface modification and interaction (e.g., plasma modification studies showing enhanced adhesion with treatment periods around 10 minutes) [389]. Therefore, optimizing the duration of plasma exposure could lead to improved outcomes by ensuring better surface activation and stronger bonding between layers.

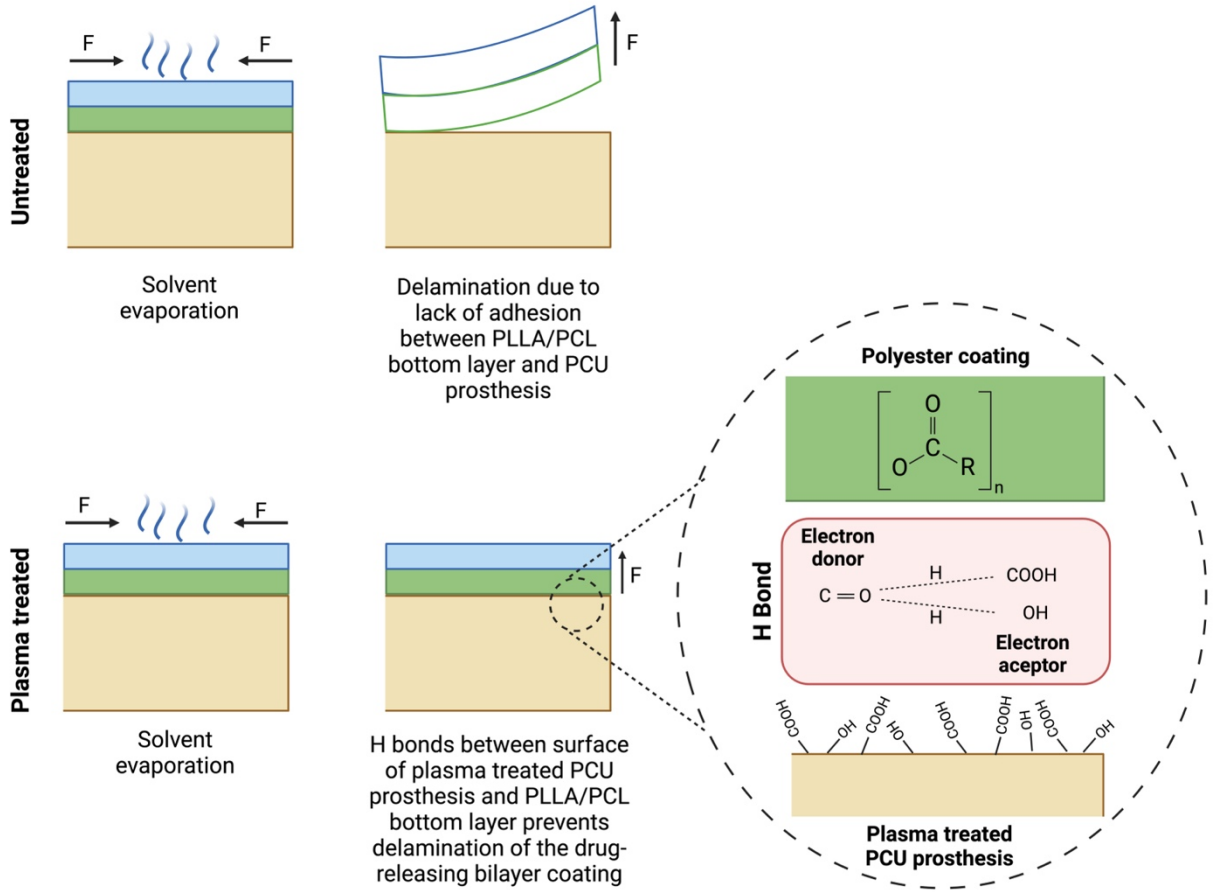

Figure 2.43. Schematic representation of the expected mechanism of action of oxygen plasma treatment to improve adhesion between the polymer coating and the treated prosthesis.

Abbreviations: F: Force. PLLA: poly(L-lactide). PCL: poly(caprolactone). PCU: Polycarbonate urethane. Created with https://www.biorender.com/

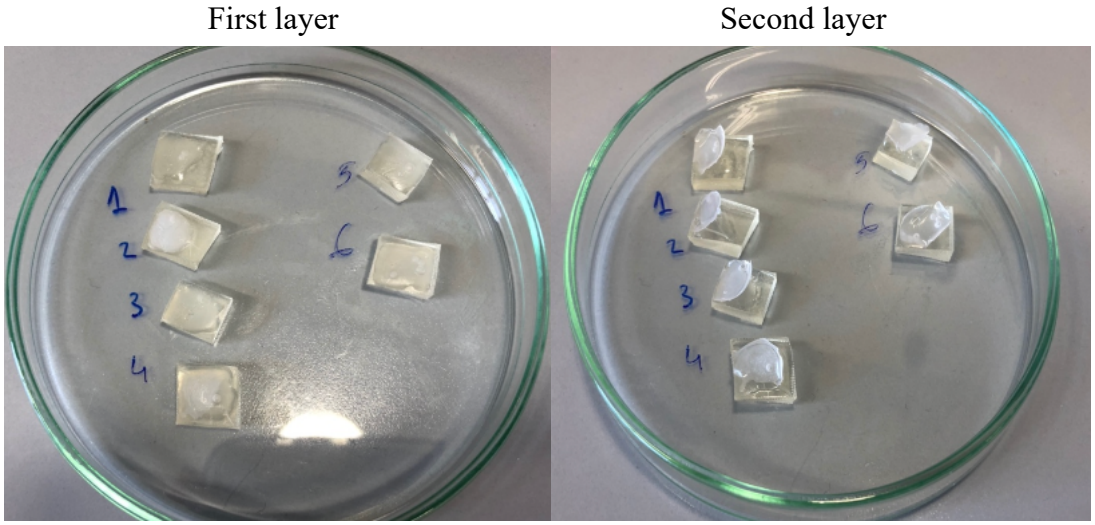

Figure 2.44. Outcomes of synthesis of the bilayer polymer film system by solvent casting after functionalizing the square PCU prosthesis by oxygen plasma treatment.

Table 2.10. Oxygen plasma treatment parameters set up.

Prototype	Time (s)	Power (W)
1	30	52
2	30	150
3	30	190
4	30	20
5	30	80
6	30	120

The effect of longer plasma treatment times on the adhesion between the drug-releasing bilayer system and the PCU prosthesis was evaluated, increasing the initial 30 seconds of processing time to 10 minutes. Extending the plasma treatment time significantly improved the interaction between the bilayer polymer coating and the prosthesis. The enhanced adhesion was observed consistently across all power settings, indicating that the longer processing times, rather than the power of the electromagnetic field, were responsible for the improvement. This suggests that longer exposure times may lead to increased functional groups (e.g., -OH or -COOH) on the prosthesis surface, facilitating the formation of additional H bonds between the prosthesis and the coating (Figure 2.7 and Table 2.3).

However, previous research has shown that plasma treatment can also modify surface roughness depending on the gas used, power, pressure, and processing time. Notably, plasma treatment was reported to increase surface roughness in some polymeric materials but can decrease it in others, such as stainless steel [390–393]. Since both pressure and the type of gas used were fixed variables, it was decided to focus on reducing processing time and power to maintain the integrity of the prosthesis' surface regarding roughness and ensure optimal adhesion without structural alterations.

First layer Second layer

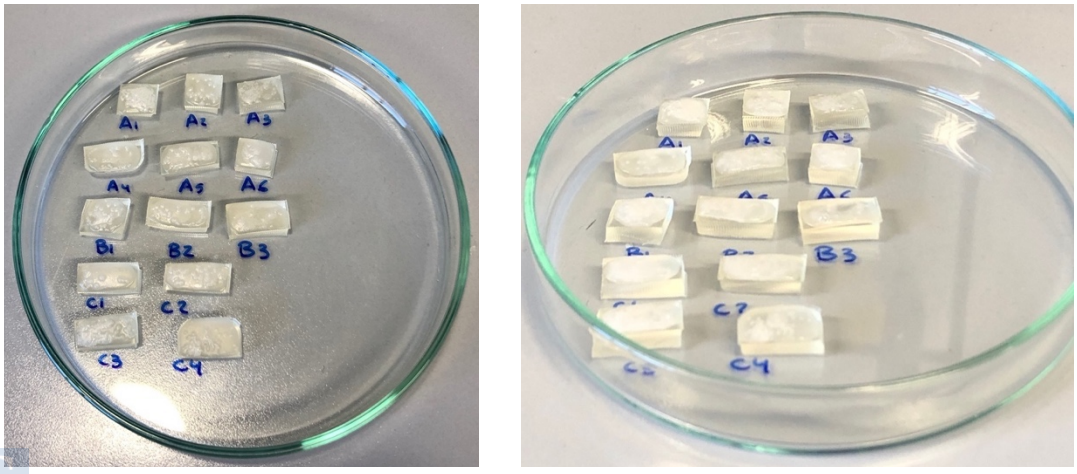

Figure 2.45. Outcomes of synthesis of the bilayer polymer film system by solvent casting after functionalizing the square PCU prosthesis by oxygen plasma treatment.

Table 2.11. Oxygen plasma treatment parameters set up.

Prototype	Time (min)	Power (W)
A1	8	200
A2	8	200
A3	8	200
A4	8	52
A5	8	52
A6	8	52
B1	8	100
B2	8	100
B3	8	100
C1	10	52
C2	10	52
C3	10	100
C4	10	100

The treatment time was reduced from 8 or 10 minutes to 6 minutes without compromising the optimized interaction, as shown in Figure 2.8 and Table 2.4. Additionally, processing powers between 50W and 100W were tested, revealing no significant differences. Based on these findings, the optimized setup was the mildest processing condition, 6 minutes at 52W.

This approach ensures efficient adhesion in dry conditions relying on the H bonds without unnecessarily extending treatment time or increasing the power, thus minimizing potential material degradation. However, when tested in wet conditions, these bonds' effectiveness was limited (image not shown), raising concerns about their functionality in the hydrophilic microenvironment of the knee cavity, where water molecules can replace polymer-surface interactions. Additionally, the surface modifications induced by plasma treatment are temporary, requiring the prosthesis to be processed and coated promptly to ensure the improved adhesion persists [43]. Thus, based on this initial macroscopic evaluation, the method was deemed unsuitable.

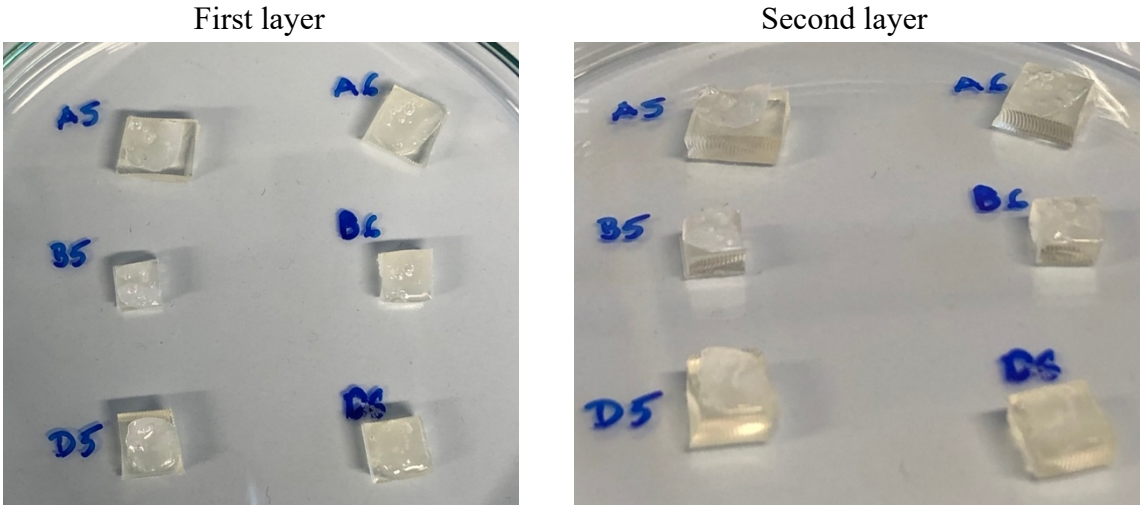

Figure 2.46. Outcomes of synthesis of the bilayer polymer film system by solvent casting after functionalizing the square PCU prosthesis by oxygen plasma treatment.

Table 2.12. Oxygen plasma treatment parameters set up.

Prototype	Time (min)	Power (W)
A5	6	100
A6	6	100
B5	6	52
B6	6	52
D5	8	100
D6	8	100

5.4.3 Chemical modification of PCU prosthesis: Polydopamine (PDA) coating

Another approach to improve adhesion inspired by mussel adhesive proteins and the self-polymerization of dopamine to polydopamine (PDA) was tested [44]. PDA has gained significant attention in tissue engineering due to its strong adhesion, hydrophilicity, biodegradability, biocompatibility, and potential for post-functionalization, making it highly suitable for gentle processing conditions [394]. Its ability to form thin adherent films on a wide range of surfaces, including superhydrophobic materials like PCU, while preserving the prosthesis's original geometry and structural integrity made PDA ideal for improving the adhesion between prostheses and drug-releasing polymer coatings [370,395]. In the case of PCU prostheses, PDA was hypothesized to adhere through noncovalent interactions such as π-π stacking, hydrogen bonding, and quinhydrone charge-transfer complexes, depending on media conditions [396]. These bonds would be facilitated by catechol and amine functional

groups within the PDA structure, which makes it conducive to forming bonds with a wide range of materials [397].

Optimal PDA deposition conditions remain under discussion, but typical parameters include a dopamine concentration of 2 mg/mL, pH of 8.5, and room temperature [394]. These oxidative conditions allow dopamine to self-polymerize into PDA, with the thickness of the film increasing over time and reaching equilibrium around 24 hours [398]. Furthermore, pre-treatment with oxygen plasma has enhanced PDA uniformity by generating active oxygen radicals that facilitate deposition [40]. This PDA coating and plasma treatment combination significantly boosts interfacial interaction without compromising the prosthesis structure [399].

Various characterization techniques, including visual inspection, dynamic light scattering (DLS), and water contact angle measurements, were employed to assess the polymerization of PDA under shaking conditions and the formation of a PDA film on square PCU prostheses pre-treated with plasma. These methods were chosen for their simplicity and efficiency in optimizing variables. However, other methods, such as UV/Vis spectrophotometry, XPS, FTIR, and TGA, have been reported in the literature for evaluating PDA polymerization [396].

As discussed, PDA film formation involves the synthesis of PDA particles in solution followed by their adsorption onto the prosthesis surface. DLS was used to monitor the size of these particles over time as an indirect measure of dopamine polymerization, which increased consistently up to 24 hours. The bigger the particles, the more PDA polymerized. The particle sizes grew from around 240 nm after 30 minutes to approximately 2700 nm after 24 hours, confirming a progressive polymerization process in line with earlier reports (Figure 2.9A). Moreover, the DLS analysis showed an unimodal particle size distribution throughout the reaction, indicating uniform particle growth without oligomers or other intermediates. Visually, the reaction was tracked by a change in color from colorless to dark brown, indicating dopamine oxidation and polymerization, with black insoluble material precipitating under static conditions (Figure 2.9B). Therefore, it was concluded that gentle shaking during polymerization resulted in a homogeneous PDA solution and uniform coating formation on the prosthesis.

A. B.

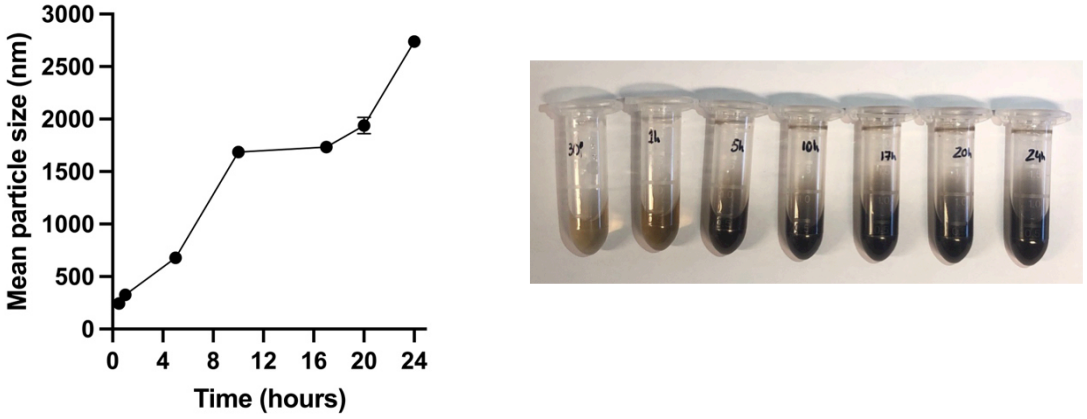

Figure 2.47. Mean particle size of PDA granules measured by DLS indirectly addressing PDA polymerization (A). Visual inspection tracking the color change of reaction medium with time during PDA polymerization (B).

Values represent the mean ± standard deviation (n=3).

After 24 hours of PDA film formation and drying, drug-releasing polymer coatings were applied via solvent casting to evaluate adhesion. However, the polymer coatings detached easily during macroscopic scratch tests. This observation led to the hypothesis that a sacrificial layer, capable of interacting with the PDA surface and the hydrophobic drug-releasing polymer, could enhance adhesion. Previous studies suggest that hydroxyl-terminated polymers, such as polyethylene glycol (PEG), can strongly interact with PDA through non-covalent bonds [370]. PEG, a biocompatible polyether, had been previously used as a sacrificial layer to prevent coatings from cracking during mechanical stress [400]. Thus, to further improve adhesion, an amphiphilic copolymer, PLA-PEG was chosen, where the hydrophilic PEG domain could interact with the PDA-modified surface and the hydrophobic PLA domain could enhance attachment to the drug-releasing polymer coatings.

The optimal approach was found to be the combination of a PDA coating, followed by a PLA-PEG layer, and the subsequent bilayer polymer functionalization (Figure 2.10A). Under dry conditions, macroscopic evaluations revealed a significant improvement in adhesion between the polymer coatings and PDA-functionalized prostheses compared to oxygen plasma-treated prototypes. As shown in Figure 2.10B, the visible interaction between the coating and the PDA-modified surface impeded detachment when attempting to delaminate the polymer coating with tweezers.

A.

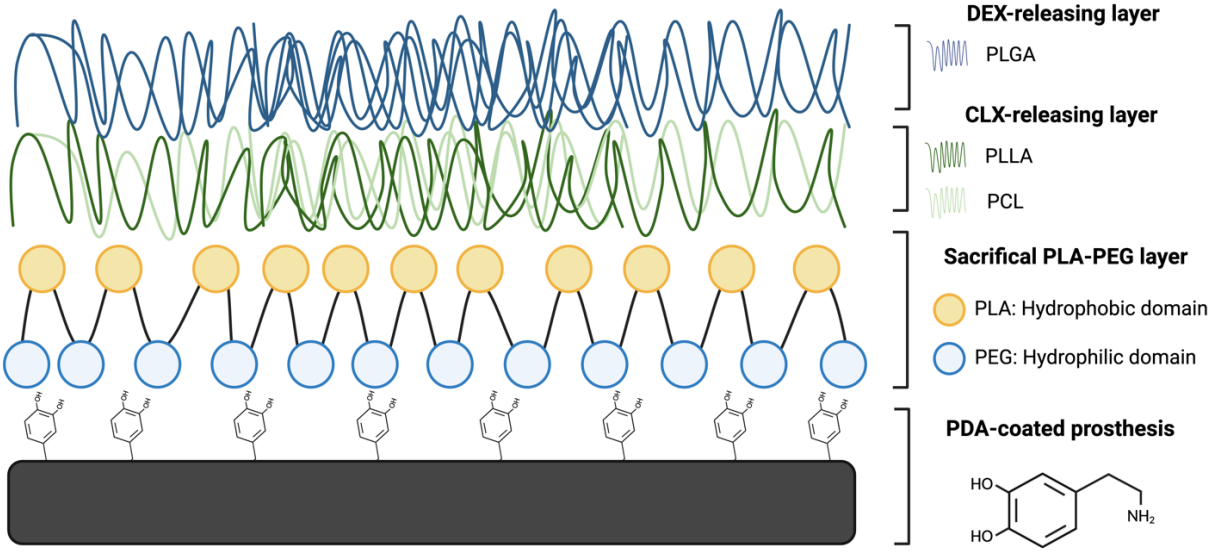

B.

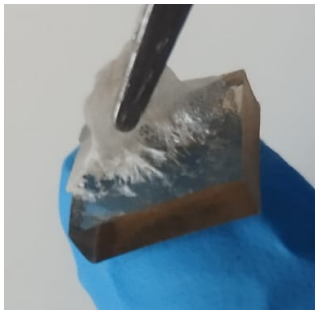

Figure 2.48. Schematic representation of the polymer-coated prosthesis incorporating the PDA film and the PLA-PEG sacrificial layer (A). Macroscopic evaluation of the system by scratch test (B).

Abbreviations: CLX: Celecoxib. DEX: Dexamethasone. PLA-PEG: poly(lactic acid)-poly(ethylene glycol) di-block copolymer. PLGA: Poly(lactic-co-glycolic) acid. PLLA: poly(L-lactide). PCL: poly(caprolactone). PDA: Polydopamine. Figure A created with https://www.biorender.com/.

Unfortunately, the polymer coatings readily detached from the prosthesis when tested under wet conditions. This behavior was attributed to the formation of H bonds between water molecules and the PDA layer surrounding the PCU prosthesis in the aqueous environment, which superseded the interactions between the polyester coatings and the PDA. Although alternative strategies, such as using amine- or thiol-terminated polymers to form covalent bonds with PDA, could potentially improve adhesion under wet conditions, they were not pursued. This decision was based on the necessity to maintain physiological pH within the knee cavity post-implantation, which ranges from neutral (7.4) in healthy knees to slightly acidic (6.8–7.1) in osteoarthritic knees, rendering the basic conditions required for these reactions impractical.

In conclusion, the PDA modification significantly enhances the hydrophilicity of the material compared to other treatments, such as plasma. Also, it is versatile enough to be applied to nearly any material, regardless of its properties [401]. Furthermore, PDA coatings can be uniformly deposited on prostheses of varying shapes and geometries under mild basic conditions at room temperature, making it a non-invasive method for the prosthesis structure. However, the process is time-intensive, requiring an oxygen plasma pre-treatment and 24 hours of dopamine polymerization to ensure uniform film formation. While adding a PLA-PEG sacrificial layer greatly improved adhesion in dry conditions, this benefit was lost in wet environments due to the higher affinity of hydrogen bonds for water. Consequently, despite the initial promise, the method was discarded in favor of exploring new alternatives that ensure strong adhesion in both dry and wet conditions.

5.4.4 Chemical modification of PCU prosthesis: Ethyl-2-cyanoacrylate (ECA) adhesive layer

Alkyl-2-cyanoacrylates (ACAs), including ethyl-2-cyanoacrylate (ECA), are widely recognized for their rapid adhesion properties, attributed to their electronegative cyano (-CN) and ester (-COOR) groups. These groups initiate fast anionic polymerization in the presence of weak bases such as water, forming high molecular weight polymers. The stability of the carbanion formed during polymerization contributes to these adhesive solid properties [371]. This makes ACAs especially useful for bonding both low and high-surface energy materials. Regarding biodegradation, ACAs undergo hydrolytic degradation, forming byproducts such as formaldehyde, minimizing toxicity with longer alkyl chains (Comparative evaluation of polycyanoacrylates). In particular, ECA has been evaluated and certified under USP Class VI and ISO-10993 standards, making it suitable for medical applications, such as surgical adhesives and biomedical device coatings [45–47,47]. Moreover, previous studies have utilized cyanoacrylates to adhere polymeric structures to polyurethane substrates for biomedical applications, such as antibacterial surfaces [48].

Our approach used medical-grade ECAs to enhance the adhesion between the prosthesis and drug-releasing bilayer polymer coatings. Their rapid polymerization under moisture and ability to form flexible bonds were advantageous in counteracting the limitations observed with PDA and plasma treatments under wet conditions. ECAs are resistant to body temperature conditions (stability goes up to 80 °C), and while they degrade over time, their mass loss in

aqueous conditions is comparable to other stable longer-chain ACAs [45]. Additionally, ECAs degradation is hypothesized to be hindered or slowed by the hydrophobic bilayer polymer coatings deposited on top. Moreover, compared to these longer-chain ACAs, ECAs form stronger bonds, which is particularly useful for dealing with the forces in the knee cavity [402]. Certified by toxicity standards, ECAs offer biocompatibility, very low toxicity (especially post-curing), and mechanical resilience, including excellent stress and scratch resistance, making them an ideal candidate for this application [403,404].

Due to the requirement to coat the entire prosthesis, combined with the inherent viscosity and rapid polymerization of ECAs, direct dip-coating with pure ECA was deemed impractical. To address this, ECA was dissolved in acetone, a commonly used solvent for cyanoacrylates [49]. After evaluating various concentrations, a 40% (w/v) ECA solution in acetone was selected as optimal, as it maintained adhesive properties while significantly reducing viscosity, making it suitable for dip-coating applications. Prostheses treated with ECA were macroscopically evaluated both in dry and wet conditions, showing no significant differences in adhesion. However, prototypes immersed in simulated synovial fluid (SSF) exhibited slightly enhanced interaction, likely due to the accelerated ECA polymerization upon contact with water [50] (Data not shown).

The potential influence of the ECA layer on the drug-release kinetics of CLX from the PLLA/PCL layer was also investigated. While the release profile for DEX remained relatively unchanged regardless of the presence of the ECA layer, a slightly faster release of CLX was noted in prostheses with the ECA layer (Figure 2.11). This accelerated release was hypothesized to be attributed to polymer restructuring due to the chemical interaction between the cyano group in ECA and the polyesters, leading to a marginally faster release than coatings without ECA.

A.

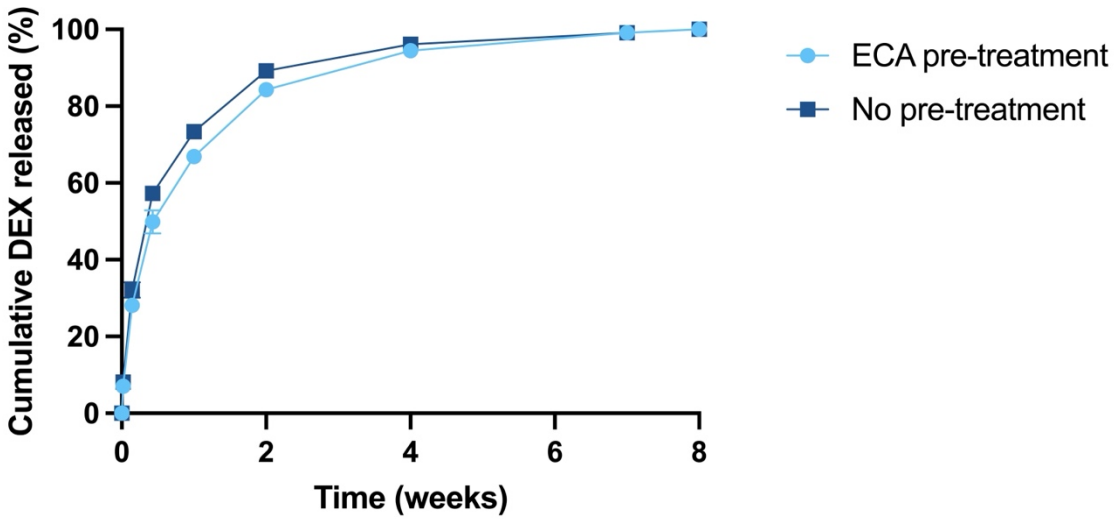

B.

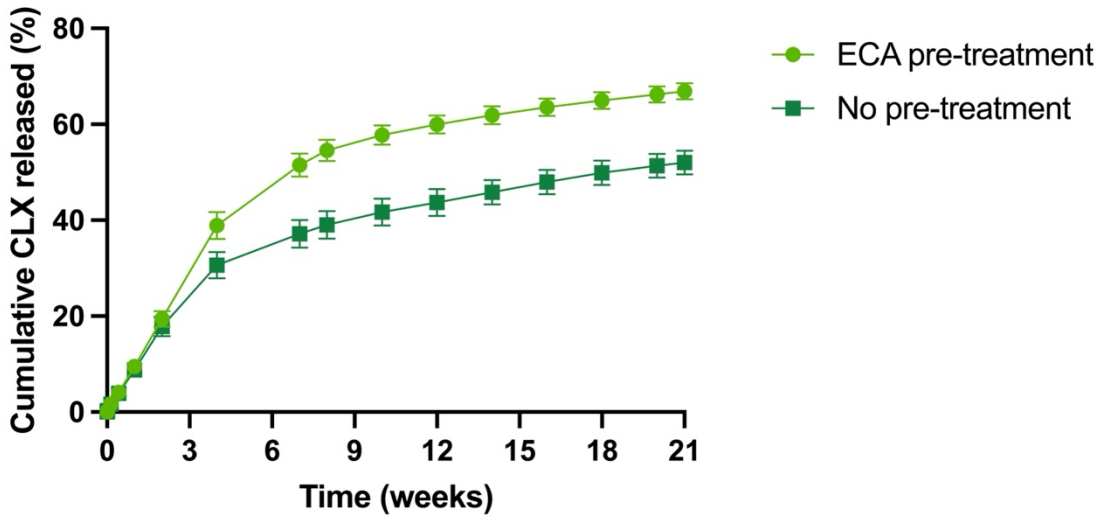

Figure 2.49. Sequential cumulative release of DEX and CLX from bilayer polymer coatings composed of a first polymer coating of PLLA/PCL, prepared at 150 mg/mL at 80/70 (w/w) with CLX loading of 16.6%, and a second polymer coating of LMW-PLGA prepared at 200 mg/mL with DEX loading of 2.44%, deposited on top of an adhesive ECA layer coating the PCU prosthesis or on top of the untreated PCU prosthesis.

Abbreviations: CLX: Celecoxib. DEX: Dexamethasone. PLA-PEG: poly(lactic acid)-poly(ethylene glycol) di-block copolymer. PLGA: Poly(lactic-co-glycolic) acid. PLLA: poly(L-lactide). PCL: poly(caprolactone). ECA: Ethyl-2-cyanoacrylate. Values represent the mean ± standard deviation (n=3).

The improvement in adhesion was confirmed by microscopic analysis (Figure 2.12). As can be seen, oxygen plasma treatment already notably improved the interaction between the polymer coating and the PCU prosthesis, enhancing adhesion. However, the orange arrow points to areas where adhesion was still lacking, even in dry conditions, suggesting that delamination under wet conditions could be worse due to hydrogen bond breakage. In contrast, the sagittal cut of the coated prosthesis using the ECA adhesive layer showed complete and robust interaction between the coating and the prosthesis, with no noticeable points of poor adhesion. This confirms macroscopic observations that the ECA layer presents a promising method for achieving consistent and enhanced adhesion.

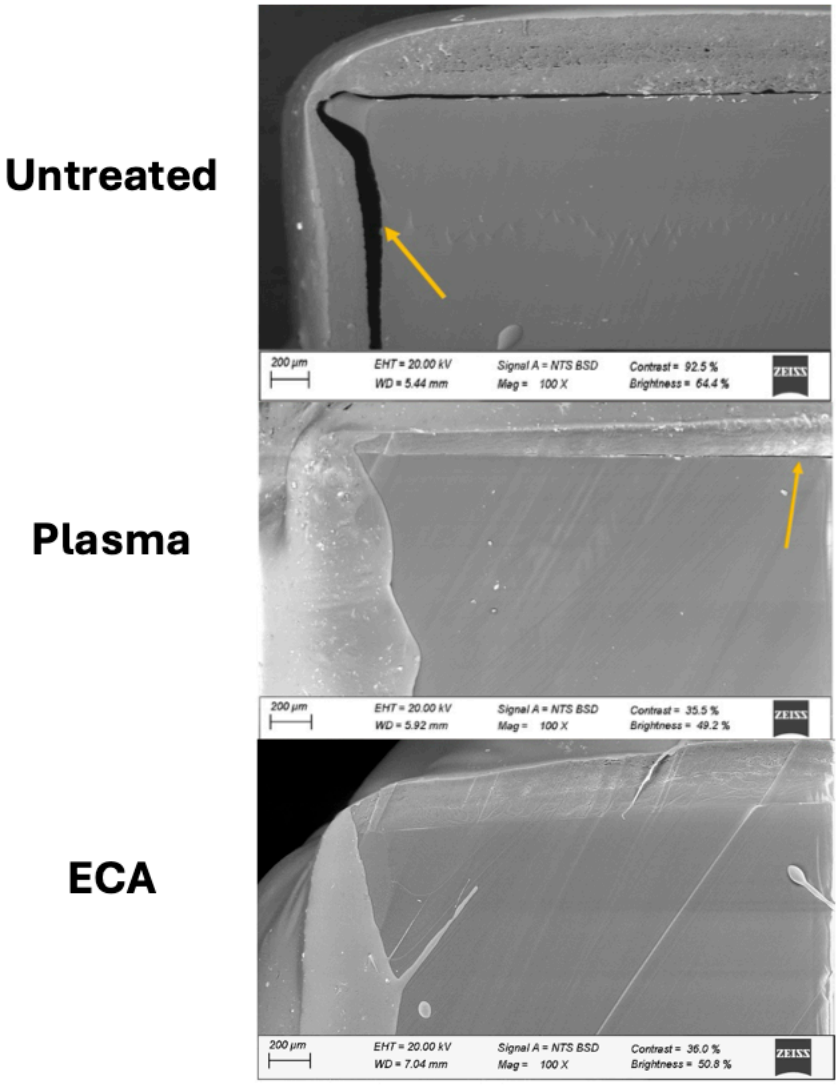

Figure 2.50. FESEM images of sagittal cut showing the bilayer polymer coating interaction with unmodified or chemically modified PCU prostheses with oxygen plasma treatment or ECA adhesive layer.

Abbreviations: ECA: Ethyl-2-cyanoacrylate.

Overall, macroscopically and microscopically, the application of the ECA adhesive layer appears the most promising approach for the functionalization of prosthesis surfaces. This ensures an adhered, complete, and uniform coating of the PCU prosthesis and does not present the limitation of lack of adhesion under wet conditions. However, quantitative studies such as DMA were needed to confirm these observations further.

5.4.5 Quantitative analysis of the prosthesis mechanical properties by DMA

Although the previous sections evaluated the different modifications macroscopically and microscopically, it was necessary to quantitatively determine which modification best met the mechanical properties of the coated prostheses. Dynamic Mechanical Analysis (DMA) using a three-point bending (TPB) setup was employed to assess the viscoelastic properties of the prototypes (Figure 2.13). DMA is a well-established technique for evaluating the storage

modulus (G'), loss modulus (G''), and damping coefficient (tan δ) of materials, offering insight into their viscoelastic behavior [405]. This method allows temperature-dependent measurements, revealing materials' engineering suitability and interfacial bonding quality (Figure 2.13A) [406]. In this experiment, it was expected that the forces applied to the upper surface of the polymer coating in a TPB setup would create compression on the top side and tension on the underside (Figure 2.13B) [407,408]. The G' and tan δ of the prototype were measured over a temperature range from -80ºC to 100ºC to evaluate thermal behavior, showing varying moduli at different temperatures because of the thermal transitions of the polymers coating the prosthesis. However, the data presented correspond to values obtained at 37 ºC, simulating the body temperature at which the prosthesis will be exposed *in vivo* (Figure 2.14).

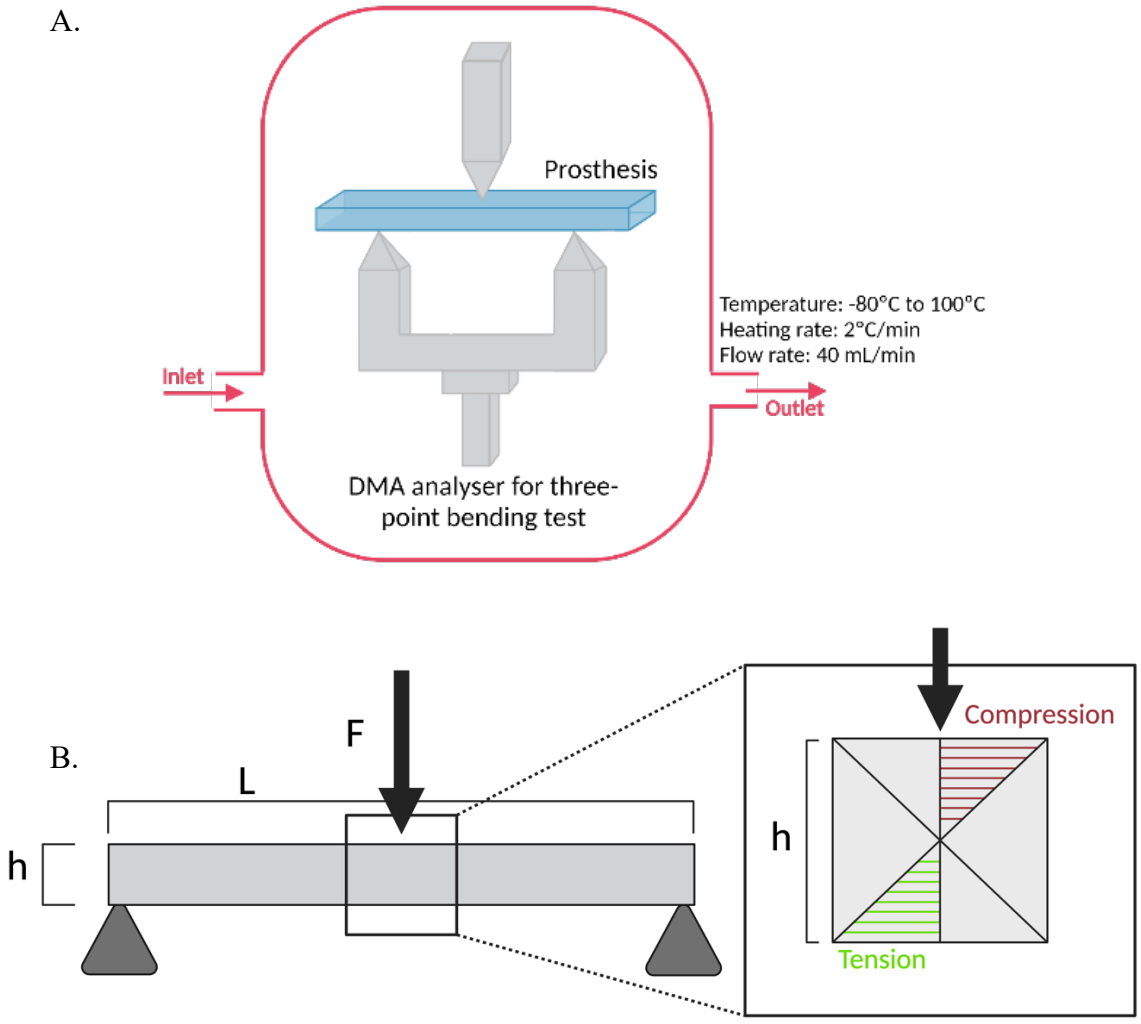

Figure 2.51. Schematic representation of the three-point bending test (TPB) used for the DMA (A). Summary of the forces applied to the bilayer drug-releasing polymer coating the prosthesis (B).

Abbreviations: h: Height. F: Force. L: Length. Created with https://www.biorender.com/

The G' reflects a material's ability to store energy elastically, indicating its solid-like behavior [409]. A higher G' corresponds to greater mechanical rigidity, which is particularly beneficial for meniscus prostheses, as they must provide mechanical support in the load-bearing

environment of the knee. The coated prostheses exhibited a higher G' than uncoated PCU prostheses, which can be attributed to the polymer coating enhancing the overall mechanical properties. Among the tested coated prostheses, the prostheses with the ECA adhesive layer demonstrated significantly higher G', indicating superior resistance to deformation under both compression and tension. This suggests stronger adhesion between the ECA-treated prosthesis and the drug-releasing polymer coating, further supporting the effectiveness of this approach in enhancing prosthesis stability for its applicability in the knee cavity (Figure 2.14A).

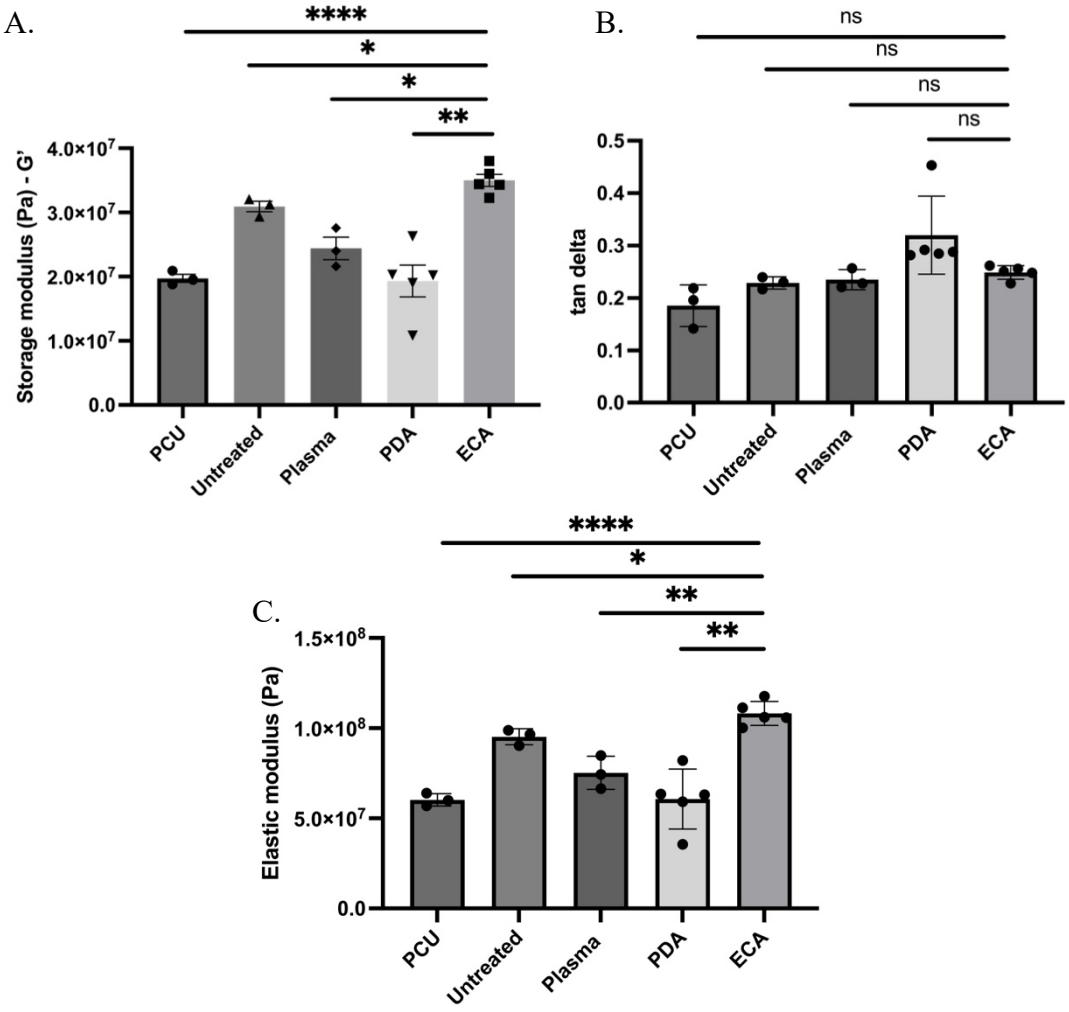

Figure 2.52. G', tan δ, and E measured by DMA.

Abbreviations: G': Storage modulus. E: Elastic modulus. PCU: Polycarbonate urethane. PDA: Polydopamine ECA: Ethyl-2-cyanoacrylate. Delta: δ. A significant comparison was performed using unpaired Welch's t-test between ECA and the rest of the groups. p-values < 0.05 were considered statistically significant (*). Also, (**) if p-value < 0.01, (***) if p-value < 0.001, (****) if p-value < 0.0001. When ns is displayed, no significative differences are observed. Columns represent the mean ± standard deviation (n ≥ 3).

Tan δ represents the ratio between energy dissipated (G") and energy stored (G'), providing insight into the material's solid or viscous behavior. A lower tan δ indicates a more solid-like material, which can elastically recover after deformation. In our case, a lower tan δ is favorable, as it shows that the coated prosthesis can retain more energy through elastic recovery, minimizing energy loss via deformation. As illustrated in Figure 2.14B, the tan δ for the

prosthesis with the ECA adhesive layer, alongside other prototypes, was very low, indicating that energy dissipated contributed significantly less than energy stored. This implied that all tested prototypes exhibit solid-like properties, suitable for the knee's mechanically demanding environment. Moreover, there were no significant differences in tan δ values between ECA-treated and uncoated prostheses, indicating that the ECA treatment did not compromise the balance between the elastic and viscous behavior of the PCU prosthesis, maintaining the prosthesis' ideal properties. Furthermore, the ECA-coated prosthesis displayed the highest G", suggesting greater flexibility, which could offer an advantage in accommodating the diverse movements that occur within the knee joint.

Finally, the elastic modulus (E), which reflects material stiffness, was significantly higher for the coated prosthesis using the ECA adhesive layer than other prototypes. This result underscored the improved interaction between the prosthesis and polymer coating, enhancing mechanical stability. The increased stiffness made it particularly suited for the demanding environment of the knee cavity, contributing to greater prosthesis durability and effectiveness (Figure 2.14C).

In summary, DMA analysis confirmed the superior mechanical properties of the ECA adhesive layer prototype, making it the most promising candidate for meniscus substitution. This prototype exhibited significantly higher G', G", and E while maintaining a favorable tan δ, ensuring resistance to knee forces while accommodating movement. The ECA-coated prostheses retained the optimal properties of the uncoated prostheses, outperforming those modified with PDA or plasma treatments.

However, despite all the described advances in terms of adapting the prosthesis surface for subsequent functionalization, a limitation inherent to the polymer coating applied via dip coating was identified. The multilayer coating introduces internal forces that could lead to delamination. Traditional adhesion tests, such as peel and lap shear tests, though effective for single-layer coatings or films, may not fully capture the complexity of the multilayer system proposed in this study. This limitation underscores the need for further investigations into adhesion measurements and optimization of the coating process to ensure a comprehensive assessment of adhesion under realistic physiological conditions [407].

5.4.6 Performance evaluation of the functionalized prosthesis in a sheep model

For the successful translation of results from animal models to humans, the chosen species must closely mimic human anatomical and biomechanical characteristics. Various animal models, including goats, sheep, dogs, and pigs, have been used in orthopedic research, specifically for meniscus repair and regeneration. Historically, sheep have emerged as the most widely used model due to their close anatomical resemblance to the human meniscus [51–53]. In all species used, the lateral meniscus tends to be larger than the medial meniscus in circumference, width, and height. Importantly, the sheep's medial meniscus closely matches the size of the human medial meniscus, which has been the primary focus of repair due to its increased susceptibility to injury [410].

Furthermore, the sheep model exhibits similarities with the human meniscus in terms of viscoelastic properties, vascularization patterns, cell density, and collagen ultrastructure [411–413]. There are, however, some kinematic differences. Biomechanically, sheep knees operate

in a flexed position compared to human knees, which bear weight in full extension. The range of motion in sheep knees is between 40-146°, while humans exhibit 2.5-137.5°. This is counterbalanced by the steeper tibial slope in sheep compared to humans [51,414,415]. Despite these variations, sheep knees are considered a size-scaled model of human knees, capable of bearing comparable joint forces. For example, the maximum force in ovine knees is up to 2.27 times body weight (BW), similar to human knees, which can experience forces ranging from 2.1-2.7 times BW during walking and up to 4.2 times BW while running [51,416].

Given their similarities in size, biomechanics, and joint forces, sheep were chosen as ideal models for studying meniscus and orthopedic applications.

5.4.7 Adapting the drug-releasing polymer coating to the geometry of the sheep meniscus prosthesis

Due to the complex structure of the sheep meniscus prosthesis (Figure 2.15), adjustments to the optimized coating parameters developed in Chapter 1 were necessary. The modifications were intended to adapt the coating process while maintaining the prosthesis' structural and mechanical integrity. The key goals of this modification are indicated in the following sections.

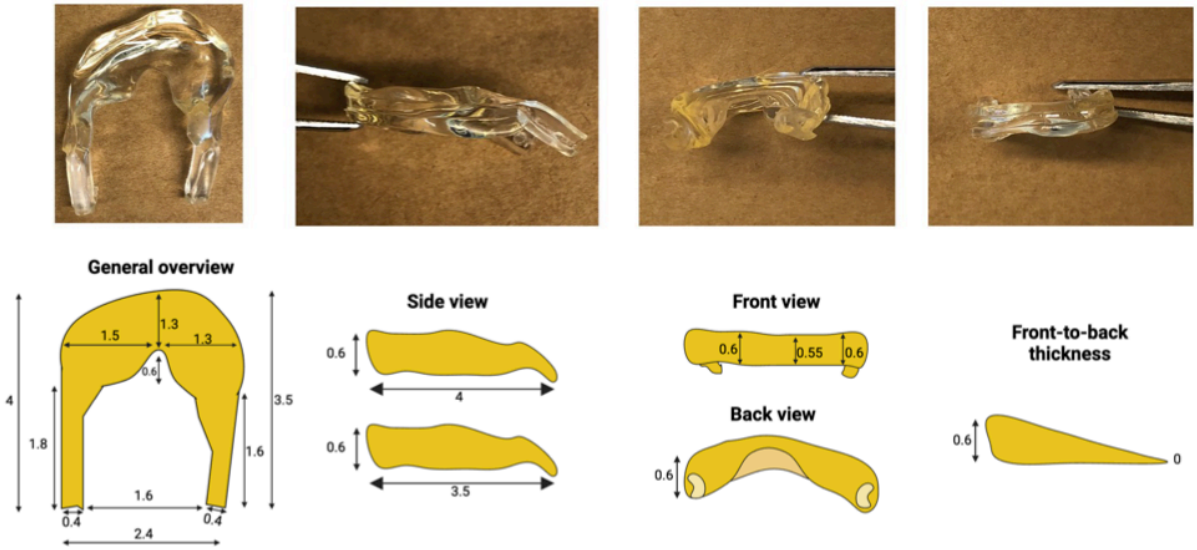

Figure 2.53. Sheep meniscus prosthesis.
Measures made in centimeters. Created with https://www.biorender.com/

5.4.7.1 Prosthesis orientation during dip coating

Previously, all dip coating processes were conducted with the square-shaped PCU prosthesis oriented horizontally during immersion in the polymer-drug solution. To ensure a uniform coating on the sheep meniscus prosthesis, the orientation was adjusted from horizontal to vertical. Immersing the prosthesis vertically during the dip-coating process resulted in a more uniform polymer distribution across the surface. This vertical orientation minimized the surface area in contact with the polymer solution at an initial time, thereby reducing polymer buildup

on the upper sections of the prosthesis and preventing uneven drug and polymer distribution (Figure 2.16).

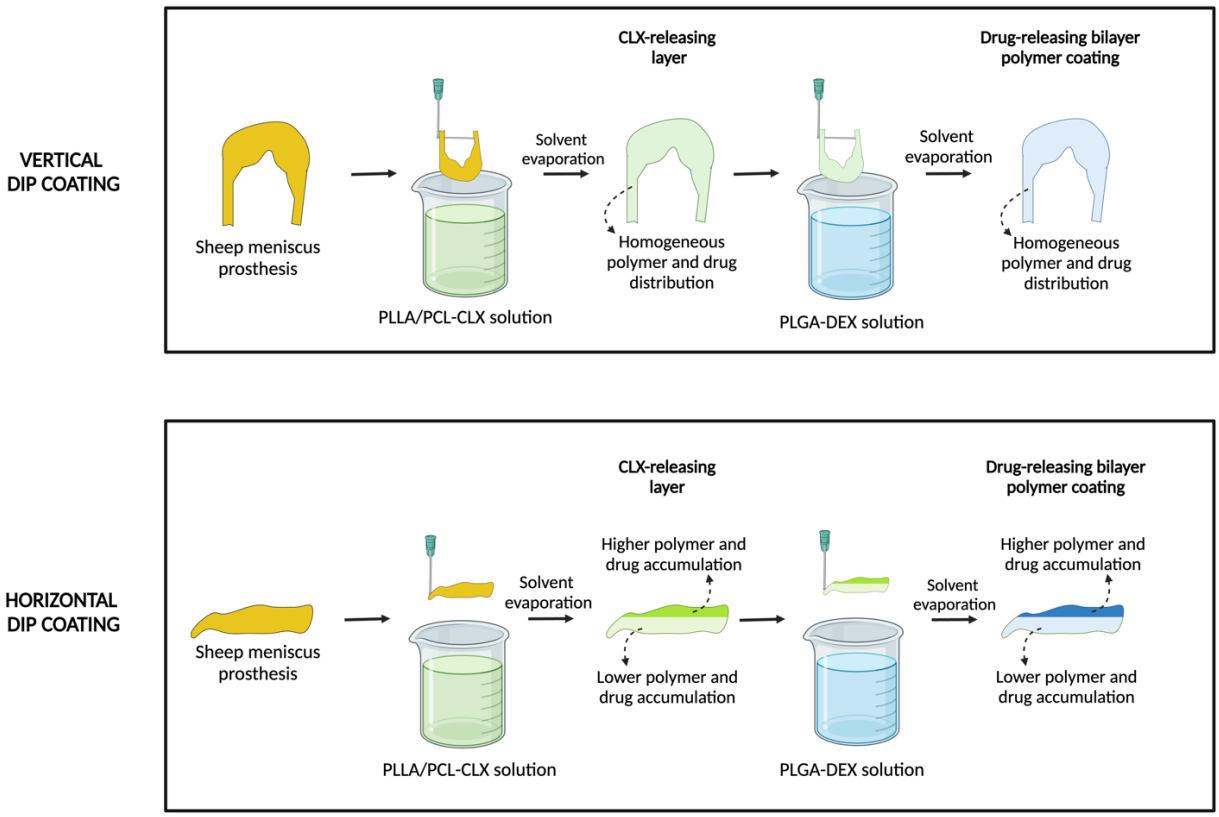

Figure 2.54. Schematic representation of the sheep prosthesis's orientation during dip coating.

Abbreviations: CLX: Celecoxib. DEX: Dexamethasone. PLA-PEG: Poly(lactic acid)-poly(ethylene glycol) di-block copolymer. PLGA: Poly(lactic-co-glycolic) acid. PLLA: poly(L-lactide). PCL: poly(caprolactone). PDA: Polydopamine. Created with https://www.biorender.com/

To determine whether the prosthesis orientation (vertical vs horizontal) impacted drug release kinetics, the release profiles of DEX and CLX were compared. Figure 2.17 demonstrates that no significant differences were observed in the percentage of drugs released between the two orientations. Both vertical and horizontal immersion produced consistent release kinetics. This result was anticipated, as the concentrations of materials used for coating remained unchanged; the primary difference was the distribution of polymer and drug due to orientation during the process.

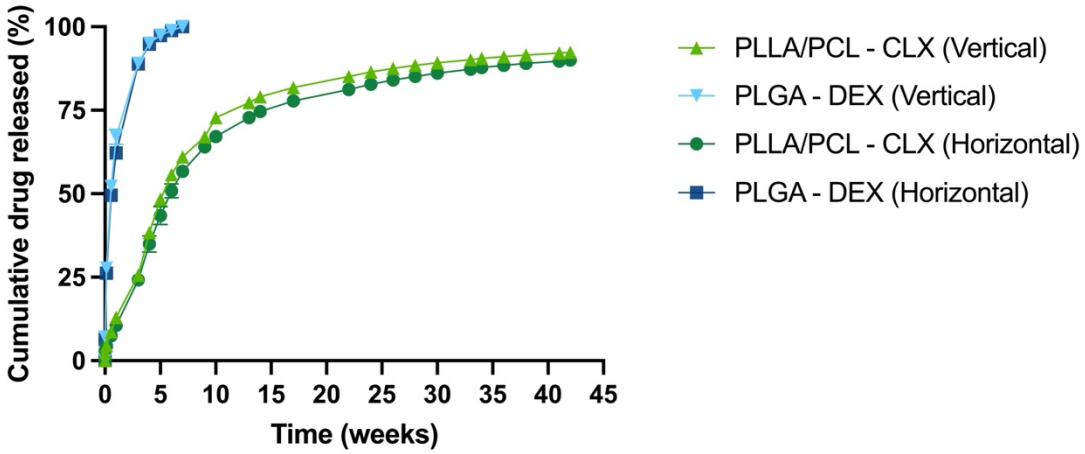

Figure 2.55. Sequential cumulative release of DEX and CLX from bilayer polymer coatings composed of a first polymer coating of PLLA/PCL, prepared at 150 mg/mL at 80/70 (w/w) with CLX loading of 16.6%; and a second polymer coating of LMW-PLGA prepared at 200 mg/mL with DEX loading of 2.44%, deposited by dip coating horizontally or vertically immersing the PCU prosthesis.

Abbreviations: CLX: Celecoxib. DEX: Dexamethasone. PLA-PEG: Poly(lactic acid)-poly(ethylene glycol) di-block copolymer. PLGA: Poly(lactic-co-glycolic) acid. PLLA: poly(L-lactide). PCL: poly(caprolactone). Values represent the mean ± standard deviation (n=3).

5.4.7.2 Preservation of prosthesis structure and properties

Given the sheep prosthesis' varying thickness, particularly in the thinner regions (Figure 2.14, front-to-back thickness), the polymer concentration of the CLX-releasing layer was reduced from 150 mg/mL to 100 mg/mL. This ensured that the coating did not compromise the mechanical properties or disrupt the prosthesis's structure due to exerted forces during curing.

As indicated by the red arrows in Figure 2.18A, vertical deposition of the polymer coating using the previously optimized concentrations (PLLA/PCL 80/70 (w/w) – CLX 16.67% and PLGA 200 mg/mL – DEX 2.44%) led to visible folds and bends in the thinner sections of the sheep meniscus prosthesis. These structural deformations were primarily attributed to the tension generated by the repeated dip cycles in DCM used to dissolve PLLA/PCL and CLX, as well as the mechanical stress induced by the PLLA/PCL – CLX coating. To address this issue, the concentrations of both the PLLA/PCL polymer and CLX were reduced proportionally by 1.5-fold, resulting in a low-concentration prototype while maintaining a constant CLX loading of 16.67%. This adjustment successfully prevented the formation of folds, thereby preserving the structural integrity of the prosthesis (data not shown).

As shown in Figure 2.18B, the release kinetics of both DEX and CLX, though slightly altered, remained consistent regardless of the polymer concentration in the CLX-releasing layer. Notably, the low-concentration prototype exhibited a faster initial release of CLX during the first five weeks, followed by a slower, sustained release over the subsequent weeks. This outcome contradicted the initial hypothesis that reducing polymer concentration would accelerate drug release. The data suggests that drug distribution within the matrix may vary based on polymer concentration, with lower concentrations potentially fostering more robust interactions between CLX and the polymer matrix. This might explain the slower, more sustained release in the long term.

A.

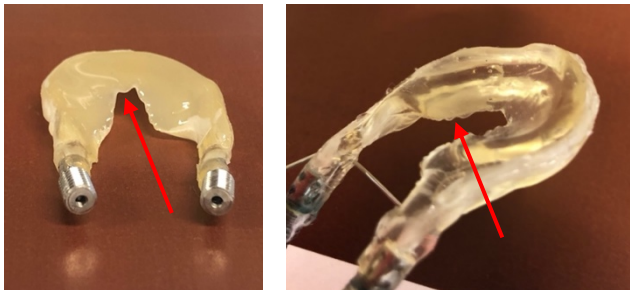

B.

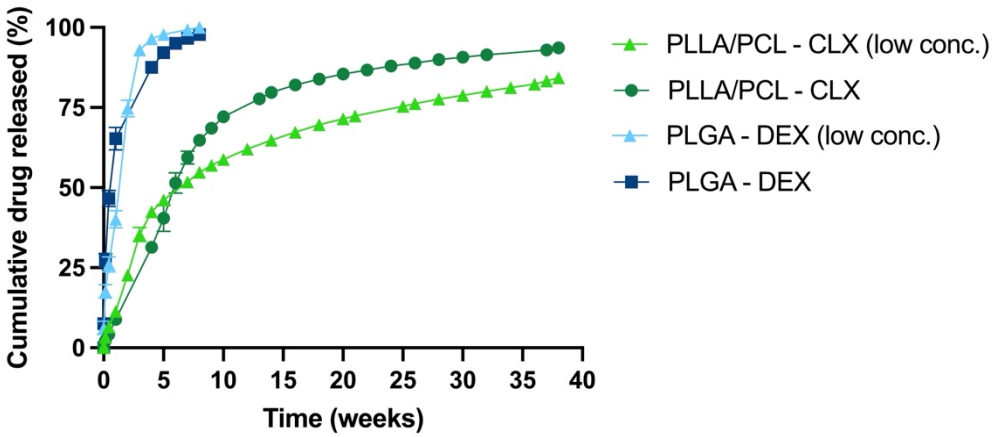

Figure 2.56. Visual aspect of sheep meniscus prosthesis coated with PLLA/PCL 80/70 (w/w)- CLX 16.67%; and PLGA 200 mg/mL - DEX 2.44%, denoting folds in the thinner parts of the prosthesis (A). Sequential cumulative release of DEX and CLX from bilayer polymer coatings composed of a first polymer coating of either PLLA/PCL, prepared at 150 mg/mL at 80/70 (w/w) with CLX loading of 16.6%, or PLLA/PCL, prepared at 100 mg/mL at 53/47 (w/w) with CLX loading of 16.6%; and a second polymer coating of LMW-PLGA prepared at 200 mg/mL with DEX loading of 2.44% in both cases (B).

Abbreviations: CLX: Celecoxib. DEX: Dexamethasone. PLA-PEG: Poly(lactic acid)-poly(ethylene glycol) di-block copolymer. PLGA: Poly(lactic-co-glycolic) acid. PLLA: poly(L-lactide). PCL: poly(caprolactone). Values represent the mean ± standard deviation (n=3).

5.4.8 *Ex vivo* simulation: Bioreactor test

Apart from joint stabilization, lubrication, and nutrient distribution, the meniscus plays a critical role in shock absorption and load distribution within the knee joint. To better understand how polymer-coated prostheses behave under these conditions, a bioreactor was selected to simulate the two predominant forces acting on the meniscus during movement: compression and shear [54,55]. The bioreactor mimicked the mechanical environment to which the prostheses are exposed during gait, serving as a bridge between the drug release profiles and degradation rates obtained *in vitro* and the expected performance *in vivo*. The influence of these mechanical forces was monitored for 3 weeks by comparing polymer-coated prostheses subjected to dynamic stimulation inside the bioreactor with unstimulated controls kept outside of the bioreactor. Additionally, simulated synovial fluid (SSF), with a composition mimicking the synovial fluid found in osteoarthritis (OA) patients (different HA molecular weight and concentration), was used as the release medium. The design of the experiment is schematized in Figure 2.1. Due to the geometric constraints of the bioreactor, the PCU prosthesis used in this study was not the actual sheep meniscus prosthesis but a cylindrical PCU sample.

Mechanical stress was anticipated to accelerate drug release by compromising the stability of the polymer coating. Our results confirmed this: both drugs were released more rapidly from stimulated prostheses inside the bioreactor than from non-stimulated controls. Notably, the difference in drug release became more pronounced over time, with 67% of DEX and 40% of CLX released from the stimulated prostheses, compared to 59% of DEX and 25% of CLX from the controls (Figure 2.19). Although the total amount of drugs released differed, the release profiles remained consistent, indicating that mechanical forces primarily accelerated the release without significantly damaging the polymer structure or drug integrity.

Thus, it was hypothesized that these forces may influence drug release by mechanically altering the interaction between the drugs and the polymer matrices rather than solely by accelerating the polymer degradation rate. This hypothesis was supported by the differences in DEX and CLX released. The upper DEX-releasing layer, composed of amorphous PLGA, degrades relatively quickly and is directly exposed to mechanical stress. However, the release of DEX showed minimal differences between conditions, suggesting that mechanical stress did not drastically affect the DEX layer. Conversely, the CLX-releasing layer, composed of semi-crystalline PLLA and PCL, was not directly exposed to mechanical stress but exhibited significantly faster release in the bioreactor. This could be attributed to the brittleness of PLLA, which is more susceptible to compression and shear forces, leading to increased degradation and faster CLX release [417]. This aligns with prior observations (Chapter 1) that CLX's interaction with the PLLA/PCL polymer blend is more complex, making it more responsive to mechanical stimulation. However, despite the accelerated release, the drugs were extrapolated to still adhere to the planned release timelines (1-4 weeks DEX release, 6-9 months CLX release).

Following the experimental setup described in Figure 2.1, macroscopic and microscopic evaluations were conducted in the bioreactor in order to understand how mechanical stimulation affects the degradation of polymer coatings. During the first two weeks, the macroscopic appearance of the coated PCU prostheses from both mechanically stimulated and non-stimulated groups remained similar, with only slight surface changes observed in the stimulated prostheses. These irregularities suggest that shear and compressive forces significantly alter the polymer’s structure or induce degradation. This mechanical impact likely compromised the integrity of the polymer coating, affecting drug release kinetics by disrupting its stability and uniformity. By the third week, the polymer-coated prostheses in the bioreactor showed a smoother, thinner surface compared to the control-coated prostheses, indicating expected surface erosion due to ongoing shear and compression forces.

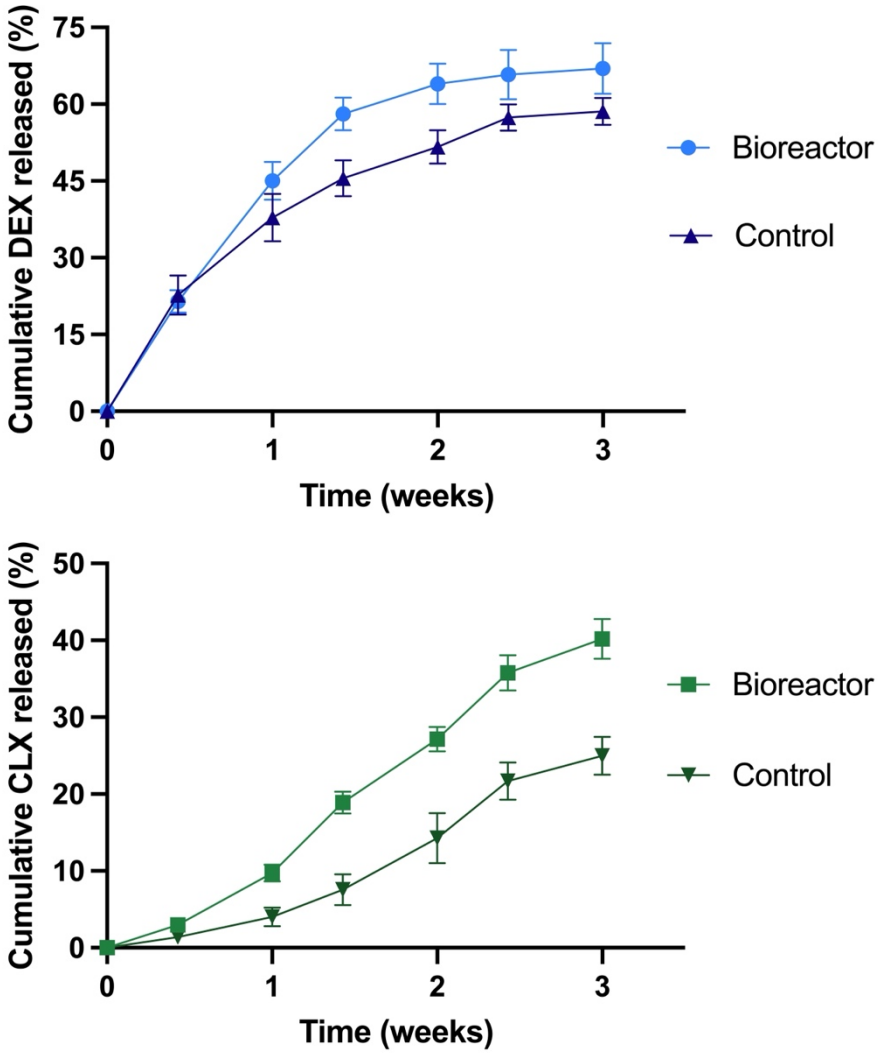

Figure 2.57. Cumulative release of DEX and CLX from bilayer polymer coatings composed of a first polymer coating of PLLA/PCL, prepared at 100 mg/mL at 53/47 (w/w) with CLX loading of 16.6%; and a second polymer coating of LMW-PLGA prepared at 200 mg/mL with DEX loading of 2.44%, deposited on top of an adhesive ECA layer coating the PCU prosthesis. Coated prostheses were analyzed under mechanical stimulation (bioreactor) or without mechanical stimulation (control).

Abbreviations: CLX: Celecoxib. DEX: Dexamethasone. PLA-PEG: Poly(lactic acid)-poly(ethylene glycol) di-block copolymer. PLGA: Poly(lactic-co-glycolic) acid. PLLA: poly(L-lactide). PCL: poly(caprolactone). Values represent the mean ± standard deviation (n≥3).

Figure 2.20 also shows the results of the scratch test conducted on the surface of both the bioreactor and control prostheses after three weeks. This test confirmed the presence of the polymer coating under both conditions, indicating that while some degradation was observed (as evidenced by macroscopic analysis and faster drug release), the overall structure and integrity of the coating were maintained during the three weeks that the experiment lasted. Importantly, there was no delamination of the polymer coating under mechanical stress, further supporting the enhanced adhesion provided by the ECA adhesive layer.

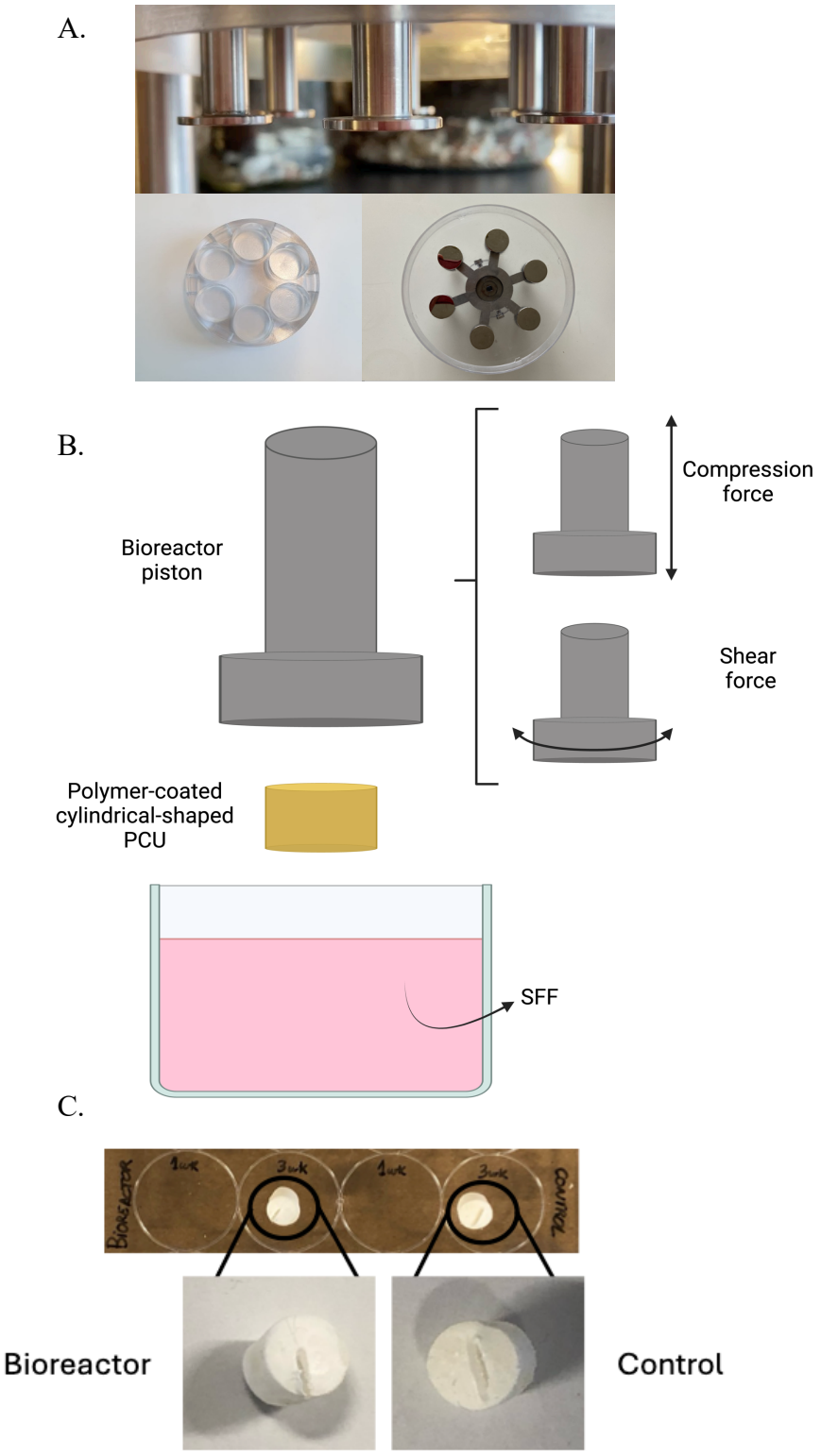

Figure 2.58. Bioreactor that mimics gait and its force-exerting pistons (A). Schematic representation of the bioreactor setup specifying the mechanical forces exerted by the pistons (B). Scratch test on the polymer surface of non-stimulated (control) or mechanically stimulated (bioreactor) after three weeks of evaluation (C).

Abbreviations: PCU: Polycarbonate urethane. Figure B was created with https://www.biorender.com/.

The microscopic evaluation of the polymer-coated prostheses further reinforced the findings from the macroscopic observations. On day 3, the non-mechanically stimulated control prostheses exhibited the expected hydration of the PLGA upper layer, revealing the porous structure of the PLLA/PCL bottom layer, characteristic of this polymer system [418]. In contrast, the bioreactor-tested prostheses, exposed to simulated gait forces, presented a more granular surface. This structural change indicates that the mechanical stress, particularly the shearing and compressive forces applied by the bioreactor, influenced the integrity of the PLGA layer. By week 1, the control prostheses began to show surface microstructures as part of their typical degradation process. On the other hand, the prostheses tested under mechanical stimulation displayed a smoother surface with trails likely caused by the movements of the bioreactor's pistons. At week 2, the degradation of the PLGA layer in both conditions had progressed, revealing more of the porous structure of the bottom PLLA/PCL layer in the control prostheses. However, the surface of the bioreactor prostheses remained notably smoother, lacking the granular structures observed in the control group, indicating that the forces had further smoothened the material surrounding the pores. By week 3, the degradation of the upper PLGA layer in both conditions was evident, fully exposing the porous structure of the PLLA/PCL bottom layer. However, the bioreactor prostheses exhibited a smoother surface around the pores than the control prostheses. Notably, the pore size in the bioreactor group decreased significantly from ~80 μm at week 2 to ~40 μm by week 3, while in the control group, the pore size slightly increased from ~47 μm to ~58 μm. This reduction in pore size for the mechanically stimulated prostheses can be attributed to the shear forces, which could displace polymer material across the surface, resulting in pore narrowing (Figure 2.21).

These microscopic observations confirmed that the polymer coatings remained stable upon exposure to the bioreactor's mechanical forces. Surface smoothness and the reduction in pore size indicate that mechanical loading influenced the polymer structure, which may explain the faster drug release observed in bioreactor-tested prostheses. However, the coating's overall presence after testing highlights its durability and the strong adhesion to the PCU prosthesis provided by the ECA adhesive layer, demonstrating the suitability of this system for use in demanding environments like the knee cavity.

A.

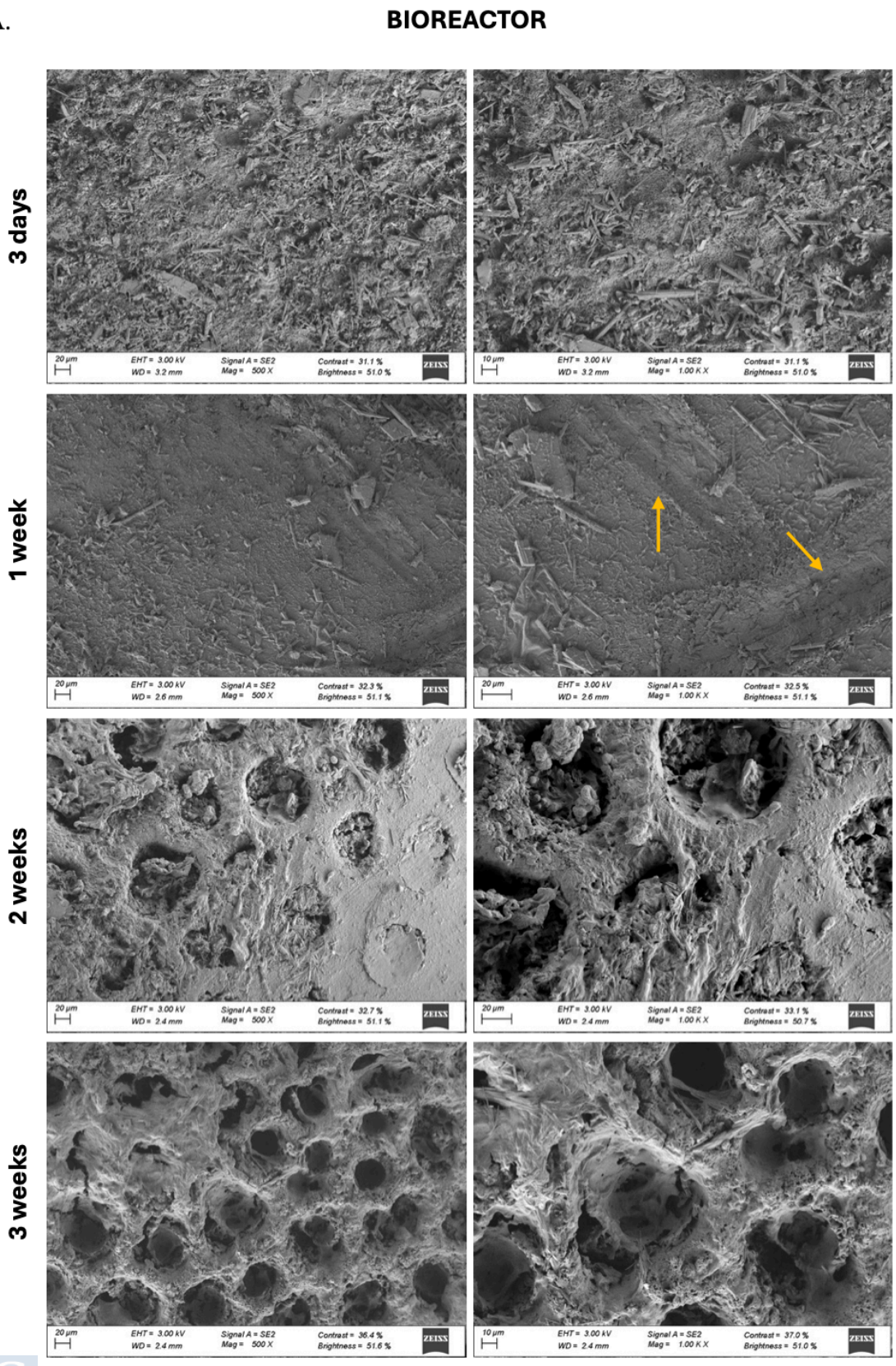

B. **CONTROL**

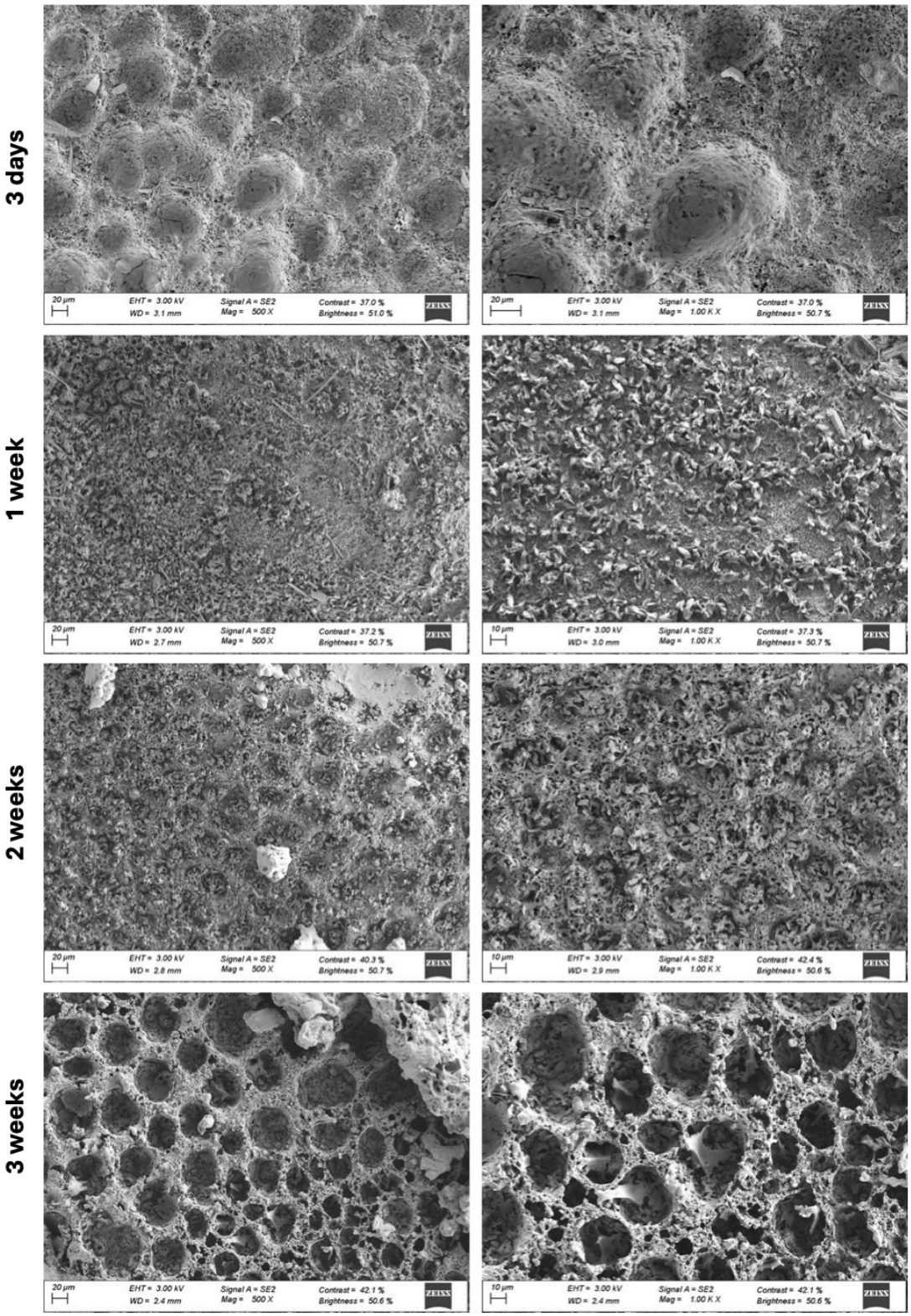

Figure 2.59. FESEM images of the aerial view showing the polymer coating under mechanical stimulation in the bioreactor (A) or without mechanical stimulation (B) at different times.

Abbreviations: FESEM: Field emission scanning electron microscopy. µm: micrometers. EHT: Electron high tension. WD: Working distance. Mag: Magnification.

5.4.9 *In vivo* preparation

5.4.9.1 Sterilization of the drug-releasing polymer-coated meniscus prostheses

The literature reports different sterilization methods, with hydrogen peroxide (H_2O_2) plasma and ethylene oxide (ETO) sterilization being the mildest treatments for polymer-coated prostheses. Both methods preserve drug release kinetics while operating at temperatures low enough to avoid exceeding the polymers' glass transition (Tg) or melting temperatures (Tm). They also prevent excessive UV light exposure, which is essential given DEX's photosensitivity [56,57].

First, H_2O_2 plasma was tested, as it is a standard sterilization method in hospitals. However, as shown in Figure 2.22A, this treatment severely damaged the polymer coatings, mainly affecting the PLGA upper layer, leading to its complete removal and exposing the PCU prosthesis. Furthermore, H_2O_2 plasma sterilization in this specific protocol required operating at 55 ºC, within the Tg range of PLLA and PLGA and the Tm of PCL, posing a risk to the polymers' integrity. Additionally, the generation of H_2O_2 plasma required UV light for more extended periods than expected (hours), which could degrade DEX, making this option unsuitable. Consequently, H_2O_2 plasma was discarded as an option for sterilizing our coated prostheses.

ETO sterilization was then evaluated. As shown in Figure 2.22B, there were minimal differences between sterilized and non-sterilized polymer coatings, and the method was optimized to be conducted at 38 ºC, below the critical Tg and Tm of the polymers. Furthermore, the ETO process did not involve UV light, thus protecting DEX from photodegradation. A significant concern with ETO is the potential for toxic residues, such as the proper ETO, 2-chloroethanol, and 1,4-dioxane, to remain on the prostheses after sterilization [45,56]. Thus, an extended 48-hour aeration step was suggested to address this issue, ensuring no toxic residues remained in the coating.

Furthermore, the ETO sterilization process unaffected the DEX and CLX release kinetics, as shown in Figure 2.23A. Additionally, drug loading studies confirmed no significant differences in the amount of CLX and DEX loaded in sterilized and non-sterilized polymer coatings (Figure 2.23B). Thus, it suggests that the drugs were not compromised during the ETO sterilization, maintaining their integrity and availability within the system.

Consequently, ETO was the selected method to sterilize the sheep prostheses for the *in vivo* studies, ensuring drug stability, maintaining release kinetics, and avoiding structural damage to the polymer coatings.

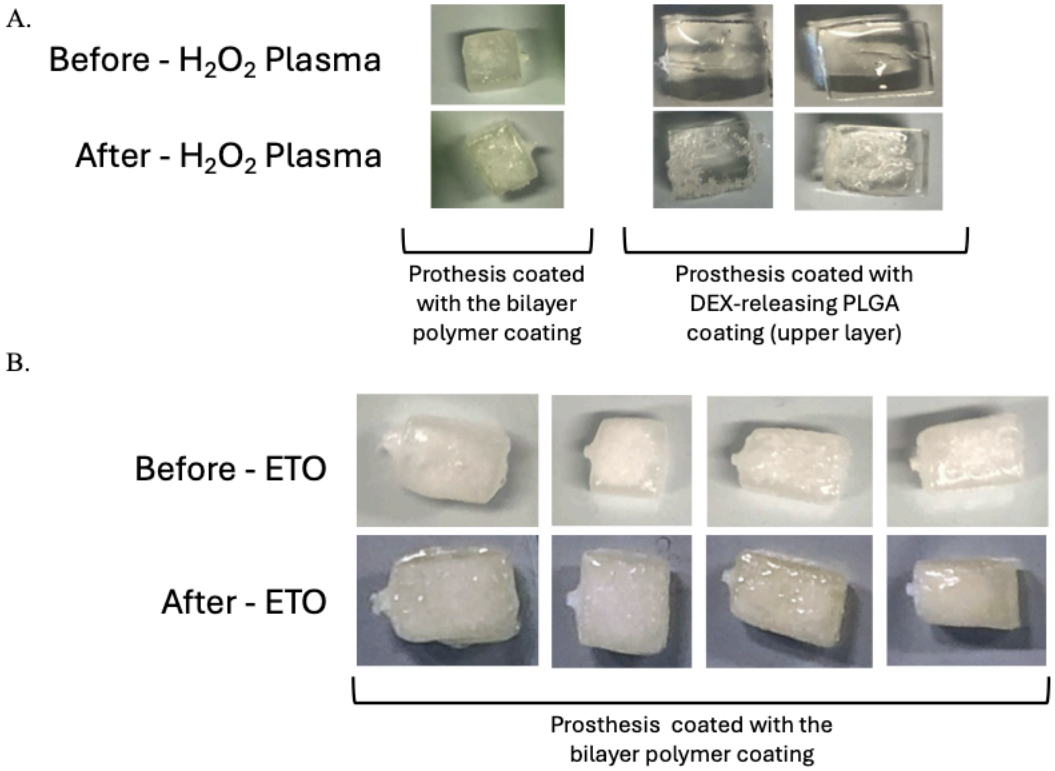

Figure 2.60. Images of coated prostheses sterilized by H_2O_2 plasma (A) and ETO (B).

Abbreviations: H_2O_2: Hydrogen peroxide. DEX: Dexamethasone. PLGA: Poly(lactic-co-glycolic) acid. ETO: Ethylene oxide.

A.

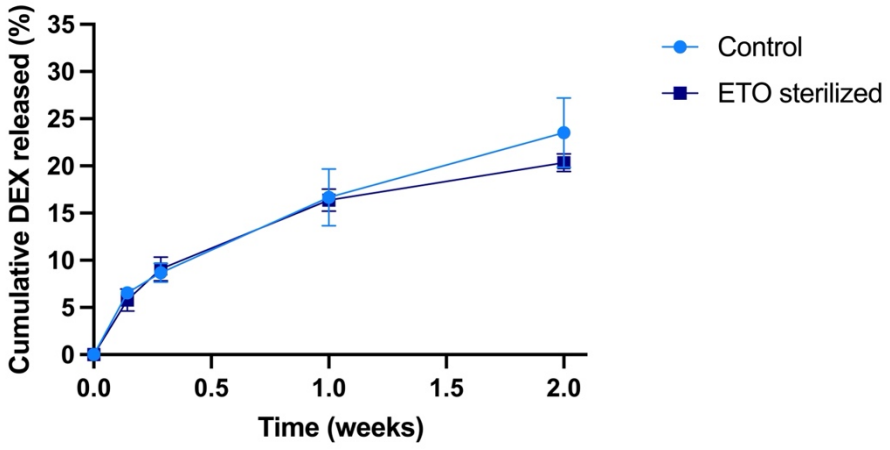

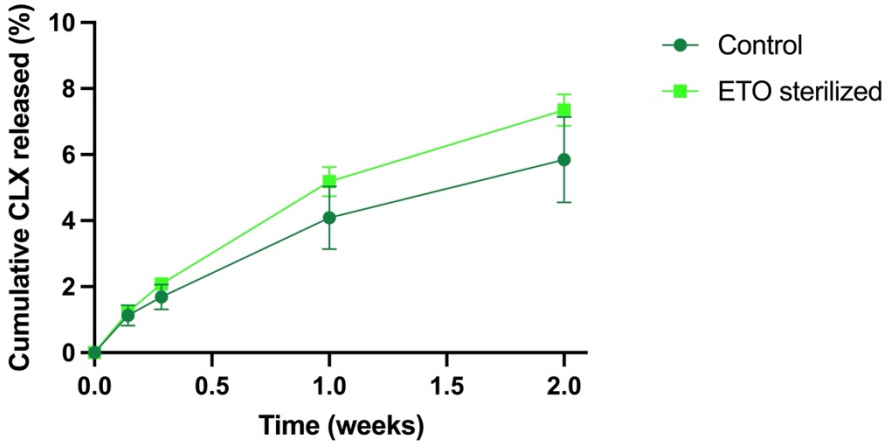

B.

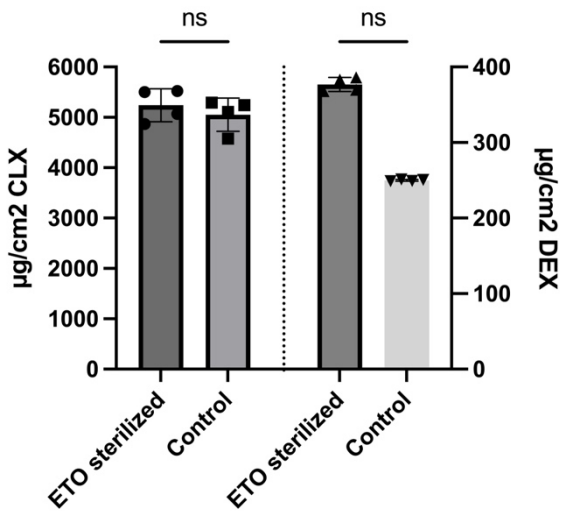

Figure 2.61. Cumulative release of DEX and CLX from bilayer polymer coatings composed of a first polymer coating of PLLA/PCL, prepared at 100 mg/mL at 53/47 (w/w) with CLX loading of 16.6%; and a second polymer coating of LMW-PLGA prepared at 200 mg/mL with DEX loading of 2.44%, deposited on top of an adhesive ECA layer coating the PCU prosthesis. Coated prostheses were analyzed after sterilization (ETO sterilized) or without sterilization (control) (A). Amount of DEX and CLX (µg/cm2) loaded in each of the bilayer polymer coatings analyzed (ETO sterilized and Control) (B).

Abbreviations: DEX: Dexamethasone. CLX: Celecoxib. ETO: Ethylene oxide. Columns represent the mean ± standard deviation (n = 4).

5.4.9.2 Comparison of initial and final coating procedures of the sheep meniscus prosthesis

The modification of the dip-coating orientation, along with the reduction in the polymer concentration of the PLLA/PCL layer from 80/70 (w/w) to 53/47 (w/w) and the introduction of ECA to improve adhesion, resulted in the disappearance of the air gaps that previously indicated poor interaction between layers (Figure 2.24 A and B). This showed that the polymer-coated sheep meniscus prosthesis behaved as a cohesive unit rather than as two distinct systems layered on top of each other. Additionally, following surgeons' recommendations to improve the fixation of the prostheses to the knee bones through the anterior and posterior root tunnels, the screws in the original design were replaced with nylon fixation fibers. These fibers facilitated a quicker surgical procedure and prevented the detachment of screws from the fixation nuts in the tibia (Figure 2.24 C and D).

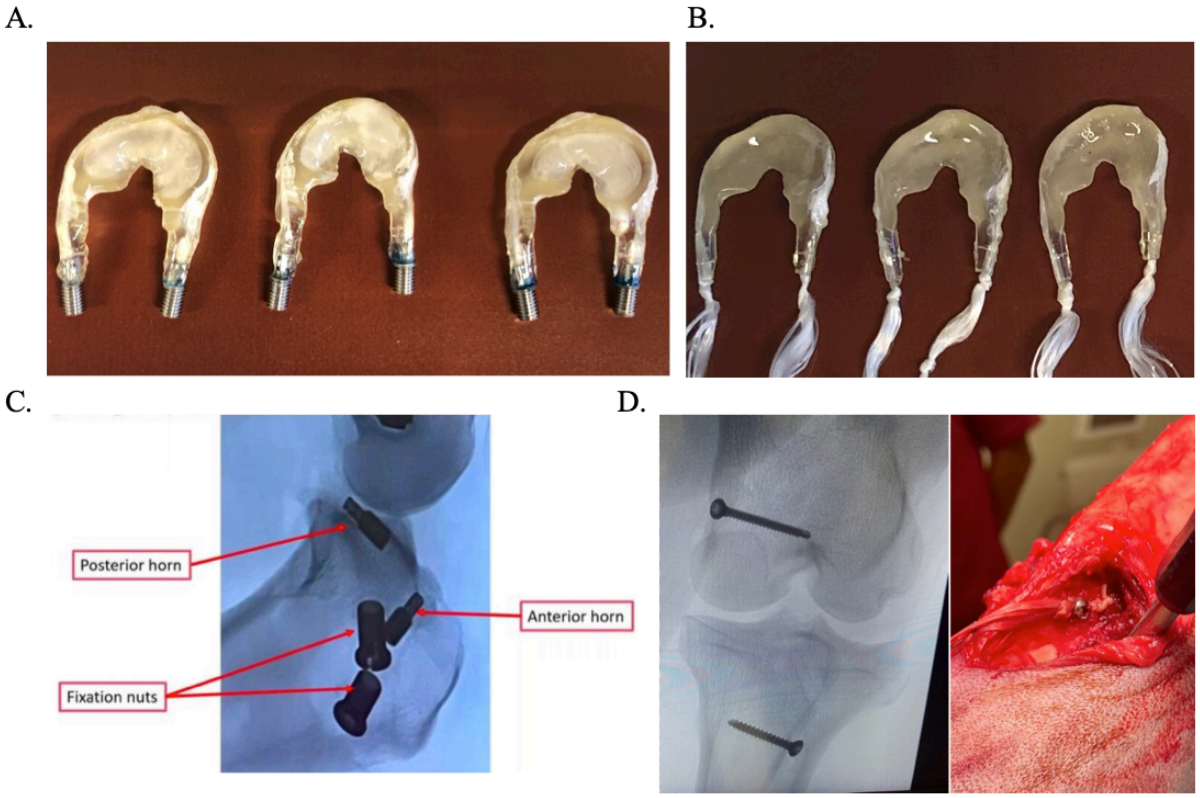

Figure 2.62. Final coating configuration of the bilayer drug-releasing polymer coating before optimization (A) and after optimization of adhesion (B). Fixation of the prosthesis to knee bones using screws (C), and fixation using nylon fibers (D).

5.4.10 *In vivo* evaluation: Sheep test

A pilot *in vivo* study was performed to address the development of a successful fixation technique and to confirm that the polymer coatings of the coated meniscus prostheses could withstand the mechanical forces in the knee cavity of the sheep.

Four sheep underwent total meniscectomy of the medial meniscus, followed by different treatments to evaluate the efficacy of the drug-releasing polymer-coated prostheses.

i. Control Group 1 (No meniscus prosthesis): One sheep underwent total meniscectomy without receiving any meniscus replacement.
ii. Control Group 2 (Uncoated meniscus prosthesis): One sheep received a bare, uncoated meniscus prosthesis using screws immediately after meniscectomy.
iii. Implanted Group (Coated meniscus prosthesis): Another two sheep received drug-releasing polymer-coated meniscus prostheses using fixation fibers immediately after meniscectomy.

Throughout the experiment, sheep were monitored for biomechanical behavior (lameness) and weight changes (alterations in feed intake and rumination), assessing pain, recovery, and potential setbacks [419,420]. Due to complications caused by the screws detaching from the fixation nuts, the sheep implanted with the uncoated prosthesis was sacrificed after one month and used as control group 2. One month post-implantation, sheep recovered without significant weight loss or noticeable lameness, indicating that the surgical procedures and implantations had a minimal adverse impact on their quality of life (data not shown). After three months, sheep were sacrificed for further evaluation, including synovial fluid analysis, prosthesis status, and histopathological assessment of the cartilage in the knee cavity. Synovial fluid samples were clear and viscous, typical of healthy joints, with no signs of inflammation, white blood cell overactivity, or significant joint injury. At the time of explantation, the two coated prostheses remained securely fixed to the medial tibial plateau, demonstrating the success of the fixation method using fibers.

Moreover, the coated meniscus prostheses showed the expected degradation of the top DEX-releasing polymer coating of the bilayer system while the bottom CLX-releasing polymer coating was still present. Lastly, a detailed histopathological analysis of the knee joints was performed using a semi-quantitative grading scale to evaluate any histological changes on different OA hallmarks. This method provided insights into the tissue response to the presence of prostheses and the overall condition of the knee post-experiment:

5.4.10.1 Articular Cartilage Structure Analysis

Fibrillation´s reduction indicates the prosthesis's ability to mitigate cartilage damage, promote joint function, and extend prosthesis longevity [421,422]. The meniscectomy group showed an average score of 0.857, indicating no fibrillation and a normal cartilage structure. In contrast, the uncoated implant group scored 3.142, reflecting significant fibrillation involving more than half of the plateau. The coated implant group had an intermediate score of 2.321, showing a reduction in fibrillation compared to the uncoated group, but with mild superficial fibrillation still present (Figure 2.25A).

5.4.10.2 Toluidine Blue Staining

The toluidine blue staining revealed that the uncoated implant group exhibited the most severe cartilage damage, with an average score of 1.85, indicating a significant loss of staining in the superficial half of the cartilage across more than half of the plateau. The coated implant group scored lower at 1.28, closer to the meniscectomy group's 1.14, indicating milder cartilage damage. This suggests that the drug-releasing polymer coating protected against cartilage degradation, reducing damage compared to the uncoated group. The meniscectomy group exhibited the least damage, although mild degradation was expected due to the absence of the meniscus (Figure 2.25A).

5.4.10.3 Chondrocyte Cloning Activity

Chondrocyte clusters indicate cartilage stress, degeneration, or repair attempts. In this study, the meniscectomy group had minimal cloning activity (score 0.71), suggesting minimal cartilage repair and no significant OA progression. The uncoated implant group showed higher cloning activity (score 1.357), reflecting higher cartilage stress and early signs of OA. The coated implant group scored 1.10, indicating that the coating may reduce cartilage stress and delay OA progression as compared to the uncoated prosthesis. Variability in the results, however, suggests the need for further investigation to confirm the coating's impact on OA development (Figure 2.25A) [421].

5.4.10.4 Osteophyte formation

Osteophytes, or bony outgrowths, are a common feature of degenerative joint diseases and are often used to diagnose OA. Though the cause of osteophyte growth and their pathogenic role in knee OA are unclear, they may represent a response to local damage in a specific compartment, a whole-knee reaction, or a combination [423]. The meniscectomy group showed no osteophyte formation. While most regions in both the coated and uncoated implant groups were free of osteophytes, some osteophyte formation was observed in the medial tibial plateau (MTP) of the uncoated implant. The anti-inflammatory releasing polymer coating appeared to reduce osteophyte formation in this region, though not to the extent observed in the meniscectomy group.

5.4.10.5 Subchondral bone

Subchondral bone thickening indicates OA progression, one of the primary distinctions between OA and rheumatoid arthritis [424,425]. In this study, the coated implant group exhibited notably less subchondral bone thickening than the uncoated implant group, suggesting that the drug-releasing coating helps mitigate OA-related bone changes. Conversely, the uncoated group showed mild thickening, indicating more advanced OA progression. The meniscectomy group displayed no significant changes, reinforcing the association between subchondral bone thickening and the prosthesis's presence, with the coating offering some protection (Figure 2.25A).

5.4.10.6 Fibrocartilage formation

Fibrous tissue formation, a key contributor to joint stiffness and pain during OA progression, also correlates with cartilage damage. Fibrocartilage formation, a mechanical substitute for damaged articular cartilage, suggests repair after tissue damage, although it is mechanically inferior to hyaline cartilage [426]. The uncoated implant group exhibited the highest level of fibrocartilage formation, indicating more pronounced OA progression. In contrast, the coated implant group displayed significantly less fibrocartilage formation, suggesting a protective effect against cartilage damage and OA development. Interestingly, the meniscectomy group exhibited a slightly higher fibrocartilage score than the coated implant group, implying that the release of DEX and CLX from the polymer coating successfully suppresses the inflammatory cascade and subsequent fibrous tissue formation, confirming the hypothesis and the *in vitro* results described in Chapter 1 (Figure 2.25A).

All in all, the meniscectomy group displayed the best outcomes, as fewer OA progression hallmarks were observed. In contrast, the groups implanted with the meniscus prostheses showed specific indicators of OA progression, such as fibrillation of the articular cartilage surface and an increased presence of chondrocytes compared to the meniscectomy group. The most critical disease status was observed for the uncoated meniscus prostheses. This was expected as the sheep in the control group had to be sacrificed at one month post-implantation due to the incorrect function of the meniscus prosthesis using the screws and nuts approach to fix the prosthesis in the knee cavity.

Nevertheless, the drug-releasing polymer coating, using the fixation fibers, remarkably improved the functionality of the meniscus prosthesis. The coated prosthesis reduced synovial inflammation and minimized or prevented the expression of OA progression hallmarks, showing more favorable results across different evaluations than the bare prosthesis. Furthermore, in some cases, such as fibrocartilage or osteophyte formation, the coated prosthesis presented outcomes comparable to or better than the meniscectomy control group.

Additionally, the observations related to fibrocartilage formation could be extrapolated to provide insights into the foreign body response (FBR). Despite the different triggers for fibrous tissue formation—tissue repair after cartilage injury and fibrous capsule formation in response to prosthesis implantation—similar inflammatory pathways, including TNF-α and IL-1, are involved in both processes. The system's ability to suppress these cytokines, primarily due to the action of DEX and CLX in fibrocartilage formation, suggests that it could also mitigate fibrous tissue formation in FBR. This, again, aligns with the *in vitro* findings in Chapter 1, further supporting the hypothesis that this bilayer coating could reduce acute and chronic inflammation, arguably preventing FBR [58,59].

Regarding specific joint regions, the medial tibial plateau (MTP), the most affected by the surgery because of the direct contact with the meniscus prosthesis, displayed consistent results with the overall findings. The coated prosthesis outperformed the uncoated prosthesis across all evaluations, particularly in toluidine blue staining, which suggests that the anti-inflammatory drugs released from the polymer coating remarkably reduced damage to the articular cartilage surface in direct contact with the meniscus prosthesis, thereby improving knee function and potentially delaying OA progression (Figure 2.25B).

Despite these promising findings, one of the study's limitations is the small number of sheep analyzed. This limits the statistical power of the results and affects the robustness of the conclusions drawn. A larger sample size is necessary to validate these observations. Moreover, a more extended follow-up period beyond the three months used in this study would provide a more comprehensive understanding of the long-term impact of meniscus resection and prosthesis implantation on OA development.

It has been previously described in the literature that partial or total meniscectomy is associated with OA onset and a poorer prognosis compared to meniscus repair, reinforcing the need for long-term evaluations, as the meniscectomy group is likely to experience setbacks over time [427–430]. Cartilage damage would likely progress over the years without an unloading device such as our meniscus prosthesis, leading to OA. Ideally, meniscus repair surgery would be the preferred treatment, but it is often not feasible in older patients. Surgeons typically avoid meniscal repairs in older individuals due to concerns about reduced healing potential and preexisting degenerative changes, as the meniscus's limited blood supply decreases with age, resulting in higher failure rates, as noted in previous studies [431].

As highlighted above, meniscectomy remains the standard clinical practice because of its positive outcomes in the short term [432]. Removing the injured meniscus reduces friction against the knee cartilage, alleviating symptoms and improving function in the early post-surgical period. Consequently, in this pilot *in vivo* study, it was expected that the meniscectomy group would show the best outcomes during the three-month period of this pilot study. Thus, these findings underscore the need for longer evaluation periods to fully assess the potential of meniscus prostheses in mitigating OA progression and providing sustained cartilage-protective benefits compared to meniscectomy.

Finally, while the histological evaluations revealed that the bilayer polymer coating releasing anti-inflammatory drugs significantly improved outcomes compared to the uncoated prosthesis, it is important to note that the uncoated prosthesis control group was sacrificed two months before the three-month endpoint due to complications associated with the fixation. X-rays performed post-sacrifice indicated that, although the meniscus prosthesis remained in place throughout the study, the fixation screws were not securely attached to the nuts, highlighting that the fixation method was not optimal. This necessitated a modification of the fixation technique for the coated meniscus prostheses, replacing screws with fibers to enhance stability.

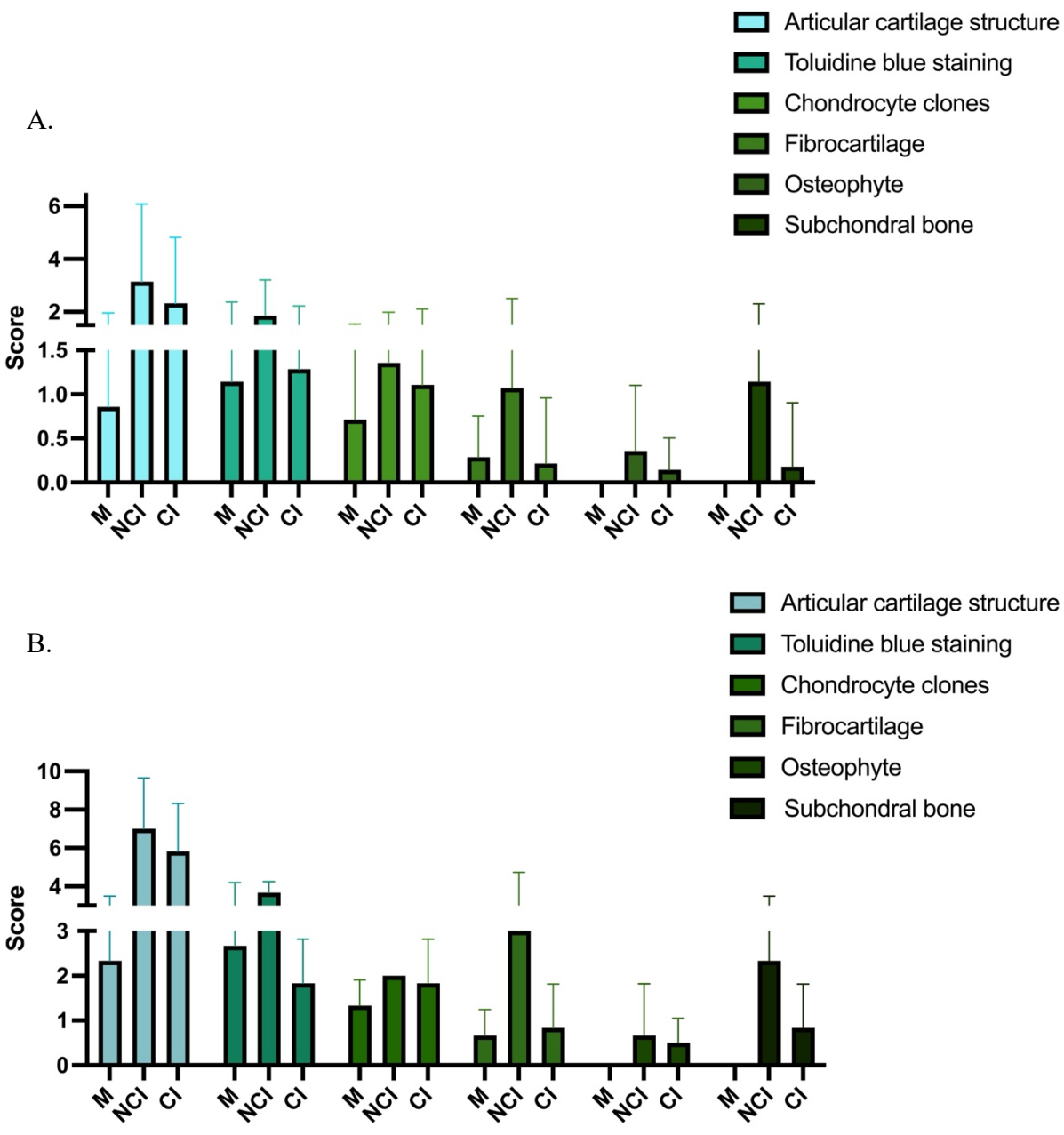

Figure 2.63. Histological scores average of all areas (A) or MTP (B).

Abbreviations: M: Meniscectomy (no meniscus prosthesis). NCI: Non-coated implant (meniscectomy + uncoated meniscus prosthesis). CI: Coated implant (meniscectomy + coated meniscus prosthesis).

Thus, although the results for the uncoated prosthesis control group are displayed in the graphs, they are not directly comparable to the coated prosthesis group. Differences in the fixation technique and the shorter experimental duration for the uncoated group preclude a true head-to-head comparison. However, the data can still be used to provide a general trend for this pilot *in vivo* study.

The primary objectives of this experiment were to develop a successful fixation technique and confirm that the polymer coatings of the coated meniscus prostheses could withstand the mechanical forces in the sheep's knee cavity. These objectives were achieved, as the coated

prostheses demonstrated both mechanical integrity and improved fixation outcomes compared to the uncoated prosthesis. Future studies employing the same fixation technique for both groups would enable a more robust, direct comparison.

In conclusion, the study underscores the need for a larger sample size, extended follow-up periods, and more precise controls to fully validate these promising initial findings. The bilayer drug-releasing polymer coating demonstrates considerable potential in improving meniscus prosthesis outcomes and preventing OA progression. Thus, this study should be regarded as a pilot *in vivo* investigation, providing valuable insights into the ability of the polymeric coatings to withstand the mechanical forces in the knee cavity and identifying the most effective prosthesis fixation technique within the joint.

5.5 CONCLUSIONS

In this work, we investigated strategies to achieve the adhesion of a drug-releasing polymer bilayer coating a PCU meniscus prosthesis. The most performant and singular strategy relied on the use of an ECA adhesive layer between the PCU and the polymer bilayer. Mechanical analysis revealed that the prostheses coated with this adhesive layer exhibited adequate mechanical properties (G', G'', and elastic modulus), while preserving the mechanical integrity of the prosthesis.

Furthermore, the optimized drug-releasing polymer coating was adapted from the square-shaped PCU meniscus prostheses to meet the physical and mechanical requirements of the sheep meniscus prosthesis. The modification of the CLX-releasing PLLA/PCL layer concentration, along with the change in the orientation of the meniscus prosthesis during the dip-coating process, resulted in a more homogeneous polymer coating. This adjustment ensured that the complex and demanding structure of the sheep meniscus prosthesis was preserved while improving the uniformity, drug distribution, and overall effectiveness of the coating.

A selected prototype was analyzed in a bioreactor that mimicked gait forces. This evaluation revealed that although the applied forces influenced the microscopic surface distribution of the coating, the polymer coating remained intact, with no delamination.

Finally, the optimized polymer-coated sheep meniscus prostheses were successfully implanted and evaluated over a set period. Although the *in vivo* results are not yet conclusive, the functionalized prostheses showed improved biomechanical parameters and better integration compared to the uncoated version. Histological evaluations confirmed the coated prosthesis outperformed the uncoated one, and while the meniscectomy group showed better outcomes in the short term, these results suggest that, with a larger sample size and longer-term studies, the coated prosthesis could offer a more effective treatment for meniscus injuries, addressing the limitations of meniscectomy.

CHAPTER 3

3D Encapsulation of thymic organoids in ECM-mimicking IPNs to evaluate morphogenesis *in vitro*

6 3D ENCAPSULATION OF THYMIC ORGANOIDS IN ECM-MIMICKING IPNS TO EVALUATE MORPHOGENESIS *IN VITRO*

This work was done during my research visit at Harvard University (School of Engineering and Applied Sciences - SEAS) under the supervision of Prof. David J. Mooney. In collaboration with Andrew Khalil, Ph.D. (Havard University), Junzhe Lou, Ph.D. (Harvard University), Grace Bingham (Harvard University), and Bryan Nerger (Harvard University). And in collaboration with Prof. Rudolf Jaenisch (Whitehead Institute for Biomedical Research - Massachusetts Institute of Technology) and Tenzin Lungjangwa (Whitehead Institute for Biomedical Research - Massachusetts Institute of Technology).

6.1 ABSTRACT

The thymus is crucial for the maturation and differentiation of T cells, playing an essential role in maintaining immune system function. However, as the thymus involutes with age, the body's ability to generate new T cells becomes increasingly limited, reducing the efficacy of innovative therapies like CAR-T cells, which rely on re-educating the existing T cell population. Moreover, the demand for advanced *ex vivo* models in research has spurred progress in technologies such as organoids and organ-on-a-chip systems, which aim to minimize animal experimentation. While these models successfully replicate many organ functions, they often lack an integrated immune system. The objective of this work was to investigate new immunocompetent thymus organoids, emphasizing the impact of the extracellular matrix (ECM) on organ development.

The hypothesis of this work was that mechanical signals regulate thymus morphogenesis in a 3D culture setting. Thymus organoids were encapsulated within alginate-based hydrogels containing Matrigel® (interpenetrating polymer networks, IPNs), which were designed with varying stress relaxation rates and stiffness. The results demonstrated that matrix viscoelasticity significantly influenced tissue organization during the first week of organoid incorporation. Furthermore, the expression of key thymus developmental markers, including K8, FOXN1, EpCAM, and VCAM1, was remarkably enhanced in those IPNs closely mimicking the mechanical properties of native thymus tissue. These findings suggest that IPN hydrogels enable precise modulation of thymus organoid development and morphology, underscoring the importance of the mechanical microenvironment as a critical design parameter for thymus tissue engineering.

6.2 GENERAL INTRODUCTION TO HYDROGELS IN TISSUE ENGINEERING

In recent decades, the advancement of bioinks, bioprinting, and sophisticated 3D models has increasingly incorporated natural polymers like alginate, chitosan, hyaluronic acid, and collagen, among others. These materials are favored for their ability to closely mimic the properties of biological tissues, enabling the creation of *in vitro* structures that closely resemble human biology [433–435]. Table 3.1 shows some of their latest applications in tissue engineering.

Table 3.13. Relevant examples of polymers for tissue engineering applications.

Biomedical application	Polymer	Target	Technology	References
Tissue engineering	Alginate	Cardiac	Hydrogel, nanoparticles	[436–439]
		Bone	Hydrogel	[440,441]
		Cartilage	Scaffold	[442,443]
		Muscle	Hydrogel	[444]
		Soft tissue	Hydrogel, scaffold	[445,446]
		Connective tissue	-	[447]
	Chitosan	Cardiac	Nanoparticles	[448]
		Cartilage	Nanoparticles, scaffold	[449,450]
		Soft tissue	Hydrogel	[451]
	HA	Bone	Hydrogel	[452]
		Cartilage	Hydrogel, microparticles, scaffold	[453–455]
		Adipose	Hydrogel	[456]
	Collagen	Bone	Scaffold	[457]
		Cartilage	Scaffold	[458]
		Adipose	Hydrogel	[459]
		Oral mucosa	Scaffold	[460]

Abbreviations: HA: Hyaluronic acid.

6.2.1 Hydrogels

Hydrogels are three-dimensional polymeric networks that can absorb and retain large volumes of water or biological fluids due to their hydrophilic nature. This ability to swell and maintain a hydrated state makes them highly versatile for numerous biomedical applications, such as tissue regeneration and drug delivery. The fabrication of hydrogels through various cross-linking methods allows for precise control over their physical and chemical properties, enabling customization for multiple biomedical applications [461,462].

6.2.1.1 Types of cross-linking

a) Physical Cross-Linking:

Physical cross-linking involves the formation of hydrogel networks through non-covalent interactions, such as hydrogen bonding, self-assembly, and crystallization. External stimuli can influence these interactions, including temperature changes (heating or cooling), pH alterations, or mechanical processes like freeze-thaw cycles. The resulting hydrogels are typically reversible and responsive to environmental conditions, making them suitable for applications requiring dynamic behavior and tunability [463].

b) *Chemical Cross-Linking:*

Chemical cross-linking forms hydrogel networks through covalent bonds, providing a more permanent and stable structure. This process can involve copolymerization with multifunctional monomers, exposure to high-energy radiation, or specific chemical reactions between complementary groups or with added cross-linkers. Standard chemical cross-linking methods include free radical polymerization, click chemistry, and Schiff base cross-linking. These hydrogels often exhibit enhanced mechanical strength and stability, ideal for applications requiring long-term durability and controlled release properties [463].

6.2.1.2 Applications

Hydrogels have become essential in various biomedical applications due to their versatility and adaptability. In contact lenses, hydrogels are valued for their biocompatibility, antifouling properties, and mechanical performance, closely mimicking natural ocular tissues. Commercial examples include Clariti® 1 day, ACUVUE OASYS®, and Airsoft™ [464]. For wound healing, hydrogel-based dressings provide a moist, oxygen-permeable, and biocompatible environment that supports tissue regeneration while preventing contamination. Products such as DermaSyn® and Purilon® highlight their clinical effectiveness [465,466]. Similarly, in drug delivery, hydrogels enable controlled spatial and temporal release of therapeutic agents, with commercialized examples like AndroGel® (used for testosterone replacement therapy in men), REGRANEX® (used for the treatment of diabetic foot ulcers), and VANTAS® (used for the palliative treatment of advanced prostate cancer) demonstrating their success across various delivery methods [11,467].

This chapter will focus on the application of hydrogels in tissue engineering, emphasizing their potential to advance regenerative medicine and advanced cellular models *in vitro*.

Developing strategies for engineering tissues and creating functional constructs to restore, maintain, and rejuvenate damaged or lost tissues and organs has profoundly influenced medicine and healthcare. Over the last two decades, hydrogels have become some of the most widely used scaffolds in tissue engineering due to their ability to maintain a defined three-dimensional structure, provide mechanical support to cells, and mimic the native extracellular matrix (ECM) of various tissues through their polymer network. The high water content of hydrogels creates an environment conducive to cell viability and mirrors the structural properties of natural tissues. Additionally, hydrogels offer customizable physical properties, controllable degradability, and excellent compatibility with biological tissues, which enhance cell attachment and support cell survival, making them ideal for tissue engineering [468,469].

6.2.1.2.1 Hydrogels in immune system tissue engineering

Hydrogels have emerged as key tools for modulating the immune system through the controlled release of molecules and their intrinsic properties, playing a pivotal role in this field. For instance, alginate hydrogels have been utilized to mediate dendritic cell (DC) accumulation *in vivo*, forming the basis for therapeutic vaccines [470], while alginate cryogels injected near inguinal lymph nodes have been shown to recruit DCs and induce antigen-specific immune responses [471]. Additionally, hydrogels have been employed to enhance anti-tumor immune responses by facilitating cell and drug delivery, on-site immune cell activation and transport, and immune cell recruitment [472].

The increasing emphasis on understanding, modulating, and regenerating the immune system has intensified research in immune system tissue engineering, aiming to replicate the complex structure and function of immune organs such as the thymus, lymph nodes, and bone marrow [473,474]. Beyond hydrogels, other approaches have utilized decellularized or polymeric scaffolds for engineering immune system tissues. Notable examples include alginate scaffolds engineered for T-cell modulation and CAR-T cell generation [475]. This section highlights recent advances in bioengineered hydrogels designed to mimic immune system organs (Table 3.2).

Table 3.14. Relevant examples of recently developed hydrogels for immune tissue engineering.

Material	Function	Observations and Results	Reference
HA hydrogel engineered with DLL4, VCAM1 and collagen derived proteins	Thymus-like hydrogel Differentiation of T cells from hematopoietic stem cells	Production of CD4+CD8b+ progenitor (Pro) T cells and functional CD3+CD8b+ T cells. First hydrogel-based platform able to produce T cells from iPSC-derived hematopoietic stem and Pro cells.	[476]
EAK16-II/EAKIIH6 peptide hydrogel	Generate a functional mini thymus clustering TECs	Retainment of molecular properties of TECs *in vitro*. TEC/EAK mini clusters allow T cell development *in vivo*.	[477]
Alginate hydrogel	Promote TEPC differentiation and maturation from iPSCs	iPSC-TEPCs were put together with $CD34^+$ HPCs in a decellularized thymic scaffold to create a human thymic organoid. Thymus organoid supported T cell programming *in vitro*. TCR repertoire expressed *in vivo* in hu mice.	[478]
Composite scaffold consisting of Gel-HA hydrogel and GFs	Bone marrow-mimicking composite Support expansion of HSCs *in vitro*	Proliferation of HSCs. Gel-HA/GF maintains CD34+CD38− immunophenotype of HSCs. Mimics bone marrow niches.	[479]
PEG-MAL	3D ex vivo immune tissue model to induce antigen-specific B cell responses	Hydrogel acts as an engineered immune tissue able to modulate GC B cell activation and differentiation *ex vivo*. PEG-MAL facilitates GC B cell enrichment based on antigen affinity *ex vivo*.	[480]

Abbreviations: HA: Hyaluronic acid. DLL: Delta-like ligand. VCAM: Vascular cell adhesion molecule. CD: Cluster of differentiation. iPSC: Induced pluripotent stem cell. EAK: Endothelial-adipocyte kinase. TEC: Thymic epithelial cell. TEPC: Thymic epithelial progenitor cells. HPC: Hematopoietic progenitor cell. TCR: T cell receptor. HSC: Hematopoietic stem cell. GF: Graphene foam. MAL: Maleimide. GC: Germinal center.

Over the last decades, advances in technological fields such as chemistry, materials science, and cross-linking methods have supported using hydrogels as matrices for tissue engineering. A search for "hydrogel tissue engineering" in PubMed reveals 11,484 articles since 2019, highlighting the growing interest in this area. However, despite the increasing development of hydrogel-based technologies to improve regeneration, many challenges and unmet clinical needs still need to be addressed.

The trend nowadays is shifting towards advanced 3D cell cultures, which can replicate live tissue's biological and physicochemical properties *in vitro*, reducing the number of *in vivo* assays [481,482]. Hydrogels are increasingly used as 3D models to mimic the ECM and evaluate the development of stem cells. Nevertheless, to produce *in vitro* 3D models that accurately replicate the anatomy and function of human tissues and organs, it is essential to understand functional human tissues at the microenvironment scale, including interactions with the immune system. This is particularly challenging due to the complexity of immune responses and the limited availability of immune system cells [483,484]. Tissue engineering using hydrogels to recreate the immune system could enhance our understanding of immune responses and interactions and provide a sustainable source of immune cells, advancing the clinical relevance of current *in vitro* 3D models.

As research expands, the role of hydrogels in modulating and recreating the immune system is expected to become increasingly significant.

6.3 INTRODUCTION

The therapeutic potential of T cells has gained considerable attention, particularly for treating cancers and autoimmune disorders. Their value as therapeutic agents stems from their ability to specifically target and eliminate diseased cells, making them crucial for managing immune responses. Central to this function is the T cell receptor (TCR), which enables T cells to recognize antigens presented by other cells. The specificity and diversity of TCRs are essential for T cell-based therapies, such as CAR-T therapy, which reprograms T cells to target specific cancer cells.

TCR repertoire formation occurs during T cell development and maturation in the thymus through tightly regulated events within specialized zones, where distinct signals and cell types direct thymocyte differentiation into fully functional T cells. Immature thymocytes undergo Positive Selection (PS) in the thymic cortex, ensuring only those recognizing self-MHC molecules survive. This is followed by Negative Selection (NS) in the medulla, where autoreactive thymocytes are eliminated to prevent autoimmunity (Figure 3.1). The thymic microenvironment's spatial organization and mechanical properties, including the ECM and tissue architecture, play critical roles in this process [60].

The spatial and temporal patterning is crucial for proper tissue and organ development, growth, and function. These patterns are guided significantly by mechanical cues generated by the ECM [485,486]. The viscoelastic properties of the ECM, which range from solid-like (elastic) to liquid-like (viscous) responses, have a profound impact on tissue organization [245]. Additionally, the stiffness and composition of the ECM are key factors that influence cell behavior, such as proliferation [487], differentiation [488], migration [245], and tissue structure [489]. The time-dependent mechanical properties of the ECM are particularly crucial for guiding morphogenesis, as shown for organs like the kidney [61]. Understanding and recreating these dynamics is essential for developing functional engineered tissues.

Recent advances in bioengineering have enabled the creation of human tissues *in vitro*, opening new possibilities for regenerative medicine and drug testing. Center for Biologics Evaluation and Research (CBER) and FDA-approved engineered tissues, such as skin and cartilage, offer alternatives to organ transplants and support personalized medicine [490,491]. Organoids and organs-on-chip provide valuable models for studying human development, disease, and therapeutic responses while reducing the need for animal testing [492].

However, challenges persist in tissue engineering, including sourcing diverse cell types to replicate complex human tissues, designing matrices that support functional multicellular structures, and integrating immune cells for accurate modeling of tissue responses. Addressing these issues is critical for advancing the therapeutic potential of engineered tissues. Focusing on thymus biology, despite progress in its understanding, many aspects still need to be clarified, particularly how mechanical signals from the thymic microenvironment regulate T cell maturation. Improving *in vitro* models, such as thymus organoids, to mimic this complexity better is essential.

This chapter investigates how the mechanical properties of ionically crosslinked alginate hydrogels, modified to incorporate ECM-associated proteins and form interpenetrating polymer networks (IPNs), influence thymus organoid development. Unlike native ECM, alginate

hydrogels resist mammalian cell degradation, allowing for independent tuning of viscoelasticity, stiffness, and ligand density. Furthermore, ionically crosslinked alginate hydrogels can adapt to the different stress relaxation rates of developing tissues while maintaining stability in culture over several weeks [61]. Thymus organoids consist of two cell types derived from human embryonic pluripotent stem cells (hESCs): thymus epithelial progenitor cells (TEPCs) and neural crest cells (NCCs). TEPCs are essential to creating the thymus microenvironment and structural framework, giving rise to the various types of thymic epithelial cells (TECs): medullary TEC (mTEC) and cortical TEC (cTEC) [493,494]. NCCs result in the mesenchymal capsule and the pericytes in the thymus [495]. In particular, four gel conditions presenting different viscoelasticity and stiffness were designed and used to encapsulate thymus organoids. These organoids were cultured and tracked for one week to evaluate how cells rearrange depending on the mechanical cues generated by the IPNs. Finally, after one week, the organoids were analyzed by immunohistochemistry (IHC) to evaluate the influence of the IPNs in the expression of markers characteristic of thymus development. Encapsulation studies of thymic organoids demonstrate that matrix mechanics regulate thymic tissue development and patterning, providing valuable insights into the design principles for engineering biomaterials for thymus organogenesis.

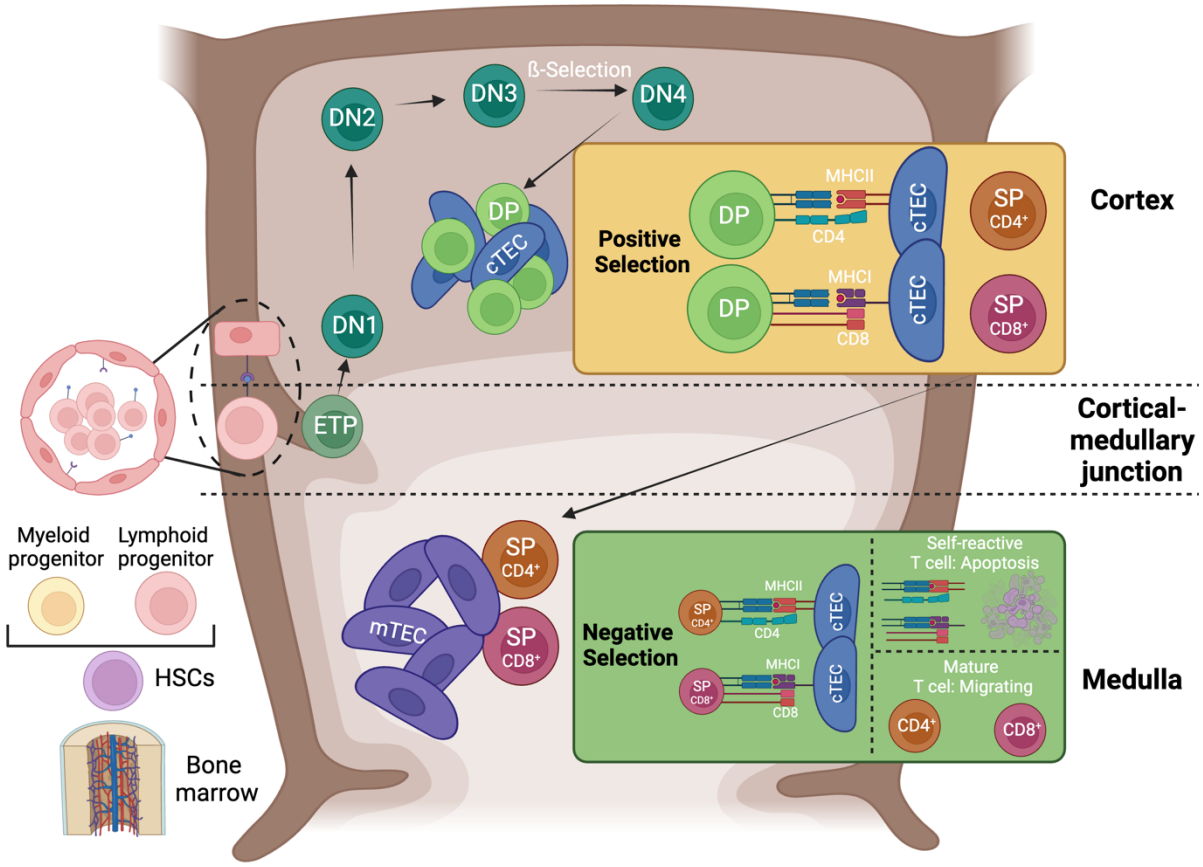

Figure 3.64. Schematic representation of a sagittal section of the thymus illustrating the T cell maturation process.

Abbreviations: HSC: Hematopoietic stem cells. ETP: Early T-lineage progenitors. DN: Double negative. DP: Double positive. cTEC: Cortical thymic epithelial cells. SP: Single positive. mTEC: Medullary thymic epithelial cells. MHC: Major histocompatibility complex. Created with https://www.biorender.com/

6.4 MATERIALS AND METHODS

6.4.1 Materials

Sodium alginate (Protanal LF10/60) was obtained from FMC (Sandvika, Norway). Calcium sulfate dihydrate ($CaSO_4$) was supplied by Sigma-Aldrich (St. Louis, MO, USA). Phosphate-buffered saline (PBS) was purchased from Corning (NY, USA). Tissue-Tek O.C.T. compound was sourced from Sakura (Torrance, CA, USA). Superfrost Plus microscope slides were provided by VWR (Radnor, PA, USA). Paraformaldehyde (PFA) was obtained from Electron Microscopy Sciences (Hatfield, PA, USA). Sucrose, MES hydrate (M8250), sodium chloride, N-(3-Dimethylaminopropyl)-N′-ethylcarbodiimide hydrochloride (EDC), hydroxylamine hydrochloride, and activated charcoal were all supplied by Sigma-Aldrich (St. Louis, MO, USA). N-hydroxysulfosuccinimide (sulfo-NHS) was purchased from Thermo Fisher Scientific (Waltham, MA, USA). TrueBlack® Background Suppressor and Cover-Grip coverslip sealant were purchased from Biotium (Fremont, CA, USA). No. 1.5 glass coverslips were purchased from VWR (Radnor, PA, USA). RGD peptide (GGGGRGDSP) was obtained from Peptide 2.0 (Chantilly, VA, USA). Dialysis membranes (MW cutoff 3.5 kDa) were acquired from Spectra/Por 6 (Repligen, Waltham, MA, USA). Luer-Lok syringes were purchased from BD (Franklin Lakes, NJ, USA). X-Vivo 10 medium was obtained from Lonza (Basel, Switzerland). Matrigel was purchased from Corning (NY, USA).

6.4.2 Alginate functionalization

RGD functionalization of alginate was performed using aqueous carbodiimide chemistry [496], as described previously [497]. Briefly, alginate functionalization was conducted with a 1% solution of sodium alginate in 0.1 M MES buffer [0.1 M MES hydrate + 0.3 M sodium chloride] using empirically determined reaction conditions [497]. N-(3-Dimethylaminopropyl)-N′-ethylcarbodiimide hydrochloride (EDC) and N-hydroxysulfosuccinimide (sulfo-NHS) were used to link a linear RGD peptide (GGGGRGDSP) to the carboxylate moieties on the alginate backbone. The reaction was performed at room temperature for 20 h and quenched with 125 mg hydroxylamine hydrochloride/g alginate. High MW alginate was functionalized with a degree of substitution (DS) of 20, which corresponds to 166.67 × 10−6 m RGD per gram of alginate. Low MW alginate was functionalized using the same molar concentrations of reactants. Functionalized alginate was dialyzed (MW cutoff 3.5 kDa) for 3 d in decreasing NaCl solutions in DI water (starting at 0.13 M NaCl). After dialysis, alginate was treated with 0.5 g of activated charcoal/g alginate for 30 min with continuous stirring. Finally, alginate was sterile-filtered (0.22 μm), lyophilized, and stored at −20 °C. Unless stated otherwise, all alginate hydrogels had a final alginate concentration of 20 mg/mL and were functionalized with RGD peptide as described above.

6.4.3 ECM-mimicking IPN preparation

IPNs were prepared using 1 mL Luer-Lok syringes and a female Luer thread style coupler. Alginate was dissolved in X-Vivo 10 medium and combined with Matrigel® in one syringe. In another syringe, $CaSO_4$ was combined with cell culture medium. The contents of the syringes were mixed (10-12 times) and deposited between glass plates to generate 1-mm-thick gels.

Alginate was incubated at 37 °C and 5% CO2 for 1 h and then mechanically characterized (Figure 3.2A).

6.4.4 Mechanical characterization by nanoindentation

Nanoindentation was performed using a KLA (Milpitas, CA, USA) iNano nanoindenter equipped with a 1.3 mm diameter flat punch to measure the mechanical properties of the samples. Samples were prepared to ensure flat, parallel surfaces and mounted securely to minimize displacement during testing. The following parameters were used for all tests: a pre-test compression of 10 µm was applied to ensure consistent sample contact, followed by testing at a frequency of 100 Hz with a test amplitude of 20 µN. A surface approach frequency of 140 Hz was employed to precisely identify the sample surface, with a phase change of 0.5º used to define the point of contact. A Poisson's ratio (v) of 0.50 was assumed for the calculations. Data were collected and analyzed to determine the storage modulus (G'), loss modulus (G''), and tan δ. Elastic modulus (E) was calculated using Equation (1).

$$E = 2G\,(1+v) \text{ and } G = \sqrt{G'^2 + G''^2} \quad (1)$$

6.4.5 Mechanical characterization by compression test

IPNs were subjected to compression testing using a Bose ElectroForce® mechanical testing system equipped with parallel plates (TA instruments) to determine their elastic modulus and stress relaxation properties. IPNs (1 mm thickness), immediately after synthesis, were placed between the compression plates, ensuring parallel alignment and no pre-load force. The compression test was performed by applying a ramp displacement at a rate of 0.05 mm/s up to 0.2 mm (20% of the total IPN thickness) while continuously recording force and displacement. The elastic modulus was calculated from the slope of the stress-strain curve in the linear elastic region, with stress derived as force divided by the sample cross-sectional area and strain as displacement divided by the initial sample height. Following the ramp displacement, stress relaxation was assessed by maintaining the 0.3 mm displacement for 185 seconds while recording the decay in force over time. The relaxation data were analyzed by fitting to an exponential decay model to extract time constants and equilibrium stress values. The relaxation time was defined as the time required for the normalized stress to decrease to 70% of its initial value after applying a constant displacement during the stress relaxation phase.

6.4.6 Neural crest cell (NCC) differentiation

Neural crest cells (NCCs) were thawed and expanded five days before harvesting TEPCs. A vial of NCCs was thawed and plated onto a 15 cm Matrigel-coated dish in NCC Expansion Media. NCC Expansion Media was prepared using N2B27 Base Media, which consisted of DMEM/F12 (500 mL), 2% B27 (10 mL), 1% N2 (5 mL), 1% penicillin/streptomycin (5 mL), 1 mM L-glutamine (5 mL), and 1% non-essential amino acids (5 mL). The N2B27 Base Media was supplemented with 3 µM CHIR99021, 20 ng/mL bFGF, and 20 ng/mL EGF. NCCs were maintained in this media until they were ready for use in organoid formation. Fluorescent NCCs

were differentiated from hPSC-RFP. Non-fluorescent NCCs were differentiated from hPSC-WT.

6.4.7 Thymic epithelial progenitor cell (TEPC) differentiation

Human pluripotent stem cells (hPSCs) were seeded at a density of 1×10^6 cells per 10 cm Matrigel-coated dish in E8 medium supplemented with 10 μM ROCK inhibitor. On Day 1, the medium was replaced with Step 1 medium, consisting of Lonza X-Vivo 10 base medium supplemented with 100 ng/mL Activin A. The cells were maintained in Step 1 medium until Day 4, with a media change on Day 3. On Day 4, TEPCs were harvested using TrypLE, centrifuged, and resuspended in Step 1 medium. Fluorescent TEPCs were differentiated from hPSC-GFP. Non-fluorescent TEPCs were differentiated from hPSC-WT.

6.4.8 Thymic organoid formation

On Day 4, TEPCs (10,000 cells per organoid) were combined with NCCs (30,000 cells per organoid) in Step 1 medium supplemented with 10 μM ROCK inhibitor. The TEPC-NCC mixture was seeded into ultra-low attachment 96-well U-bottom plates at a density of 150 μL per well. The plates were centrifuged at 300 × g for 3 minutes to promote cell aggregation and incubated at 37°C.

6.4.9 Encapsulation of thymic organoids in ECM-mimicking IPNs

On Day 6, the organoids were encapsulated in a matrix, similarly as described in 3.5.3 (Figure 3.2B). Briefly, IPNs were prepared using 1 mL Luer-Lok syringes and a female Luer thread style coupler. Alginate was dissolved in X-Vivo 10 medium and combined with Matrigel® and the thymic organoids in one syringe. In another syringe, $CaSO_4$ was combined with cell culture medium. The contents of the syringes were mixed (10-12 times) and deposited between glass plates to generate 1-mm-thick gels. Alginate was incubated at 37 °C and 5% CO2 for 1 h and then mechanically characterized.

Then, organoids encapsulated in IPNs were transferred to a 6 cm dish containing 4 mL of Step 3 medium, which consisted of Lonza X-Vivo 10 base medium supplemented with 1 μM all-trans retinoic acid and 2.5 μM IWR1. On Day 8, 2 mL of Step 3 medium was added to the dish.

On Day 10, the medium was replaced with Step 4 medium, consisting of Lonza X-Vivo 10 base medium supplemented with 10 ng/mL BMP-4 and 50 ng/mL WNT3a. On Day 12, fresh Step 4 medium was added to the culture. Organoids were harvested on Day 14 for further analysis or co-culture experiments with pro-T cells.

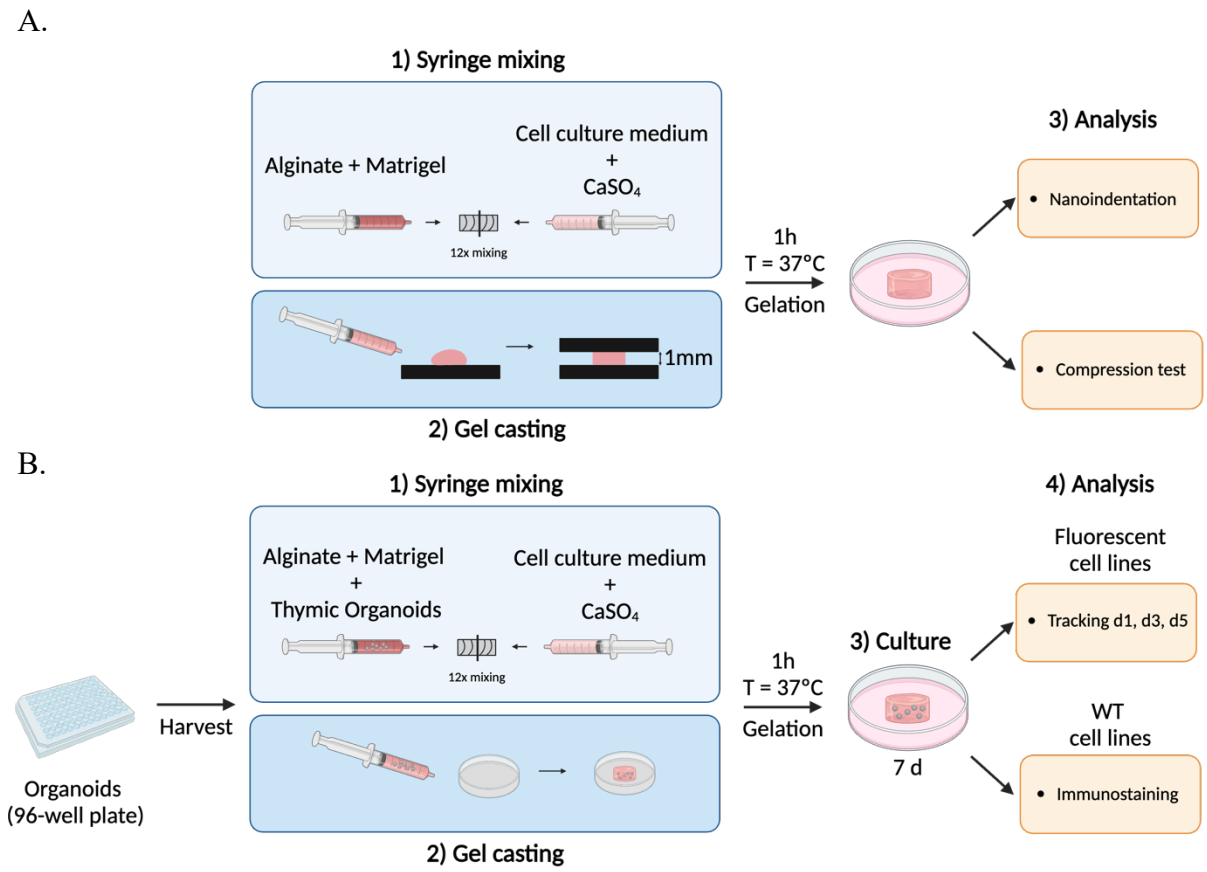

Figure 3.65. Schematic of IPN synthesis for mechanical characterization (A). Schematic of thymic organoids embedding and post-fixation analysis.

Abbreviations: $CaSO_4$: Calcium sulfate dihydrate. Created with https://www.biorender.com/

6.4.10 Widefield microscopy

Widefield microscopy was performed using an Eclipse Ti inverted fluorescence microscope (Nikon), equipped with brightfield and fluorescence imaging capabilities for imaging live cells in 6 cm culture dishes. Samples were visualized under 4× and 10× magnifications. Brightfield images were captured to assess overall structure, followed by fluorescence imaging using GFP (excitation: 488 nm, emission: 509 nm) and RFP (excitation: 561 nm, emission: 582 nm) filters to detect specific signals. Images were acquired sequentially for each channel and saved for subsequent analysis.

6.4.11 Cryosectioning

Organoids encapsulated in IPNs were rinsed in PBS, fixed in 4% paraformaldehyde overnight at room temperature, and washed three times with PBS. After washing, organoids were immersed in 30% sucrose in PBS overnight (>12 h) at 4 ºC. Next, organoids were embedded in Tissue-Tek O.C.T. compound, frozen on dry ice, and immediately cryosectioned or stored at −80 ºC. 50-µm-thick sections were cut throughout the entire height of the organoid-loaded IPNs using a cryostat (CM 1950, Leica) at a temperature of ≈−17 ºC. Sections were

placed on Superfrost Plus microscope slides and stored at −80 ºC until immunofluorescence staining.

6.4.12 Immunofluorescence staining

To ensure sample hydration during processing, a humidity chamber was constructed using a pipette box with wet paper towels saturated with diH_2O placed at the bottom, providing a consistent humid environment. Fresh-frozen sections were immediately outlined with a hydrophobic pap pen and processed without drying. O.C.T compound was removed from fresh-frozen sections through three consecutive PBS washes (5–10 minutes each). Blocking was conducted at room temperature for 1 h using a solution of TrueBlack® Background Suppressor, 5% (w/v) donkey serum, and Fc block. Primary antibody staining was performed overnight at 4°C with antibodies diluted in a blocking solution, ensuring even distribution using parafilm. Samples were washed and stained with secondary antibody cocktails at room temperature for 2 hours, followed by two consecutive PBS washes (5–10 minutes each) and nuclear staining with SYTOX Green at a 1:30,000 dilution for 30 minutes. Finally, slides were mounted with an anti-fade prolong medium and dried overnight in a dark, light-shielded area.

6.4.13 Fluorescent microscopy

Fluorescence microscopy was conducted using a Zeiss Axioscan 7 laser scanning confocal microscope and a 20× objective. The 488, 555, and 647 nm channels were acquired sequentially. Unless stated otherwise, images in the chapter represent single confocal slices of 50-µm-thick organoid-loaded IPN cryosections.

6.4.14 Quantification of area, circularity, and fraction of segments

During the live tracking of fluorescent organoids, each marker's total fluorescent area (A) and perimeter (P) were quantified using the analyze particles command. The circularity (C) of the organoids was calculated using Equation (1). The marker’s area was quantified using ImageJ. Fluorescence images of organoids were converted to binary images. Each marker's total A and P were quantified using the analyze particles command. The C of segments was calculated using Equation (2).

$$C = \frac{4\pi A}{P^2} \qquad (2)$$

6.5 Results and Discussion

The aim of this chapter was to investigate the combination of engineered biomaterials and stem cell progenitors for creating an *ex vivo* human thymic tissue. The biomaterials selected were a combination of alginate and Matrigel® interpenetrating polymer networks (IPNs). The experimental objectives were established in order to analyze the influence of the composition variables in the mechanical properties and their subsequent influence on the development, differentiation, and organization of thymic organoids :

1) Developing IPNs with different levels of viscoelasticity and stiffness to provide varied mechanical environments.
2) Mimicking the mechanical properties of the native thymus using these IPNs to create a supportive matrix.
3) Encapsulating neural crest cell (NCC) and thymic epithelial progenitor cell (TEPC) derived thymic organoids within the IPNs.
4) Analyzing the development and structural organization of the thymic organoids within the IPNs to understand how mechanical properties influence their maturation and differentiation.

This systematic approach aims to create a biomimetic environment for thymic organoid growth. It provides insights into how mechanical cues affect thymic tissue development and offers potential strategies for regenerative medicine applications and T cell production.

6.5.1 Mechanical properties of the thymus

The thymus is a complex organ that undergoes a progressive involution over time, characterized by the replacement of thymopoietic tissue—containing thymocytes and supporting TECs—with adipose tissue. This process begins early, around 4–6 weeks of age in mice (rapidly increasing in mice 1 day after birth to 4-6 weeks) and approximately 1 year in humans, when other organs show minimal signs of aging, suggesting that thymic involution may be an evolutionarily conserved phenomenon. This thymic involution finds a reason occurring in two phases: an initial growth-dependent phase, where energy is redirected to other organs once the TCR repertoire is established, and a subsequent age-dependent phase, mirroring the aging processes seen in different tissues. This involution reduces the production of new naïve T cells and a constricted peripheral TCR repertoire. Consequently, thymic involution is linked to an increased susceptibility to diseases such as cancer, infections, and autoimmune disorders [498–500]. Therefore, understanding how the mechanical properties of the thymus change over time during involution is crucial for accurately replicating its structural and functional characteristics in experimental models.

Previous investigations from Prof. D. J. Mooney's lab revealed that the mouse and embryonic human thymus present comparable mechanical properties in terms of storage modulus (G'), loss modulus (G''), and viscoelasticity measured by tan delta (tan δ) when analyzed by nanoindentation. Thus, in Figure 3.3, it could be observed that the thymus was relatively soft and viscoelastic, that these mechanical properties were comparable between post-natal and embryonic thymus, and that the thymus of embryos was very similar across species.

The mouse embryonic thymus exhibited mechanical properties with a G' of approximately 1,500 Pa, a G" of roughly 700 Pa, and a tan δ of approximately 0.48.

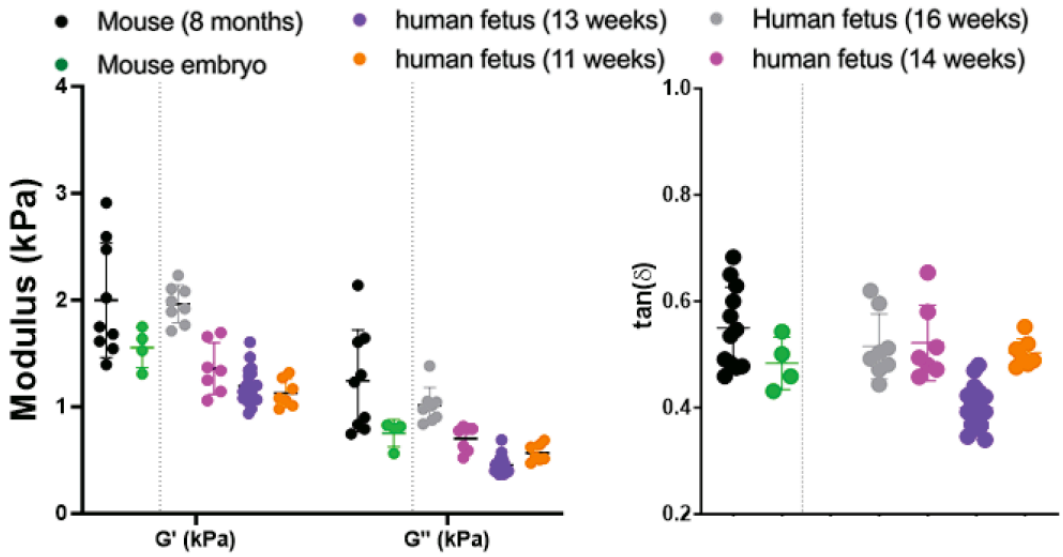

Figure 3.66. Murine and human thymus present comparable soft viscoelastic mechanical properties. G', G'', tan δ of human and murine thymus were measured with nanoindenter.

Abbreviations: G': Storage modulus. G'': Loss modulus. Tan δ: tan delta. Values represent the mean ± standard deviation (n≥4).

6.5.2 ECM-mimicking IPN design and mechanical characterization

Mechanical cues within tissues and their surrounding three-dimensional (3D) extracellular matrix (ECM) regulate tissue organization and morphogenesis. Previous studies have indicated that the ECM's passive viscoelastic properties significantly influence spatiotemporal tissue organization [67,69]. Furthermore, the interplay between ECM stiffness and viscoelasticity is essential for tissue growth dynamics, as recently demonstrated using spheroidal breast epithelial cell cultures [245]. Thus, thymus morphogenesis is expected to be impacted by the matrix's viscoelastic properties and stiffness.

Four gel conditions were developed to establish a controlled matrix environment, encompassing a spectrum from viscoelastic to elastic properties (fast-relaxing to slow-relaxing) and from soft to stiff mechanical characteristics (Figure 3.4A). Viscoelasticity was quantified by measuring the relaxation time of the initially applied stress. Alginate was selected as the base polymer due to its stability in mammalian systems; since mammalian cells lack the enzymes to degrade alginate, any effects related to matrix degradation are minimized [434,497]. Moreover, by adjusting the molecular weight (MW) of alginate and the density of calcium crosslinking (Figure 3.4B and Table 3.1), the relative viscoelastic properties of these gels were independently tuned without altering stiffness, pore size or adhesive ligand density [488]. To ensure consistent cell adhesion across all conditions and previous literature, Arg-Gly-Asp (RGD) peptides were conjugated to the alginate polymer backbone, providing uniform cell binding sites [245,497]. Additionally, prior studies have demonstrated that Matrigel and

alginate can form homogeneous IPNs, which were leveraged in this design to enhance the matrix's structural and biochemical compatibility [501].

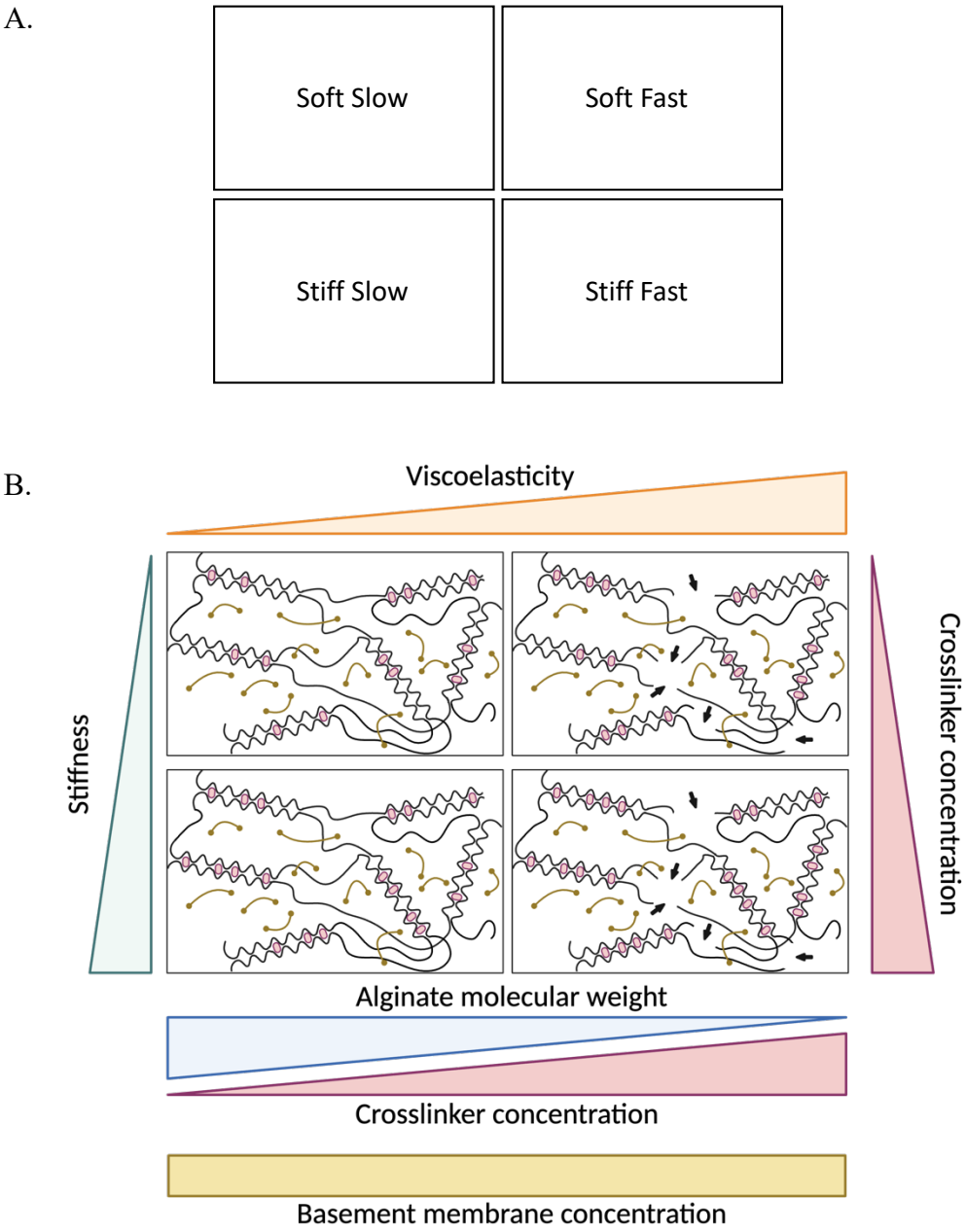

Figure 3.67. Murine and human thymus present comparable soft viscoelastic mechanical properties measured with nanoindenter.

Created with https://www.biorender.com/

First, the mechanical properties of the gels were measured using a nanoindenter, the same instrument as the one employed for measuring the mechanical properties of the thymus.

Thus, stiff gels were produced with constant G' ≈ 7,000 Pa, G" ≈ 1,000 Pa, and E ≈ 21,500 Pa; soft gels with G' ≈ 1,200 Pa, G" ≈ 270 Pa, and E ≈ 3,750 Pa (Figure 3.5A, B and C). Soft gels were in the G' and G" range of the analyzed thymus. Viscoelasticity is addressed by tan δ,

being more viscoelastic for those with higher ratios and more elastic for those with lower ratios. However, in this case, no significant differences were observed between the fast-relaxing gels (using LMW alginate) and the slow-relaxing gels (using HMW alginate) (Figure 3.5D). This outcome can be explained by the manufacturer's recommendation that the punch diameter should be approximately 1.3 mm for very soft gels. This requirement affected a large percentage of the gel's surface, limiting the number of indentations performed on each gel and addressing bulk instead of zone-specific properties.

Table 3.15. IPN conditions and parameters set up

IPN condition	Alginate MW	[Alginate] (%wt)	[Matrigel] (mg/mL)	[$CaSO_4$] (mM)
Stiff Slow	HMW	1	3.69	11.71
Stiff Fast	HMW	1	3.69	19
Soft Slow	LMW	1	3.69	5
Soft Slow	LMW	1	3.69	7.8

Abbreviations: IPN: Interpenetrating polymer network. MW: Molecular weight. $CaSO_4$: Calcium Sulfate. HMW: High molecular weight. LMW: Low molecular weight.

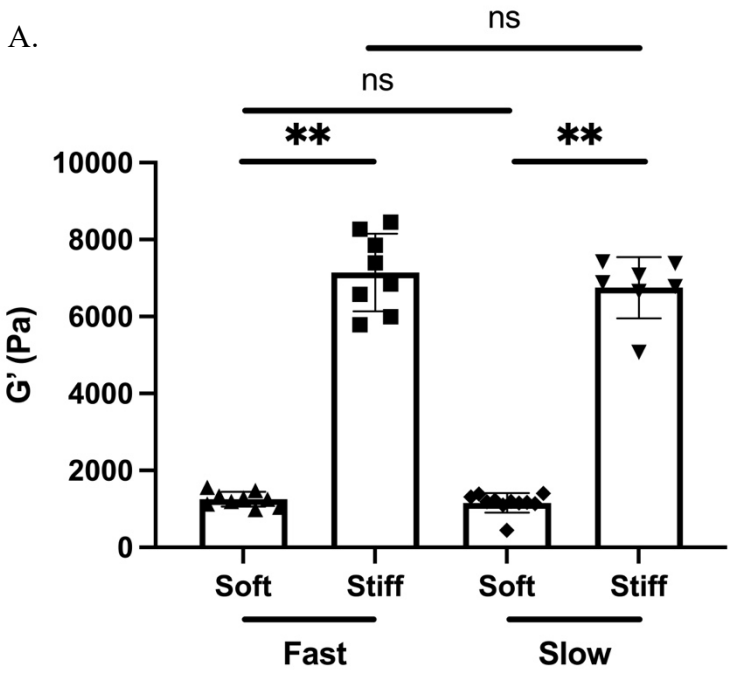

B.

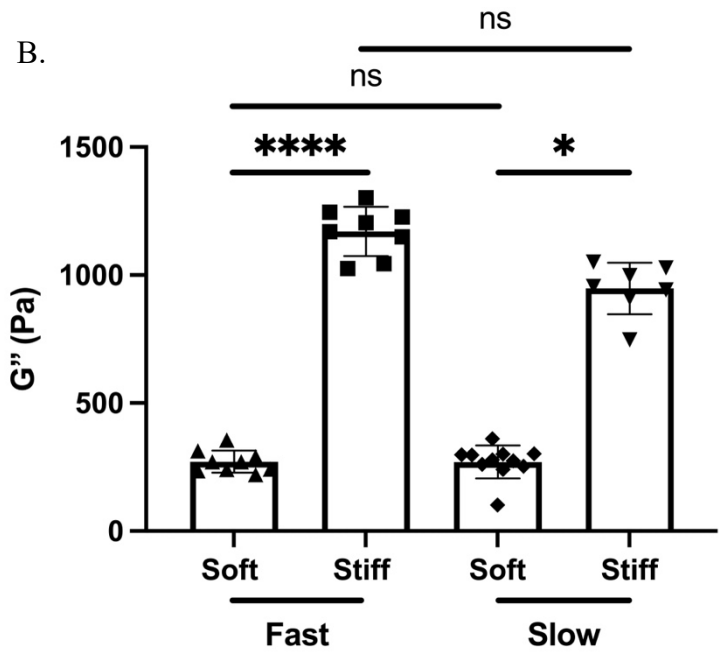

C.

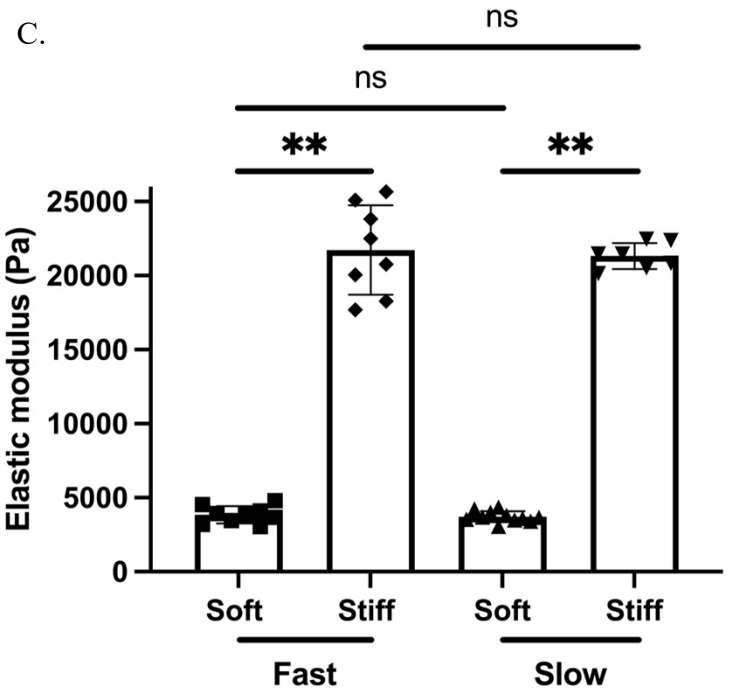

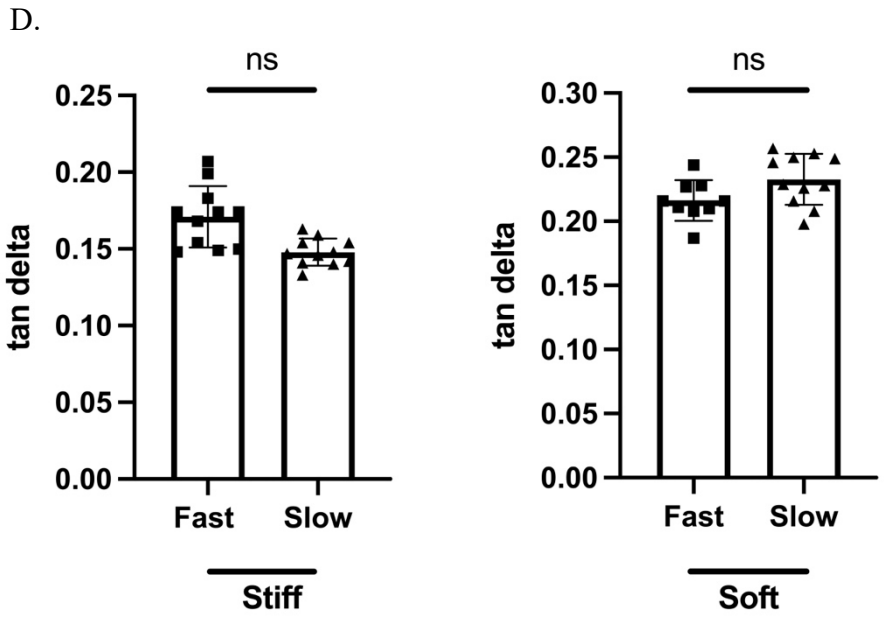

Figure 3.68. Soft Fast-relaxing IPNs approximate the soft viscoelastic mechanical properties of the native thymus. G' (A), G''(B), E (C), and tan δ (D) of the four IPN conditions were measured with nanoindenter.

Abbreviations: G': Storage modulus. G'': Loss modulus. E: Elastic modulus. Values represent the mean ± standard deviation (n≥7).

Thus, an alternative mechanical characterization approach was decided upon, utilizing a compression test. This method allowed for E analysis and stress relaxation times. In this case, the moduli ranged from soft E ≈ 4,100 Pa to stiff E ≈ 15,000 Pa, and the viscoelasticity from more elastic, slower τ70% relaxation time to more viscoelastic, faster τ70% relaxation time (Figure 3.6).

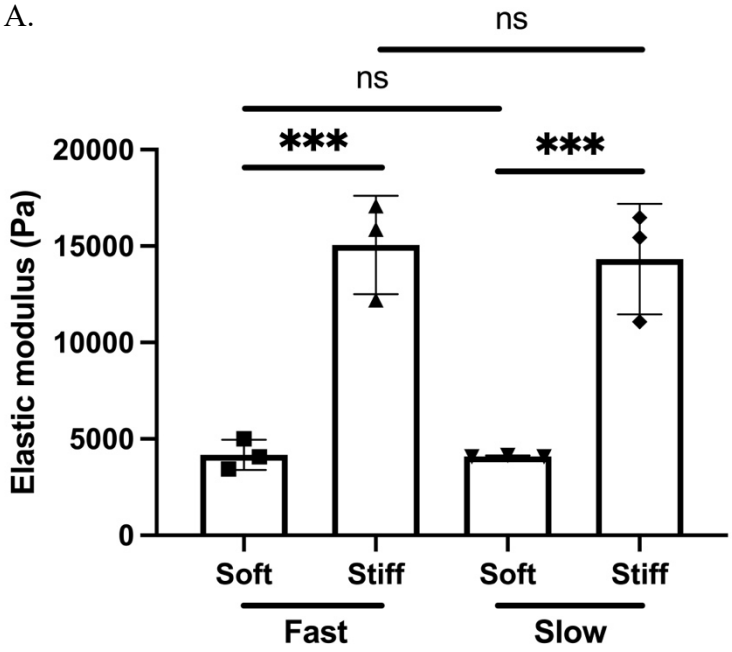

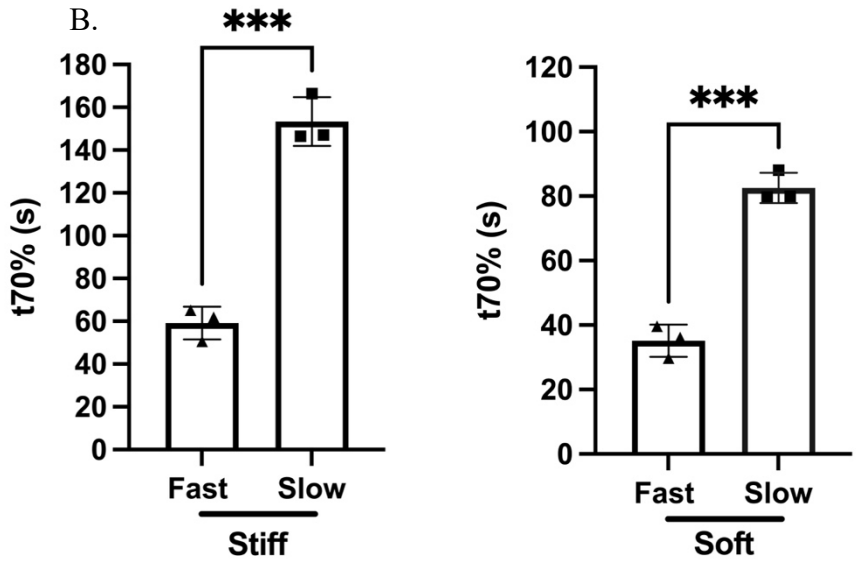

Figure 3.69. Results of the bulk mechanical characterization using compression test unveiled similar results to those of characterization with nanoindenter. Soft Fast-relaxing IPNs approximate the soft viscoelastic mechanical properties of the native thymus. E (A) and τ70% relaxation time (B) of the four IPN conditions were measured with compression test.

Abbreviations: E: Elastic modulus. τ70%: Time needed to reduce 70% of the initial stress. Values represent the mean ± standard deviation (n=3, experimental replicates). Each point is the mean of n ≥ 3 technical replicates.

The differences between the E obtained by nanoindentation and the compression test lay in the nature of these tests. Nanoindentation and compression testing differ significantly in their measurement scale, type of loading, and the mechanical properties they assess. Nanoindentation operates at the microscale or nanoscale, applying a localized load through a sharp or spherical indenter to measure surface properties such as elastic modulus and hardness. In contrast, compression testing evaluates bulk properties at the macroscale by applying a uniform load across the sample's cross-section. It provides insights into compressive modulus, yield strength, and time-dependent properties like stress relaxation. While nanoindentation focuses on localized deformation, compression tests examine the overall structural response [502–504].

6.5.3 Organoid preparation

TECs, originating from the bipotent precursors called thymic epithelial progenitor cells (TEPCs), differentiate into two distinct subsets: cTECs and mTECs. cTECs play a key role in the positive selection of thymocytes, ensuring the survival of T cells with functional TCRs. Meanwhile, mTECs are essential for negative selection, eliminating autoreactive T cells by expressing tissue-specific antigens regulated by the transcription factor AIRE. On the other hand, NCCs serve as crucial precursors for the mesenchymal cells involved in the organization and structure of the thymus. During embryonic development, migrating NCCs contribute to the mesenchymal compartment of the thymic microenvironment, providing structural support and instructive signals essential for TEC development and organization. These mesenchymal cells play a critical role in shaping the 3D architecture of the thymus and supporting TEC differentiation into cortical and medullary subsets. The thymic stroma, formed by the coordinated contributions of TECs, NCC-derived mesenchymal cells, and endothelial cells,

establishes the functional environment necessary for T cell maturation. This stroma provides a scaffold for thymocyte migration and selection while producing cytokines, chemokines, and extracellular matrix components essential for developing a functional immune repertoire [71,505].

Recent advancements in hPSC-derived thymic tissue engineering have highlighted the critical role of supporting mesenchyme in promoting the development of TEPCs. However, the mesenchyme studied to date has not been systematically engineered for thymic development or designed to replicate the native thymic environment. During embryogenesis, TEPCs arise from the third pharyngeal pouch of the differentiating endoderm, which interacts with mesenchyme derived from migrating and differentiating NCCs. This interaction provides essential supportive and instructive cues for thymic maturation [495,506–508]. Building on this developmental framework, our approach combines differentiated TEPCs and NCCs to generate thymic organoids.

6.5.4 ECM-mimicking IPN viscoelasticity regulates thymus morphogenesis

TEPCs and NCCs were differentiated from the pluripotent human embryonic stem cell line H1 (H1), which was used in either fluorescent (H1-Fl) or wild-type (H1-WT) form, depending on the experiment. TEPCs derived from H1-Fl expressed green fluorescent protein (GFP), while NCCs expressed the red fluorescent protein (RFP) tdTomato. TEPCs and NCCs were combined at a TEPC-to-NCC ratio (TEPC:NCC) of 1:3 to form thymic organoids before being encapsulated in the IPNs of different conditions. H1-Fl-derived organoids were used to track their reorganization and morphological changes during the first week. On the other hand, H1-WT-derived organoids were collected at day 7 post-encapsulation and analyzed by immunohistochemistry.

During the development of thymic organoids, NCCs initially outnumber TEPCs with a proportion of 3 to 1 and become increasingly dominant over time, encapsulating the TEPCs and contributing to the global organoid structure. Circularity remained largely stable in stiffer IPNs, while softer gels exhibited distinct trends. In Soft Slow-relaxing IPNs, circularity decreased significantly by day 3 and stabilized by day 5, whereas Soft Fast-relaxing IPNs showed a progressive decrease in circularity throughout the observation period. In contrast, Stiff IPNs maintained consistent circularity over time regardless of viscoelasticity (Figure 3.7).

These results highlight gel stiffness and viscoelasticity's significant and complementary roles in influencing thymic organoid morphology and spatial organization, underscoring their pivotal role in shaping organoid structure. NCCs initially formed a ring-like structure around the middle of the organoid, positioning TEPCs toward the poles and inner regions. Over the week, this arrangement progressed to near-complete encapsulation of TEPCs by NCCs (Figure 3.8). This observation aligns with previous studies emphasizing the critical role of mechanical cues in tissue morphogenesis and organoid development [62,63].

6.5.4.1 Circularity analysis for assessing thymic organoid spatial reorganization in ECM-mimicking IPNs

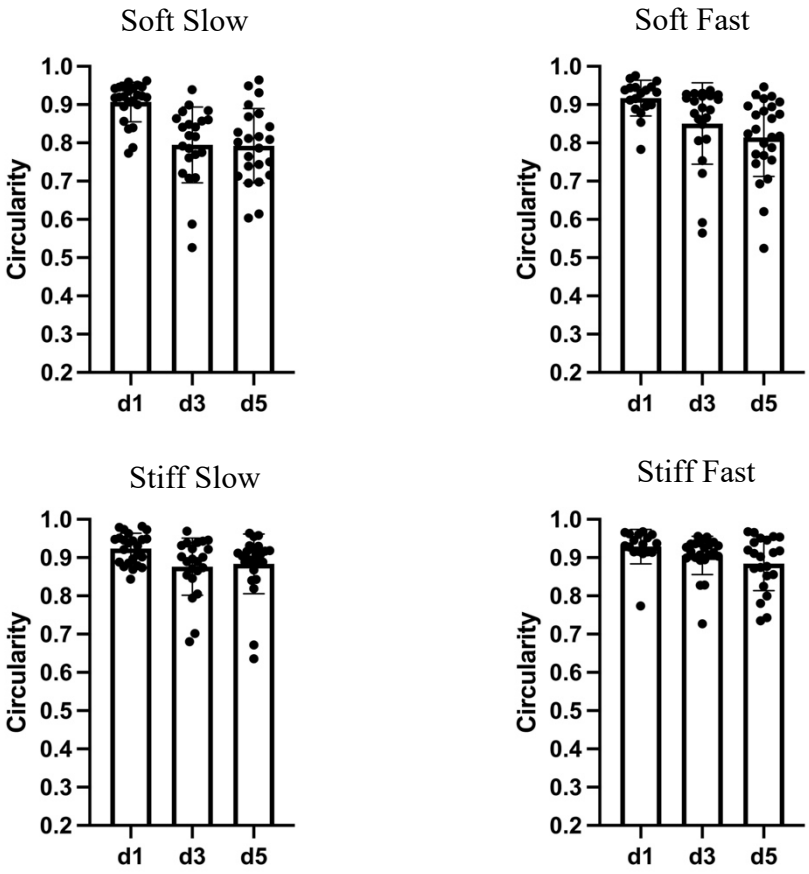

Figure 3.70. Thymus organoids' circularity changes depending on the mechanical properties of the ECM-mimicking IPNs.

Abbreviations: IPN: Interpenetrating polymer network. Values represent the mean ± standard deviation (n ≥ 18).

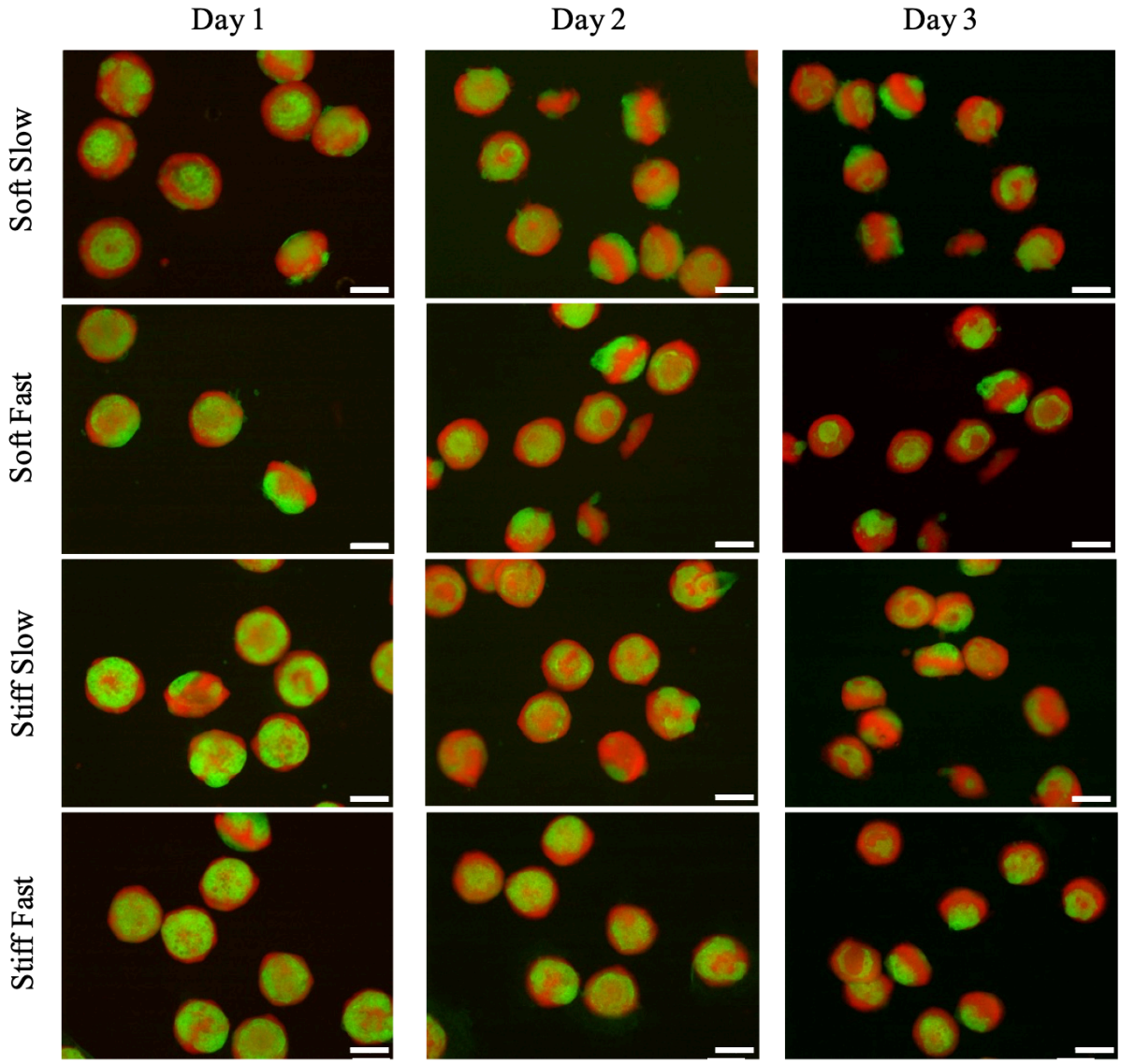

Figure 3.71. Live tracking of the fluorescent thymic organoids with widefield microscopy.

Abbreviations: Interpenetrating polymer network. GFP represents TEPC. RFP represents NCCs. Images were captured at 4× magnification, providing an overview of the organoid distribution within the field. Scale bars represent 500 µm.

6.5.4.2 Changes in TEPCs and NCCs area over time in ECM-mimicking IPN

To investigate these findings further, TEPCs and NCCs were independently analyzed to examine their spatial organization within the different IPNs over time. By day 5, NCCs displayed a homogeneous distribution within the organoid, with a remarkably higher concentration around the ring-like structure. Conversely, TEPCs were observed to relocate toward the poles and interior of the organoid, leaving the middle zone predominantly occupied by NCCs. This redistribution confirmed our observations of distinct spatial organization between TEPCs and NCCs (Figure 3.9).

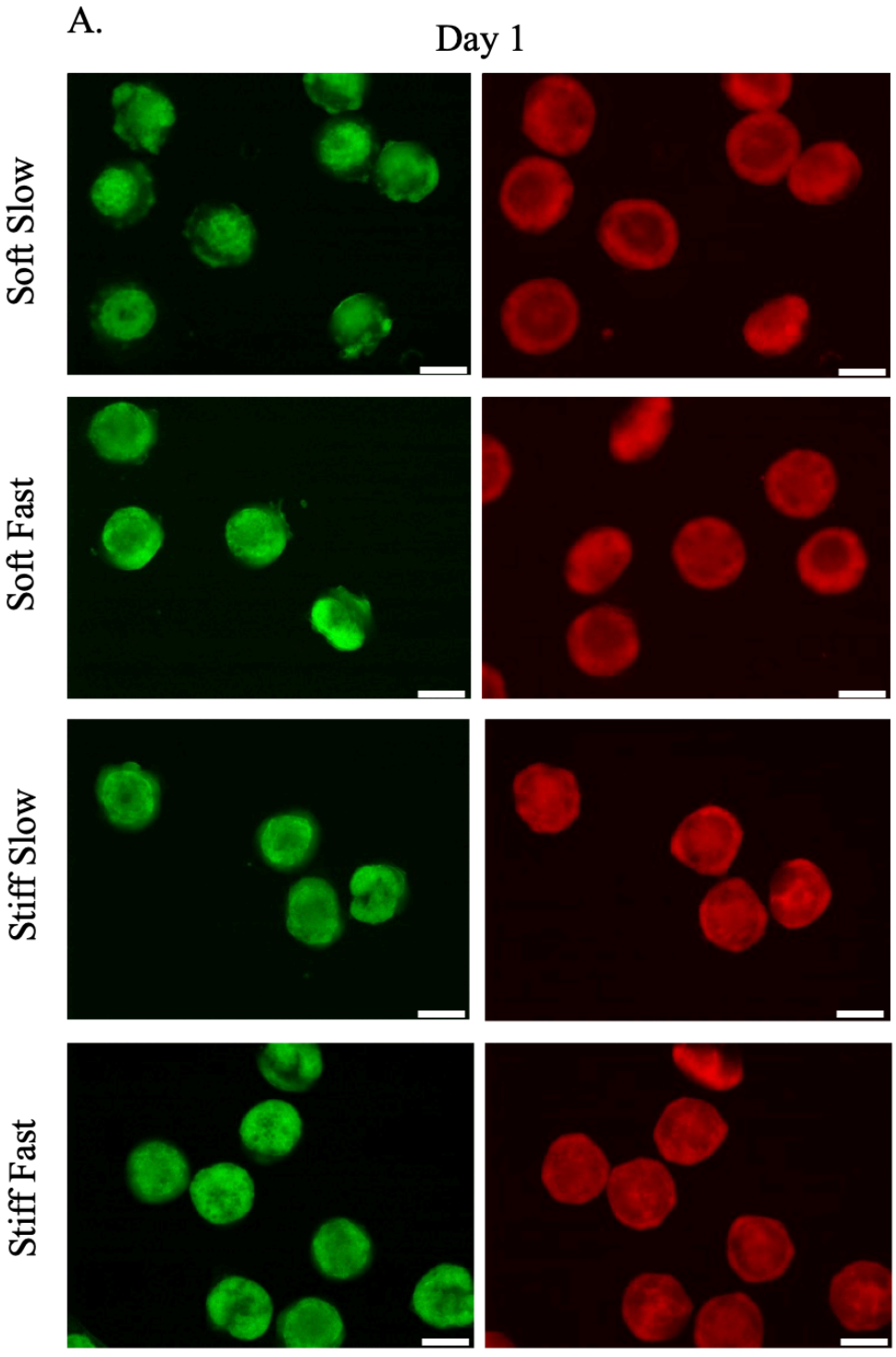

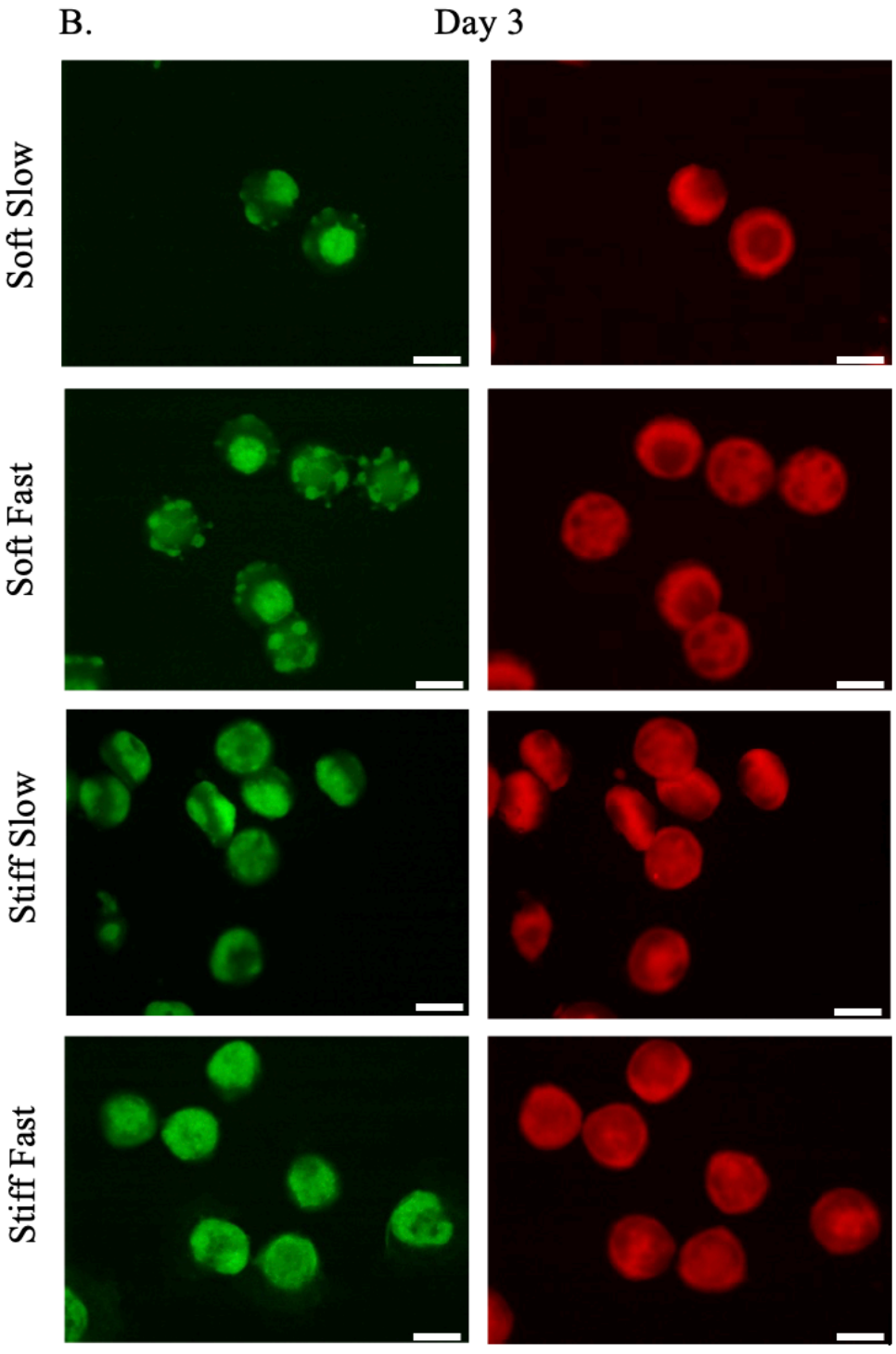

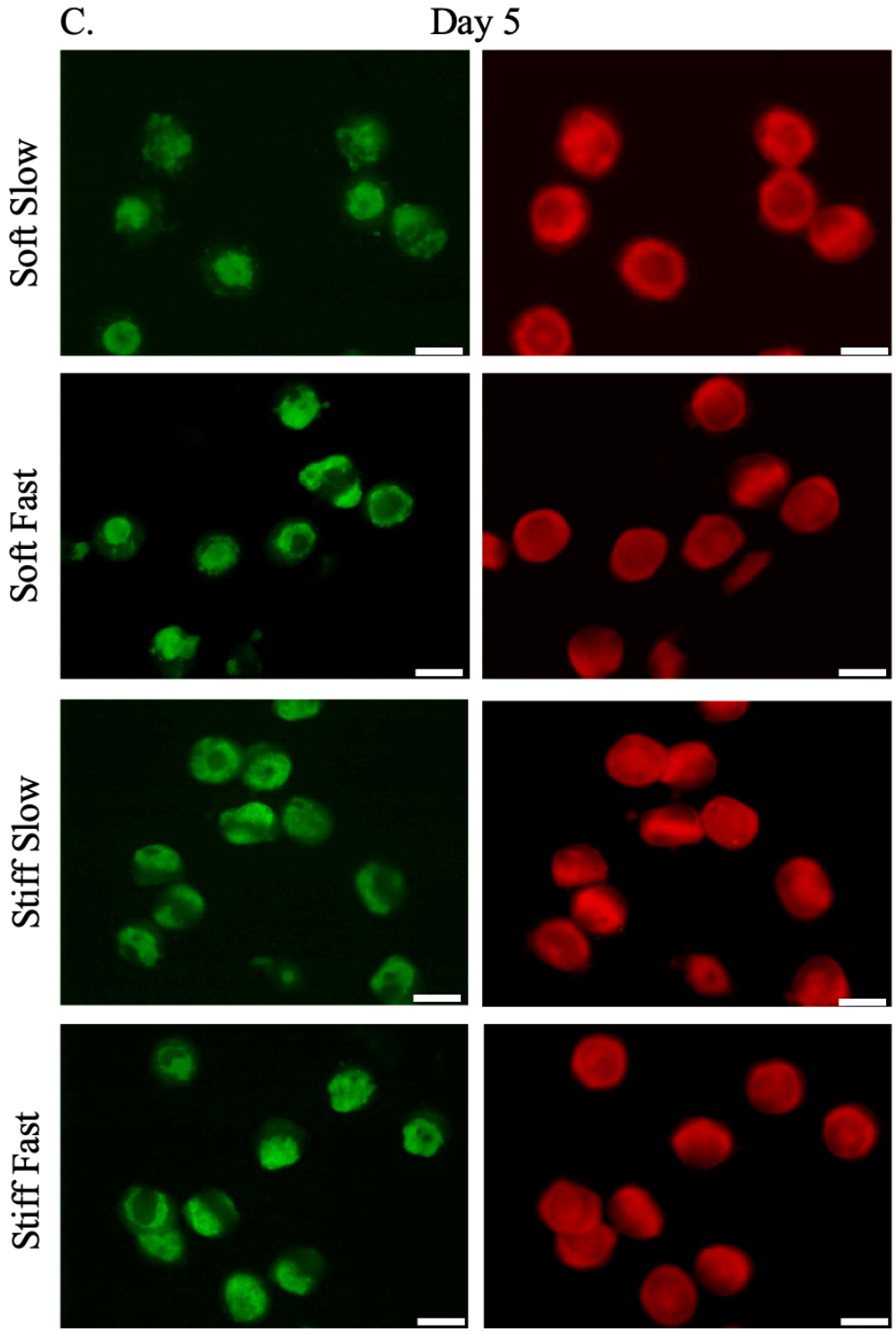

Figure 3.72. Redistribution of TEPCs and NCCs within the organoid during the first week of encapsulation in IPNs with varying mechanical properties imaged with widefield microscopy. Images show spatial organization on day 1 (A), day 3 (B), and day 5 (C).

Abbreviations: TEPC: Thymic epithelial progenitor cell. NCC: Neural crest cell. IPN: Interpenetrating polymer network. GFP represents TEPC. RFP represents NCCs. Images were captured at 4× magnification, providing an overview of the organoid distribution within the field. Scale bars represent 500 µm.

The total area of TEPCs and NCCs within the organoids decreased over time, with NCCs consistently maintaining a larger and more constant area than TEPCs throughout the observed period (Figure 3.10). This trend aligned with the observed spatial reorganization of TEPCs, which progressively relocate toward the poles of the organoid. This dynamic suggests that, as expected, NCCs may influence the structural arrangement and compaction of the organoid, guiding the positioning of TEPCs regardless of the mechanical properties of the IPNs. Moreover, these findings highlight the interplay between cell types during thymic organoid development and suggest a coordinated process influenced by cellular interactions and microenvironmental mechanical cues exerted by the IPNs.

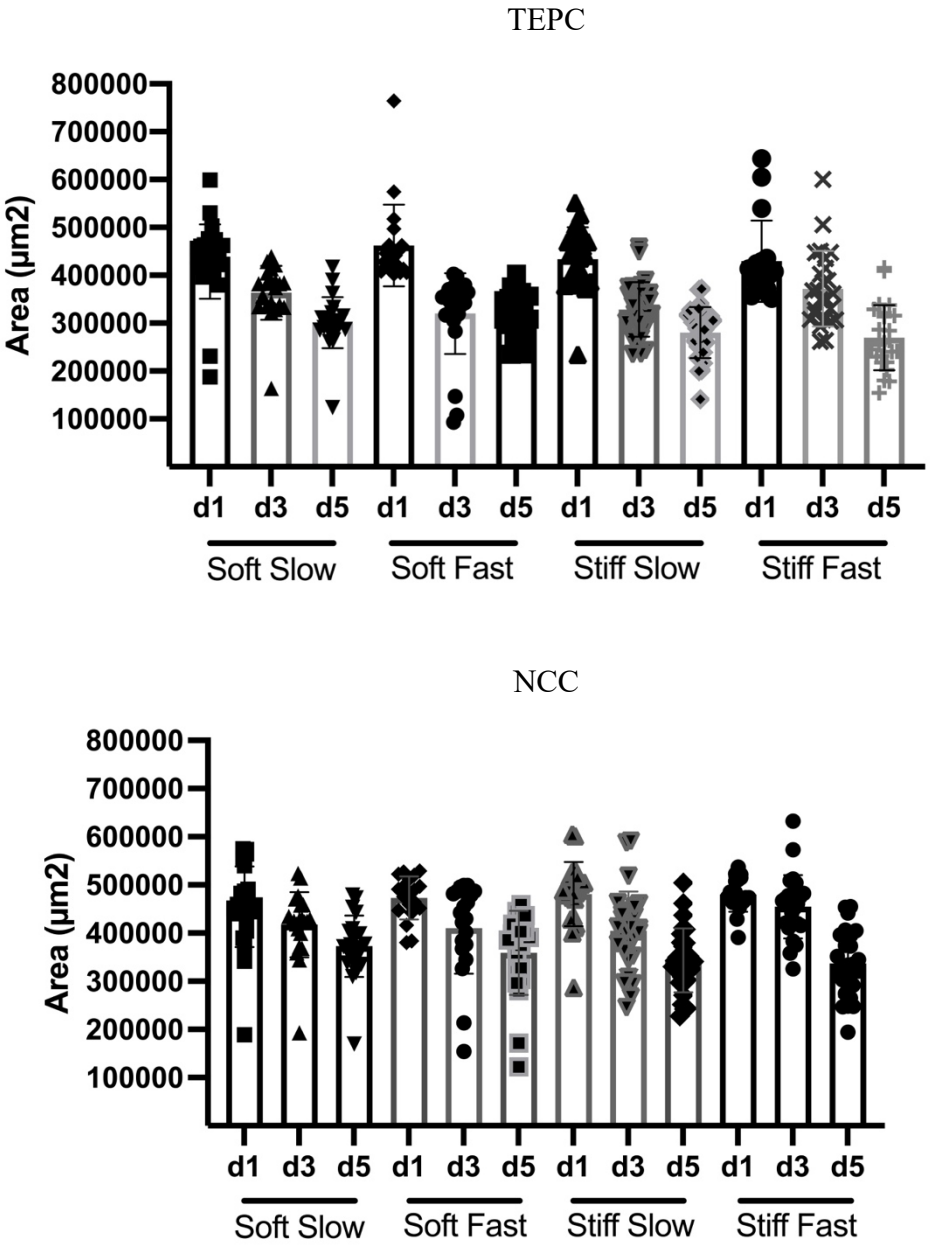

Figure 3.73. Thymus organoids' circularity changes depending on the mechanical properties of the IPNs. **Abbreviations:** TEPC: Thymic epithelial progenitor cell. NCC: Neural crest cell. Values represent the mean ± standard deviation (n ≥ 17).

6.5.5 Expression of thymus development markers in encapsulated thymic organoids

To investigate how viscoelasticity and stiffness influence thymus organogenesis, self-organizing thymic organoids were encapsulated within IPNs with varying mechanical properties and analyzed using immunohistochemistry (IHC) seven days post-encapsulation. The analysis focused on detecting specific thymus development markers, including Keratin 8 (K8), Forkhead-box n1 (FOXN1), Epithelial cell adhesion molecule (EpCAM), and Vascular cell adhesion molecule-1 (VCAM1).

K8 is an intermediate filament (IF) protein often paired with K18 to form a keratin IF network. Its expression is predominantly observed in cTECs, with a key subset of K5+K8+ cells located at the corticomedullary boundary of the thymus. Interestingly, previous studies described that while the loss of K8 does not impair thymocyte development, it significantly disrupts TEC morphology in both the cortex and medulla, leading to a marked depletion of cTECs [509]. Consequently, K8 was selected as a marker for the thymic cortex and the structural integrity of both TEC types in the thymus organogenesis.

FOXN1 is a key transcription factor required for complete thymus morphogenesis. The absence of functional FOXN1 leads to aberrant epithelial morphogenesis and an inability to recruit lymphoid precursors to the thymus primordium [510]. Consequently, the loss of FOXN1 results in athymia, where the growth and differentiation of TECs are severely impaired, restricting their development beyond an immature phenotype and preventing the attraction of hematopoietic precursor cells. These two processes are essential for normal T cell lymphopoiesis. FOXN1 is pivotal in regulating TEC patterning during the fetal stage and maintaining TEC homeostasis in the postnatal thymus [511,512].

Although EpCAM is present in almost all adult organs and glands, it is a critical adhesion molecule and structural marker in the thymus. It is essential for TEC function and thymocyte development, playing a key role in positive and negative selection and maturation. EpCAM expression is generally higher in mTEC [513,514].

VCAM1 is a high-affinity adhesive ligand for the integrin α4β1 (VLA-4) on thymocytes. It is expressed in the thymic cortex by cTECs and in the corticomedullary junction by endothelial cells. In the cortex, VCAM1 mediates interactions between immature thymocytes and selecting elements on epithelial cells, playing a crucial role in thymocyte positive selection. At the corticomedullary junction, VCAM1 facilitates the migration of hematopoietic precursor cells into the thymus, a necessary step for T cell development [70,515].

First, the formation of tissue-like structures in the thymic organoids was evaluated. Soft IPNs showed different marker expressions within structures depending on their viscoelasticity. Slow-relaxing IPNs diminished the expression of the markers K8 and FOXN1. Regarding EpCAM, its expression was distributed throughout the thymic organoid, with a notably higher expression in a structured pattern localized to a circular zone (Figure 3.11, white box). However, VCAM1 expression was also notably diminished. On the other hand, in Soft Fast-relaxing IPNs, the organoids exhibited a more structured pattern than in the Soft Slow-relaxing IPNs, with regions resembling the organization characteristic of native tissue with a lumen

towards the inner part of the structure (Figure 3.12, white boxes). Fast-relaxing IPNs demonstrated high expression of the markers K8, FOXN1, and EpCAM; while VCAM1 expression remained dimmed, it was observed within the same circular zone where EpCAM was expressed.

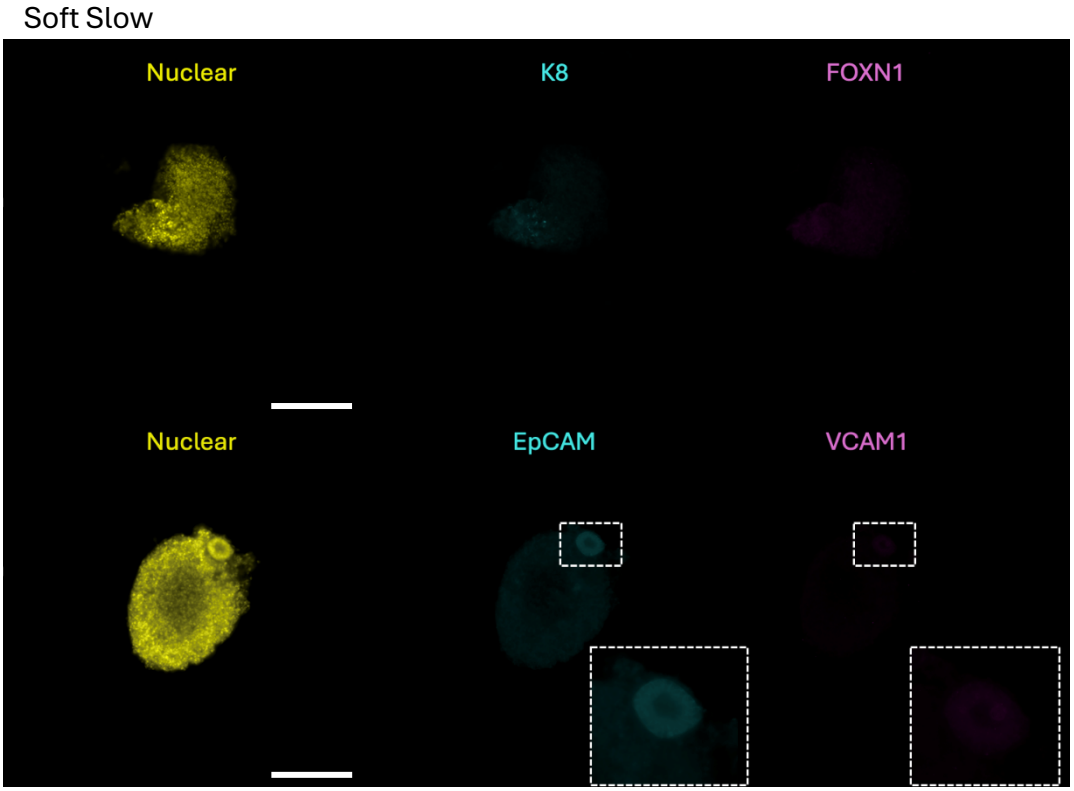

Figure 3.74. Representative fluorescent images of thymic organoids encapsulated and differentiated in Soft Slow-relaxing ECM-mimicking IPNs.

Abbreviations: K8: Keratin 8. FOXN1: Forkhead-box n1. EpCAM: Epithelial cell adhesion molecule. VCAM1: Vascular cell adhesion molecule-1. The images in each panel were captured at 20x magnification. The images in dotted square white boxes present a zoomed-in view of a part of the organoid, allowing for a more detailed observation of its morphology and structural features. Scale bars represent 200 µm.

Stiff IPNs demonstrated a viscoelastic trend similar to Soft IPNs; however, the overall marker expression was reduced, and the distinct localized and structured patterns typical of Soft IPNs were markedly diminished. Slow-relaxing IPNs exhibited faint marker expression, minimal tissue-like patterns, and limited cellular organization. Structures highlighted within the white boxes (Figure 3.13) appeared reminiscent of early differentiation and organogenesis stages, as the absence of lumens—a hallmark of more advanced tissue and organ development—indicates insufficiently coordinated mechanical and biochemical interactions [64–66]. In contrast, Fast-relaxing IPNs, while exhibiting reduced marker expression compared to Soft IPNs, displayed distinctly defined and organized patterns with clearly visible lumens (Figure 3.14, white box).

These findings highlight the pivotal role of viscoelasticity in driving the development of differentiated and organized structures in thymic organoids. Although stiffness influenced tissue organization, its effect was less pronounced. The most structured patterns, including defined lumens, were observed in Soft Fast-relaxing IPNs, demonstrating their superior

capacity to support advanced tissue organization during thymic organoid development. Stiff Fast-relaxing and Soft Slow-relaxing IPNs showed comparable outcomes, with Stiff Fast-relaxing IPNs exhibiting a more distinct presence of lumens. In contrast, Stiff Slow-relaxing IPNs produced the least differentiated organoids, underscoring that a stiffer, less elastic ECM microenvironment hinders thymus organogenesis.

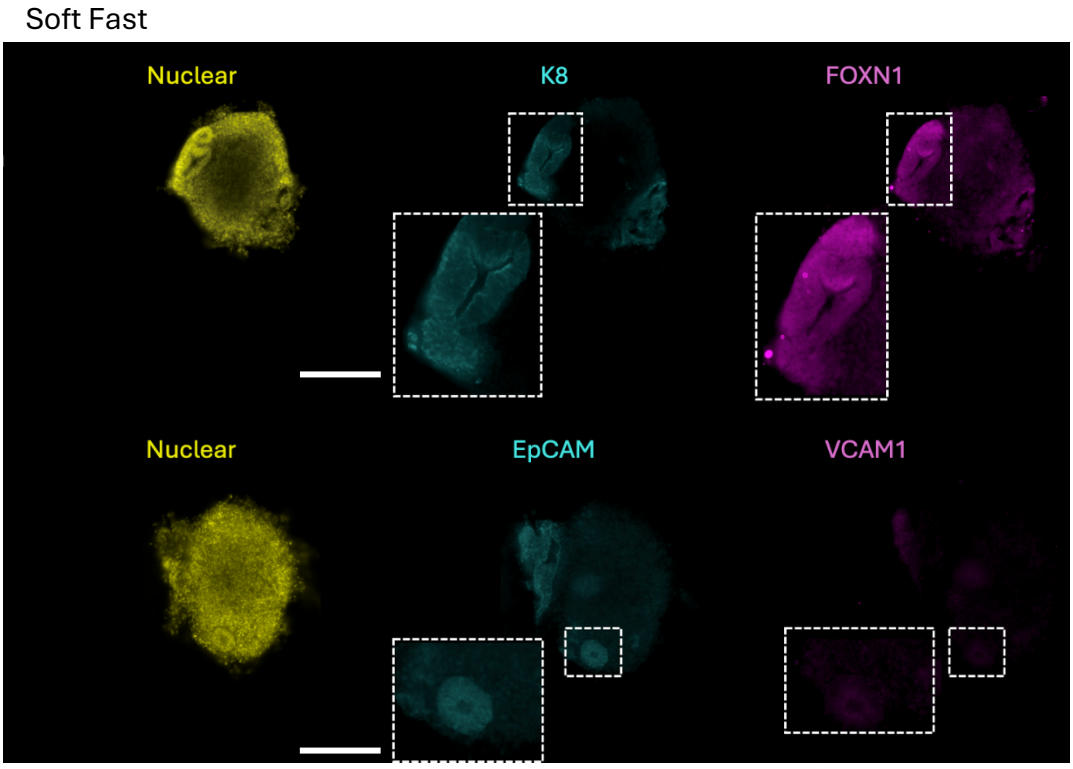

Figure 3.75. Representative fluorescent images of thymic organoids encapsulated and differentiated in Soft Fast-relaxing ECM-mimicking IPNs.

Abbreviations: K8: Keratin 8. FOXN1: Forkhead-box n1. EpCAM: Epithelial cell adhesion molecule. VCAM1: Vascular cell adhesion molecule-1. The images in each panel were captured at 20x magnification. The images in dotted square white boxes present a zoomed-in view of a part of the organoid, allowing for a more detailed observation of its morphology and structural features. Scale bars represent 200 µm.

To quantitatively assess thymus development markers, the fractions of segments expressing each marker were quantified relative to total nuclear staining within the organoids.

Soft Fast-relaxing IPNs exhibited the highest K8 expression, showing significant differences from Stiff Slow-relaxing IPNs but no statistically significant differences with the other IPN conditions. Notably, K8 expression in Soft Slow-relaxing and Stiff Fast-relaxing IPNs was comparable, suggesting that their respective microenvironments exerted similar effects on the expression of K8 during thymus organoid development. These findings emphasize the dominant role of viscoelasticity in enhancing K8 expression, with Fast-relaxing IPNs consistently showing higher K8 fractions compared to Slow-relaxing elastic counterparts. Stiffness also influenced K8 expression, as stiffer IPNs exhibited lower levels, particularly in Stiff Slow-relaxing IPNs. Again, this underscores the combined effects of viscoelasticity and stiffness in shaping a microenvironment conducive to optimal K8 expression (Figure 3.15A).

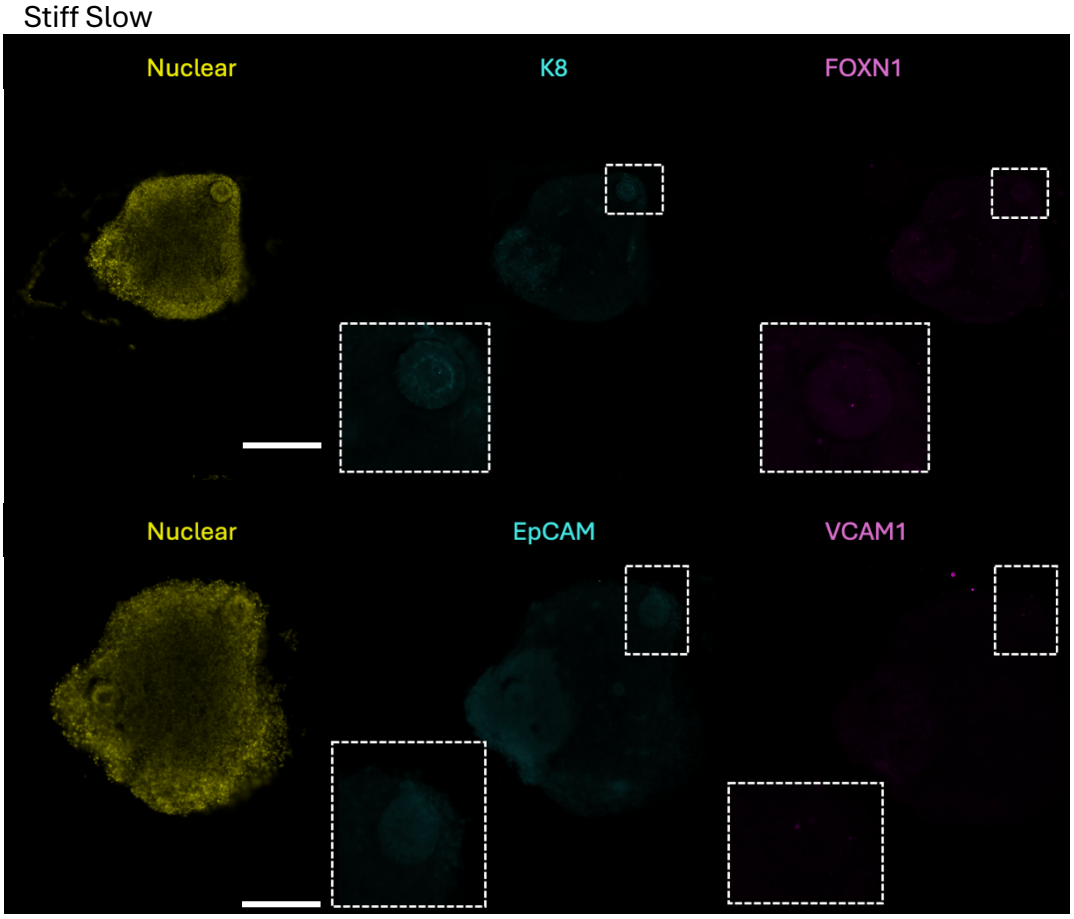

Figure 3.76. Representative fluorescent images of thymic organoids encapsulated and differentiated in Stiff Slow-relaxing ECM-mimicking IPNs.

Abbreviations: K8: Keratin 8. FOXN1: Forkhead-box n1. EpCAM: Epithelial cell adhesion molecule. VCAM1: Vascular cell adhesion molecule-1. The images in each panel were captured at 20x magnification. The images in dotted square white boxes present a zoomed-in view of a part of the organoid, allowing for a more detailed observation of its morphology and structural features. Scale bars represent 200 µm.

Significant differences in FOXN1 expression were observed between Soft Fast-relaxing IPNs and all other conditions (Figure 3.15B). FOXN1, a critical transcription factor required for complete thymus morphogenesis, was expressed at higher levels in Soft Fast-relaxing IPNs, indicating that this condition supports a more advanced stage of thymus organoid differentiation during the analysis period. Although no significant differences were detected between Stiff Fast-relaxing and Soft Slow-relaxing IPNs, a slight trend toward higher FOXN1 expression was observed in the Stiff Fast-relaxing condition. Conversely, Stiff Slow-relaxing IPNs consistently exhibited the lowest FOXN1 expression, highlighting their unfavorable microenvironment for thymus organoid development.

Similar results were observed for the fraction of EpCAM, with significant differences between Soft Fast-relaxing IPNs and the other conditions (Figure 3.15C). Stiff Slow-relaxing IPNs consistently exhibited the lowest EpCAM expression, highlighting their limited capacity to support thymus development. EpCAM, a key marker for thymus development and epithelial

organization, reflects the structural and functional integrity of thymic TECs. The elevated EpCAM expression in Soft Fast-relaxing IPNs underscores the critical role of a more viscoelastic and softer microenvironment in promoting advanced tissue organization and differentiation of the organoids.

The combined findings for FOXN1 and EpCAM further solidify the conclusion that viscoelasticity is the primary factor driving thymus organoid development. While stiffness is a secondary, complementary factor, IPNs with viscoelastic properties consistently supported higher marker expression levels, correlating with more advanced differentiation stages. These results highlight the critical importance of designing IPNs that closely mimic ECM-like mechanical properties to recreate a native thymus microenvironment, thereby optimizing the conditions necessary to support thymus organogenesis.

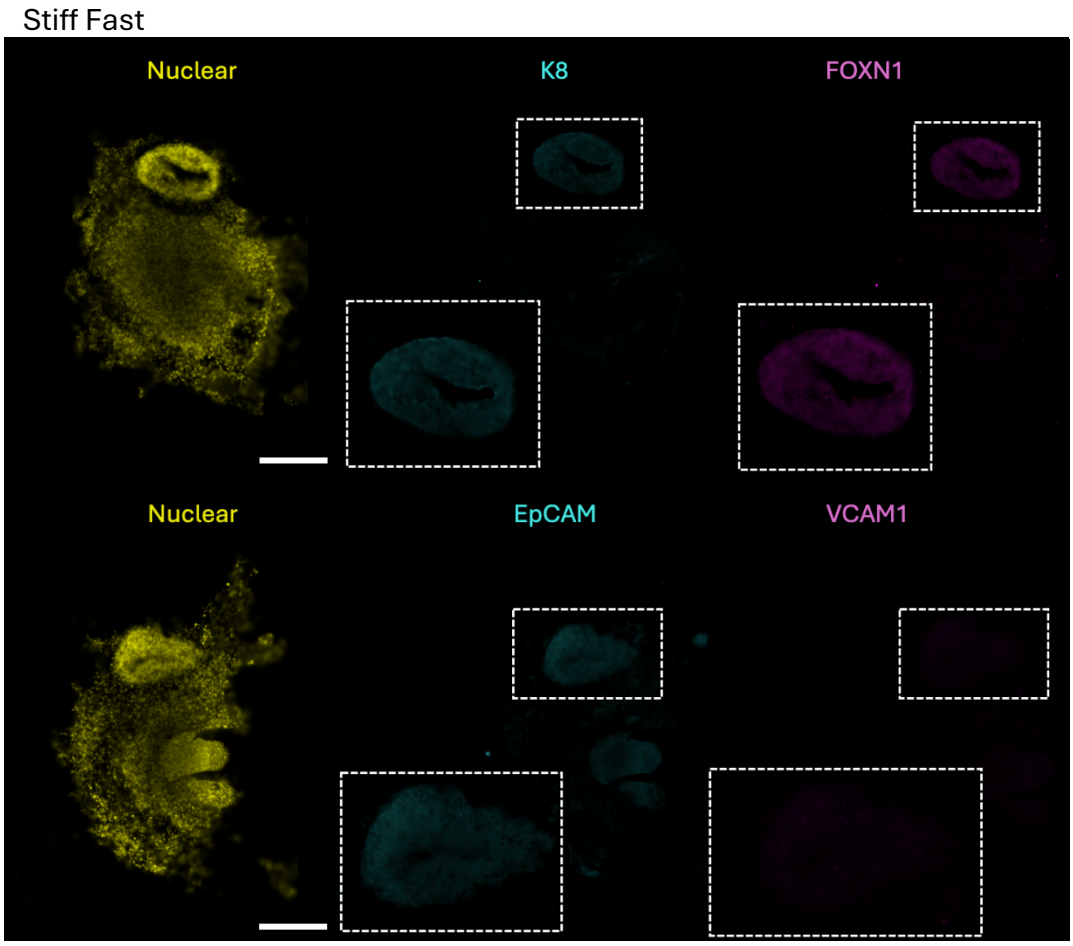

Figure 3.77. Representative fluorescent images of thymic organoids encapsulated and differentiated in Stiff Fast-relaxing ECM-mimicking IPNs.

Abbreviations: K8: Keratin 8. FOXN1: Forkhead-box n1. EpCAM: Epithelial cell adhesion molecule. VCAM1: Vascular cell adhesion molecule-1. The images in each panel were captured at 20x magnification. The images in dotted square white boxes present a zoomed-in view of a part of the organoid, allowing for a more detailed observation of its morphology and structural features. Scale bars represent 200 μm.

Finally, the fraction of VCAM1 was meager across all conditions, with no significant differences observed (Figure 3.15D). This suggests that this marker was not yet prominently expressed after one week of encapsulation at this stage of organoid development. This result

aligns with expectations, as VCAM1 is a protein typically associated with vascularization, which occurs at later stages of thymus development [70,71].

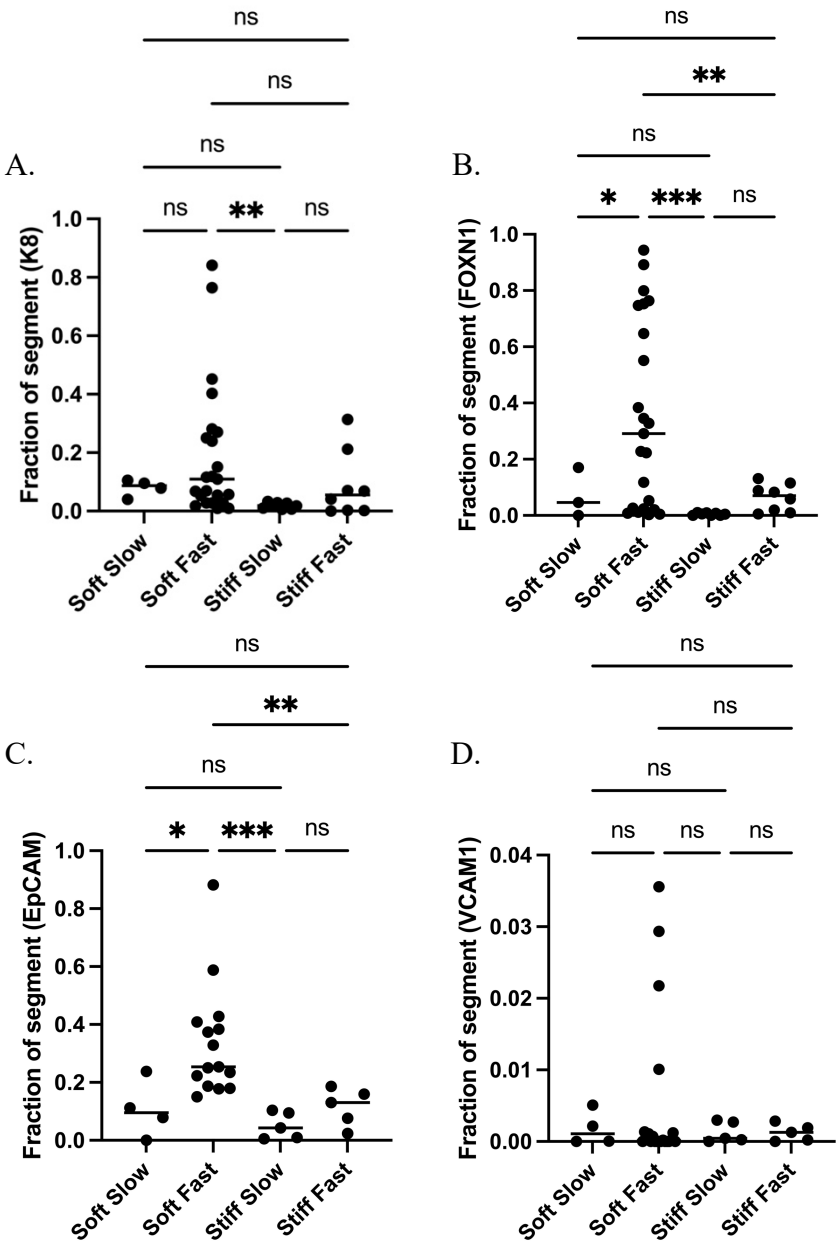

Figure 3.78. Fraction of K8, FOXN1, EpCAM, and VCAM1 in thymic organoids encapsulated in ECM-mimicking IPNs.

Abbreviations: K8: Keratin 8. FOXN1: Forkhead-box n1. EpCAM: Epithelial cell adhesion molecule. VCAM1: Vascular cell adhesion molecule-1. Values represent the mean ± standard deviation (n ≥ 4).

6.6 CONCLUSIONS

The role of stiffness in tissue organization has been extensively discussed [516,517]. However, the interplay between viscosity and elasticity in regulating tissue response has been less understood until recent studies underscored its critical importance. The time-dependent viscoelastic properties of the ECM are now recognized as key regulators of morphogenesis [67,245]. While matrix viscoelasticity has been shown to influence single-cell behavior, its effects on collective cell behavior still need to be understood. However, it is expected that tissue organization is linked to the matrix's viscoelastic spectrum.

Considering our observations, Soft Fast-relaxing IPNs created an optimal ECM-mimicking microenvironment for thymic organoids, providing mechanical cues that closely mimic the mechanical properties of the native thymus. These mechanical cues promoted faster and more advanced stages of thymus differentiation and development, highlighting their critical role in guiding thymus organogenesis. Viscoelasticity emerged as a key regulator of spatiotemporal tissue organization during thymus morphogenesis, initially guiding the reorganization of TEPCs and NCCs within the thymus organoids and subsequently promoting the expression of essential thymic markers, including K8, FOXN1, and EpCAM. Stiffness, while secondary, was shown to play a complementary role in supporting proper thymus development.

This study highlights the synergistic yet distinct effects of viscoelasticity and stiffness on tissue spatiotemporal organization. Beyond validating prior studies on the role of ECM viscoelasticity [245], this research introduces a novel approach for achieving advanced thymic differentiation in organoids. By incorporating mechanical cues alongside biological signals, this work underscores the importance of engineering the mechanical microenvironment to support correct thymus development.

Future perspectives for this work include developing a streamlined system to directly facilitate TEPC and NCC reorganization and thymic structure formation within Soft Fast-relaxing IPNs, bypassing the need for pre-synthesized organoids. Additionally, replacing Matrigel with defined ECM proteins such as fibronectin, laminin, or collagen IV could enhance the translational potential of this technology. These thymic structures could also be advanced to a stage where pro-T cells are introduced into the gel, promoting their differentiation into fully functional, mature T cells.

GENERAL DISCUSSION

7 GENERAL DISCUSSION

Integrating biomaterials into medicine has revolutionized the treatment of a wide range of medical conditions, offering innovative solutions through advanced implants and polymer technologies. The versatility, biocompatibility, and capacity for tailored engineering of biomaterials have established their critical role in various applications, ranging from implantable devices and drug delivery systems to tissue engineering and regenerative medicine [433–435,518]. Among these biomaterials, polymers have been pivotal in advancing medical technologies, enabling targeted therapies, supporting tissue regeneration, and creating advanced *in vitro* 3D models that mimic native tissue properties [519]. A significant challenge within this field is the interaction between the immune system and biomaterials, which often leads to complex biological reactions that can compromise implant performance and tissue integration [8,9]. Addressing these issues has become a significant research focus, driving innovations such as polymer coatings functionalized to release anti-inflammatory drugs. These coatings enhance implant integration, minimize foreign body reaction (FBR), and reduce post-surgical complications [13,14]. Within this framework, this thesis addresses two distinct challenges.

The first part focused on designing drug-releasing polymer coatings for meniscus prostheses to provide localized, sustained delivery of anti-inflammatory drugs. This approach directly addresses a critical gap in the management of meniscus-related degenerative pathologies, aiming to improve therapeutic efficacy, reduce systemic side effects, and minimize the need for repeated intra-articular (IA) injections [269]. Incorporating drug delivery technologies into prostheses and implants is crucial for achieving site-specific effects, which can help manage pain, reduce inflammation and fibrosis, promote biocompatibility, and combat bacterial infections [7,188–194].

Moreover, the knee joint is particularly dynamic, subject to continuous mechanical stress from compression, tension, and shear forces during movement, such as walking and running. These forces are compounded by the synovial fluid's motion and the articular cartilage's deformation. This creates a complex environment for the meniscus prosthesis and its drug-releasing polymer coatings that require optimized adhesion between materials [359]. Current methods for surface modification have demonstrated significant potential in enhancing the interface adherence between materials [360,361]. Thus, in this thesis, various surface modification strategies, including physical and chemical modifications, were explored to address these challenges to improve adhesion [367–371].

The second part of this thesis focused on hydrogels, characterized by their high water content and tunable mechanical and biochemical properties. Hydrogels have emerged as powerful platforms for tissue engineering due to their ability to mimic the extracellular matrix (ECM), providing an optimal environment for cell growth, differentiation, and tissue morphogenesis. Hydrogels also enable the creation of three-dimensional cellular models, which are invaluable for replicating native conditions *in vitro*, simulating organ-like structures, and studying immune system interactions through tissue engineering approaches. In particular, spatial and temporal patterning is critical for proper tissue and organ development, growth, and function. These patterns are significantly influenced by mechanical cues generated by the ECM [485,486]. Among them, the time-dependent viscoelastic properties of the ECM, which range from solid-like (elastic) to liquid-like (viscous) responses, have a profound impact on tissue organization guiding morphogenesis, as demonstrated in organs such as the kidney [61,245].

Additionally, the stiffness and composition of the ECM are key factors that influence cell behavior, such as proliferation [487], differentiation [488], migration [245], and tissue structure [489]. Understanding and recreating these dynamics is essential for developing functional engineered tissues. The increasing emphasis on modulating and regenerating the immune system has intensified research in immune system tissue engineering, aiming to replicate the complex structure and function of immune organs such as the thymus, lymph nodes, and bone marrow [473,474].

Together, these two parts show the versatility and potential of advanced biomaterials in addressing critical challenges in drug delivery and tissue engineering. Building upon this foundation, this PhD thesis was organized into three distinct chapters, addressing the following topics:

1. The design of polymer coatings of meniscus prosthesis for the sustained release of anti-inflammatory drugs.

2. The assessment of the adhesion of the anti-inflammatory-releasing polymer coatings to meniscus prostheses to improve mechanical performance and its *in vitro* and *in vivo* evaluation.

3. The 3D encapsulation of thymic organoids in ECM-mimicking hydrogels to evaluate their morphogenesis *in vitro* under varying mechanical conditions.

Figures previously mentioned in the thesis are referred to by their original names, as introduced in their respective chapters.

7.1 POLYMER COATINGS FOR THE SUSTAINED RELEASE OF ANTI-INFLAMMATORY DRUGS FROM A MENISCUS IMPLANT

Meniscus implants or scaffolds that promote regeneration are a promising alternative to avoid the onset of osteoarthritis (OA) after a meniscectomy [12]. For older patients, meniscus self-regeneration is limited by the meniscus biology and aging biology [12]. Consequently, a non-biodegradable prosthesis could be used as an artificial meniscus substitute. For those patients who have undergone total meniscectomy and have incorporated the non-biodegradable NUsurface® meniscus prosthesis, the use of anti-inflammatory drugs will be necessary for the management of the post-surgical and long-term inflammation, providing symptomatic pain relief and ensuring the integration of the prosthesis into the surrounding native tissues in the knee cavity managing the FBR [13,14].

COX-2 inhibitors like celecoxib (CLX) and corticosteroids such as dexamethasone (DEX) are widely used for inflammation and pain management. CLX, administered orally, is effective in alleviating pain and chronic inflammation but can cause significant systemic side effects with prolonged use, particularly in the gastrointestinal, renal, cardiac, and hematological systems [15,16]. While topical application has fewer side effects, its efficacy in pain relief is often limited [17]. CLX has demonstrated superior outcomes in improving knee function in OA patients and protecting against cartilage degeneration, suggesting its potential as a disease-modifying osteoarthritis drug (DMOAD) [18–22]. Similarly, DEX, commonly used via IA

injection for severe knee pain, has shown promise as a chondroprotective corticosteroid at low doses.

Given this context, our goal was to develop a novel delivery system for the localized, sustained release of CLX to manage pain and control long-term inflammation with a targeted release over 6 to 9 months and DEX to address excessive post-surgery inflammation with a rapid release over 1 to 4 weeks. This approach aims to overcome the limitations of current IA injections and systemic therapies, offering a more effective and targeted solution for managing OA [20] (Figure 4.1).

An initial screening phase evaluated a range of polymer and drug combinations to optimize release kinetics, considering factors such as polymer type and concentration, drug loading, solubility, interaction with the polymeric matrix, and crystallinity. A PLLA/PCL (80/70 (w/w)) blend was selected for CLX release among the tested polymers. Including PCL in the PLLA matrix accelerated CLX release, achieving an almost complete release after 1 year. Moreover, the blend's ability to incorporate a higher CLX concentration (30 mg/mL) than other polymer-drug combinations positioned it as a strong candidate for facilitating meniscus prosthesis integration, requiring higher CLX doses and faster release kinetics [23,24]. For DEX delivery, LMW-PLGA and PLA-PEG were identified as the most suitable candidates, offering controlled release profiles beyond one week or sustained release within the first week, respectively.

Although solvent casting was initially explored for the synthesis of polymeric films based on its simplicity, cost-effectiveness, and rapid preparation [25,26], dip coating was ultimately employed. This technique, well-suited to the complex geometry of implants, enabled precise layering and consistent drug release, making it ideal for fabricating the bilayer coatings [27,28].

Figure 1.17 shows a comparative release study that highlighted differences in the release kinetics between the two prototypes (Prototype PLA-PEG and Prototype PLGA) which were considered to be the best from the performance screening carried out (Figure 1.17). The faster degradation and swelling of LMW-PLGA in Prototype PLGA facilitated a quicker release of CLX from the underlying PLLA/PCL matrix compared to the slower, sustained release observed with Prototype PLA-PEG. This discrepancy was attributed to the faster loss of tortuosity in the PLGA layer, allowing direct buffer access to the CLX layer earlier. Measurements of pH proved to be a more reliable indicator of the degradation of the bilayer polymer coatings compared to thickness changes, which were directly influenced by the microscope's angle and the sagittal cut's nature (Figure 1.18). The reduction in pH of the release buffer observed in the *in vitro* setup indicated polymer degradation, with the acidification of the medium resulting from this process. This acidic environment, in turn, affected the further degradation of the remaining polymer coating through autocatalysis, accelerating the overall degradation rate. However, these degradation results cannot be directly extrapolated to *in vivo* degradation, where pH levels are expected to remain stable due to the synovial fluid turnover. Despite this limitation, previous studies have shown that the degradation profiles of PLGA *in vitro* and *in vivo* are comparable in terms of molecular weight reduction [29]. This similarity may stem from the complex interactions between polymers and tissues, including potential enzymatic involvement in the degradation process.

It was demonstrated that buffer media where Prototype PLGA and Prototype PLA-PEG were incubated exhibited excellent biocompatibility with human primary macrophages (HMDMs), with no impact on macrophage viability at any assessed time point (Figure 1.23). Since the release buffer included both the drugs and polymer degradation byproducts, these results indicate that the hydrolytic degradation byproducts of the polyesters did not compromise cell survival, aligning with previous studies and underscoring the non-toxic nature and biocompatibility of the developed prototypes [30].

Importantly, the anti-inflammatory efficacy of the released drugs was also validated using macrophages HMDMs. ELISA results demonstrated that both DEX and CLX maintained their ability to regulate cytokine secretion (TNFα, CCL2, and PGE2) after being encapsulated and subsequently released from the polymer coatings (Figure 1.25).

DEX effectively suppressed TNFα and CCL2 secretion at early time points, while CLX primarily reduced PGE2 levels, consistent with its role in inhibiting the COX-2 inflammatory pathway [31]. These findings confirm the synergistic anti-inflammatory effects of the two drugs, with each playing a distinct role in inflammation modulation.

In summary, the development of a non-cytotoxic and biocompatible bilayer drug-releasing polymer coating, consisting of a first layer of PLLA/PCL for the sustained release of CLX over 6-9 months and a second layer of LMW-PLGA for the fast release of DEX over 1-4 weeks, presents a promising strategy for enhancing meniscus prosthesis integration and addressing inflammation during post-surgical recovery through tailored drug release profiles.

7.2 OPTIMIZING THE ADHESION OF THE DRUG-RELEASING BILAYER POLYMER COATING TO A MENISCUS PROSTHESIS

The drug-releasing polymer-coated meniscus prostheses must withstand substantial mechanical forces within the knee cavity, requiring enhanced adhesion between the polymer coating and the polycarbonate urethane (PCU) prosthesis to prevent delamination. To achieve this, surface modification techniques are essential for improving the attachment of the drug-polymer coatings and ensuring their durability under physiological conditions. However, while PCU is biocompatible and durable, its hydrophobic nature, sensitivity to organic solvents, and the need to preserve the geometrical wedge shape of the meniscus prosthesis present significant challenges [32,33]. These factors render traditional modification methods, such as sand-blasting [34], less effective and highlight the necessity for innovative approaches to enhance surface interactions and maintain the coating's integrity.

This study evaluated four surface modification strategies to improve the adhesion between polymer coatings and the meniscus prosthesis through macroscopic and microscopic analyses. Among these, femtosecond (fs)-pulse laser treatment was investigated for its capability to precisely control surface roughness and structure across macro-, micro-, and nano-scales, attributes particularly beneficial for biomedical applications [35]. Fs-pulse lasers are recognized for minimizing thermal effects while generating complex surface geometries that promote cellular activity [36]. The laser treatment allowed fine-tuning of parameters such as energy input, modified surface area, pattern geometry, hole separation, and exposure time (Table 2.1), providing a versatile tool for tailoring surface properties.

While the grid-pattern modification improved the interaction between the coating and the prosthesis, the laser treatment induced visible color changes, indicating potential alterations in the prosthesis's mechanical properties and structure caused by thermal effects. This color change, likely caused by carbonization from excessive heat, indicated material decomposition and the formation of a carbon-rich residue [37]. Consequently, this method was deemed unsuitable for improving coating adhesion and was discontinued in favor of more reliable approaches.

Then, chemical modification of the PCU prosthesis using oxygen plasma treatment was evaluated as a strategy to enhance adhesion. This approach preserved the bulk properties of the PCU prosthesis, maintaining its structural integrity [38,39]. The oxygen plasma treatment was expected to introduce carboxyl (-COOH) and hydroxyl (-OH) groups on the prosthesis surface, enhancing hydrophilicity and wettability [40,41]. These functional groups were hypothesized to form hydrogen bonds with ester (COO) groups in the polymer coating, collectively providing sufficient strength to improve adhesion under dry conditions [42].

The setup of this procedure was optimized to 6 minutes of processing at 52W (Figure 2.8 – conditions B5 and B6). This approach ensures efficient adhesion in dry conditions relying on the H bonds without unnecessarily extending treatment time or increasing the power of the electromagnetic field, thus minimizing potential material degradation. However, when tested in wet conditions, these bonds' effectiveness was limited, raising concerns about their functionality in the hydrophilic microenvironment of the knee cavity, where water molecules can replace polymer-surface interactions. Additionally, the surface modifications induced by plasma treatment are temporary, requiring the prosthesis to be processed and coated promptly to ensure the improved adhesion persists [43].

Another chemical modification of the PCU prosthesis using a polydopamine (PDA) was evaluated. PDA coating formation relies on the self-polymerization of dopamine [44]. This was monitored by DLS, revealing consistent particle size growth up to 24 hours, confirming progressive polymerization (Figure 2.9A). The reaction's visual transition from colorless to dark brown further indicated dopamine oxidation and uniform PDA formation (Figure 2.9B). While the resulting PDA coatings enhanced hydrophilicity and offered a versatile, noninvasive method suitable for varying prosthesis geometries, the process required extended preparation time, including oxygen plasma pre-treatment and 24 hours of polymerization. To further address drug-releasing polymer coating adhesion challenges, a sacrificial PLA-PEG layer was introduced after PDA coating. It was hypothesized that the hydrophilic PEG domain interacted with the PDA surface, while the hydrophobic PLA domain facilitated attachment to the polymer coatings. This approach significantly improved adhesion under dry conditions, with macroscopic evaluations showing visible interaction fibers resisting delamination (Figure 2.10). However, in wet conditions, the adhesion weakened as water molecules disrupted hydrogen bonding between the prosthesis and coatings. Despite its promise, the method was ultimately deemed unsuitable. These findings highlighted the need for alternative strategies to achieve robust adhesion under both dry and wet conditions.

Finally, chemical modification of the PCU prosthesis with ethyl-2-cyanoacrylate (ECA) was evaluated. ECA has been certified under USP Class VI and ISO-10993 standards, making

it suitable for medical applications, such as surgical adhesives and biomedical device coatings [45–47], and has already been described to adhere polymers to polyurethane [48].

ECA was dissolved in acetone [49] and optimized to a 40% (w/v) ECA solution, as it maintained adhesive properties while significantly reducing viscosity, making it suitable for the dip-coating of the meniscus prosthesis. ECA presented better stability of the adhesion under wet conditions because it polymerizes under moisture [50], counteracting the limitations observed with PDA and plasma treatments. Moreover, the ability to form flexible bonds was advantageous for the dynamic environment of the knee cavity. The release kinetics remained unchanged for DEX but were slightly accelerated for CLX, likely due to polymer restructuring caused by chemical interactions between the cyano group in ECA and the PLLA/PCL. This hypothesis was supported by the observation that DEX release from PLGA, which does not contact the ECA layer, was unaffected by its presence (Figure 2.11).

Mechanical evaluation using Dynamic Mechanical Analysis (DMA) with a three-point bending (TPB) setup was then conducted to quantitatively assess the physical and mechanical properties of the modified PCU prosthesis, ensuring they closely mimicked the mechanical needs of natural menisci. The mechanical properties of the ECA-coated prostheses were superior compared to other modifications. The ECA adhesive layer significantly increased the storage modulus (G'), indicating enhanced rigidity and solid-like behavior critical for providing mechanical support in the knee's load-bearing environment (Figure 2.14A). Additionally, the elastic modulus (E) of the ECA-coated prostheses was substantially higher than other prototypes, reflecting improved stiffness and stability, essential for durability in the knee cavity (Figure 2.14B). Despite these enhancements, the tan δ values remained low and comparable to uncoated prostheses, indicating that the ECA treatment preserved the balance between elastic and viscous behaviors, ensuring optimal energy recovery during movement (Figure 2.14C). Moreover, the ECA adhesive layer prototype exhibited the highest loss modulus (G"), suggesting greater flexibility to accommodate diverse knee joint movements. All these properties collectively demonstrate that the ECA adhesive layer not only improved adhesion and mechanical stability but also retained the prosthesis's ability to respond to dynamic forces. Overall, the ECA-coated prostheses outperformed those untreated or treated with PDA or plasma, establishing the ECA modification as the most promising candidate for meniscus prostheses in the mechanically demanding knee environment.

PCU meniscus prostheses were evaluated *in vivo* in a sheep model due to their anatomical similarity to the human meniscus [51–53]. To accommodate the geometrical characteristics of the sheep meniscus prosthesis, the dip coating process was optimized. The prosthesis orientation was adjusted from horizontal to vertical, and the concentration of the PLLA/PCL layer was modified from 80/70 (w/w) with a CLX loading of 16.67% to 53/47 (w/w) with a CLX loading of 16.6%. These adjustments preserved the prosthesis's mechanical properties, prevented structural disruption during curing, and maintained the release kinetics relatively unchanged, ensuring compatibility with *in vivo* conditions.

The final configuration using the ECA adhesive layer, the new orientation of the prosthesis during the dip coating process, and the reduction of the polymer concentration of the CLX-releasing layer was evaluated in a bioreactor simulating gait and the two predominant forces acting on the meniscus during movement: compression and shear [54,55]. Mechanical stress accelerated drug release from prostheses in a bioreactor compared to non-stimulated controls,

with 67% of DEX and 40% of CLX released under stimulation versus 59% and 25%, respectively, in controls. Despite the faster release, the profiles remained consistent, suggesting that mechanical forces primarily altered drug-polymer interactions rather than significantly increasing polymer degradation. The DEX layer, composed of amorphous PLGA, showed minimal differences in the release under stress, while the semi-crystalline PLLA/PCL layer for CLX exhibited a more pronounced response, likely due to PLLA's brittleness under compression [417]. Importantly, the release timelines remained aligned with the original design. Moreover, macroscopic and microscopic evaluations demonstrated that mechanical stimulation in the bioreactor influenced the degradation of polymer-coated prostheses (Figure 2.21). By week three, stimulated prostheses exhibited smoother surfaces and reduced pore sizes (~80 μm to ~40 μm), likely due to shear forces displacing polymer material, compared to slight pore enlargement in controls. Despite these changes, the polymer coatings remained attached to the PCU prostheses with no delamination, showcasing the durability and strong adhesion provided by the ECA adhesive layer. These findings confirm the coating's stability and suitability for the demanding mechanical environment of the knee cavity.

Ethylene oxide (ETO) was selected as the sterilization method for the coated sheep prostheses due to its ability to preserve drug stability, maintain release kinetics, and avoid structural damage to the polymer coatings. While hydrogen peroxide (H_2O_2) plasma sterilization was initially considered, it severely damaged the polymer coatings, particularly the PLGA upper layer, and posed risks due to high operating temperatures and extended UV-light exposure, which could degrade DEX [56,57]. In contrast, ETO sterilization was conducted at a safe temperature of 38ºC, below the critical Tg and Tm of the polymers, and avoided UV exposure. To address concerns about potential toxic residues [45,56], a 48-hour aeration step was implemented, ensuring residue-free prostheses. ETO sterilization also demonstrated no adverse effects on drug release kinetics or drug loading (Figure 2.23), making it the most suitable method for *in vivo* studies. Finally, the optimized drug-releasing polymer-coated meniscus prostheses were tested *in vivo* in sheep. The primary objectives of this experiment were to develop a successful fixation technique and confirm that the polymer coatings of the coated meniscus prostheses could withstand the mechanical forces in the sheep's knee cavity. These objectives were achieved, as the coated prostheses demonstrated both mechanical integrity and improved fixation outcomes compared to the uncoated prosthesis. Future studies employing the same fixation technique for both groups would enable a more robust, direct comparison.

Histological analyses revealed differences between the groups (Figure 2.25). The meniscectomy group (no implanted meniscus prosthesis) exhibited the best outcomes in the short term, with minimal cartilage damage and no osteophyte formation or significant subchondral bone thickening. However, this group lacked an unloading device like the meniscus prosthesis, potentially leading to progressive degeneration of the knee cavity structures over time. In contrast, the uncoated prosthesis group showed the most severe indicators of OA, including significant cartilage fibrillation, extensive fibrocartilage formation, and notable subchondral bone thickening. These outcomes reflected the lack of an anti-inflammatory mechanism and poor fixation stability, necessitating early sacrifice in this group.

The coated prostheses appear to perform better than the uncoated group across all evaluations. Toluidine blue staining revealed that the coated prosthesis minimized cartilage damage, with scores approaching those of the meniscectomy group. Additionally, the coated

prostheses reduced chondrocyte clustering, fibrocartilage formation, and osteophyte presence compared to the uncoated prostheses, suggesting a protective effect generated by the sustained release of DEX and CLX. Subchondral bone thickening was also less pronounced in the coated group, further indicating its role in mitigating OA progression. However, all these data should be taken cautiously due to the lack of statistical significance associated with the small number of animals.

Importantly, the coated prostheses showed potential in mitigating the FBR, as evidenced by reduced fibrocartilage formation. This process is linked to inflammatory pathways, including TNF-α and IL-1, which are involved in fibrous capsule formation. The anti-inflammatory drugs released from the coating were hypothesized to be the reason for effectively decreasing this process in the sheep. These results align with our *in vitro* findings, further supporting the hypothesis that the drug-releasing bilayer polymer coating reduces acute and chronic inflammation, thereby minimizing fibrous tissue formation associated with FBR around the meniscus prosthesis [58,59].

In conclusion, the study underscores the need for a larger sample size, extended follow-up periods, and more precise controls to fully validate these promising initial findings. The bilayer drug-releasing polymer coating demonstrates considerable potential in improving meniscus prosthesis outcomes and preventing OA progression. Thus, this study should be regarded as a pilot *in vivo* investigation, providing valuable insights into the ability of the polymeric coatings to withstand the mechanical forces in the knee cavity and identifying the most effective prosthesis fixation technique within the joint.

7.3 3D ENCAPSULATION OF THYMIC ORGANOIDS IN ECM-MIMICKING IPNS TO EVALUATE MORPHOGENESIS *IN VITRO*

T cell receptor (TCR) repertoire formation occurs during T cell development and maturation in the thymus through tightly regulated events within specialized zones. During this process, distinct signals and cell types direct thymocyte differentiation into fully functional T cells. The thymic microenvironment's spatial organization and mechanical properties, including the ECM and tissue architecture, play critical roles [60].

This chapter explores how the mechanical properties of ionically crosslinked alginate hydrogels, modified to incorporate ECM-associated proteins and form interpenetrating polymer networks (IPNs), impact thymus organoid development. The hydrogels' ability to resist mammalian cell degradation allows for independent tuning of viscoelasticity, stiffness, and ligand density. Also, their ionic crosslinking can adapt to the different stress relaxation rates of developing tissues while maintaining stability in culture over several weeks [61].

Thymus organoids, composed of thymus epithelial progenitor cells (TEPCs) and neural crest cells (NCCs) derived from human embryonic stem cells, were encapsulated in four IPN formulations with distinct mechanical properties. The moduli ranged from soft $E \approx 4{,}100$ Pa to stiff $E \approx 15{,}000$ Pa, and the viscoelasticity from more elastic, slower $\tau 70\%$ relaxation time to more viscoelastic, faster $\tau 70\%$ relaxation time (Figure 3.6).

These organoids were cultured and tracked over one week to assess cell rearrangement in response to mechanical cues. During thymic organoid development, NCCs initially outnumber

TEPCs in a 3:1 ratio and progressively encapsulate the TEPCs, shaping the organoid structure. Circularity analysis revealed stable morphology in Stiff IPNs, regardless of viscoelasticity, while Soft IPNs showed distinct trends: Soft Slow-relaxing IPNs experienced a sharp decrease in circularity by day 3, stabilizing by day 5, whereas Soft Fast-relaxing IPNs showed a gradual decrease throughout the observation period (Figure 3.7). These findings highlight the complementary roles of stiffness and viscoelasticity in influencing organoid morphology and spatial organization. NCCs formed a ring-like structure around the organoid's middle, progressively encapsulating TEPCs over time (Figure 3.8), demonstrating the importance of mechanical cues in organoid development and tissue morphogenesis [62,63].

Immunohistochemistry analysis revealed that the mechanical properties of the ECM significantly influence thymic tissue development, including the formation of tissue-like structures and the expression of key developmental markers, underscoring the pivotal role of viscoelasticity in establishing structured, tissue-like patterns within thymic organoids. Regarding the formation of tissue-like structures, Soft Fast-relaxing IPNs demonstrated the most advanced structures, with the presence of lumens indicating progression toward mature tissue organization (Figure 3.12). Conversely, the absence of lumens in other conditions indicated limited differentiation, highlighting insufficient coordination of mechanical and biochemical cues [64–66]. Stiff Fast-relaxing IPNs slightly supported lumen formation and tissue-like structures, suggesting that stiffness complements viscoelasticity in driving thymic morphogenesis. In contrast, Soft Slow-relaxing IPNs displayed limited complexity with less lumen formation, and Stiff Slow-relaxing IPNs lacked lumens and organization altogether, emphasizing the necessity of a viscoelastic ECM-like environment for proper thymic tissue development, supporting previous investigations highlighting its role in tissue development and cell instruction [67–69].

Lastly, the analysis of thymus development markers revealed significant differences in expression across IPNs with varying mechanical properties. Soft Fast-relaxing IPNs consistently promoted the highest expression levels of K8, FOXN1, and EpCAM, markers critical for thymus organogenesis. Significant differences in K8 expression were observed between Soft Fast-relaxing and Stiff Slow-relaxing IPNs, while other conditions showed comparable levels, highlighting the dominant role of viscoelasticity in enhancing K8 expression. FOXN1, essential for thymus morphogenesis, exhibited significantly higher levels in Soft Fast-relaxing IPNs compared to all other conditions, with Stiff Slow-relaxing IPNs showing the lowest expression. Similarly, EpCAM, associated with the epithelial organization, was significantly elevated in Soft Fast-relaxing IPNs compared to other conditions, emphasizing their superior capacity to support advanced tissue differentiation. Conversely, VCAM1 expression was uniformly low across all conditions, with no significant differences, consistent with its role in later stages of thymus development [70,71].

This part of the thesis underscores viscoelasticity as the primary driver of thymus organoid maturation, while stiffness plays a secondary yet complementary role. It emphasizes the importance of optimal mechanical properties of the ECM-mimicking IPNs to optimize thymus organogenesis.

CONCLUSIONS

8 CONCLUSIONS

C1: A bilayer polymer coating technology was designed for the sequential release of two anti-inflammatory drugs, DEX and CLX, with distinct release kinetics. Two prototypes—Prototype PLGA and Prototype PLA-PEG—achieved the targeted release profiles of DEX over 1–4 weeks and CLX over 6–9 months, demonstrating the feasibility of localized, controlled drug delivery.

C2: Prototype PLGA demonstrated more consistent and reproducible drug loading compared to Prototype PLA-PEG and supported sustained release kinetics without interference from the degradation of the upper DEX-loaded layer. Its faster degradation rate resulted in an earlier acidification of the medium. In contrast, the slower degradation of the PLA-PEG upper layer delayed acidification and contributed to a slower release of CLX from the bottom PLLA/PCL layer. Both prototypes displayed distinct hydrolytic degradation profiles influenced by the properties of their polymeric matrices.

C3: When tested with human macrophages (HMDMs), both prototypes showed excellent biocompatibility, no toxicity, and effective anti-inflammatory activity *in vitro*.

C4: Prototype PLGA was selected for further development due to its reproducible drug loading, controlled degradation, and ability to maintain desired release kinetics. These characteristics make it a more reliable candidate for application on anatomically relevant meniscus prostheses in preclinical studies.

C5: The incorporation of an ECA adhesive layer significantly improved the adhesion of the bilayer drug-releasing polymer coating to the PCU meniscus prosthesis, as confirmed through macroscopic and microscopic evaluations. Compared to other adhesion enhancement methods explored in the chapter, such as PDA coating and plasma treatment, the ECA-based approach exhibited superior mechanical properties (G', G'', and elastic modulus), making it highly suitable for the knee cavity's demanding mechanical environment. The ECA layer preserved the viscoelastic balance (tan δ) of the uncoated PCU prosthesis, ensuring the mechanical integrity of the prosthesis was maintained. Additionally, the incorporation of this ECA layer maintained the drug release kinetics relatively unaltered.

C6: The drug-releasing polymer coating was successfully adapted to the sheep meniscus prosthesis by modifying the CLX-releasing PLLA/PCL layer concentration and reorienting the prosthesis during the dip-coating process. These adjustments ensured a homogeneous polymer coating while preserving the prosthesis's complex structure, improving drug distribution and overall coating effectiveness. This optimization aligned the coating with the physical and mechanical demands of the sheep meniscus prosthesis.

C7: *Ex vivo* evaluations in early-OA simulated synovial fluid (SSF) within a bioreactor revealed that mechanical forces did not significantly damage the polymer coating but influenced its surface structure and accelerated drug release kinetics, particularly CLX.

C8: ETO sterilization was selected as the optimal method to preserve coating and drug integrity, with no adverse effects on drug release kinetics or loading.

C9: *In vivo* studies demonstrated that the optimized coated prostheses outperformed uncoated prostheses in reducing osteoarthritis progression markers while remaining securely attached without delamination. Although, as expected, the meniscectomy group showed superior outcomes in the short term, the coated prosthesis showed significant promise as an alternative treatment, warranting further evaluation with larger sample sizes and longer study durations.

C10: Mechanical cues provided by the ECM, particularly viscoelasticity, played a critical role in guiding the spatial reorganization of TEPCs and NCCs within thymus organoids. Soft Fast-relaxing IPNs effectively mimicked the mechanical properties of the native thymus, promoting the formation of organized cellular patterns where NCCs encapsulated TEPCs, supporting early morphogenesis.

C11: Viscoelasticity emerged as the primary factor driving the development of tissue-like structures within thymic organoids. Soft Fast-relaxing IPNs facilitated the formation of advanced structures, including lumens, indicative of native thymus organization and tissue development. In contrast, stiffer and purely elastic environments hindered lumen formation and limited structural complexity.

C13: The viscoelastic properties of the ECM significantly enhanced the expression of key thymic markers such as K8, FOXN1, and EpCAM, crucial for thymic differentiation and tissue development. Soft Fast-relaxing IPNs showed the highest marker expression, demonstrating their ability to support advanced thymus organogenesis. Conversely, slower-relaxing and stiffer environments exhibited reduced marker expression, underscoring the importance of tuning ECM mechanics to achieve optimal thymic differentiation.

REFERENCES

9 REFERENCES

[1] Chavda VP, Jogi G, Paiva-Santos AC, Kaushik A. Biodegradable and removable implants for controlled drug delivery and release application. Expert Opin Drug Deliv 2022;19:1177–81. https://doi.org/10.1080/17425247.2022.2110065.

[2] Maitz MF. Applications of synthetic polymers in clinical medicine. Biosurf Biotribol 2015;1:161–76. https://doi.org/10.1016/J.BSBT.2015.08.002.

[3] Ulery BD, Nair LS, Laurencin CT. Biomedical Applications of Biodegradable Polymers. J Polym Sci B Polym Phys 2011;49:832. https://doi.org/10.1002/POLB.22259.

[4] Kauffman GB. Polymer pioneers: a popular history of the science and technology of large molecules (Morris, Peter J.T.). J Chem Educ 1988;65:A301. https://doi.org/10.1021/ED065PA301.2.

[5] Kravanja KA, Finšgar M. A review of techniques for the application of bioactive coatings on metal-based implants to achieve controlled release of active ingredients. Mater Des 2022;217:110653. https://doi.org/10.1016/J.MATDES.2022.110653.

[6] Atay HY. Fabrication Methods for Polymer Coatings. Polymer Coatings 2020:1–20. https://doi.org/10.1002/9781119655145.CH1.

[7] Lebaudy E, Fournel S, Lavalle P, Vrana NE, Gribova V. Recent Advances in Antiinflammatory Material Design. Adv Healthc Mater 2021;10. https://doi.org/10.1002/ADHM.202001373.

[8] Tripathi AS, Zaki MEA, Al-Hussain SA, Dubey BK, Singh P, Rind L, et al. Material matters: exploring the interplay between natural biomaterials and host immune system. Front Immunol 2023;14:1269960. https://doi.org/10.3389/FIMMU.2023.1269960/BIBTEX.

[9] Salthouse D, Novakovic K, Hilkens CMU, Ferreira AM. Interplay between biomaterials and the immune system: Challenges and opportunities in regenerative medicine. Acta Biomater 2023;155:1–18. https://doi.org/10.1016/J.ACTBIO.2022.11.003.

[10] Chen J, Li S, Zhang Y, Wang W, Zhang X, Zhao Y, et al. A Reloadable Self-Healing Hydrogel Enabling Diffusive Transport of C-Dots Across Gel–Gel Interface for Scavenging Reactive Oxygen Species. Adv Healthc Mater 2017;6:1700746. https://doi.org/10.1002/ADHM.201700746.

[11] Li J, Mooney DJ. Designing hydrogels for controlled drug delivery. Nature Reviews Materials 2016 1:12 2016;1:1–17. https://doi.org/10.1038/natrevmats.2016.71.

[12] Makris EA, Hadidi P, Athanasiou KA. The knee meniscus: Structure–function, pathophysiology, current repair techniques, and prospects for regeneration. Biomaterials 2011;32:7411–31. https://doi.org/10.1016/J.BIOMATERIALS.2011.06.037.

[13] Kwon H, Brown WE, Lee CA, Wang D, Paschos N, Hu JC, et al. Surgical and tissue engineering strategies for articular cartilage and meniscus repair. Nat Rev Rheumatol 2019;15:550–70. https://doi.org/10.1038/S41584-019-0255-1.

[14] Carnicer-Lombarte A, Chen ST, Malliaras GG, Barone DG. Foreign Body Reaction to Implanted Biomaterials and Its Impact in Nerve Neuroprosthetics. Front Bioeng Biotechnol 2021;9. https://doi.org/10.3389/FBIOE.2021.622524.

[15] Aweid O, Haider Z, Saed A, Kalairajah Y. Treatment modalities for hip and knee osteoarthritis: A systematic review of safety. J Orthop Surg (Hong Kong) 2018;26. https://doi.org/10.1177/2309499018808669.

[16] Caldwell B, Aldington S, Weatherall M, Shirtcliffe P, Beasley R. Risk of cardiovascular events and celecoxib: a systematic review and meta-analysis. J R Soc Med 2006;99:132–40. https://doi.org/10.1258/jrsm.99.3.132.

[17] Mora JC, Przkora R, Cruz-Almeida Y. Knee osteoarthritis: Pathophysiology and current treatment modalities. J Pain Res 2018;11:2189–96. https://doi.org/10.2147/JPR.S154002.

[18] Rowan-Robinson K. Celecoxib for osteoarthritis. Br J Community Nurs 2019;24:501–2. https://doi.org/10.12968/bjcn.2019.24.10.501.

[19] Puljak L, Marin A, Vrdoljak D, Markotic F, Utrobicic A, Tugwell P. Celecoxib for osteoarthritis. Cochrane Database Syst Rev 2017;5. https://doi.org/10.1002/14651858.CD009865.PUB2.

[20] El-Gogary RI, Khattab MA, Abd-Allah H. Intra-articular multifunctional celecoxib loaded hyaluronan nanocapsules for the suppression of inflammation in an osteoarthritic rat model. Int J Pharm 2020;583:119378. https://doi.org/10.1016/J.IJPHARM.2020.119378.

[21] Jiang D, Zou J, Huang L, Shi Q, Zhu X, Wang G, et al. Efficacy of intra-articular injection of celecoxib in a rabbit model of osteoarthritis. Int J Mol Sci 2010;11:4106–13. https://doi.org/10.3390/IJMS11104106.

[22] Maudens P, Jordan O, Allémann E. Recent advances in intra-articular drug delivery systems for osteoarthritis therapy. Drug Discov Today 2018;23:1761–75. https://doi.org/10.1016/j.drudis.2018.05.023.

[23] Can E, Udenir G, Kanneci AI, Kose G, Bucak S. Investigation of PLLA/PCL Blends and Paclitaxel Release Profiles. AAPS PharmSciTech 2011;12:1442. https://doi.org/10.1208/S12249-011-9714-Y.

[24] Sakai F, Nishikawa K, Inoue Y, Yazawa K. Nucleation enhancement effect in poly(L-lactide) (PLLA)/poly(ε- caprolactone) (PCL) blend induced by locally activated chain mobility resulting from limited miscibility. Macromolecules 2009;42:8335–42. https://doi.org/10.1021/MA901547A/SUPPL_FILE/MA901547A_SI_001.PDF.

[25] Wahid F, Khan T, Hussain Z, Ullah H. Nanocomposite scaffolds for tissue engineering; properties, preparation and applications. Applications of Nanocomposite Materials in Drug Delivery 2018:701–35. https://doi.org/10.1016/B978-0-12-813741-3.00031-5.

[26] Borbolla-Jiménez F V., Peña-Corona SI, Farah SJ, Jiménez-Valdés MT, Pineda-Pérez E, Romero-Montero A, et al. Films for Wound Healing Fabricated Using a Solvent Casting Technique. Pharmaceutics 2023;15. https://doi.org/10.3390/PHARMACEUTICS15071914.

[27] Chen Y, Chen BZ, Wang QL, Jin X, Guo XD. Fabrication of coated polymer microneedles for transdermal drug delivery. Journal of Controlled Release 2017;265:14–21. https://doi.org/10.1016/J.JCONREL.2017.03.383.

[28] Haj-Ahmad R, Khan H, Arshad MS, Rasekh M, Hussain A, Walsh S, et al. Microneedle Coating Techniques for Transdermal Drug Delivery. Pharmaceutics 2015;7:486. https://doi.org/10.3390/PHARMACEUTICS7040486.

[29] Park TG. Degradation of poly(lactic-co-glycolic acid) microspheres: effect of copolymer composition. Biomaterials 1995;16:1123–30. https://doi.org/10.1016/0142-9612(95)93575-X.

[30] Grizzi I, Garreau H, Li S, Vert M. Hydrolytic degradation of devices based on poly(dl-lactic acid) size-dependence. Biomaterials 1995;16:305–11. https://doi.org/10.1016/0142-9612(95)93258-F.

[31] Kulesza A, Paczek L, Burdzinska A. The Role of COX-2 and PGE2 in the Regulation of Immunomodulation and Other Functions of Mesenchymal Stromal Cells. Biomedicines 2023;11. https://doi.org/10.3390/BIOMEDICINES11020445.

[32] van Minnen BS, van Tienen TG. The Current State of Meniscus Replacements. Curr Rev Musculoskelet Med 2024;17:293. https://doi.org/10.1007/S12178-024-09902-1.

[33] Geary C, Birkinshaw C, Jones E. Characterisation of Bionate polycarbonate polyurethanes for orthopaedic applications. J Mater Sci Mater Med 2008;19:3355–63. https://doi.org/10.1007/S10856-008-3472-8/TABLES/7.

[34] Yoshida T, Makino S, Ayato Y, - al, Aoki Y, Tsuji J, et al. Sand-blasting treatment as a way to improve the adhesion strength of hydroxyapatite coating on titanium implant. J Phys Conf Ser 2017;830:012109. https://doi.org/10.1088/1742-6596/830/1/012109.

[35] Riveiro A, Maçon ALB, del Val J, Comesaña R, Pou J. Laser surface texturing of polymers for biomedical applications. Front Phys 2018;5:330240. https://doi.org/10.3389/FPHY.2018.00016/BIBTEX.

[36] Kryszak B, Szustakiewicz K, Dzienny P, Junka A, Paleczny J, Szymczyk-Ziółkowska P, et al. Functionalization of the PLLA surface with a femtosecond laser: Tailored substrate properties for cellular response. Polym Test 2022;116:107815. https://doi.org/10.1016/J.POLYMERTESTING.2022.107815.

[37] Devi M, Wang H, Moon S, Sharma S, Strauss V. Laser-Carbonization – A Powerful Tool for Micro-Fabrication of Patterned Electronic Carbons. Advanced Materials 2023;35:2211054. https://doi.org/10.1002/ADMA.202211054.

[38] Yoshida S, Hagiwara K, Hasebe T, Hotta A. Surface modification of polymers by plasma treatments for the enhancement of biocompatibility and controlled drug release. Surf Coat Technol 2013;233:99–107. https://doi.org/10.1016/J.SURFCOAT.2013.02.042.

[39] Pizzorni M, Parmiggiani A, Prato M. Adhesive bonding of a mixed short and continuous carbon-fiber-reinforced Nylon-6 composite made via fused filament fabrication. Int J Adhes Adhes 2021;107:102856. https://doi.org/10.1016/J.IJADHADH.2021.102856.

[40] Ghorbani F, Zamanian A, Torabinejad B. The effect of oxygen plasma pretreatment on

the properties of mussel-inspired polydopamine-decorated polyurethane nanofibers. Journal of Polymer Engineering 2020;40:109–19. https://doi.org/10.1515/POLYENG-2019-0219/MACHINEREADABLECITATION/RIS.

[41] Kuwabara A, Kuroda SI, Kubota H. Polymer Surface Treatment by Atmospheric Pressure Low Temperature Surface Discharge Plasma: Its Characteristics and Comparison with Low Pressure Oxygen Plasma Treatment. Plasma Science and Technology 2007;9:181. https://doi.org/10.1088/1009-0630/9/2/14.

[42] Yoon SJ, Jeon IY. Reinforcement of Poly(vinyl alcohol) using hydrogen bonding of carboxylic acid-functionalized graphitic nanoplatelets. Polymer (Guildf) 2023;285:126376. https://doi.org/10.1016/J.POLYMER.2023.126376.

[43] Novák I, Popelka A, Luyt AS, Chehimi MM, Špírková M, Janigová I, et al. Adhesive properties of polyester treated by cold plasma in oxygen and nitrogen atmospheres. Surf Coat Technol 2013;235:407–16. https://doi.org/10.1016/J.SURFCOAT.2013.07.057.

[44] Lee H, Dellatore SM, Miller WM, Messersmith PB. Mussel-inspired surface chemistry for multifunctional coatings. Science (1979) 2007;318:426–30. https://doi.org/10.1126/SCIENCE.1147241/SUPPL_FILE/LEE.SOM.PDF.

[45] Barkan Y, Levinman M, Veprinsky-Zuzuliya I, Tsach T, Merqioul E, Blum G, et al. Comparative evaluation of polycyanoacrylates. Acta Biomater 2017;48:390–400. https://doi.org/10.1016/J.ACTBIO.2016.11.011.

[46] Pascual G, Rodríguez M, Mesa-Ciller C, Pérez-Köhler B, Fernández-Gutiérrez M, San Román J, et al. Sutures versus new cyanoacrylates in prosthetic abdominal wall repair: a preclinical long-term study. J Surg Res 2017;220:30–9. https://doi.org/10.1016/J.JSS.2017.06.074.

[47] Habib A, Mehanna A, Medra A. Cyanoacrylate: a handy tissue glue in maxillofacial surgery: our experience in alexandria, egypt. J Maxillofac Oral Surg 2013;12:243–7. https://doi.org/10.1007/S12663-012-0433-Z.

[48] Wang W, Lu Y, Zhu H, Cao Z. Superdurable Coating Fabricated from a Double-Sided Tape with Long Term "Zero" Bacterial Adhesion. Adv Mater 2017;29. https://doi.org/10.1002/ADMA.201606506.

[49] Ethyl 2-cyanoacrylate - American Chemical Society n.d. https://www.acs.org/molecule-of-the-week/archive/e/ethyl-2-cyanoacrylate.html (accessed September 26, 2024).

[50] Cary R. Methyl cyanoacrylate and ethyl cyanoacrylate. Geneva: World Health Organization; 2001.

[51] Brzezinski A, Ghodbane SA, Patel JM, Perry BA, Gatt CJ, Dunn MG. The Ovine Model for Meniscus Tissue Engineering: Considerations of Anatomy, Function, Implantation, and Evaluation. Tissue Eng Part C Methods 2017;23:829. https://doi.org/10.1089/TEN.TEC.2017.0192.

[52] Proffen BL, McElfresh M, Fleming BC, Murray MM. A comparative anatomical study of the human knee and six animal species. Knee 2012;19:493–9. https://doi.org/10.1016/J.KNEE.2011.07.005.

[53] Kon E, Filardo G, Tschon M, Fini M, Giavaresi G, Reggiani LM, et al. Tissue engineering for total meniscal substitution: animal study in sheep model--results at 12 months. Tissue Eng Part A 2012;18:1573–82. https://doi.org/10.1089/TEN.TEA.2011.0572.

[54] Schwer J, Ignatius A, Seitz AM. The biomechanical properties of human menisci: A systematic review. Acta Biomater 2024;175:1–26. https://doi.org/10.1016/J.ACTBIO.2023.12.010.

[55] Raj MA, Bubnis MA. Knee Meniscal Tears. StatPearls 2023.

[56] Our Current Understanding of Ethylene Oxide (EtO) | US EPA n.d. https://www.epa.gov/hazardous-air-pollutants-ethylene-oxide/our-current-understanding-ethylene-oxide-eto (accessed October 5, 2024).

[57] Wang D, Zhang A, Guo W, Zhu B, Yu H, Chen Y. Identification of residues in ethylene oxide sterilized hard gelatin capsule shells by gas chromatography-mass spectrometry and development of a simple gas chromatography-flame ionization detector method for the determination of residues. Journal of Chromatography Open 2022;2:100061. https://doi.org/10.1016/J.JCOA.2022.100061.

[58] Carnicer-Lombarte A, Chen ST, Malliaras GG, Barone DG. Foreign Body Reaction to Implanted Biomaterials and Its Impact in Nerve Neuroprosthetics. Front Bioeng Biotechnol 2021;9. https://doi.org/10.3389/FBIOE.2021.622524.

[59] Armiento AR, Alini M, Stoddart MJ. Articular fibrocartilage - Why does hyaline cartilage fail to repair? Adv Drug Deliv Rev 2019;146:289–305. https://doi.org/10.1016/J.ADDR.2018.12.015.

[60] Gameiro J, Nagib P, Verinaud L. The thymus microenvironment in regulating thymocyte differentiation. Cell Adh Migr 2010;4:382. https://doi.org/10.4161/CAM.4.3.11789.

[61] Nerger BA, Sinha S, Lee NN, Cheriyan M, Bertsch P, Johnson CP, et al. 3D Hydrogel Encapsulation Regulates Nephrogenesis in Kidney Organoids. Adv Mater 2024;36. https://doi.org/10.1002/ADMA.202308325.

[62] Gan Z, Qin X, Liu H, Liu J, Qin J. Recent advances in defined hydrogels in organoid research. Bioact Mater 2023;28:386. https://doi.org/10.1016/J.BIOACTMAT.2023.06.004.

[63] Vining KH, Mooney DJ. Mechanical forces direct stem cell behaviour in development and regeneration. Nature Reviews Molecular Cell Biology 2017 18:12 2017;18:728–42. https://doi.org/10.1038/nrm.2017.108.

[64] Muñoz JJ, Cejalvo T, Tobajas E, Fanlo L, Cortés A, Zapata AG. 3D immunofluorescence analysis of early thymic morphogenesis and medulla development. Histol Histopathol 2015;30:589–99. https://doi.org/10.14670/HH-30.589.

[65] Figueiredo M, Zilhão R, Neves H. Thymus Inception: Molecular Network in the Early Stages of Thymus Organogenesis. International Journal of Molecular Sciences 2020, Vol 21, Page 5765 2020;21:5765. https://doi.org/10.3390/IJMS21165765.

[66] Navis A, Nelson CM. Pulling together: Tissue-generated forces that drive lumen morphogenesis. Semin Cell Dev Biol 2016;55:139.

https://doi.org/10.1016/J.SEMCDB.2016.01.002.

[67] Chaudhuri O, Cooper-White J, Janmey PA, Mooney DJ, Shenoy VB. Effects of extracellular matrix viscoelasticity on cellular behaviour. Nature 2020 584:7822 2020;584:535–46. https://doi.org/10.1038/s41586-020-2612-2.

[68] Wu DT, Diba M, Yang S, Freedman BR, Elosegui-Artola A, Mooney DJ. Hydrogel viscoelasticity modulates migration and fusion of mesenchymal stem cell spheroids. Bioeng Transl Med 2022;8. https://doi.org/10.1002/BTM2.10464.

[69] Wu DT, Diba M, Yang S, Freedman BR, Elosegui-Artola A, Mooney DJ. Hydrogel viscoelasticity modulates migration and fusion of mesenchymal stem cell spheroids. Bioeng Transl Med 2023;8:e10464. https://doi.org/10.1002/BTM2.10464.

[70] Salomon DR, Crisa L, Mojcik CF, Ishii JK, Klier G, Shevach EM. Vascular Cell Adhesion Molecule-1 Is Expressed by Cortical Thymic Epithelial Cells and Mediates Thymocyte Adhesion. Implications for the Function of α4β1 (VLA4) Integrin in T-Cell Development. Blood 1997;89:2461–71. https://doi.org/10.1182/BLOOD.V89.7.2461.

[71] Han J, Zúñiga-Pflücker JC. A 2020 View of Thymus Stromal Cells in T Cell Development. J Immunol 2021;206:249. https://doi.org/10.4049/JIMMUNOL.2000889.

[72] Maadani AM, Salahinejad E. Performance comparison of PLA- and PLGA-coated porous bioceramic scaffolds: Mechanical, biodegradability, bioactivity, delivery and biocompatibility assessments. Journal of Controlled Release 2022;351:1–7. https://doi.org/10.1016/J.JCONREL.2022.09.022.

[73] Barik A, Chakravorty N. Targeted Drug Delivery from Titanium Implants: A Review of Challenges and Approaches. Adv Exp Med Biol 2020;1251:1–17. https://doi.org/10.1007/5584_2019_447.

[74] Rykowska I, Nowak I, Nowak R. Drug-Eluting Stents and Balloons—Materials, Structure Designs, and Coating Techniques: A Review. Molecules 2020, Vol 25, Page 4624 2020;25:4624. https://doi.org/10.3390/MOLECULES25204624.

[75] Talebian S, Mendes B, Conniot J, Farajikhah S, Dehghani F, Li Z, et al. Biopolymeric Coatings for Local Release of Therapeutics from Biomedical Implants. Advanced Science 2023;10:2207603. https://doi.org/10.1002/ADVS.202207603.

[76] Welch NG, Winkler DA, Thissen H. Antifibrotic strategies for medical devices. Adv Drug Deliv Rev 2020;167:109–20. https://doi.org/10.1016/J.ADDR.2020.06.008.

[77] Ulery BD, Nair LS, Laurencin CT. Biomedical Applications of Biodegradable Polymers. J Polym Sci B Polym Phys 2011;49:832. https://doi.org/10.1002/POLB.22259.

[78] AW L. Interfacial bioengineering to enhance surface biocompatibility. Med Device Technol 2002;13:18–21.

[79] Gu L, Shan T, Ma Y xuan, Tay FR, Niu L. Novel Biomedical Applications of Crosslinked Collagen. Trends Biotechnol 2019;37:464–91. https://doi.org/10.1016/J.TIBTECH.2018.10.007.

[80] Li X, Xue W, Zhu C, Fan D, Liu Y, Xiaoxuan M. Novel hydrogels based on carboxyl

pullulan and collagen crosslinking with 1, 4-butanediol diglycidylether for use as a dermal filler: initial in vitro and in vivo investigations. Materials Science and Engineering: C 2015;57:189–96. https://doi.org/10.1016/J.MSEC.2015.07.059.

[81] Fadlallah A, Zhu H, Arafat S, Kochevar I, Melki S, Ciolino JB. Corneal Resistance to Keratolysis After Collagen Crosslinking With Rose Bengal and Green Light. Invest Ophthalmol Vis Sci 2016;57:6610–4. https://doi.org/10.1167/IOVS.15-18764.

[82] Fan L, Ren Y, Emmert S, Vučković I, Stojanovic S, Najman S, et al. The Use of Collagen-Based Materials in Bone Tissue Engineering. Int J Mol Sci 2023;24. https://doi.org/10.3390/IJMS24043744.

[83] Ning C, Li P, Gao C, Fu L, Liao Z, Tian G, et al. Recent advances in tendon tissue engineering strategy. Front Bioeng Biotechnol 2023;11:1115312. https://doi.org/10.3389/FBIOE.2023.1115312/BIBTEX.

[84] Chen F, Fan J, Hui D, Wang C, Yuan F, Wu X. Mechanisms of the improved stiffness of flexible polymers under impact loading. Nanotechnol Rev 2022;11:3281–91. https://doi.org/10.1515/NTREV-2022-0437/ASSET/GRAPHIC/J_NTREV-2022-0437_FIG_010.JPG.

[85] Chen J. Design and Synthesis of Biomedical Polymer Materials. Int J Mol Sci 2024;25:5088. https://doi.org/10.3390/IJMS25105088.

[86] Yuce-Erarslan E, Domb A (Avi) J, Kasem H, Uversky VN, Coskuner-Weber O. Intrinsically Disordered Synthetic Polymers in Biomedical Applications. Polymers 2023, Vol 15, Page 2406 2023;15:2406. https://doi.org/10.3390/POLYM15102406.

[87] Tanaka M, Sato K, Kitakami E, Kobayashi S, Hoshiba T, Fukushima K. Design of biocompatible and biodegradable polymers based on intermediate water concept. Polymer Journal 2015 47:2 2014;47:114–21. https://doi.org/10.1038/pj.2014.129.

[88] Weber M, Renkawitz T, Voellner F, Craiovan B, Greimel F, Worlicek M, et al. Revision Surgery in Total Joint Replacement Is Cost-Intensive. Biomed Res Int 2018;2018. https://doi.org/10.1155/2018/8987104.

[89] Fang CJ, Shaker JM, Ward DM, Jawa A, Mattingly DA, Smith EL. Financial Burden of Revision Hip and Knee Arthroplasty at an Orthopedic Specialty Hospital: Higher Costs and Unequal Reimbursements. J Arthroplasty 2021;36:2680–4. https://doi.org/10.1016/J.ARTH.2021.03.044.

[90] Alentorn-Geli E, Clark NJ, Assenmacher AT, Samuelsen BT, Sánchez-Sotelo J, Cofield RH, et al. What Are the Complications, Survival, and Outcomes After Revision to Reverse Shoulder Arthroplasty in Patients Older Than 80 Years? Clin Orthop Relat Res 2017;475:2744–51. https://doi.org/10.1007/S11999-017-5406-6.

[91] Pflüger MJ, Frömel DE, Meurer A. Total Hip Arthroplasty Revision Surgery: Impact of Morbidity on Perioperative Outcomes. J Arthroplasty 2021;36:676–81. https://doi.org/10.1016/J.ARTH.2020.08.005.

[92] Day CW, Costi K, Pannach S, Atkins GJ, Hofstaetter JG, Callary SA, et al. Long-Term Outcomes of Staged Revision Surgery for Chronic Periprosthetic Joint Infection of Total Hip Arthroplasty. Journal of Clinical Medicine 2022, Vol 11, Page 122 2021;11:122.

https://doi.org/10.3390/JCM11010122.

[93] Czumbel LM, Kerémi B, Gede N, Mikó A, Tóth B, Csupor D, et al. Sandblasting reduces dental implant failure rate but not marginal bone level loss: A systematic review and meta-analysis. PLoS One 2019;14. https://doi.org/10.1371/JOURNAL.PONE.0216428.

[94] Baleani M, Viceconti M, Toni A. The effect of sandblasting treatment on endurance properties of titanium alloy hip prostheses. Artif Organs 2000;24:296–9. https://doi.org/10.1046/J.1525-1594.2000.06486.X.

[95] Bosshardt DD, Chappuis V, Buser D. Osseointegration of titanium, titanium alloy and zirconia dental implants: current knowledge and open questions. Periodontol 2000 2017;73:22–40. https://doi.org/10.1111/PRD.12179.

[96] Sadati Tilebon SM, Emamian SA, Ramezanpour H, Yousefi H, Özcan M, Naghib SM, et al. Intelligent modeling and optimization of titanium surface etching for dental implant application. Sci Rep 2022;12. https://doi.org/10.1038/S41598-022-11254-0.

[97] Villapún VM, Man K, Carter L, Penchev P, Dimov S, Cox S. Laser texturing of additively manufactured implants: A tool to programme biological response. Biomaterials Advances 2023;153:213574. https://doi.org/10.1016/J.BIOADV.2023.213574.

[98] Kang HK, Chu TM, Dechow P, Stewart K, Kyung HM, Liu SSY. Laser-treated stainless steel mini-screw implants: 3D surface roughness, bone-implant contact, and fracture resistance analysis. Eur J Orthod 2016;38:154–62. https://doi.org/10.1093/EJO/CJV017.

[99] Accioni F, Vázquez J, Merinero M, Begines B, Alcudia A. Latest Trends in Surface Modification for Dental Implantology: Innovative Developments and Analytical Applications. Pharmaceutics 2022;14. https://doi.org/10.3390/PHARMACEUTICS14020455.

[100] Yoshida S, Hagiwara K, Hasebe T, Hotta A. Surface modification of polymers by plasma treatments for the enhancement of biocompatibility and controlled drug release. Surf Coat Technol 2013;233:99–107. https://doi.org/10.1016/J.SURFCOAT.2013.02.042.

[101] Barry JJA, Silva MMCG, Shakesheff KM, Howdle SM, Alexander MR. Using Plasma Deposits to Promote Cell Population of the Porous Interior of Three-Dimensional Poly(D,L-Lactic Acid) Tissue-Engineering Scaffolds. Adv Funct Mater 2005;15:1134–40. https://doi.org/10.1002/ADFM.200400562.

[102] Wan Y, Qu X, Lu J, Zhu C, Wan L, Yang J, et al. Characterization of surface property of poly(lactide-co-glycolide) after oxygen plasma treatment. Biomaterials 2004;25:4777–83. https://doi.org/10.1016/j.biomaterials.2003.11.051.

[103] Lee H, Dellatore SM, Miller WM, Messersmith PB. Mussel-inspired surface chemistry for multifunctional coatings. Science (1979) 2007;318:426–30. https://doi.org/10.1126/SCIENCE.1147241.

[104] Kim BH, Lee DH, Kim JY, Shin DO, Jeong HY, Hong S, et al. Mussel-inspired block copolymer lithography for low surface energy materials of teflon, graphene, and gold. Adv Mater 2011;23:5618–22. https://doi.org/10.1002/ADMA.201103650.

[105] Hemmatpour H, De Luca O, Crestani D, Stuart MCA, Lasorsa A, van der Wel PCA, et

al. New insights in polydopamine formation via surface adsorption. Nat Commun 2023;14:1–12. https://doi.org/10.1038/s41467-023-36303-8.

[106] Diez-Escudero A, Hailer NP. The role of silver coating for arthroplasty components. Bone Joint J 2021;103-B:423–9. https://doi.org/10.1302/0301-620X.103B3.BJJ-2020-1370.R1.

[107] Li B, Xia X, Guo M, Jiang Y, Li Y, Zhang Z, et al. Biological and antibacterial properties of the micro-nanostructured hydroxyapatite/chitosan coating on titanium. Scientific Reports 2019 9:1 2019;9:1–10. https://doi.org/10.1038/s41598-019-49941-0.

[108] Łukaszewska-Kuska M, Krawczyk P, Martyla A, Hędzelek W, Dorocka-Bobkowska B. Hydroxyapatite coating on titanium endosseous implants for improved osseointegration: Physical and chemical considerations. Adv Clin Exp Med 2018;27:1055–9. https://doi.org/10.17219/ACEM/69084.

[109] Zhu Y, Gao C, Guan J, Shen J. Engineering porous polyurethane scaffolds by photografting polymerization of methacrylic acid for improved endothelial cell compatibility. J Biomed Mater Res A 2003;67A:1367–73. https://doi.org/10.1002/JBM.A.20058.

[110] Maadani AM, Salahinejad E. Performance comparison of PLA- and PLGA-coated porous bioceramic scaffolds: Mechanical, biodegradability, bioactivity, delivery and biocompatibility assessments. J Control Release 2022;351:1–7. https://doi.org/10.1016/J.JCONREL.2022.09.022.

[111] Kim SM, Park S Bin, Bedair TM, Kim MH, Park BJ, Joung YK, et al. The effect of solvents and hydrophilic additive on stable coating and controllable sirolimus release system for drug-eluting stent. Materials Science and Engineering: C 2017;78:39–46. https://doi.org/10.1016/J.MSEC.2017.04.024.

[112] Hanas T, Sampath Kumar TS, Perumal G, Doble M. Tailoring degradation of AZ31 alloy by surface pre-treatment and electrospun PCL fibrous coating. Mater Sci Eng C Mater Biol Appl 2016;65:43–50. https://doi.org/10.1016/J.MSEC.2016.04.017.

[113] Noel S, Hachem A, Merhi Y, De Crescenzo G. Development of a polyester coating combining antithrombogenic and cell adhesive properties: Influence of sequence and surface density of adhesion peptides. Biomacromolecules 2015;16:1682–94. https://doi.org/10.1021/ACS.BIOMAC.5B00219/SUPPL_FILE/BM5B00219_SI_001.PDF.

[114] Pan CJ, Tang JJ, Weng YJ, Wang J, Huang N. Preparation and characterization of rapamycin-loaded PLGA coating stent. J Mater Sci Mater Med 2007;18:2193–8. https://doi.org/10.1007/S10856-007-3075-9.

[115] Panchal M, Khare S, Khamkar P, Suresh Bhole K. Dental implants: A review of types, design analysis, materials, additive manufacturing methods, and future scope. Mater Today Proc 2022;68:1860–7. https://doi.org/10.1016/J.MATPR.2022.08.049.

[116] Ahadi F, Azadi M, Biglari M, Bodaghi M, Khaleghian A. Evaluation of coronary stents: A review of types, materials, processing techniques, design, and problems. Heliyon 2023;9:e13575. https://doi.org/10.1016/J.HELIYON.2023.E13575.

[117] Cockerill I, See CW, Young ML, Wang Y, Zhu D. Designing Better Cardiovascular Stent Materials: A Learning Curve. Adv Funct Mater 2021;31:2005361. https://doi.org/10.1002/ADFM.202005361.

[118] Stöver T, Lenarz T. Biomaterials in cochlear implants. GMS Curr Top Otorhinolaryngol Head Neck Surg 2009;8:Doc10. https://doi.org/10.3205/CTO000062.

[119] Jensen MJ, Claussen AD, Higgins T, Vielman-Quevedo R, Mostaert B, Xu L, et al. Cochlear implant material effects on inflammatory cell function and foreign body response. Hear Res 2022;426:108597. https://doi.org/10.1016/J.HEARES.2022.108597.

[120] Szczęsny G, Kopec M, Politis DJ, Kowalewski ZL, Łazarski A, Szolc T. A Review on Biomaterials for Orthopaedic Surgery and Traumatology: From Past to Present. Materials 2022;15. https://doi.org/10.3390/MA15103622.

[121] Buechel FF, Pappas MJ. Properties of Materials Used in Orthopaedic Implant Systems. Principles of Human Joint Replacement 2011:1–35. https://doi.org/10.1007/978-3-642-23011-0_1.

[122] Tapscott DC, Wottowa C. Orthopedic Implant Materials. StatPearls 2023.

[123] Grosso D. How to exploit the full potential of the dip-coating process to better control film formation. J Mater Chem 2011;21:17033–8. https://doi.org/10.1039/C1JM12837J.

[124] Glynn C, Creedon D, Geaney H, Armstrong E, Collins T, Morris MA, et al. Linking Precursor Alterations to Nanoscale Structure and Optical Transparency in Polymer Assisted Fast-Rate Dip-Coating of Vanadium Oxide Thin Films. Scientific Reports 2015 5:1 2015;5:1–15. https://doi.org/10.1038/srep11574.

[125] Naveas N, Pulido R, Torres-Costa V, Agulló-Rueda F, Santibáñez M, Malano F, et al. Antibacterial Films of Silver Nanoparticles Embedded into Carboxymethylcellulose/Chitosan Multilayers on Nanoporous Silicon: A Layer-by-Layer Assembly Approach Comparing Dip and Spin Coating. International Journal of Molecular Sciences 2023, Vol 24, Page 10595 2023;24:10595. https://doi.org/10.3390/IJMS241310595.

[126] Borges J, Mano JF. Molecular interactions driving the layer-by-layer assembly of multilayers. Chem Rev 2014;114:8883–942. https://doi.org/10.1021/CR400531V.

[127] Gulati K, Ramakrishnan S, Aw MS, Atkins GJ, Findlay DM, Losic D. Biocompatible polymer coating of titania nanotube arrays for improved drug elution and osteoblast adhesion. Acta Biomater 2012;8:449–56. https://doi.org/10.1016/J.ACTBIO.2011.09.004.

[128] Douroumis D, Onyesom I. Novel Coating Technologies of Drug Eluting Stents. Studies in Mechanobiology, Tissue Engineering and Biomaterials 2011;8:87–125. https://doi.org/10.1007/8415_2010_54.

[129] Almeida AC, Vale AC, Pires RA, Reis RL, Alves NM. Layer-by-layer films based on catechol-modified polysaccharides produced by dip- and spin-coating onto different substrates. J Biomed Mater Res B Appl Biomater 2020;108:1412–27. https://doi.org/10.1002/JBM.B.34489.

[130] Knebel A, Caro J. Metal–organic frameworks and covalent organic frameworks as disruptive membrane materials for energy-efficient gas separation. Nature Nanotechnology 2022 17:9 2022;17:911–23. https://doi.org/10.1038/s41565-022-01168-3.

[131] Naveas N, Naveas N, Manso-Silván M, Pulido R, Pulido R, Agulló-Rueda F, et al. Fabrication and characterization of nanostructured porous silicon-silver composite layers by cyclic deposition: dip-coating vs spin-coating. Nanotechnology 2020;31:365704. https://doi.org/10.1088/1361-6528/AB96E5.

[132] Abu-Thabit NY, Uwaezuoke OJ, Abu Elella MH. Superhydrophobic nanohybrid sponges for separation of oil/ water mixtures. Chemosphere 2022;294:133644. https://doi.org/10.1016/J.CHEMOSPHERE.2022.133644.

[133] Nadeem H, Athar M, Dehghani M, Garnier G, Batchelor W. Recent advancements, trends, fundamental challenges and opportunities in spray deposited cellulose nanofibril films for packaging applications. Science of The Total Environment 2022;836:155654. https://doi.org/10.1016/J.SCITOTENV.2022.155654.

[134] Choudhary K, Chen AX, Pitch GM, Runser R, Urbina A, Dunn TJ, et al. Comparison of the Mechanical Properties of a Conjugated Polymer Deposited Using Spin Coating, Interfacial Spreading, Solution Shearing, and Spray Coating. ACS Appl Mater Interfaces 2021;13:51436–46. https://doi.org/10.1021/ACSAMI.1C13043/SUPPL_FILE/AM1C13043_SI_005.MP4.

[135] Liu S, Zhang X, Zhang L, Xie W. Ultrasonic spray coating polymer and small molecular organic film for organic light-emitting devices. Sci Rep 2016;6. https://doi.org/10.1038/SREP37042.

[136] Liu HS, Chang WC, Chou CY, Pan BC, Chou YS, Liou GS, et al. Controllable Electrochromic Polyamide Film and Device Produced by Facile Ultrasonic Spray-coating. Scientific Reports 2017 7:1 2017;7:1–10. https://doi.org/10.1038/s41598-017-11862-1.

[137] Ren W, Yang M, Zhou L, Fan Y, He S, Pan J, et al. Scalable Ultrathin All-Organic Polymer Dielectric Films for High-Temperature Capacitive Energy Storage. Advanced Materials 2022;34:2207421. https://doi.org/10.1002/ADMA.202207421.

[138] Alf ME, Asatekin A, Barr MC, Baxamusa SH, Chelawat H, Ozaydin-lnce G, et al. Chemical Vapor Deposition of Conformal, Functional, and Responsive Polymer Films. Advanced Materials 2010;22:1993–2027. https://doi.org/10.1002/ADMA.200902765.

[139] Chen N, Kim DH, Kovacik P, Sojoudi H, Wang M, Gleason KK. Polymer Thin Films and Surface Modification by Chemical Vapor Deposition: Recent Progress. Https://DoiOrg/101146/Annurev-Chembioeng-080615-033524 2016;7:373–93. https://doi.org/10.1146/ANNUREV-CHEMBIOENG-080615-033524.

[140] Khlyustova A, Cheng Y, Yang R. Vapor-deposited functional polymer thin films in biological applications. J Mater Chem B 2020;8:6588–609. https://doi.org/10.1039/D0TB00681E.

[141] Gleason KK. Nanoscale control by chemically vapour-deposited polymers. Nature Reviews Physics 2020 2:7 2020;2:347–64. https://doi.org/10.1038/s42254-020-0192-6.

[142] Christian P, Tumphart S, Ehmann HMA, Riegler H, Coclite AM, Werzer O. Controlling Indomethacin Release through Vapor-Phase Deposited Hydrogel Films by Adjusting the Cross-linker Density. Scientific Reports 2018 8:1 2018;8:1–12. https://doi.org/10.1038/s41598-018-24238-w.

[143] Zhi B, Mao Y. Vapor-Deposited Nanocoatings for Sustained Zero-Order Release of Antiproliferative Drugs. ACS Appl Bio Mater 2020;3:1088–96. https://doi.org/10.1021/ACSABM.9B01044/ASSET/IMAGES/MEDIUM/MT9B01044_0010.GIF.

[144] Ghasemi-Mobarakeh L, Werzer O, Keimel R, Kolahreez D, Hadley P, Coclite AM. Manipulating drug release from tridimensional porous substrates coated by initiated chemical vapor deposition. J Appl Polym Sci 2019;136:47858. https://doi.org/10.1002/APP.47858.

[145] Christian P, Ehmann HMA, Coclite AM, Werzer O. Polymer Encapsulation of an Amorphous Pharmaceutical by initiated Chemical Vapor Deposition for Enhanced Stability. ACS Appl Mater Interfaces 2016;8:21177–84. https://doi.org/10.1021/ACSAMI.6B06015.

[146] Moreira J, Vale AC, Alves NM. Spin-coated freestanding films for biomedical applications. J Mater Chem B 2021;9:3778–99. https://doi.org/10.1039/D1TB00233C.

[147] Tran DT, Chen FH, Wu GL, Ching PCO, Yeh ML. Influence of Spin Coating and Dip Coating with Gelatin/Hydroxyapatite for Bioresorbable Mg Alloy Orthopedic Implants: In Vitro and In Vivo Studies. ACS Biomater Sci Eng 2023;9:705–18. https://doi.org/10.1021/ACSBIOMATERIALS.2C01122/ASSET/IMAGES/LARGE/AB2C01122_0012.JPEG.

[148] Eliaz N. Corrosion of Metallic Biomaterials: A Review. Materials 2019;12. https://doi.org/10.3390/MA12030407.

[149] Ude CC, Dzidotor GK, Iloeje K, Nair LS, Laurencin CT. Corrosion of Metals During Use in Arthroplasty. ACS Appl Bio Mater 2023;6:2029–42. https://doi.org/10.1021/ACSABM.2C01082.

[150] Manam NS, Harun WSW, Shri DNA, Ghani SAC, Kurniawan T, Ismail MH, et al. Study of corrosion in biocompatible metals for implants: A review. J Alloys Compd 2017;701:698–715. https://doi.org/10.1016/J.JALLCOM.2017.01.196.

[151] Yang H, Jia B, Zhang Z, Qu X, Li G, Lin W, et al. Alloying design of biodegradable zinc as promising bone implants for load-bearing applications. Nat Commun 2020;11. https://doi.org/10.1038/S41467-019-14153-7.

[152] Harb SV, Uvida MC, Trentin A, Oliveira Lobo A, Webster TJ, Pulcinelli SH, et al. PMMA-silica nanocomposite coating: Effective corrosion protection and biocompatibility for a Ti6Al4V alloy. Materials Science and Engineering: C 2020;110:110713. https://doi.org/10.1016/J.MSEC.2020.110713.

[153] Zhang R, Han B, Liu X. Functional Surface Coatings on Orthodontic Appliances: Reviews of Friction Reduction, Antibacterial Properties, and Corrosion Resistance. International Journal of Molecular Sciences 2023, Vol 24, Page 6919 2023;24:6919. https://doi.org/10.3390/IJMS24086919.

[154] Kurtz SM, Devine JN. PEEK biomaterials in trauma, orthopedic, and spinal implants. Biomaterials 2007;28:4845–69. https://doi.org/10.1016/j.biomaterials.2007.07.013.

[155] Moaref R, Shahini MH, Eivaz Mohammadloo H, Ramezanzadeh B, Yazdani S. Application of sustainable polymers for reinforcing bio-corrosion protection of magnesium implants–a review. Sustain Chem Pharm 2022;29:100780. https://doi.org/10.1016/J.SCP.2022.100780.

[156] Catauro M, Bollino F, Giovanardi R, Veronesi P. Modification of Ti6Al4V implant surfaces by biocompatible TiO2/PCL hybrid layers prepared via sol-gel dip coating: Structural characterization, mechanical and corrosion behavior. Mater Sci Eng C Mater Biol Appl 2017;74:501–7. https://doi.org/10.1016/J.MSEC.2016.12.046.

[157] Goodman SB. Wear particles, periprosthetic osteolysis and the immune system. Biomaterials 2007;28:5044–8. https://doi.org/10.1016/J.BIOMATERIALS.2007.06.035.

[158] Zhai W, Bai L, Zhou R, Fan X, Kang G, Liu Y, et al. Recent Progress on Wear-Resistant Materials: Designs, Properties, and Applications. Advanced Science 2021;8:2003739. https://doi.org/10.1002/ADVS.202003739.

[159] Ren Y, Zhang L, Xie G, Li Z, Chen H, Gong H, et al. A review on tribology of polymer composite coatings. Friction 2021;9:429–70. https://doi.org/10.1007/S40544-020-0446-4/METRICS.

[160] Saurer EM, Flessner RM, Sullivan SP, Prausnitz MR, Lynn DM. Layer-by-layer assembly of DNA- and protein-containing films on microneedles for drug delivery to the skin. Biomacromolecules 2010;11:3136–43. https://doi.org/10.1021/BM1009443/SUPPL_FILE/BM1009443_SI_001.PDF.

[161] Batasheva S, Fakhrullin R. Sequence Does Not Matter: The Biomedical Applications of DNA-Based Coatings and Cores. Int J Mol Sci 2021;22:12884. https://doi.org/10.3390/IJMS222312884.

[162] Labhasetwar V. A DNA Controlled-Release Coating for Gene Transfer: Transfection in Skeletal and Cardiac Muscle. J Pharm Sci 1998;87:1347–50. https://doi.org/10.1021/js980077+.

[163] Cado G, Aslam R, Séon L, Garnier T, Fabre R, Parat A, et al. Self-Defensive Biomaterial Coating Against Bacteria and Yeasts: Polysaccharide Multilayer Film with Embedded Antimicrobial Peptide. Adv Funct Mater 2013;23:4801–9. https://doi.org/10.1002/ADFM.201300416.

[164] Tang W, Wang J, Hou H, Li Y, Wang J, Fu J, et al. Review: Application of chitosan and its derivatives in medical materials. Int J Biol Macromol 2023;240:124398. https://doi.org/10.1016/J.IJBIOMAC.2023.124398.

[165] Lee KY, Mooney DJ. Alginate: properties and biomedical applications. Prog Polym Sci 2012;37:106–26. https://doi.org/10.1016/J.PROGPOLYMSCI.2011.06.003.

[166] Yu H, Liu L, Li X, Zhou R, Yan S, Li C, et al. Fabrication of polylysine based antibacterial coating for catheters by facile electrostatic interaction. Chemical Engineering Journal 2019;360:1030–41. https://doi.org/10.1016/J.CEJ.2018.10.160.

[167] Xie X, Mao C, Liu X, Zhang Y, Cui Z, Yang X, et al. Synergistic Bacteria Killing through Photodynamic and Physical Actions of Graphene Oxide/Ag/Collagen Coating. ACS Appl Mater Interfaces 2017;9:26417–28. https://doi.org/10.1021/ACSAMI.7B06702/ASSET/IMAGES/LARGE/AM-2017-06702G_0005.JPEG.

[168] Rasal RM, Janorkar A V., Hirt DE. Poly(lactic acid) modifications. Prog Polym Sci 2010;35:338–56. https://doi.org/10.1016/J.PROGPOLYMSCI.2009.12.003.

[169] Trivedi AK, Gupta MK, Singh H. PLA based biocomposites for sustainable products: A review. Advanced Industrial and Engineering Polymer Research 2023;6:382–95. https://doi.org/10.1016/J.AIEPR.2023.02.002.

[170] Lei Z, Liang H, Sun W, Chen Y, Huang Z, Yu B. A biodegradable PVA coating constructed on the surface of the implant for preventing bacterial colonization and biofilm formation. J Orthop Surg Res 2024;19:1–19. https://doi.org/10.1186/S13018-024-04662-7/FIGURES/8.

[171] Prete S, Dattilo M, Patitucci F, Pezzi G, Parisi OI, Puoci F. Natural and Synthetic Polymeric Biomaterials for Application in Wound Management. J Funct Biomater 2023;14:455. https://doi.org/10.3390/JFB14090455.

[172] Theocharidis G, Veves A. Greater foreign-body responses to big implants. Nature Biomedical Engineering 2023 7:11 2023;7:1340–2. https://doi.org/10.1038/s41551-023-01118-x.

[173] Foroushani FT, Dzobo K, Khumalo NP, Mora VZ, de Mezerville R, Bayat A. Advances in surface modifications of the silicone breast implant and impact on its biocompatibility and biointegration. Biomaterials Research 2022 26:1 2022;26:1–27. https://doi.org/10.1186/S40824-022-00314-1.

[174] Carnicer-Lombarte A, Chen ST, Malliaras GG, Barone DG. Foreign Body Reaction to Implanted Biomaterials and Its Impact in Nerve Neuroprosthetics. Front Bioeng Biotechnol 2021;9. https://doi.org/10.3389/FBIOE.2021.622524.

[175] Mikhail AS, Ranger JJ, Liu L, Longenecker R, Thompson DB, Sheardown HD, et al. Rapid and efficient assembly of functional silicone surfaces protected by PEG: cell adhesion to peptide-modified PDMS. J Biomater Sci Polym Ed 2010;21:821–42. https://doi.org/10.1163/156856209X445311.

[176] Trantidou T, Elani Y, Parsons E, Ces O. Hydrophilic surface modification of PDMS for droplet microfluidics using a simple, quick, and robust method via PVA deposition. Microsystems & Nanoengineering 2017 3:1 2017;3:1–9. https://doi.org/10.1038/micronano.2016.91.

[177] Chen A, Chen D, Lv K, Li G, Pan J, Ma D, et al. Zwitterionic Polymer/Polydopamine Coating of Electrode Arrays Reduces Fibrosis and Residual Hearing Loss after Cochlear Implantation. Adv Healthc Mater 2023;12. https://doi.org/10.1002/ADHM.202200807.

[178] Wang K, Yu Y, Li W, Li D, Li H. Preparation of fully bio-based multilayers composed of heparin-like carboxymethylcellulose sodium and chitosan to functionalize poly (l-lactic acid) film for cardiovascular implant applications. Int J Biol Macromol 2023;231:123285. https://doi.org/10.1016/J.IJBIOMAC.2023.123285.

[179] Chau Nguyen TT, Shin CM, Lee SJ, Koh ES, Kwon HH, Park H, et al. Ultrathin Nanostructured Films of Hyaluronic Acid and Functionalized β-Cyclodextrin Polymer Suppress Bacterial Infection and Capsular Formation of Medical Silicone Implants. Biomacromolecules 2022;23:4547–61. https://doi.org/10.1021/ACS.BIOMAC.2C00687/ASSET/IMAGES/LARGE/BM2C00687_0012.JPEG.

[180] Wu S, Xu J, Zou L, Luo S, Yao R, Zheng B, et al. Long-lasting renewable antibacterial porous polymeric coatings enable titanium biomaterials to prevent and treat peri-implant infection. Nature Communications 2021 12:1 2021;12:1–14. https://doi.org/10.1038/s41467-021-23069-0.

[181] Xi W, Hegde V, Zoller SD, Park HY, Hart CM, Kondo T, et al. Point-of-care antimicrobial coating protects orthopaedic implants from bacterial challenge. Nature Communications 2021 12:1 2021;12:1–15. https://doi.org/10.1038/s41467-021-25383-z.

[182] Zhou W, Peng X, Ma Y, Hu Y, Wu Y, Lan F, et al. Two-staged time-dependent materials for the prevention of implant-related infections. Acta Biomater 2020;101:128–40. https://doi.org/10.1016/J.ACTBIO.2019.10.023.

[183] Van de Belt H, Neut D, Schenk W, Van Horn JR, Van der Mei HC, Busscher HJ. Infection of orthopedic implants and the use of antibiotic-loaded bone cements. A review. Acta Orthop Scand 2001;72:557–71. https://doi.org/10.1080/000164701317268978.

[184] Liu Z, Ma S, Duan S, Xuliang D, Sun Y, Zhang X, et al. Modification of Titanium Substrates with Chimeric Peptides Comprising Antimicrobial and Titanium-Binding Motifs Connected by Linkers to Inhibit Biofilm Formation. ACS Appl Mater Interfaces 2016;8:5124–36. https://doi.org/10.1021/ACSAMI.5B11949/ASSET/IMAGES/MEDIUM/AM-2015-119495_0014.GIF.

[185] Catalano A, Iacopetta D, Ceramella J, Scumaci D, Giuzio F, Saturnino C, et al. Multidrug Resistance (MDR): A Widespread Phenomenon in Pharmacological Therapies. Molecules 2022;27. https://doi.org/10.3390/MOLECULES27030616.

[186] Nikaido H. Multidrug Resistance in Bacteria. Annu Rev Biochem 2009;78:119. https://doi.org/10.1146/ANNUREV.BIOCHEM.78.082907.145923.

[187] Nikam SP, Nettleton K, Everitt JI, Barton HA, Becker ML. Antibiotic eluting poly(ester urea) films for control of a model cardiac implantable electronic device infection. Acta Biomater 2020;111:65–79. https://doi.org/10.1016/J.ACTBIO.2020.04.025.

[188] Boehler C, Oberueber F, Asplund M. Tuning drug delivery from conducting polymer films for accurately controlled release of charged molecules. Journal of Controlled Release 2019;304:173–80. https://doi.org/10.1016/J.JCONREL.2019.05.017.

[189] Jahanmard F, Croes M, Castilho M, Majed A, Steenbergen MJ, Lietaert K, et al. Bactericidal coating to prevent early and delayed implant-related infections. Journal of Controlled Release 2020;326:38–52. https://doi.org/10.1016/J.JCONREL.2020.06.014.

[190] Barik A, Chakravorty N. Targeted Drug Delivery from Titanium Implants: A Review of Challenges and Approaches. Adv Exp Med Biol 2020;1251:1–17. https://doi.org/10.1007/5584_2019_447/COVER.

[191] Carlyle WC, McClain JB, Tzafriri AR, Bailey L, Zani BG, Markham PM, et al. Enhanced drug delivery capabilities from stents coated with absorbable polymer and crystalline drug. Journal of Controlled Release 2012;162:561–7. https://doi.org/10.1016/J.JCONREL.2012.07.004.

[192] Gulati K, Ramakrishnan S, Aw MS, Atkins GJ, Findlay DM, Losic D. Biocompatible polymer coating of titania nanotube arrays for improved drug elution and osteoblast adhesion. Acta Biomater 2012;8:449–56. https://doi.org/10.1016/J.ACTBIO.2011.09.004.

[193] Agarwal R, García AJ. Biomaterial strategies for engineering implants for enhanced osseointegration and bone repair. Adv Drug Deliv Rev 2015;94:53–62. https://doi.org/10.1016/J.ADDR.2015.03.013.

[194] Pauly S, Luttosch F, Morawski M, Haas NP, Schmidmaier G, Wildemann B. Simvastatin locally applied from a biodegradable coating of osteosynthetic implants improves fracture healing comparable to BMP-2 application. Bone 2009;45:505–11. https://doi.org/10.1016/J.BONE.2009.05.010.

[195] McManamon C, De Silva JP, Delaney P, Morris MA, Cross GLW. Characteristics, interactions and coating adherence of heterogeneous polymer/drug coatings for biomedical devices. Mater Sci Eng C Mater Biol Appl 2016;59:102–8. https://doi.org/10.1016/J.MSEC.2015.09.103.

[196] Vallejo-Heligon SG, Klitzman B, Reichert WM. Characterization of Porous, Dexamethasone-Releasing Polyurethane Coatings for Glucose Sensors. Acta Biomater 2014;10:4629. https://doi.org/10.1016/J.ACTBIO.2014.07.019.

[197] Kunrath MF, Rubensam G, Rodrigues FVF, Marinowic DR, Sesterheim P, de Oliveira SD, et al. Nano-scaled surfaces and sustainable-antibiotic-release from polymeric coating for application on intra-osseous implants and trans-mucosal abutments. Colloids Surf B Biointerfaces 2023;228:113417. https://doi.org/10.1016/J.COLSURFB.2023.113417.

[198] Stefanini GG, Holmes DR. Drug-eluting coronary-artery stents. N Engl J Med 2013;368:254–65. https://doi.org/10.1056/NEJMRA1210816.

[199] Product Classification n.d. https://www.accessdata.fda.gov/scripts/cdrh/cfdocs/cfPCD/classification.cfm?ID=NIQ (accessed October 16, 2024).

[200] Use of International Standard ISO 10993-1, "Biological evaluation of medical devices - Part 1: Evaluation and testing within a risk management process" | FDA n.d. https://www.fda.gov/regulatory-information/search-fda-guidance-documents/use-international-standard-iso-10993-1-biological-evaluation-medical-devices-part-1-evaluation-and (accessed October 16, 2024).

[201] Anderson JM, Rodriguez A, Chang DT. FOREIGN BODY REACTION TO BIOMATERIALS. Semin Immunol 2008;20:86. https://doi.org/10.1016/J.SMIM.2007.11.004.

[202] Lu D, Han Y, Liu D, Chen S, Qie J, Qu J, et al. Centrifugally concentric ring-patterned drug-loaded polymeric coating as an intraocular lens surface modification for efficient prevention of posterior capsular opacification. Acta Biomater 2022;138:327–41.

https://doi.org/10.1016/J.ACTBIO.2021.11.018.

[203] Zhang X, Lai K, Li S, Wang J, Li J, Wang W, et al. Drug-eluting intraocular lens with sustained bromfenac release for conquering posterior capsular opacification. Bioact Mater 2022;9:343–57. https://doi.org/10.1016/J.BIOACTMAT.2021.07.015.

[204] Chen H, Xiang Z, Zhang T, Wang H, Li X, Chen H, et al. Heparinized self-healing polymer coating with inflammation modulation for blood-contacting biomedical devices. Acta Biomater 2024;186:201–14. https://doi.org/10.1016/J.ACTBIO.2024.07.010.

[205] Lehner E, Honeder C, Knolle W, Binder W, Scheffler J, Plontke SK, et al. Towards the optimization of drug delivery to the cochlear apex: Influence of polymer and drug selection in biodegradable intracochlear implants. Int J Pharm 2023;643:123268. https://doi.org/10.1016/J.IJPHARM.2023.123268.

[206] Khoshnood N, Yarmand B, Badri A, Jahanpanah M, Zamanian A. Improvement of biological and corrosion behavior of plasma electrolytic oxidized Mg implant by 3D printed scaffold of amine-terminated PEG/PCL loaded with dexamethasone. Prog Org Coat 2024;196:108705. https://doi.org/10.1016/J.PORGCOAT.2024.108705.

[207] Yan H, Wang L, Wu H, An Y, Qin Y, Xiang Z, et al. Anti-fouling coating with ROS-Triggered On-Demand regulation of inflammation to favor tissue healing on vascular devices. Chemical Engineering Journal 2024;490:151893. https://doi.org/10.1016/J.CEJ.2024.151893.

[208] Yu H, Tan H, Huang Y, Pan J, Yao J, Liang M, et al. Development of a rapidly made, easily personalized drug-eluting polymer film on the electrode array of a cochlear implant during surgery. Biochem Biophys Res Commun 2020;526:328–33. https://doi.org/10.1016/J.BBRC.2020.02.171.

[209] Xu M, Ma D, Chen D, Cai J, He Q, Shu F, et al. Preparation, characterization and application research of a sustained dexamethasone releasing electrode coating for cochlear implantation. Mater Sci Eng C Mater Biol Appl 2018;90:16–26. https://doi.org/10.1016/J.MSEC.2018.04.033.

[210] Wulf K, Goblet M, Raggl S, Teske M, Eickner T, Lenarz T, et al. PLLA Coating of Active Implants for Dual Drug Release. Molecules 2022, Vol 27, Page 1417 2022;27:1417. https://doi.org/10.3390/MOLECULES27041417.

[211] Behrends W, Wulf K, Raggl S, Fröhlich M, Eickner T, Dohr D, et al. Dual Drug Delivery in Cochlear Implants: In Vivo Study of Dexamethasone Combined with Diclofenac or Immunophilin Inhibitor MM284 in Guinea Pigs. Pharmaceutics 2023;15. https://doi.org/10.3390/PHARMACEUTICS15030726.

[212] Yuan P, Qiu X, Liu T, Tian R, Bai Y, Liu S, et al. Substrate-independent polymer coating with stimuli-responsive dexamethasone release for on-demand fibrosis inhibition. J Mater Chem B 2020;8:7777–84. https://doi.org/10.1039/D0TB01127D.

[213] Patil SD, Papadimitrakopoulos F, Burgess DJ. Dexamethasone-loaded poly(lactic-co-glycolic) acid microspheres/poly(vinyl alcohol) hydrogel composite coatings for inflammation control. Diabetes Technol Ther 2004;6:887–97. https://doi.org/10.1089/DIA.2004.6.887.

[214] Tipnis N, Kastellorizios M, Legassey A, Papadimitrakopoulos F, Jain F, Burgess DJ. Sterilization of Drug-Loaded Composite Coatings for Implantable Glucose Biosensors. J Diabetes Sci Technol 2019;15:646–54. https://doi.org/10.1177/1932296819890620/ASSET/IMAGES/LARGE/10.1177_1932296819890620-FIG8.JPEG.

[215] Han X, Lu B, Zou D, Luo X, Liu L, Maitz MF, et al. Allicin-Loaded Intelligent Hydrogel Coating Improving Vascular Implant Performance. ACS Appl Mater Interfaces 2023;15:38247–63. https://doi.org/10.1021/ACSAMI.3C05984/ASSET/IMAGES/LARGE/AM3C05984_0008.JPEG.

[216] Wang Y, Wu H, Zhou Z, Maitz MF, Liu K, Zhang B, et al. A thrombin-triggered self-regulating anticoagulant strategy combined with anti-inflammatory capacity for blood-contacting implants. Sci Adv 2022;8:3378. https://doi.org/10.1126/SCIADV.ABM3378/SUPPL_FILE/SCIADV.ABM3378_SM.PDF.

[217] You Y, Wang W, Li Y, Song Y, Jiao J, Wang Y, et al. Aspirin/PLGA coated 3D-printed Ti-6Al-4V alloy modulate macrophage polarization to enhance osteoblast differentiation and osseointegration. J Mater Sci Mater Med 2022;33. https://doi.org/10.1007/S10856-022-06697-W.

[218] Rožanc J, Žižek M, Milojević M, Maver U, Finšgar M. Dexamethasone-Loaded Bioactive Coatings on Medical Grade Stainless Steel Promote Osteointegration. Pharmaceutics 2021;13. https://doi.org/10.3390/PHARMACEUTICS13040568.

[219] Shi Y, Lai Y, Guo Y, Cai Z, Mao C, Lu M, et al. Aspirin/amoxicillin loaded chitosan microparticles and polydopamine modified titanium implants to combat infections and promote osteogenesis. Scientific Reports 2024 14:1 2024;14:1–13. https://doi.org/10.1038/s41598-024-57156-1.

[220] Qian J, Wang J, Zhang W, Mao J, Qin H, Ling X, et al. Corrosion-tailoring, osteogenic, anti-inflammatory, and antibacterial aspirin-loaded organometallic hydrogel composite coating on biodegradable Zn for orthopedic applications. Biomaterials Advances 2023;153. https://doi.org/10.1016/J.BIOADV.2023.213536.

[221] Uskoković V, Velie PN, Wu VM. Toward chronopharmaceutical drug delivery patches and biomaterial coatings for the facilitation of wound healing. J Colloid Interface Sci 2024;659:355–63. https://doi.org/10.1016/J.JCIS.2023.12.156.

[222] Al-Khoury H, Espinosa-Cano E, Aguilar MR, Román JS, Syrowatka F, Schmidt G, et al. Anti-inflammatory Surface Coatings Based on Polyelectrolyte Multilayers of Heparin and Polycationic Nanoparticles of Naproxen-Bearing Polymeric Drugs. Biomacromolecules 2019;20:4015–25. https://doi.org/10.1021/ACS.BIOMAC.9B01098/SUPPL_FILE/BM9B01098_SI_001.PDF.

[223] Selig DJ, Kress AT, Horton IM, Livezey JR, Sadik EJ, DeLuca JP. Pharmacokinetics, safety and efficacy of intra-articular non-steroidal anti-inflammatory drug injections for the treatment of osteoarthritis: A narrative review. J Clin Pharm Ther 2022;47:1122–33. https://doi.org/10.1111/JCPT.13669.

[224] van Minnen BS, van der Veen AJ, van de Groes SAW, Verdonschot NJJ, van Tienen TG. An anatomically shaped medial meniscus prosthesis is able to partially restore the contact mechanics of the meniscectomized knee joint. J Exp Orthop 2022;9:91. https://doi.org/10.1186/S40634-022-00531-6.

[225] Kluyskens L, Debieux P, Wong KL, Krych AJ, Saris DBF. Biomaterials for meniscus and cartilage in knee surgery: state of the art. Journal of ISAKOS 2022;7:67–77. https://doi.org/10.1136/JISAKOS-2020-000600.

[226] Di Francesco M, Bedingfield SK, Di Francesco V, Colazo JM, Yu F, Ceseracciu L, et al. Shape-Defined microPlates for the Sustained Intra-articular Release of Dexamethasone in the Management of Overload-Induced Osteoarthritis. ACS Appl Mater Interfaces 2021;13:31379–92. https://doi.org/10.1021/ACSAMI.1C02082/ASSET/IMAGES/MEDIUM/AM1C02082_M004.GIF.

[227] Wang Q-S, Xu B-X, Fan K-J, Fan Y-S, Teng H, Wang T-Y. Dexamethasone-loaded thermo-sensitive hydrogel attenuates osteoarthritis by protecting cartilage and providing effective pain relief. Ann Transl Med 2021;9:1120–1120. https://doi.org/10.21037/ATM-21-684.

[228] Condello V, Dei Giudici L, Perdisa F, Screpis DU, Guerriero M, Filardo G, et al. Polyurethane scaffold implants for partial meniscus lesions: delayed intervention leads to an inferior outcome. Knee Surg Sports Traumatol Arthrosc 2021;29:109–16. https://doi.org/10.1007/S00167-019-05760-4.

[229] Murakami T, Otsuki S, Nakagawa K, Okamoto Y, Inoue T, Sakamoto Y, et al. Establishment of novel meniscal scaffold structures using polyglycolic and poly-l-lactic acids. Http://DxDoiOrg/101177/0885328217713631 2017;32:150–61. https://doi.org/10.1177/0885328217713631.

[230] Li Y, Chen M, Yan J, Zhou W, Gao S, Liu S, et al. Tannic acid/Sr2+-coated silk/graphene oxide-based meniscus scaffold with anti-inflammatory and anti-ROS functions for cartilage protection and delaying osteoarthritis. Acta Biomater 2021;126:119–31. https://doi.org/10.1016/J.ACTBIO.2021.02.046.

[231] Li C, Deng Z, Gillies ER. Designing polymers with stimuli-responsive degradation for biomedical applications. Curr Opin Biomed Eng 2023;25:100437. https://doi.org/10.1016/J.COBME.2022.100437.

[232] Amin Yavari S, Croes M, Akhavan B, Jahanmard F, Eigenhuis CC, Dadbakhsh S, et al. Layer by layer coating for bio-functionalization of additively manufactured meta-biomaterials. Addit Manuf 2020;32:100991. https://doi.org/10.1016/J.ADDMA.2019.100991.

[233] Udduttula A, Jakubovics N, Khan I, Pontiroli L, Rankin KS, Gentile P, et al. Layer-by-Layer Coatings of Collagen-Hyaluronic acid Loaded with an Antibacterial Manuka Honey Bioactive Compound to Fight Metallic Implant Infections. ACS Appl Mater Interfaces 2023;15:58119–35. https://doi.org/10.1021/ACSAMI.3C11910/ASSET/IMAGES/LARGE/AM3C11910_0008.JPEG.

[234] Zhang Z, Nong J, Zhong Y. Antibacterial, anti-inflammatory and neuroprotective layer-

by-layer coatings for neural implants. J Neural Eng 2015;12. https://doi.org/10.1088/1741-2560/12/4/046015.

[235] Guan J, Wang J, Jia F, Jiang W, Song L, Xie L, et al. Layer-by-layer self-assembly coatings on strontium titanate nanotubes with antimicrobial and anti-inflammatory properties to prevent implant-related infections. Colloids Surf B Biointerfaces 2024;244:114183. https://doi.org/10.1016/J.COLSURFB.2024.114183.

[236] Ayar Z, Shafieian M, Mahmoodi N, Sabzevari O, Hassannejad Z. A rechargeable drug delivery system based on pNIPAM hydrogel for the local release of curcumin. J Appl Polym Sci 2021;138:51167. https://doi.org/10.1002/APP.51167.

[237] Horecka A, Hordyjewska A, Blicharski T, Kurzepa J. Osteoarthritis of the knee - biochemical aspect of applied therapies: a review. Bosn J Basic Med Sci 2022;22:488–98. https://doi.org/10.17305/BJBMS.2021.6489.

[238] Hurmuz M, Ionac M, Hogea B, Miu CA, Tatu F. Osteoarthritis Development Following Meniscectomy vs. Meniscal Repair for Posterior Medial Meniscus Injuries: A Systematic Review. Medicina (Kaunas) 2024;60. https://doi.org/10.3390/MEDICINA60040569.

[239] Makris EA, Hadidi P, Athanasiou KA. The knee meniscus: structure-function, pathophysiology, current repair techniques, and prospects for regeneration. Biomaterials 2011;32:7411–31. https://doi.org/10.1016/J.BIOMATERIALS.2011.06.037.

[240] Sun J, Vijayavenkataraman S, Liu H. An Overview of Scaffold Design and Fabrication Technology for Engineered Knee Meniscus. Materials (Basel) 2017;10. https://doi.org/10.3390/MA10010029.

[241] Mora JC, Przkora R, Cruz-Almeida Y. Knee osteoarthritis: pathophysiology and current treatment modalities. J Pain Res 2018;11:2189. https://doi.org/10.2147/JPR.S154002.

[242] El-Gogary RI, Khattab MA, Abd-Allah H. Intra-articular multifunctional celecoxib loaded hyaluronan nanocapsules for the suppression of inflammation in an osteoarthritic rat model. Int J Pharm 2020;583:119378. https://doi.org/10.1016/J.IJPHARM.2020.119378.

[243] Chen T, Wang M, Chen Y, Liu Y. Current challenges and therapeutic advances of CAR-T cell therapy for solid tumors. Cancer Cell International 2024 24:1 2024;24:1–24. https://doi.org/10.1186/S12935-024-03315-3.

[244] Sterner RC, Sterner RM. CAR-T cell therapy: current limitations and potential strategies. Blood Cancer Journal 2021 11:4 2021;11:1–11. https://doi.org/10.1038/s41408-021-00459-7.

[245] Elosegui-Artola A, Gupta A, Najibi AJ, Seo BR, Garry R, Tringides CM, et al. Matrix viscoelasticity controls spatiotemporal tissue organization. Nature Materials 2022 22:1 2022;22:117–27. https://doi.org/10.1038/s41563-022-01400-4.

[246] Horecka A, Hordyjewska A, Blicharski T, Kurzepa J. Osteoarthritis of the knee - biochemical aspect of applied therapies: a review. Bosn J Basic Med Sci 2022;22:488–98. https://doi.org/10.17305/BJBMS.2021.6489.

[247] Cui A, Li H, Wang D, Zhong J, Chen Y, Lu H. Global, regional prevalence, incidence

and risk factors of knee osteoarthritis in population-based studies. EClinicalMedicine 2020;29–30:100587. https://doi.org/10.1016/j.eclinm.2020.100587.

[248] Heidari B. Knee osteoarthritis prevalence, risk factors, pathogenesis and features: Part I. Caspian J Intern Med 2011;2:205.

[249] Vignes H, Conzatti G, Hua G, Benkirane-Jessel N. Meniscus Repair: From In Vitro Research to Patients. Organoids 2022;1:116–34. https://doi.org/10.3390/ORGANOIDS1020010.

[250] Klarmann GJ, Gaston J, Ho VB. A review of strategies for development of tissue engineered meniscal implants. Biomaterials and Biosystems 2021;4:100026. https://doi.org/10.1016/J.BBIOSY.2021.100026.

[251] Hussain SM, Neilly DW, Baliga S, Patil S, Meek RMD. Knee osteoarthritis: A review of management options. Scott Med J 2016;61:7–16. https://doi.org/10.1177/0036933015619588.

[252] Abbadessa A, Crecente-Campo J, Alonso MJ. Engineering Anisotropic Meniscus: Zonal Functionality and Spatiotemporal Drug Delivery. Tissue Eng Part B Rev 2021;27:133–54. https://doi.org/10.1089/ten.teb.2020.0096.

[253] Pillai MM, Gopinathan J, Selvakumar R, Bhattacharyya A. Human Knee Meniscus Regeneration Strategies: a Review on Recent Advances. Curr Osteoporos Rep 2018;16:224–35. https://doi.org/10.1007/S11914-018-0436-X.

[254] Abbadessa A, Crecente-Campo J, Alonso MJ. Engineering Anisotropic Meniscus: Zonal Functionality and Spatiotemporal Drug Delivery. Tissue Eng Part B Rev 2021;27:133–54. https://doi.org/10.1089/TEN.TEB.2020.0096.

[255] Kwon H, Brown WE, Lee CA, Wang D, Paschos N, Hu JC, et al. Surgical and tissue engineering strategies for articular cartilage and meniscus repair. Nat Rev Rheumatol 2019;15:550–70. https://doi.org/10.1038/S41584-019-0255-1.

[256] Vignes H, Conzatti G, Hua G, Benkirane-Jessel N. Meniscus Repair: From In Vitro Research to Patients. Organoids 2022;1:116–34. https://doi.org/10.3390/ORGANOIDS1020010.

[257] Klarmann GJ, Gaston J, Ho VB. A review of strategies for development of tissue engineered meniscal implants. Biomaterials and Biosystems 2021;4:100026. https://doi.org/10.1016/J.BBIOSY.2021.100026.

[258] Cengiz IF, Pereira H, Espregueira-Mendes J, Oliveira JM, Reis RL. Treatments of Meniscus Lesions of the Knee: Current Concepts and Future Perspectives. Regenerative Engineering and Translational Medicine 2017 3:1 2017;3:32–50. https://doi.org/10.1007/S40883-017-0025-Z.

[259] Hurmuz M, Ionac M, Hogea B, Miu CA, Tatu F. Osteoarthritis Development Following Meniscectomy vs. Meniscal Repair for Posterior Medial Meniscus Injuries: A Systematic Review. Medicina 2024, Vol 60, Page 569 2024;60:569. https://doi.org/10.3390/MEDICINA60040569.

[260] Shimomura K, Hamamoto S, Hart DA, Yoshikawa H, Nakamura N. Meniscal repair and

regeneration: Current strategies and future perspectives. J Clin Orthop Trauma 2018;9:247. https://doi.org/10.1016/J.JCOT.2018.07.008.

[261] Sun J, Vijayavenkataraman S, Liu H. An overview of scaffold design and fabrication technology for engineered knee meniscus. Materials 2017;10. https://doi.org/10.3390/ma10010029.

[262] Orteq Sports Medicine - The ACTIfit Procedure n.d. https://www.orteq.com/patients/the-actifit-procedure (accessed July 5, 2021).

[263] Menaflex - Medical Clinical Policy Bulletins | Aetna n.d. http://www.aetna.com/cpb/medical/data/700_799/0786.html (accessed July 5, 2021).

[264] Rodkey WG. Menaflex (TM) collagen meniscus implant: Basic science. The Meniscus, Springer Berlin Heidelberg; 2010, p. 367–71. https://doi.org/10.1007/978-3-642-02450-4_46.

[265] Knee & Joint Pain Treatment Options | Meniscus Pain | Active Implants n.d. https://activeimplants.com/knee-joint-pain-treatment-options/ (accessed July 5, 2021).

[266] Active-Implants. NUsurface® Meniscus Implant for Persistent Knee Pain n.d.

[267] Zhang D, Chen Q, Shi C, Chen M, Ma K, Wan J, et al. Dealing with the Foreign-Body Response to Implanted Biomaterials: Strategies and Applications of New Materials. Adv Funct Mater 2021;31:2007226. https://doi.org/10.1002/ADFM.202007226.

[268] Talebian S, Mendes B, Conniot J, Farajikhah S, Dehghani F, Li Z, et al. Biopolymeric Coatings for Local Release of Therapeutics from Biomedical Implants. Advanced Science 2023;10:2207603. https://doi.org/10.1002/ADVS.202207603.

[269] Khella CM, Horvath JM, Asgarian R, Rolauffs B, Hart ML. Anti-Inflammatory Therapeutic Approaches to Prevent or Delay Post-Traumatic Osteoarthritis (PTOA) of the Knee Joint with a Focus on Sustained Delivery Approaches. Int J Mol Sci 2021;22. https://doi.org/10.3390/IJMS22158005.

[270] Gómez-Gaete C, Tsapis N, Besnard M, Bochot A, Fattal E. Encapsulation of dexamethasone into biodegradable polymeric nanoparticles. Int J Pharm 2007;331:153–9. https://doi.org/10.1016/j.ijpharm.2006.11.028.

[271] McCarron PA, Donnelly RF, Marouf W. Celecoxib-loaded poly(D,L-lactide-co-glycolide) nanoparticles prepared using a novel and controllable combination of diffusion and emulsification steps as part of the salting-out procedure. J Microencapsul 2006;23:480–98. https://doi.org/10.1080/02652040600682390.

[272] Makadia HK, Siegel SJ. Poly Lactic-co-Glycolic Acid (PLGA) as biodegradable controlled drug delivery carrier. Polymers (Basel) 2011;3:1377–97. https://doi.org/10.3390/polym3031377.

[273] Kalam MA. The potential application of hyaluronic acid coated chitosan nanoparticles in ocular delivery of dexamethasone. Int J Biol Macromol 2016;89:559–68. https://doi.org/10.1016/j.ijbiomac.2016.05.016.

[274] IFPMA:Geneva. ICH - Harmonised Tripartity Guideline; Validation of Analytical Proce

dures: Text and Methodology Q2(R1). 2005.

[275] Kalam MA. The potential application of hyaluronic acid coated chitosan nanoparticles in ocular delivery of dexamethasone. Int J Biol Macromol 2016;89:559–68. https://doi.org/10.1016/j.ijbiomac.2016.05.016.

[276] IFPMA:Geneva. ICH - Harmonised Tripartity Guideline; Validation of Analytical Proce dures: Text and Methodology Q2(R1). 2005.

[277] Ummarino A, Anfray C, Maeda A, Andón FT, Allavena P. In Vitro Methods to Evaluate Macrophage Polarization and Function in Cancer. Methods Mol Biol 2023;2614:81–91. https://doi.org/10.1007/978-1-0716-2914-7_6.

[278] Phillips DJ, Pygall SR, Cooper VB, Mann JC. Overcoming sink limitations in dissolution testing: a review of traditional methods and the potential utility of biphasic systems. Journal of Pharmacy and Pharmacology 2012;64:1549–59. https://doi.org/10.1111/J.2042-7158.2012.01523.X.

[279] Yoon SD, Kwon YS, Lee KS. Biodegradation and biocompatibility of poly L-lactic acid implantable mesh. Int Neurourol J 2017;21:48–54. https://doi.org/10.5213/inj.1734882.441.

[280] Arakawa CK, DeForest CA. Polymer Design and Development. Elsevier Inc.; 2017. https://doi.org/10.1016/B978-0-12-802734-9.00019-6.

[281] Braunecker J, Baba M, Milroy GE, Cameron RE. The effects of molecular weight and porosity on the degradation and drug release from polyglycolide. Int J Pharm 2004;282:19–34. https://doi.org/10.1016/J.IJPHARM.2003.08.020.

[282] Abdelghafour MM, Orbán Á, Deák Á, Lamch Ł, Frank É, Nagy R, et al. Biocompatible poly(ethylene succinate) polyester with molecular weight dependent drug release properties. Int J Pharm 2022;618:121653. https://doi.org/10.1016/J.IJPHARM.2022.121653.

[283] Ochi M, Wan B, Bao Q, Burgess DJ. Influence of PLGA molecular weight distribution on leuprolide release from microspheres. Int J Pharm 2021;599. https://doi.org/10.1016/J.IJPHARM.2021.120450.

[284] Visan AI, Popescu-Pelin G, Socol G. Degradation Behavior of Polymers Used as Coating Materials for Drug Delivery—A Basic Review. Polymers (Basel) 2021;13. https://doi.org/10.3390/POLYM13081272.

[285] Im D, Gavande V, Lee HY, Lee WK. Influence of Molecular Weight on the Enzymatic Degradation of PLA Isomer Blends by a Langmuir System. Materials 2023, Vol 16, Page 5087 2023;16:5087. https://doi.org/10.3390/MA16145087.

[286] Nevoralová M, Koutný M, Ujčić A, Starý Z, Šerá J, Vlková H, et al. Structure Characterization and Biodegradation Rate of Poly(ε-caprolactone)/Starch Blends. Front Mater 2020;7:487523. https://doi.org/10.3389/FMATS.2020.00141/BIBTEX.

[287] Mota J. Solid solutions vs. solid dispersions: the impact of formulation parameters. Journal Biomedical and Biopharmaceutical Research 2013;10:235–48. https://doi.org/10.19277/bbr.10.2.68.

[288] Cetindag E, Pentangelo J, Arrieta Cespedes T, Davé RN. Effect of Solvents and Cellulosic Polymers on Quality Attributes of Films Loaded with a Poorly Water-Soluble Drug. Carbohydr Polym 2020;250:117012. https://doi.org/10.1016/J.CARBPOL.2020.117012.

[289] Ljungberg N, Wesslén B. Tributyl citrate oligomers as plasticizers for poly (lactic acid): thermo-mechanical film properties and aging. Polymer (Guildf) 2003;44:7679–88. https://doi.org/10.1016/J.POLYMER.2003.09.055.

[290] Alamri HR, El-Hadi AM, Al-Qahtani SM, Assaedi HS, Alotaibi AS. Role of lubricant with a plasticizer to change the glass transition temperature as a result improving the mechanical properties of poly(lactic acid) PLLA. Mater Res Express 2020;7. https://doi.org/10.1088/2053-1591/AB715A.

[291] Lin G, Wang J, Lv N, Wang H, Wang H, Yu B, et al. Simultaneously Strengthening and Toughening Poly(lactic acid) by Co-Additions of Poly(ε-caprolactone), Tributyl Citrate Plasticizer and Functionalized Multiwall Carbon Nanotube. Sci Adv Mater 2020;12:950–7. https://doi.org/10.1166/SAM.2020.3717.

[292] Qin Y, Cheng L, Zhang Y, Chen X, Wang X, He X, et al. Efficient preparation of poly(lactic acid) nanofibers by melt differential electrospinning with addition of acetyl tributyl citrate. J Appl Polym Sci 2018;135:46554. https://doi.org/10.1002/APP.46554.

[293] Yang Z, Feng X, Bi Y, Zhou Z, Yue J, Xu M. Bleached extruder chemi-mechanical pulp fiber-PLA composites: Comparison of mechanical, thermal, and rheological properties with those of wood flour-PLA bio-composites. J Appl Polym Sci 2016;133:44241. https://doi.org/10.1002/APP.44241.

[294] Tatu RR, Oria M, Rao MB, Peiro JL, Lin CY. Biodegradation of poly(l-lactic acid) and poly(ε-caprolactone) patches by human amniotic fluid in an in-vitro simulated fetal environment. Scientific Reports 2022 12:1 2022;12:1–11. https://doi.org/10.1038/s41598-022-07681-8.

[295] Harting R, Johnston K, Petersen S. Correlating in vitro degradation and drug release kinetics of biopolymer-based drug delivery systems. International Journal of Biobased Plastics 2019;1:8–21. https://doi.org/10.1080/24759651.2018.1563358.

[296] Petit A, Sandker M, Müller B, Meyboom R, van Midwoud P, Bruin P, et al. Release behavior and intra-articular biocompatibility of celecoxib-loaded acetyl-capped PCLA-PEG-PCLA thermogels. Biomaterials 2014;35:7919–28. https://doi.org/10.1016/J.BIOMATERIALS.2014.05.064.

[297] Jiang D, Zou J, Huang L, Shi Q, Zhu X, Wang G, et al. Efficacy of intra-articular injection of celecoxib in a rabbit model of osteoarthritis. Int J Mol Sci 2010;11:4106–13. https://doi.org/10.3390/IJMS11104106.

[298] Janssen M, Timur UT, Woike N, Welting TJM, Draaisma G, Gijbels M, et al. Celecoxib-loaded PEA microspheres as an auto regulatory drug-delivery system after intra-articular injection. Journal of Controlled Release 2016;244:30–40. https://doi.org/10.1016/J.JCONREL.2016.11.003.

[299] Li Z, Meng D, Li G, Xu J, Tian K, Li Y. Celecoxib Combined with Diacerein Effectively Alleviates Osteoarthritis in Rats via Regulating JNK and p38MAPK Signaling Pathways.

Inflammation 2015;38:1563–72. https://doi.org/10.1007/S10753-015-0131-3/FIGURES/7.

[300] Hurtig M, Shive M, Kapoor M, Grizot S, Mahomed N, Foster Roberts G, et al. Intra-articular injection of a polymer/celecoxib formulation for long-term control of postoperative inflammation. Osteoarthritis Cartilage 2016;24:S526–7. https://doi.org/10.1016/j.joca.2016.01.962.

[301] Baptista C, Azagury A, Shin H, Baker CM, Ly E, Lee R, et al. The effect of temperature and pressure on polycaprolactone morphology. Polymer (Guildf) 2020;191:122227. https://doi.org/10.1016/J.POLYMER.2020.122227.

[302] Haddadin R, Qian F, Desikan S, Hussain M, Smith RL. Estimation of drug solubility in polymers via differential scanning calorimetry and utilization of the fox equation. Pharm Dev Technol 2009;14:19–27. https://doi.org/10.1080/10837450802409370.

[303] Ouazib F, Bouslah Mokhnachi N, Haddadine N, Barille R. Role of polymer/polymer and polymer/drug specific interactions in drug delivery systems. Journal of Polymer Engineering 2019;39:534–44. https://doi.org/10.1515/POLYENG-2018-0403/MACHINEREADABLECITATION/RIS.

[304] Chiu M, Prenner E. Differential scanning calorimetry: An invaluable tool for a detailed thermodynamic characterization of macromolecules and their interactions. J Pharm Bioallied Sci 2011;3:39. https://doi.org/10.4103/0975-7406.76463.

[305] Gill P, Moghadam TT, Ranjbar B. Differential Scanning Calorimetry Techniques: Applications in Biology and Nanoscience. J Biomol Tech 2010;21:167.

[306] Li Y, Pang H, Guo Z, Lin L, Dong Y, Li G, et al. Interactions between drugs and polymers influencing hot melt extrusion. Journal of Pharmacy and Pharmacology 2014;66:148–66. https://doi.org/10.1111/JPHP.12183.

[307] Valenti S, Del Valle LJ, Romanini M, Mitjana M, Puiggalí J, Tamarit JL, et al. Drug-Biopolymer Dispersions: Morphology- and Temperature- Dependent (Anti)Plasticizer Effect of the Drug and Component-Specific Johari-Goldstein Relaxations. Int J Mol Sci 2022;23. https://doi.org/10.3390/IJMS23052456.

[308] Khalyavina A, Häußler L, Lederer A. Effect of the degree of branching on the glass transition temperature of polyesters. Polymer (Guildf) 2012;53:1049–53. https://doi.org/10.1016/J.POLYMER.2012.01.020.

[309] Yang Z, Feng X, Bi Y, Zhou Z, Yue J, Xu M. Bleached extruder chemi-mechanical pulp fiber-PLA composites: Comparison of mechanical, thermal, and rheological properties with those of wood flour-PLA bio-composites. J Appl Polym Sci 2016;133:44241. https://doi.org/10.1002/APP.44241.

[310] Ouazib F, Bouslah Mokhnachi N, Haddadine N, Barille R. Role of polymer/polymer and polymer/drug specific interactions in drug delivery systems. Journal of Polymer Engineering 2019;39:534–44. https://doi.org/10.1515/POLYENG-2018-0403/MACHINEREADABLECITATION/RIS.

[311] Arbeiter D, Reske T, Teske M, Bajer D, Senz V, Schmitz KP, et al. Influence of drug incorporation on the physico-chemical properties of poly(L-lactide) implant coating

matrices—a systematic study. Polymers (Basel) 2021;13:1–19. https://doi.org/10.3390/polym13020292.

[312] Broz ME, VanderHart DL, Washburn NR. Structure and mechanical properties of poly(D,L-lactic acid)/poly(ε-caprolactone) blends. Biomaterials 2003;24:4181–90. https://doi.org/10.1016/S0142-9612(03)00314-4.

[313] Ferri JM, Fenollar O, Jorda-Vilaplana A, García-Sanoguera D, Balart R. Effect of miscibility on mechanical and thermal properties of poly(lactic acid)/ polycaprolactone blends. Polym Int 2016;65:453–63. https://doi.org/10.1002/PI.5079.

[314] Current Applications of Powder X-Ray Diffraction in Drug Discovery and Development | American Pharmaceutical Review - The Review of American Pharmaceutical Business & Technology n.d. https://www.americanpharmaceuticalreview.com/Featured-Articles/155545-Current-Applications-of-Powder-X-Ray-Diff-raction-in-Drug-Discovery-and-Development/ (accessed August 7, 2024).

[315] Vasu Dev R, Shashi Rekha K, Vyas K, Mohanti SB, Rajender Kumar P, Om Reddy G. Celecoxib, a COX-II inhibitor. Acta Crystallogr C 1999;55:IUC9900161. https://doi.org/10.1107/s0108270199098200.

[316] Brizzolara D, Cantow HJ, Diederichs K, Keller E, Domb AJ. Mechanism of the stereocomplex formation between enantiomeric poly(lactide)s. Macromolecules 1996;29:191–7. https://doi.org/10.1021/ma951144e.

[317] Karavelidis V, Karavas E, Giliopoulos D, Papadimitriou S, Bikiaris D. Evaluating the effects of crystallinity in new biocompatible polyester nanocarriers on drug release behavior. Int J Nanomedicine 2011;6:3021. https://doi.org/10.2147/IJN.S26016.

[318] Niyom Y, Phakkeeree T, Flood A, Crespy D. Synergy between polymer crystallinity and nanoparticles size for payloads release. J Colloid Interface Sci 2019;550:139–46. https://doi.org/10.1016/J.JCIS.2019.04.085.

[319] Miles CE, Bernstein AD, Osborn Popp TM, Murthy NS, Nieuwkoop AJ, Gormley AJ. Control of Drug Release from Microparticles by Tuning Their Crystalline Textures: A Structure-Activity Study. ACS Appl Polym Mater 2021;3:6548–61. https://doi.org/10.1021/ACSAPM.1C01254/ASSET/IMAGES/LARGE/AP1C01254_0008.JPEG.

[320] Jeong JC, Lee J, Cho K. Effects of crystalline microstructure on drug release behavior of poly(ε-caprolactone) microspheres. Journal of Controlled Release 2003;92:249–58. https://doi.org/10.1016/S0168-3659(03)00367-5.

[321] Makadia HK, Siegel SJ. Poly Lactic-co-Glycolic Acid (PLGA) as Biodegradable Controlled Drug Delivery Carrier. Polymers (Basel) 2011;3:1377. https://doi.org/10.3390/POLYM3031377.

[322] Vey E, Rodger C, Booth J, Claybourn M, Miller AF, Saiani A. Degradation kinetics of poly(lactic-co-glycolic) acid block copolymer cast films in phosphate buffer solution as revealed by infrared and Raman spectroscopies. Polym Degrad Stab 2011;96:1882–9. https://doi.org/10.1016/J.POLYMDEGRADSTAB.2011.07.011.

[323] Gentile P, Chiono V, Carmagnola I, Hatton P V. An Overview of Poly(lactic-co-glycolic)

Acid (PLGA)-Based Biomaterials for Bone Tissue Engineering. Int J Mol Sci 2014;15:3640. https://doi.org/10.3390/IJMS15033640.

[324] Kamaly N, Yameen B, Wu J, Farokhzad OC. Degradable Controlled-Release Polymers and Polymeric Nanoparticles: Mechanisms of Controlling Drug Release. Chem Rev 2016;116:2602. https://doi.org/10.1021/ACS.CHEMREV.5B00346.

[325] Varma MVS, Kaushal AM, Garg A, Garg S. Factors affecting mechanism and kinetics of drug release from matrix-based oral controlled drug delivery systems. American Journal of Drug Delivery 2004 2:1 2012;2:43–57. https://doi.org/10.2165/00137696-200402010-00003.

[326] Borandeh S, van Bochove B, Teotia A, Seppälä J. Polymeric drug delivery systems by additive manufacturing. Adv Drug Deliv Rev 2021;173:349–73. https://doi.org/10.1016/J.ADDR.2021.03.022.

[327] Wang Q, Jiang J, Chen W, Jiang H, Zhang Z, Sun X. Targeted delivery of low-dose dexamethasone using PCL-PEG micelles for effective treatment of rheumatoid arthritis. Journal of Controlled Release 2016;230:64–72. https://doi.org/10.1016/j.jconrel.2016.03.035.

[328] Serra T, Ortiz-Hernandez M, Engel E, Planell JA, Navarro M. Relevance of PEG in PLA-based blends for tissue engineering 3D-printed scaffolds. Materials Science and Engineering: C 2014;38:55–62. https://doi.org/10.1016/J.MSEC.2014.01.003.

[329] Meunier M, Goupil A, Lienard P. Predicting drug loading in PLA-PEG nanoparticles. Int J Pharm 2017;526:157–66. https://doi.org/10.1016/j.ijpharm.2017.04.043.

[330] Arbeiter D, Reske T, Teske M, Bajer D, Senz V, Schmitz KP, et al. Influence of Drug Incorporation on the Physico-Chemical Properties of Poly(l-Lactide) Implant Coating Matrices—A Systematic Study. Polymers 2021, Vol 13, Page 292 2021;13:292. https://doi.org/10.3390/POLYM13020292.

[331] Fredenberg S, Wahlgren M, Reslow M, Axelsson A. The mechanisms of drug release in poly(lactic-co-glycolic acid)-based drug delivery systems—A review. Int J Pharm 2011;415:34–52. https://doi.org/10.1016/J.IJPHARM.2011.05.049.

[332] Gentile P, Chiono V, Carmagnola I, Hatton P V. An overview of poly(lactic-co-glycolic) Acid (PLGA)-based biomaterials for bone tissue engineering. Int J Mol Sci 2014;15:3640–59. https://doi.org/10.3390/IJMS15033640.

[333] Chrissafis K, Paraskevopoulos KM, Bikiaris DN. Effect of molecular weight on thermal degradation mechanism of the biodegradable polyester poly(ethylene succinate). Thermochim Acta 2006;440:166–75. https://doi.org/10.1016/J.TCA.2005.11.002.

[334] Marcos MA, Cabaleiro D, Guimarey MJG, Comuñas MJP, Fedele L, Fernández J, et al. PEG 400-Based Phase Change Materials Nano-Enhanced with Functionalized Graphene Nanoplatelets. Nanomaterials 2018;8. https://doi.org/10.3390/NANO8010016.

[335] Dabbagh A, Mahmoodian R, Abdullah BJJ, Abdullah H, Hamdi M, Abu Kasim NH. Low-melting-point polymeric nanoshells for thermal-triggered drug release under hyperthermia condition. International Journal of Hyperthermia 2015;31:920–9. https://doi.org/10.3109/02656736.2015.1094147.

[336] Kumar A, Weig AR, Agarwal S. Balancing Degradability and Physical Properties of Amorphous Poly(d,l-Lactide) by Making Blends. Macromol Mater Eng 2021. https://doi.org/10.1002/MAME.202100602.

[337] da Silva D, Kaduri M, Poley M, Adir O, Krinsky N, Shainsky-Roitman J, et al. Biocompatibility, biodegradation and excretion of polylactic acid (PLA) in medical implants and theranostic systems. Chemical Engineering Journal 2018;340:9–14. https://doi.org/10.1016/J.CEJ.2018.01.010.

[338] Weir NA, Buchanan FJ, Orr JF, Dickson GR. Degradation of poly-L-lactide. Part 1: in vitro and in vivo physiological temperature degradation. Http://DxDoiOrg/101243/0954411041932782 2004;218:307–19. https://doi.org/10.1243/0954411041932782.

[339] Feng P, Jia J, Liu M, Peng S, Zhao Z, Shuai C. Degradation mechanisms and acceleration strategies of poly (lactic acid) scaffold for bone regeneration. Mater Des 2021;210:110066. https://doi.org/10.1016/J.MATDES.2021.110066.

[340] Kutikov AB, Song J. Biodegradable PEG-Based Amphiphilic Block Copolymers for Tissue Engineering Applications. ACS Biomater Sci Eng 2015;1:463–80. https://doi.org/10.1021/ACSBIOMATERIALS.5B00122/ASSET/IMAGES/MEDIUM/AB-2015-001228_0011.GIF.

[341] Mundel R, Thakur T, Chatterjee M. Emerging uses of PLA–PEG copolymer in cancer drug delivery. 3 Biotech 2022;12:1–12. https://doi.org/10.1007/S13205-021-03105-Y/TABLES/3.

[342] Gu B, Wang Y, Burgess DJ. In vitro and in vivo performance of dexamethasone loaded PLGA microspheres prepared using polymer blends. Int J Pharm 2015;496:534. https://doi.org/10.1016/J.IJPHARM.2015.10.056.

[343] Cokelaere SM, Plomp SGM, de Boef E, de Leeuw M, Bool S, van de Lest CHA, et al. Sustained intra-articular release of celecoxib in an equine repeated LPS synovitis model. Eur J Pharm Biopharm 2018;128:327–36. https://doi.org/10.1016/J.EJPB.2018.05.001.

[344] Petit A, Sandker M, Müller B, Meyboom R, van Midwoud P, Bruin P, et al. Release behavior and intra-articular biocompatibility of celecoxib-loaded acetyl-capped PCLA-PEG-PCLA thermogels. Biomaterials 2014;35:7919–28. https://doi.org/10.1016/J.BIOMATERIALS.2014.05.064.

[345] Tellegen AR, Rudnik-Jansen I, Pouran B, de Visser HM, Weinans HH, Thomas RE, et al. Controlled release of celecoxib inhibits inflammation, bone cysts and osteophyte formation in a preclinical model of osteoarthritis. Drug Deliv 2018;25:1438–47. https://doi.org/10.1080/10717544.2018.1482971.

[346] Roberge C, Cros JM, Serindoux J, Cagnon ME, Samuel R, Vrlinic T, et al. BEPO®: Bioresorbable diblock mPEG-PDLLA and triblock PDLLA-PEG-PDLLA based in situ forming depots with flexible drug delivery kinetics modulation. Journal of Controlled Release 2020;319:416–27. https://doi.org/10.1016/J.JCONREL.2020.01.022.

[347] Chen CC, Chueh JY, Tseng H, Huang HM, Lee SY. Preparation and characterization of biodegradable PLA polymeric blends. Biomaterials 2003;24:1167–73. https://doi.org/10.1016/S0142-9612(02)00466-0.

[348] Rapier CE, Shea KJ, Lee AP. Investigating PLGA microparticle swelling behavior reveals an interplay of expansive intermolecular forces. Scientific Reports 2021 11:1 2021;11:1–12. https://doi.org/10.1038/s41598-021-93785-6.

[349] Gasmi H, Danede F, Siepmann J, Siepmann F. Does PLGA microparticle swelling control drug release? New insight based on single particle swelling studies. Journal of Controlled Release 2015;213:120–7. https://doi.org/10.1016/J.JCONREL.2015.06.039.

[350] Guidance for Industry: Pyrogen and Endotoxins Testing: Questions and Answers | FDA n.d. https://www.fda.gov/regulatory-information/search-fda-guidance-documents/guidance-industry-pyrogen-and-endotoxins-testing-questions-and-answers (accessed August 16, 2024).

[351] Dinarello CA. Historical Review of Cytokines. Eur J Immunol 2007;37:S34. https://doi.org/10.1002/EJI.200737772.

[352] Zhang JM, An J. Cytokines, Inflammation and Pain. Int Anesthesiol Clin 2007;45:27. https://doi.org/10.1097/AIA.0B013E318034194E.

[353] Jang DI, Lee AH, Shin HY, Song HR, Park JH, Kang TB, et al. The Role of Tumor Necrosis Factor Alpha (TNF-α) in Autoimmune Disease and Current TNF-α Inhibitors in Therapeutics. International Journal of Molecular Sciences 2021, Vol 22, Page 2719 2021;22:2719. https://doi.org/10.3390/IJMS22052719.

[354] Zia K, Ashraf S, Jabeen A, Saeed M, Nur-e-Alam M, Ahmed S, et al. Identification of potential TNF-α inhibitors: from in silico to in vitro studies. Scientific Reports 2020 10:1 2020;10:1–9. https://doi.org/10.1038/s41598-020-77750-3.

[355] Deshmane SL, Kremlev S, Amini S, Sawaya BE. Monocyte Chemoattractant Protein-1 (MCP-1): An Overview. Journal of Interferon & Cytokine Research 2009;29:313. https://doi.org/10.1089/JIR.2008.0027.

[356] Kyriakides TR, Foster MJ, Keeney GE, Tsai A, Giachelli CM, Clark-Lewis I, et al. The CC Chemokine Ligand, CCL2/MCP1, Participates in Macrophage Fusion and Foreign Body Giant Cell Formation. Am J Pathol 2004;165:2157–66. https://doi.org/10.1016/S0002-9440(10)63265-8.

[357] Viana MN, Leiguez E, Gutiérrez JM, Rucavado A, Markus RP, Marçola M, et al. A representative metalloprotease induces PGE2 synthesis in fibroblast-like synoviocytes via the NF-κB/COX-2 pathway with amplification by IL-1β and the EP4 receptor. Scientific Reports 2020 10:1 2020;10:1–15. https://doi.org/10.1038/s41598-020-59095-z.

[358] Menarim BC, Gillis KH, Oliver A, Ngo Y, Werre SR, Barrett SH, et al. Macrophage Activation in the Synovium of Healthy and Osteoarthritic Equine Joints. Front Vet Sci 2020;7:568756. https://doi.org/10.3389/FVETS.2020.568756.

[359] Raleigh AR, W.J. McCarty, Chen AC, Meinert C, Klein TJ, Sah RL. Synovial joints: Mechanobiology and tissue engineering of articular cartilage and synovial fluid. Comprehensive Biomaterials II 2017:107–34. https://doi.org/10.1016/B978-0-12-803581-8.09304-8.

[360] Dayss E, Leps G, Meinhardt J. Surface modification for improved adhesion of a polymer–

metal compound. Surf Coat Technol 1999;116–119:986–90. https://doi.org/10.1016/S0257-8972(99)00184-X.

[361] Al-Amiery AA, Fayad MA, Abdul Wahhab HA, Al-Azzawi WK, Mohammed JK, Majdi HS. Interfacial Engineering for Advanced Functional Materials: Surfaces, Interfaces, and Applications. Results in Engineering 2024;22:102125. https://doi.org/10.1016/J.RINENG.2024.102125.

[362] Dua R, Jones H, Noble PC. Evaluation of bone formation on orthopedic implant surfaces using an ex-vivo bone bioreactor system. Scientific Reports 2021 11:1 2021;11:1–10. https://doi.org/10.1038/s41598-021-02070-z.

[363] Ladner YD, Kasper H, Armiento AR, Stoddart MJ. A multi-well bioreactor for cartilage tissue engineering experiments. IScience 2023;26:107092. https://doi.org/10.1016/J.ISCI.2023.107092.

[364] Brzezinski A, Ghodbane SA, Patel JM, Perry BA, Gatt CJ, Dunn MG. The Ovine Model for Meniscus Tissue Engineering: Considerations of Anatomy, Function, Implantation, and Evaluation. Tissue Eng Part C Methods 2017;23:829. https://doi.org/10.1089/TEN.TEC.2017.0192.

[365] Proffen BL, McElfresh M, Fleming BC, Murray MM. A comparative anatomical study of the human knee and six animal species. Knee 2012;19:493–9. https://doi.org/10.1016/J.KNEE.2011.07.005.

[366] Kon E, Filardo G, Tschon M, Fini M, Giavaresi G, Reggiani LM, et al. Tissue engineering for total meniscal substitution: animal study in sheep model--results at 12 months. Tissue Eng Part A 2012;18:1573–82. https://doi.org/10.1089/TEN.TEA.2011.0572.

[367] Kolarovszki B, Ficsor S, Frank D, Katona K, Soos B, Turzo K. Unlocking the potential: laser surface modifications for titanium dental implants. Lasers Med Sci 2024;39. https://doi.org/10.1007/S10103-024-04076-1.

[368] Saran R, Ginjupalli K, George SD, Chidangil S, V K U. LASER as a tool for surface modification of dental biomaterials: A review. Heliyon 2023;9:e17457. https://doi.org/10.1016/J.HELIYON.2023.E17457.

[369] Ghorbani F, Zamanian A. Oxygen-plasma treatment-induced surface engineering of biomimetic polyurethane nanofibrous scaffolds for gelatin-heparin immobilization. E-Polymers 2018;18:275–85. https://doi.org/10.1515/EPOLY-2017-0185/ASSET/GRAPHIC/J_EPOLY-2017-0185_FIG_006.JPG.

[370] Liu Y, Ai K, Lu L. Polydopamine and its derivative materials: Synthesis and promising applications in energy, environmental, and biomedical fields. Chem Rev 2014;114:5057–115. https://doi.org/10.1021/CR400407A/ASSET/CR400407A.FP.PNG_V03.

[371] Raja PR. Cyanoacrylate Adhesives: A Critical Review. REVIEWS OF ADHESION AND ADHESIVES 2016;4.

[372] Bortel EL, Charbonnier B, Heuberger R. Development of a Synthetic Synovial Fluid for Tribological Testing. Lubricants 2015, Vol 3, Pages 664-686 2015;3:664–86. https://doi.org/10.3390/LUBRICANTS3040664.

[373] Rothammer B, Marian M, Rummel F, Schroeder S, Uhler M, Kretzer JP, et al. Rheological behavior of an artificial synovial fluid – influence of temperature, shear rate and pressure. J Mech Behav Biomed Mater 2021;115:104278. https://doi.org/10.1016/J.JMBBM.2020.104278.

[374] Temple-Wong MM, Ren S, Quach P, Hansen BC, Chen AC, Hasegawa A, et al. Hyaluronan concentration and size distribution in human knee synovial fluid: variations with age and cartilage degeneration. Arthritis Res Ther 2016;18. https://doi.org/10.1186/S13075-016-0922-4.

[375] Kosinska MK, Ludwig TE, Liebisch G, Zhang R, Siebert HC, Wilhelm J, et al. Articular Joint Lubricants during Osteoarthritis and Rheumatoid Arthritis Display Altered Levels and Molecular Species. PLoS One 2015;10. https://doi.org/10.1371/JOURNAL.PONE.0125192.

[376] Ghosh S, Choudhury D, Das NS, Pingguan-Murphy B. Tribological role of synovial fluid compositions on artificial joints — a systematic review of the last 10 years. Lubrication Science 2014;26:387–410. https://doi.org/10.1002/LS.1266.

[377] Furmann D, Nečas D, Rebenda D, Čípek P, Vrbka M, Křupka I, et al. The Effect of Synovial Fluid Composition, Speed and Load on Frictional Behaviour of Articular Cartilage. Materials 2020;13. https://doi.org/10.3390/MA13061334.

[378] Brandt JM, Brière LK, Marr J, MacDonald SJ, Bourne RB, Medley JB. Biochemical comparisons of osteoarthritic human synovial fluid with calf sera used in knee simulator wear testing. J Biomed Mater Res A 2010;94:961–71. https://doi.org/10.1002/JBM.A.32728.

[379] Zurita R, Puiggalí J, Rodríguez-Galán A. Triclosan release from coated polyglycolide threads. Macromol Biosci 2006;6:58–69. https://doi.org/10.1002/MABI.200500147.

[380] Thing M, Mertz N, Ågårdh L, Larsen SW, Østergaard J, Larsen C. Simulated synovial fluids for in vitro drug and prodrug release testing of depot injectables intended for joint injection. J Drug Deliv Sci Technol 2019;49:169–76. https://doi.org/10.1016/J.JDDST.2018.11.012.

[381] Visco A, Yousef S, Scolaro C, Espro C, Cristani M. Tribological Behavior of Nanocomposites Based on UHMWPE Aged in Simulated Synovial Fluid. Polymers (Basel) 2018;10. https://doi.org/10.3390/POLYM10111291.

[382] Bittar IP, Neves CA, Araújo CT, Oliveira YVR, Silva SL, Borges NC, et al. Dose-Finding in the Development of an LPS-Induced Model of Synovitis in Sheep. Comp Med 2021;71:141–7. https://doi.org/10.30802/AALAS-CM-20-000032.

[383] Lang V, Roch T, Lasagni AF. High-Speed Surface Structuring of Polycarbonate Using Direct Laser Interference Patterning: Toward 1 m2 min−1 Fabrication Speed Barrier. Adv Eng Mater 2016;18:1342–8. https://doi.org/10.1002/ADEM.201600173.

[384] Clauser J, Gester K, Roggenkamp J, Mager I, Maas J, Jansen S V., et al. Micro-structuring of polycarbonate-urethane surfaces in order to reduce platelet activation and adhesion. J Biomater Sci Polym Ed 2014;25:504–18. https://doi.org/10.1080/09205063.2013.879561.

[385] Encinas N, Pantoja M, Abenojar J, Martínez MA. Control of Wettability of Polymers by Surface Roughness Modification. J Adhes Sci Technol 2010;24:1869–83. https://doi.org/10.1163/016942410X511042.

[386] Majhy B, Priyadarshini P, Sen AK. Effect of surface energy and roughness on cell adhesion and growth – facile surface modification for enhanced cell culture. RSC Adv 2021;11:15467. https://doi.org/10.1039/D1RA02402G.

[387] Obilor AF, Pacella M, Wilson A, Silberschmidt V V. Micro-texturing of polymer surfaces using lasers: a review. The International Journal of Advanced Manufacturing Technology 2022 120:1 2022;120:103–35. https://doi.org/10.1007/S00170-022-08731-1.

[388] Nyssanbek M, Kuzina N, Kondrashchenko V, Azimov A. Effects of plasma treatment on biodegradation of natural and synthetic fibers. Npj Materials Degradation 2024 8:1 2024;8:1–8. https://doi.org/10.1038/s41529-024-00437-x.

[389] Arjun GN, Menon G, Ramesh P. Plasma surface modification of fibroporous polycarbonate urethane membrane by polydimethyl siloxane: structural characterization, mechanical properties, and in vitro cytocompatibility evaluation. J Biomed Mater Res A 2014;102:947–57. https://doi.org/10.1002/JBM.A.34781.

[390] Sanchis MR, Calvo O, Fenollar O, Garcia D, Balart R. Surface modification of a polyurethane film by low pressure glow discharge oxygen plasma treatment. J Appl Polym Sci 2007;105:1077–85. https://doi.org/10.1002/APP.26250.

[391] Oguzlu H, Baldelli A, Mohammadi X, Kong A, Bacca M, Pratap-Singh A. Cold Plasma for the Modification of the Surface Roughness of Microparticles. ACS Omega 2024;9:35634–44. https://doi.org/10.1021/ACSOMEGA.4C03787/ASSET/IMAGES/LARGE/AO4C03787_0006.JPEG.

[392] Cvelbar U, Pejovnik S, Mozetiè M, Zalar A. Increased surface roughness by oxygen plasma treatment of graphite/polymer composite. Appl Surf Sci 2003;210:255–61. https://doi.org/10.1016/S0169-4332(02)01286-2.

[393] Kalel N, Darpe A, Bijwe J. Low pressure plasma induced surface changes of some stainless steels. Surf Coat Technol 2021;425:127700. https://doi.org/10.1016/J.SURFCOAT.2021.127700.

[394] Sarkari S, Khajehmohammadi M, Davari N, Li D, Yu B. The effects of process parameters on polydopamine coatings employed in tissue engineering applications. Front Bioeng Biotechnol 2022;10. https://doi.org/10.3389/FBIOE.2022.1005413.

[395] Kim BH, Lee DH, Kim JY, Shin DO, Jeong HY, Hong S, et al. Mussel-inspired block copolymer lithography for low surface energy materials of teflon, graphene, and gold. Adv Mater 2011;23:5618–22. https://doi.org/10.1002/ADMA.201103650.

[396] Hemmatpour H, De Luca O, Crestani D, Stuart MCA, Lasorsa A, van der Wel PCA, et al. New insights in polydopamine formation via surface adsorption. Nature Communications 2023 14:1 2023;14:1–12. https://doi.org/10.1038/s41467-023-36303-8.

[397] Prieto-López LO, Herbeck-Engel P, Yang L, Wu Q, Li J, Cui J. When Ultimate Adhesive Mechanism Meets Ultimate Anti-Fouling Surfaces—Polydopamine Versus SLIPS:

Which One Prevails? Adv Mater Interfaces 2020;7:2000876. https://doi.org/10.1002/ADMI.202000876.

[398] Zhou P, Deng Y, Lyu B, Zhang R, Zhang H, Ma H, et al. Rapidly-Deposited Polydopamine Coating via High Temperature and Vigorous Stirring: Formation, Characterization and Biofunctional Evaluation. PLoS One 2014;9:e113087. https://doi.org/10.1371/JOURNAL.PONE.0113087.

[399] Teng R, Meng Y, Zhao X, Liu J, Ding R, Cheng Y, et al. Combination of Polydopamine Coating and Plasma Pretreatment to Improve Bond Ability Between PEEK and Primary Teeth. Front Bioeng Biotechnol 2021;8:630094. https://doi.org/10.3389/FBIOE.2020.630094/BIBTEX.

[400] Serra T, Ortiz-Hernandez M, Engel E, Planell JA, Navarro M. Relevance of PEG in PLA-based blends for tissue engineering 3D-printed scaffolds. Materials Science and Engineering: C 2014;38:55–62. https://doi.org/10.1016/J.MSEC.2014.01.003.

[401] Bernsmann F, Ball V, Addiego F, Ponche A, Michel M, Gracio JJDA, et al. Dopamine-melanin film deposition depends on the used oxidant and buffer solution. Langmuir 2011;27:2819–25. https://doi.org/10.1021/LA104981S/SUPPL_FILE/LA104981S_SI_001.PDF.

[402] Pawar RP, Jadhav AE, Tathe SB, Khade BC, Domb AJ. Medicinal Applications of Cyanoacrylate. Biodegradable Polymers in Clinical Use and Clinical Development 2011:417–49. https://doi.org/10.1002/9781118015810.CH12.

[403] Pascual G, Sotomayor S, Rodríguez M, Pérez-Köhler B, Kühnhardt A, Fernández-Gutiérrez M, et al. Cytotoxicity of Cyanoacrylate-Based Tissue Adhesives and Short-Term Preclinical In Vivo Biocompatibility in Abdominal Hernia Repair. PLoS One 2016;11. https://doi.org/10.1371/JOURNAL.PONE.0157920.

[404] Mele E, Heredia-Guerrero JA, Bayer IS, Ciofani G, Genchi GG, Ceseracciu L, et al. Zwitterionic Nanofibers of Super-Glue for Transparent and Biocompatible Multi-Purpose Coatings. Scientific Reports 2015 5:1 2015;5:1–13. https://doi.org/10.1038/srep14019.

[405] Leng J, Lan X, Liu Y, Du S. Shape-memory polymers and their composites: Stimulus methods and applications. Prog Mater Sci 2011;56:1077–135. https://doi.org/10.1016/J.PMATSCI.2011.03.001.

[406] Saba N, Jawaid M, Alothman OY, Paridah MT. A review on dynamic mechanical properties of natural fibre reinforced polymer composites. Constr Build Mater 2016;106:149–59. https://doi.org/10.1016/J.CONBUILDMAT.2015.12.075.

[407] Lei* W-S, Mittal K, Yu Z. Adhesion Measurement of Coatings on Biodevices/Implants: A Critical Review. REVIEWS OF ADHESION AND ADHESIVES 2016;4.

[408] Lewis F, Horny P, Hale P, Turgeon S, Tatoulian M, Mantovani D. Study of the adhesion of thin plasma fluorocarbon coatings resisting plastic deformation for stent applications. J Phys D Appl Phys 2008;41:045310. https://doi.org/10.1088/0022-3727/41/4/045310.

[409] Kimbell G, Azad MA. 3D printing: Bioinspired materials for drug delivery. Bioinspired and Biomimetic Materials for Drug Delivery 2021:295–318. https://doi.org/10.1016/B978-0-12-821352-0.00011-3.

[410] Majewski M, Susanne H, Klaus S. Epidemiology of athletic knee injuries: A 10-year study. Knee 2006;13:184–8. https://doi.org/10.1016/J.KNEE.2006.01.005.

[411] Sandmann GH, Adamczyk C, Garcia EG, Doebele S, Buettner A, Milz S, et al. Biomechanical comparison of menisci from different species and artificial constructs. BMC Musculoskelet Disord 2013;14:1–8. https://doi.org/10.1186/1471-2474-14-324/FIGURES/6.

[412] Takroni T, Laouar L, Adesida A, Elliott JAW, Jomha NM. Anatomical study: comparing the human, sheep and pig knee meniscus. J Exp Orthop 2016;3. https://doi.org/10.1186/S40634-016-0071-3.

[413] Chevrier A, Nelea M, Hurtig MB, Hoemann CD, Buschmann MD. Meniscus structure in human, sheep, and rabbit for animal models of meniscus repair. J Orthop Res 2009;27:1197–203. https://doi.org/10.1002/JOR.20869.

[414] Gupte CM, Bull AMJ, Murray R, Amis AA. Comparative anatomy of the meniscofemoral ligament in humans and some domestic mammals. Anat Histol Embryol 2007;36:47–52. https://doi.org/10.1111/J.1439-0264.2006.00718.X.

[415] Giffin JR, Vogrin TM, Zantop T, Woo SLY, Harner CD. Effects of increasing tibial slope on the biomechanics of the knee. Am J Sports Med 2004;32:376–82. https://doi.org/10.1177/0363546503258880.

[416] Taylor WR, Poepplau BM, König C, Ehrig RM, Zachow S, Duda GN, et al. The medial-lateral force distribution in the ovine stifle joint during walking. J Orthop Res 2011;29:567–71. https://doi.org/10.1002/JOR.21254.

[417] Fortelny I, Ujcic A, Fambri L, Slouf M. Phase Structure, Compatibility, and Toughness of PLA/PCL Blends: A Review. Front Mater 2019;6:481142. https://doi.org/10.3389/FMATS.2019.00206/BIBTEX.

[418] Dhakal R, Peer A, Biswas R, Kim J. Transfer molding processes for nanoscale patterning of poly-L-lactic acid (PLLA) films. Https://DoiOrg/101117/122212871 2016;9705:44–9. https://doi.org/10.1117/12.2212871.

[419] Fitzpatrick J, Scott M, Nolan A. Assessment of pain and welfare in sheep. Small Ruminant Research 2006;62:55–61. https://doi.org/10.1016/J.SMALLRUMRES.2005.07.028.

[420] Assessment of pain in sheep | AWEC n.d. https://awecadvisors.org/en/farm-animals/assessment-of-pain-in-sheep/ (accessed October 6, 2024).

[421] Piperno M, Reboul P, Hellio Le Graverand MP, Peschard MJ, Annefeld M, Richard M, et al. Osteoarthritic cartilage fibrillation is associated with a decrease in chrondrocyte adhesion to fibronectin. Osteoarthritis Cartilage 1998;6:393–9. https://doi.org/10.1053/JOCA.1998.0138.

[422] Mononen ME, Mikkola MT, Julkunen P, Ojala R, Nieminen MT, Jurvelin JS, et al. Effect of superficial collagen patterns and fibrillation of femoral articular cartilage on knee joint mechanics-a 3D finite element analysis. J Biomech 2012;45:579–87. https://doi.org/10.1016/J.JBIOMECH.2011.11.003.

[423] Vincent G, Marchand R, Mont MA, Harder B, Salem HS, Conaghan PG, et al. Characterizing Osteophyte Formation in Knee Osteoarthritis: Application of Machine Learning Quantification of a Computerized Tomography Cohort: Implications for Treatment. J Arthroplasty 2024;39. https://doi.org/10.1016/J.ARTH.2024.04.083.

[424] Li G, Yin J, Gao J, Cheng TS, Pavlos NJ, Zhang C, et al. Subchondral bone in osteoarthritis: Insight into risk factors and microstructural changes. Arthritis Res Ther 2013;15:1–12. https://doi.org/10.1186/AR4405/FIGURES/3.

[425] Donell S. Subchondral bone remodelling in osteoarthritis. EFORT Open Rev 2019;4:221. https://doi.org/10.1302/2058-5241.4.180102.

[426] Rim YA, Ju JH. The Role of Fibrosis in Osteoarthritis Progression. Life 2021;11:1–13. https://doi.org/10.3390/LIFE11010003.

[427] Skinner M, Sullivan B, Conley C, Johnson D, Ireland ML, Landy D, et al. Incidence of Osteoarthritis Diagnosis Within 5 Years of Surgery Was Greater Following Partial Meniscectomy Than Meniscus Repair and/or Anterior Cruciate Ligament Reconstruction. Arthrosc Sports Med Rehabil 2024;6:100903. https://doi.org/10.1016/J.ASMR.2024.100903.

[428] Migliorini F, Schäfer L, Bell A, Weber CD, Vecchio G, Maffulli N. Meniscectomy is associated with a higher rate of osteoarthritis compared to meniscal repair following acute tears: a meta-analysis. Knee Surgery, Sports Traumatology, Arthroscopy 2023;31:5485. https://doi.org/10.1007/S00167-023-07600-Y.

[429] Hurmuz M, Ionac M, Hogea B, Miu CA, Tatu F. Osteoarthritis Development Following Meniscectomy vs. Meniscal Repair for Posterior Medial Meniscus Injuries: A Systematic Review. Medicina 2024, Vol 60, Page 569 2024;60:569. https://doi.org/10.3390/MEDICINA60040569.

[430] Bhatia S, Laprade CM, Ellman MB, Laprade RF. Meniscal root tears: significance, diagnosis, and treatment. Am J Sports Med 2014;42:3016–30. https://doi.org/10.1177/0363546514524162.

[431] Husen M, Kennedy NI, Till S, Reinholz A, Stuart MJ, Krych AJ, et al. Benefits of Meniscal Repair in Selected Patients Aged 60 Years and Older. Orthop J Sports Med 2022;10. https://doi.org/10.1177/23259671221117491.

[432] Babalola OR, Laiyemo AE, Itapke SE, Madubueze C, Shodipo O, Okanu F, et al. ARTHROSCOPIC PARTIAL MENISCECTOMY - SHORT-TERM CLINICAL OUTCOME IN AN ORTHOPAEDIC CENTER IN SOUTHWESTERN NIGERIA. J West Afr Coll Surg 2017;7:1.

[433] Mao AS, Mooney DJ. Regenerative medicine: Current therapies and future directions. Proc Natl Acad Sci U S A 2015;112:14452–9. https://doi.org/10.1073/PNAS.1508520112.

[434] Lee KY, Mooney DJ. Alginate: properties and biomedical applications. Prog Polym Sci 2012;37:106–26. https://doi.org/10.1016/J.PROGPOLYMSCI.2011.06.003.

[435] Liu F, Chen Q, Liu C, Ao Q, Tian X, Fan J, et al. Natural Polymers for Organ 3D Bioprinting. Polymers 2018, Vol 10, Page 1278 2018;10:1278.

https://doi.org/10.3390/POLYM10111278.

[436] Mousavi A, Mashayekhan S, Baheiraei N, Pourjavadi A. Biohybrid oxidized alginate/myocardial extracellular matrix injectable hydrogels with improved electromechanical properties for cardiac tissue engineering. Int J Biol Macromol 2021;180:692–708. https://doi.org/10.1016/J.IJBIOMAC.2021.03.097.

[437] Kaviani S, Talebi A, Labbaf S, Karimzadeh F. Conductive GelMA/alginate/polypyrrole/graphene hydrogel as a potential scaffold for cardiac tissue engineering; Physiochemical, mechanical, and biological evaluations. Int J Biol Macromol 2024;259:129276. https://doi.org/10.1016/J.IJBIOMAC.2024.129276.

[438] Naveenkumar S, Venkateshan N, Kaviyarasu K, Christyraj JRSS, Muthukumaran A. Optimum performance of a novel biocompatible scaffold comprising alginate-pectin-selenium nanoparticles for cardiac tissue engineering using C2C12 cells. J Mol Struct 2023;1294:136457. https://doi.org/10.1016/J.MOLSTRUC.2023.136457.

[439] Thankam FG, Muthu J. Alginate–polyester comacromer based hydrogels as physiochemically and biologically favorable entities for cardiac tissue engineering. J Colloid Interface Sci 2015;457:52–61. https://doi.org/10.1016/J.JCIS.2015.06.034.

[440] Sathain A, Monvisade P, Siriphannon P. Bioactive alginate/carrageenan/calcium silicate porous scaffolds for bone tissue engineering. Mater Today Commun 2021;26:102165. https://doi.org/10.1016/J.MTCOMM.2021.102165.

[441] Ghorbani M, Vasheghani-Farahani E, Azarpira N, Hashemi-Najafabadi S, Ghasemi A. Dual-crosslinked in-situ forming alginate/silk fibroin hydrogel with potential for bone tissue engineering. Biomaterials Advances 2023;153:213565. https://doi.org/10.1016/J.BIOADV.2023.213565.

[442] Wang CC, Yang KC, Lin KH, Liu HC, Lin FH. A highly organized three-dimensional alginate scaffold for cartilage tissue engineering prepared by microfluidic technology. Biomaterials 2011;32:7118–26. https://doi.org/10.1016/J.BIOMATERIALS.2011.06.018.

[443] Olmos-Juste R, Larrañaga-Jaurrieta G, Larraza I, Ramos-Diez S, Camarero-Espinosa S, Gabilondo N, et al. Alginate-waterborne polyurethane 3D bioprinted scaffolds for articular cartilage tissue engineering. Int J Biol Macromol 2023;253:127070. https://doi.org/10.1016/J.IJBIOMAC.2023.127070.

[444] Hu L, Li T, Wu X, Yu L, Zeng G, Han M, et al. Stretchable Alginate/GelMA Interpenetrating Network (IPN) hydrogel microsprings based on coaxial microfluidic technique for skeletal muscle tissue engineering. Colloids Surf A Physicochem Eng Asp 2024;687:133502. https://doi.org/10.1016/J.COLSURFA.2024.133502.

[445] Chawla D, Kaur T, Joshi A, Singh N. 3D bioprinted alginate-gelatin based scaffolds for soft tissue engineering. Int J Biol Macromol 2020;144:560–7. https://doi.org/10.1016/J.IJBIOMAC.2019.12.127.

[446] Wei Q, Zhou J, An Y, Li M, Zhang J, Yang S. Modification, 3D printing process and application of sodium alginate based hydrogels in soft tissue engineering: A review. Int J Biol Macromol 2023;232:123450. https://doi.org/10.1016/J.IJBIOMAC.2023.123450.

[447] Freedman BR, Mooney DJ. Biomaterials to Mimic and Heal Connective Tissues. Adv Mater 2019;31. https://doi.org/10.1002/ADMA.201806695.

[448] Kalishwaralal K, Jeyabharathi S, Sundar K, Selvamani S, Prasanna M, Muthukumaran A. A novel biocompatible chitosan–Selenium nanoparticles (SeNPs) film with electrical conductivity for cardiac tissue engineering application. Materials Science and Engineering: C 2018;92:151–60. https://doi.org/10.1016/J.MSEC.2018.06.036.

[449] Raftery RM, Tierney EG, Curtin CM, Cryan SA, O'Brien FJ. Development of a gene-activated scaffold platform for tissue engineering applications using chitosan-pDNA nanoparticles on collagen-based scaffolds. Journal of Controlled Release 2015;210:84–94. https://doi.org/10.1016/J.JCONREL.2015.05.005.

[450] Bhardwaj N, Nguyen QT, Chen AC, Kaplan DL, Sah RL, Kundu SC. Potential of 3-D tissue constructs engineered from bovine chondrocytes/silk fibroin-chitosan for in vitro cartilage tissue engineering. Biomaterials 2011;32:5773–81. https://doi.org/10.1016/J.BIOMATERIALS.2011.04.061.

[451] Yang Y, Campbell Ritchie A, Everitt NM. Recombinant human collagen/chitosan-based soft hydrogels as biomaterials for soft tissue engineering. Materials Science and Engineering: C 2021;121:111846. https://doi.org/10.1016/J.MSEC.2020.111846.

[452] Liu J, Liu Z, Zhang X, Yang R, Xu D, Li X, et al. Nanocomposite hyaluronic acid adhesive hydrogel with controllable drug release for bone regeneration. Int J Biol Macromol 2024;274:133362. https://doi.org/10.1016/J.IJBIOMAC.2024.133362.

[453] Shim HE, Kim YJ, Park KH, Park H, Huh KM, Kang SW. Enhancing cartilage regeneration through spheroid culture and hyaluronic acid microparticles: A promising approach for tissue engineering. Carbohydr Polym 2024;328:121734. https://doi.org/10.1016/J.CARBPOL.2023.121734.

[454] Wang M, Deng Z, Guo Y, Xu P. Designing functional hyaluronic acid-based hydrogels for cartilage tissue engineering. Mater Today Bio 2022;17:100495. https://doi.org/10.1016/J.MTBIO.2022.100495.

[455] Lan X, Ma Z, Dimitrov A, Kunze M, Mulet-Sierra A, Ansari K, et al. Double crosslinked hyaluronic acid and collagen as a potential bioink for cartilage tissue engineering. Int J Biol Macromol 2024;273:132819. https://doi.org/10.1016/J.IJBIOMAC.2024.132819.

[456] Pitton M, Urzì C, Farè S, Contessi Negrini N. Visible light photo-crosslinking of biomimetic gelatin-hyaluronic acid hydrogels for adipose tissue engineering. J Mech Behav Biomed Mater 2024;158:106675. https://doi.org/10.1016/J.JMBBM.2024.106675.

[457] de Brito ACF, Sousa SM de, Morais HLO de, Costa PHM da, Medrado NV, Prado M de C, et al. Cutting-edge collagen biocomposite reinforced with 2D nano-talc for bone tissue engineering. Nanomedicine 2024;60:102756. https://doi.org/10.1016/J.NANO.2024.102756.

[458] Abbadessa A, Nuñez Bernal P, Buttitta G, Ronca A, D'Amora U, Zihlmann C, et al. Biofunctionalization of 3D printed collagen with bevacizumab-loaded microparticles targeting pathological angiogenesis. Journal of Controlled Release 2023;360:747–58. https://doi.org/10.1016/J.JCONREL.2023.07.017.

[459] Li C, Ge J, Guo Q, Wang J, Wu J, Yan Z, et al. Polyvinyl alcohol/collagen composite scaffold reinforced with biodegradable polyesters/gelatin nanofibers for adipose tissue engineering. Int J Biol Macromol 2024;263:130237. https://doi.org/10.1016/J.IJBIOMAC.2024.130237.

[460] Gelin A, Masson-Meyers D, Amini F, Moharamzadeh K, Tayebi L. Collagen: The superior material for full-thickness oral mucosa tissue engineering. J Oral Biosci 2024;66:511–8. https://doi.org/10.1016/J.JOB.2024.06.006.

[461] Peppas NA, Hoffman AS. Hydrogels. Biomaterials Science: An Introduction to Materials in Medicine 2020:153–66. https://doi.org/10.1016/B978-0-12-816137-1.00014-3.

[462] Sánchez-Cid P, Jiménez-Rosado M, Romero A, Pérez-Puyana V. Novel Trends in Hydrogel Development for Biomedical Applications: A Review. Polymers (Basel) 2022;14. https://doi.org/10.3390/POLYM14153023.

[463] Hennink WE, van Nostrum CF. Novel crosslinking methods to design hydrogels. Adv Drug Deliv Rev 2012;64:223–36. https://doi.org/10.1016/J.ADDR.2012.09.009.

[464] Aswathy SH, Narendrakumar U, Manjubala I. Commercial hydrogels for biomedical applications. Heliyon 2020;6:e03719. https://doi.org/10.1016/J.HELIYON.2020.E03719.

[465] Zhang W, Liu L, Cheng H, Zhu J, Li X, Ye S, et al. Hydrogel-based dressings designed to facilitate wound healing. Mater Adv 2024;5:1364–94. https://doi.org/10.1039/D3MA00682D.

[466] Gounden V, Singh M. Hydrogels and Wound Healing: Current and Future Prospects. Gels 2024;10. https://doi.org/10.3390/GELS10010043.

[467] Thang NH, Chien TB, Cuong DX. Polymer-Based Hydrogels Applied in Drug Delivery: An Overview. Gels 2023, Vol 9, Page 523 2023;9:523. https://doi.org/10.3390/GELS9070523.

[468] Lee KY, Mooney DJ. Hydrogels for tissue engineering. Chem Rev 2001;101:1869–79. https://doi.org/10.1021/CR000108X/ASSET/IMAGES/LARGE/CR000108XF00012.JPEG.

[469] Mantha S, Pillai S, Khayambashi P, Upadhyay A, Zhang Y, Tao O, et al. Smart Hydrogels in Tissue Engineering and Regenerative Medicine. Materials 2019;12. https://doi.org/10.3390/MA12203323.

[470] Verbeke CS, Mooney DJ. Injectable, Pore-Forming Hydrogels for In Vivo Enrichment of Immature Dendritic Cells. Adv Healthc Mater 2015;4:2677. https://doi.org/10.1002/ADHM.201500618.

[471] Najibi AJ, Shih TY, Mooney DJ. Cryogel vaccines effectively induce immune responses independent of proximity to the draining lymph nodes. Biomaterials 2022;281. https://doi.org/10.1016/J.BIOMATERIALS.2021.121329.

[472] Wu C, Zhang H, Guo Y, Sun X, Hu Z, Teng L, et al. Porous Hydrogels for Immunomodulatory Applications. International Journal of Molecular Sciences 2024, Vol 25, Page 5152 2024;25:5152. https://doi.org/10.3390/IJMS25105152.

[473] Silva CS, Reis RL, Martins A, Neves NM. Recapitulation of Thymic Function by Tissue Engineering Strategies. Adv Healthc Mater 2021;10:2100773. https://doi.org/10.1002/ADHM.202100773.

[474] Provin N, Giraud M. Differentiation of Pluripotent Stem Cells Into Thymic Epithelial Cells and Generation of Thymic Organoids: Applications for Therapeutic Strategies Against APECED. Front Immunol 2022;13:930963. https://doi.org/10.3389/FIMMU.2022.930963.

[475] Agarwalla P, Ogunnaike EA, Ahn S, Froehlich KA, Jansson A, Ligler FS, et al. Bioinstructive implantable scaffolds for rapid in vivo manufacture and release of CAR-T cells. Nat Biotechnol 2022;40:1250. https://doi.org/10.1038/S41587-022-01245-X.

[476] Primbetova A, Hsu HH, Baker A, Jones R, Zimmerman C, Shoichet M, et al. T-Cell Differentiation from Hematopoietic Progenitor Cells Using 3D Thymic-like Hydrogels. Https://HomeLiebertpubCom/Genbio 2024;3:136–51. https://doi.org/10.1089/GENBIO.2024.0010.

[477] Tajima A, Liu W, Pradhan I, Bertera S, Bagia C, Trucco M, et al. Bioengineering mini functional thymic units with EAK16-II/EAKIIH6 self-assembling hydrogel. Clinical Immunology 2015;160:82–9. https://doi.org/10.1016/J.CLIM.2015.03.010.

[478] Zeleniak A, Wiegand C, Liu W, McCormick C, Ravikumar K, Alavi A, et al. De novo construction of T cell compartment in humanized mice engrafted with iPSC-derived thymus organoids. Nature Methods 2022 19:10 2022;19:1306–19. https://doi.org/10.1038/s41592-022-01583-3.

[479] Hong J, Zhu Z, Cui L, Wang Z, Hao Y, Tian X, et al. Bone marrow-inspired hydrogel/graphene composite scaffolds to support in vitro expansion of hematopoietic stem cells. J Mater Chem B 2024;12:2354–63. https://doi.org/10.1039/D3TB02448B.

[480] Purwada A, Shah SB, Béguelin W, August A, Melnick AM, Singh A. Ex vivo synthetic immune tissues with T cell signals for differentiating antigen-specific, high affinity germinal center B cells. Biomaterials 2019;198:27–36. https://doi.org/10.1016/J.BIOMATERIALS.2018.06.034.

[481] Lawko N, Plaskasovitis C, Stokes C, Abelseth L, Fraser I, Sharma R, et al. 3D Tissue Models as an Effective Tool for Studying Viruses and Vaccine Development. Front Mater 2021;8:631373. https://doi.org/10.3389/FMATS.2021.631373/BIBTEX.

[482] Urzì O, Gasparro R, Costanzo E, De Luca A, Giavaresi G, Fontana S, et al. Three-Dimensional Cell Cultures: The Bridge between In Vitro and In Vivo Models. Int J Mol Sci 2023;24. https://doi.org/10.3390/IJMS241512046.

[483] Gerardo-Nava JL, Jansen J, Günther D, Klasen L, Thiebes AL, Niessing B, et al. Transformative Materials to Create 3D Functional Human Tissue Models In Vitro in a Reproducible Manner. Adv Healthc Mater 2023;12:2301030. https://doi.org/10.1002/ADHM.202301030.

[484] Cacciamali A, Villa R, Dotti S. 3D Cell Cultures: Evolution of an Ancient Tool for New Applications. Front Physiol 2022;13. https://doi.org/10.3389/FPHYS.2022.836480.

[485] Cruz Walma DA, Yamada KM. The extracellular matrix in development. Development

2020;147:dev175596. https://doi.org/10.1242/DEV.175596.

[486] Tiemeijer LA, Sanlidag S, Bouten CVC, Sahlgren CM. Engineering tissue morphogenesis: taking it up a Notch. Trends Biotechnol 2022;40:945–57. https://doi.org/10.1016/J.TIBTECH.2022.01.007.

[487] Nam S, Gupta VK, Lee H pyo, Lee JY, Wisdom KM, Varma S, et al. Cell cycle progression in confining microenvironments is regulated by a growth-responsive TRPV4-PI3K/Akt-p27Kip1 signaling axis. Sci Adv 2019;5. https://doi.org/10.1126/SCIADV.AAW6171.

[488] Chaudhuri O, Gu L, Klumpers D, Darnell M, Bencherif SA, Weaver JC, et al. Hydrogels with tunable stress relaxation regulate stem cell fate and activity. Nature Materials 2015 15:3 2015;15:326–34. https://doi.org/10.1038/nmat4489.

[489] Barriga EH, Mayor R. Adjustable viscoelasticity allows for efficient collective cell migration. Semin Cell Dev Biol 2019;93:55–68. https://doi.org/10.1016/J.SEMCDB.2018.05.027.

[490] Tissue Engineering and Regenerative Medicine n.d. https://www.nibib.nih.gov/science-education/science-topics/tissue-engineering-and-regenerative-medicine (accessed October 22, 2024).

[491] Brockbank KGM. Tissue Engineering Constructs and Commercialization 2013.

[492] Zhu J, Ji L, Chen Y, Li H, Huang M, Dai Z, et al. Organoids and organs-on-chips: insights into predicting the efficacy of systemic treatment in colorectal cancer. Cell Death Discovery 2023 9:1 2023;9:1–12. https://doi.org/10.1038/s41420-023-01354-9.

[493] Zeleniak A, Wiegand C, Liu W, McCormick C, Ravikumar K, Alavi A, et al. De novo construction of T cell compartment in humanized mice engrafted with iPSC-derived thymus organoids. Nature Methods 2022 19:10 2022;19:1306–19. https://doi.org/10.1038/s41592-022-01583-3.

[494] Gao H, Cao M, Deng K, Yang Y, Song J, Ni M, et al. The Lineage Differentiation and Dynamic Heterogeneity of Thymic Epithelial Cells During Thymus Organogenesis. Front Immunol 2022;13:805451. https://doi.org/10.3389/FIMMU.2022.805451/BIBTEX.

[495] Gordon J, Manley NR. Mechanisms of thymus organogenesis and morphogenesis. Development 2011;138:3865. https://doi.org/10.1242/DEV.059998.

[496] Hoare DG, Koshland DE. A Method for the Quantitative Modification and Estimation of Carboxylic Acid Groups in Proteins. Journal of Biological Chemistry 1967;242:2447–53. https://doi.org/10.1016/S0021-9258(18)95981-8.

[497] Rowley JA, Madlambayan G, Mooney DJ. Alginate hydrogels as synthetic extracellular matrix materials. Biomaterials 1999;20:45–53. https://doi.org/10.1016/S0142-9612(98)00107-0.

[498] Liang Z, Dong X, Zhang Z, Zhang Q, Zhao Y. Age-related thymic involution: Mechanisms and functional impact. Aging Cell 2022;21:e13671. https://doi.org/10.1111/ACEL.13671.

[499] Boehm T, Swann JB. Thymus involution and regeneration: two sides of the same coin? Nature Reviews Immunology 2013 13:11 2013;13:831–8. https://doi.org/10.1038/nri3534.

[500] Busse PJ, Mathur SK. Age-related changes in immune function: Effect on airway inflammation. Journal of Allergy and Clinical Immunology 2010;126:690–9. https://doi.org/10.1016/J.JACI.2010.08.011.

[501] Chaudhuri O, Koshy ST, Branco Da Cunha C, Shin JW, Verbeke CS, Allison KH, et al. Extracellular matrix stiffness and composition jointly regulate the induction of malignant phenotypes in mammary epithelium. Nature Materials 2014 13:10 2014;13:970–8. https://doi.org/10.1038/nmat4009.

[502] Manalili D, Berardi M, Aardema H, Asimaki K, Sarmiento R, Imran Akca B. Parallel-plate compression test for soft materials: confocal microscopy-assisted ferrule-top nanoindentation. Biomed Opt Express 2022;13:824. https://doi.org/10.1364/BOE.447147.

[503] Nabavizadeh A, Kinnick RR, Bayat M, Amador C, Urban MW, Alizad A, et al. Automated Compression Device for Viscoelasticity Imaging. IEEE Trans Biomed Eng 2016;64:1535. https://doi.org/10.1109/TBME.2016.2612541.

[504] Arevalo SE, Ebenstein DM, Pruitt LA. A methodological framework for nanomechanical characterization of soft biomaterials and polymers. J Mech Behav Biomed Mater 2022;134:105384. https://doi.org/10.1016/J.JMBBM.2022.105384.

[505] Griffith A V., Cardenas K, Carter C, Gordon J, Iberg A, Engleka K, et al. Increased thymus- and decreased parathyroid-fated organ domains in Splotch mutant embryos. Dev Biol 2008;327:216. https://doi.org/10.1016/J.YDBIO.2008.12.019.

[506] Parent A V., Russ HA, Khan IS, Laflam TN, Metzger TC, Anderson MS, et al. Generation of functional thymic epithelium from human embryonic stem cells that supports host T cell development. Cell Stem Cell 2013;13:219–29. https://doi.org/10.1016/j.stem.2013.04.004.

[507] Anderson G, Jenkinson EJ, Moore NC, Owen JJT. MHC class II-positive epithelium and mesenchyme cells are both required for T-cell development in the thymus. Nature 1993 362:6415 1993;362:70–3. https://doi.org/10.1038/362070a0.

[508] Seet CS, He C, Bethune MT, Li S, Chick B, Gschweng EH, et al. Generation of mature T cells from human hematopoietic stem and progenitor cells in artificial thymic organoids. Nature Methods 2017 14:5 2017;14:521–30. https://doi.org/10.1038/nmeth.4237.

[509] Odaka C, Loranger A, Takizawa K, Ouellet M, Tremblay MJ, Murata S, et al. Keratin 8 Is Required for the Maintenance of Architectural Structure in Thymus Epithelium. PLoS One 2013;8:e75101. https://doi.org/10.1371/JOURNAL.PONE.0075101.

[510] Balciunaite G, Keller MP, Balciunaite E, Piali L, Zuklys S, Mathieu YD, et al. Wnt glycoproteins regulate the expression of FoxN1, the gene defective in nude mice. Nature Immunology 2002 3:11 2002;3:1102–8. https://doi.org/10.1038/ni850.

[511] Romano R, Palamaro L, Fusco A, Giardino G, Gallo V, Del Vecchio L, et al. FOXN1: A

master regulator gene of thymic epithelial development program. Front Immunol 2013;4:53666. https://doi.org/10.3389/FIMMU.2013.00187/BIBTEX.

[512] Vaidya HJ, Briones Leon A, Blackburn CC. FOXN1 in thymus organogenesis and development. Eur J Immunol 2016;46:1826. https://doi.org/10.1002/EJI.201545814.

[513] Campinoti S, Gjinovci A, Ragazzini R, Zanieri L, Ariza-McNaughton L, Catucci M, et al. Reconstitution of a functional human thymus by postnatal stromal progenitor cells and natural whole-organ scaffolds. Nature Communications 2020 11:1 2020;11:1–16. https://doi.org/10.1038/s41467-020-20082-7.

[514] Schnell U, Cirulli V, Giepmans BNG. EpCAM: Structure and function in health and disease. Biochimica et Biophysica Acta (BBA) - Biomembranes 2013;1828:1989–2001. https://doi.org/10.1016/J.BBAMEM.2013.04.018.

[515] Paessens LC, Singh SK, Fernandes RJ, van Kooyk Y. Vascular cell adhesion molecule-1 (VCAM-1) and intercellular adhesion molecule-1 (ICAM-1) provide co-stimulation in positive selection along with survival of selected thymocytes. Mol Immunol 2008;45:42–8. https://doi.org/10.1016/J.MOLIMM.2007.05.016.

[516] Thompson AJ, Pillai EK, Dimov IB, Foster SK, Holt CE, Franze K. Rapid changes in tissue mechanics regulate cell behaviour in the developing embryonic brain. Elife 2019;8. https://doi.org/10.7554/ELIFE.39356.

[517] Barriga EH, Franze K, Charras G, Mayor R. Tissue stiffening coordinates morphogenesis by triggering collective cell migration in vivo. Nature 2018 554:7693 2018;554:523–7. https://doi.org/10.1038/nature25742.

[518] Ershad-Langroudi A, Babazadeh N, Alizadegan F, Mehdi Mousaei S, Moradi G. Polymers for implantable devices. Journal of Industrial and Engineering Chemistry 2024;137:61–86. https://doi.org/10.1016/J.JIEC.2024.03.030.

[519] Kurowiak J, Klekiel T, Będziński R. Biodegradable Polymers in Biomedical Applications: A Review—Developments, Perspectives and Future Challenges. Int J Mol Sci 2023;24. https://doi.org/10.3390/IJMS242316952.

LIST OF ABBREVIATIONS

LIST OF ABBREVIATIONS

A

A: Area
ACAs: Alkyl-2-cyanoacrylates
ACN: Acetonitrile
ADAMTS: A disintegrin-like and metalloproteinase with thrombospondin motif
Al_2O_3: Aluminum oxide (Alumina)
APC: Antigen-presenting cells
Amo: Amoxicillin
Ara-C: Cytosine arabinoside hydrochloride
Asp: Aspirin
ATBC: Acetyl Tributyl Citrate

B

BDDE: 1,4-butanediol diglycidyl ether
BSA: Bovine serum albumin
Buf: Buffer

C

C: Circularity
C-HA: Catechol modification of hyaluronic acid
$CaSO_4$: Calcium sulfate dihydrate
CAR: Chimeric antigen receptor
CCL2: C-C motif chemokine ligand 2
CD: Cluster of differentiation
CMC: Carboxymethyl cellulose
CN: Cyano
COOH: Carboxyl
COOR: Ester
Co-Cr-Mo: Cobalt-Chromium-Molybdenum
CoCr: Cobalt-Chromium
CsA: Cyclosporin A
CVD: Chemical vapor deposition

D

DAMP: Damage-associated molecular pattern
DC: Dendritic cell
DCF: Diclofenac
DEX: Dexamethasone

DL: Drug loading
DLL: Delta-like ligand
DoE: Design of experiments
DN: Double negative
DP: Double positive
DSP: Dexamethasone sodium phosphate
DSC: Differential scanning calorimetry
DAMP: Damage-associated molecular patterns
DMA: Dynamic mechanical analysis

E

EAK: Endothelial-adipocyte kinase
ECA: Ethyl-2-cyanoacrylate
EHT: Electron high tension
EpCAM: Epithelial cell adhesion molecule
ETO: Ethylene oxide
EMT: Epithelial-mesenchymal transition

F

F: Force
fs: femtosecond
FBR: Foreign body reaction
FDA: Food and Drug Administration
FESEM: Field emission scanning electron microscopy
FOXN1: Forkhead-box n1

G

GF: Graphene foam
GM-CSF: Granulocyte-macrophage colony-stimulating factor
GOPs: (3-Glycidyloxypropyl) trimethoxysilane
G': Storage modulus
G": Loss modulus

H

HA: Hyaluronic acid
H&E: Hematoxylin and Eosin

HCl: Hydrochloride
HMDMs: Human monocyte-derived macrophages
HMW: High molecular weight
hESC: Human embryonic stem cells
HSC: Hematopoietic stem cells
hPSC: Human pluripotent stem cells

I

IA: Intra-articular
IHC: Immunohistochemistry
IFN: Interferon
IL: Interleukin
iNOS: Inducible nitric oxide synthase
IPN: Interpenetrating polymer network
IOLs: Intraocular lenses
IV: Intrinsic viscosity

K

K8: Keratin 8

L

LAL: Limulus amebocites lisate
LA:GA: Lactic acid:glycolic acid
LbL: Layer-by-layer
LECs: Lens epithelial cells
LOD: Limit of detection
LOQ: Limit of quantification
LMW: Low molecular weight
LPS: Lipopolysaccharide

M

M0: Unactivated macrophages
M1: Activated macrophages
M2: Activated macrophages
Mag: Magnification
MAL: Maleimide

MCL: Medial collateral ligament
MeOH: Methanol
MKP-1: Mitogen-activated protein kinase phosphatase-1
Ms: Mouse
MTP: Medial tibial plateau

N

NaN3: Sodium azide
NCCs: Neural crest cells
ns: Non significative
NSAID: Non-steroidal anti-inflammatory drug

O

OA: Osteoarthritis
Ox-HA: Oxidized hyaluronic acid

P

PAI: Polyamide-imide
PCL: Poly(caprolactone)
PCU: Polycarbonate urethane
PDDA: Poly-diallyl dimethylammonium
PDGF: Platelet-derived growth factor
PDS: Polydioxanone suture
PFA: Paraformaldehyde
PEG: Polyethylene glycol
PLA: Poly(lactic acid)
PLA-PEG: Poly(lactic acid)-poly(ethylene glycol) di-block copolymer
PLGA: Poly(lactic-co-glycolic acid)
PLLA: Poly(L-lactide)
PMMA: Polymethyl methacrylate
POM: Polyoxymethylene
PSS: Poly-styrene sulfonate
PTFE: Polytetrafluoroethylene
PVA: Polyvinyl alcohol
PGE2: Prostaglandin E2
P: Perimeter
Pos: Positive control

R

R^2: Correlation coefficient
RIMP: Rifampicin
ROS: Reactive oxygen species

S

SSF: Simulated synovial fluid

T

τ: stress
TB: Toluidine blue
TCR: T cell receptor
TEC: Thymic epithelial cells
TEPC: Thymic epithelial progenitor cells
TFA: Trifluoracetic acid
TGF: Transforming growth factor
Th: T Helper
Tg: Glass transition temperature
TCC: Cold crystallization temperature
Tm: Melting temperature

U

UPLC: Ultraperformance liquid chromatography
UV: Ultraviolet

V

v: Poisson's ratio
VCAM: Vascular cell adhesion molecule
v/v: Volume to volume

W

w/v: Weight to volume
w/w: Weight to weight

X

Xc: Crystallinity

Y

YM1: Chitinase-like protein

Z

Zn: Zinc
ZrO_2: Zirconium dioxide

ETHICAL CONSIDERATIONS

ETHICAL CONSIDERATIONS

Cell culture

Studies using human-derived monocytes in Chapter 1 were conducted at Humanitas Research Institute (Milano, Italy) in accordance with Italian and European law. Monocytes were isolated from the buffy coats of blood donations. Buffy coats were obtained from anonymous healthy blood donors at Instituto Clinico Humanitas (ICH) (Milano, Italy). The ethical committee at ICH provides favorable confirmation for their use in basic scientific research activities. Their use does not involve any ethical problem regarding the informed consent or the privacy of the donor.

The human embryonic stem cells (hESCs) used in Chapter 3 of the thesis are the cell line WA01 (H1), which has the National Institute of Health (NIH) Approval number NIHhESC-10-0043. Chapter 3 of the thesis was carried out in Boston (USA) in 2024.

The cell line received NIH approval on 01/29/2010. It is available for distribution by provider WiCell Research Institute. The cell line does not present any NIH restriction. The NIH has developed its current NIH Human Embryonic Stem Cell Registry comprised of lines that have been submitted, reviewed, and judged eligible for use in NIH-funded research per the 2009 NIH Guidelines on Human Stem Cell Research. For more information on this process, please refer to NOT-OD-10-020 (December 2, 2009) "First Human Embryonic Stem Cells Approved for use under the NIH Guidelines for Human Stem Cell Research" https://stemcells.nih.gov/registry/eligible-to-use-lines. Thymic epithelial progenitor cells (TEPCs) and neural crest cells (NCCs) were derived from this H1 cell line.

Animal studies

The animal studies in Chapter 2 were conducted in Israel at Shamir Medical Center and approved by the Shamir Medical Center Institutional Animal Care and Use Committee under permit number AHMC-IL-2303-115-3. When sheep displayed excessive discomfort, they were euthanized using potassium chloride at the end of the experiment or before. Alternatives to the study were examined in Good Search Practice on Animal Alternative-EU and deemed unsuitable for the experiment's needs. Dr. Emmanuel Loeb carried out a histopathology evaluation at Patho-Logica, Ltd. (Israel) under study number HUM-1549-HIS.

Furthermore, even though not included in this PhD thesis and due to the situation in Israel, animal studies in sheep also received approval from Ministero della Salute Italiano autorizzazione 388/2024-PR (Risp. a prot. 30111.29) to be carried out in Bari (Italy).

COMITATO ETICO INDIPENDENTE
Istituto Clinico Humanitas - IRCCS

14.11.2012

"Il Comitato etico di ICH ha esaminato il caso di impiego per attività di ricerca scientifica di base di "*buffycoats*" provenienti da processamento di campioni di sangue prelevati da donatori volontari sani e forniti a ICH da centri trasfusionali autorizzati.
I *buffy coats* vengono forniti sulla base di specifiche convenzioni in sacche anonimizzate completamente despletate da piastrine per cui essi "sono da ritenere scarti finali del frazionamento del sangue donato" non più quindi riutilizzabili per fini trasfusionali né per produzione di farmaci emoderivati.
Il Comitato etico di ICH ha pertanto espresso parere favorevole in via generale al loro impiego in attività di ricerca di base non rilevando l'insorgere di problematiche etiche in ordine al consenso informato e sotto il profilo della tutela della *privacy* del donatore."

Il Segretario
Dott. Michele Tedeschi

Rozzano, 14 Novembre 2012

Istituto Clinico Humanitas
Via Manzoni 56
20089 Rozzano (Milano)
Telefono 02.8224.7216
Fax 02.8224.7208

המרכז הרפואי אסף הרופא - הוועדה המוסדית לניסויים בבעלי חיים

Shamir Medical Center - Institutional Animal Care and Use Committee

אישור לעריכת ניסוי עם בעלי חיים

Permit for an Animal Experiment Protocol

Permit number	AHMC - IL - 2303 - 115 - 3		אישור ניסוי מספר
Valid	from 12/03/2023	מ	תוקף האישור
	to 12/03/2027	עד	
Awarded to	Udi Willenz	אודי וילנץ	ניתן ל
Institute name	Shamir Medical Center	המרכז הרפואי אסף הרופא	שם המוסד

Species	Quantity of animals מספר בעלי החיים	סוג בעלי חיים
Swine		חזיר
Sheep	18	כבש

הועדה המוסדית לניסויים בבע"ח בחנה את בקשתך לעריכת ניסויים בבעלי חיים בבקשת המחקר שכותרתה:

טיפול באובדן מניסקוס חלקי באופן שמונע OA (osteo arthritis) שלאחר כריתת המניסקוס בברך במודל כבש

ומצאה אותה מתאימה לאישור בהתאם לחוק צער בעלי חיים - ניסויים בבעלי חיים התשנ"ד. הנך מתבקש שלא לסטות מהפרוצדורות המפורטות בבקשה מבלי לקבל את אישור הוועדה המוסדית לניסויים בבע"ח.

The institutional amimal care and use committee reviewed your application to conduct experiments in animals in the research proposal entitled:

To treat partial meniscus loss in a way that prevents an epidemic of post-meniscectomy knee OA in sheep model

And found it acceptable for approval according to the Animal Welfare Law – Expermients in Animals 1994. You are requested not to deviate from the procedures outlines in you application without the approval of the IACUC.

Chairman IACUC		שי אפרתי	יו"ר הועדה המוסדית
Signature			חתימה
Date	12/03/2023		תאריך

Approval No. 3 – 115 – 2303 – IL –AHMC
The Institute Name - Shamir Medical Center (Assaf Harofeh)

The Study

The Study Subject in Hebrew	To treat partial meniscus loss in a way that prevents an epidemic of postmeniscectomy knee OA in sheep model
The Study Subject in English	To treat partial meniscus loss in a way that prevents an epidemic of postmeniscectomy knee OA in sheep model
Is this a Continued Study?	New
The Previous Study No.	
Is it a Service Study for a Third-Party Institute?	
The Ordering Institute Name	Mefisto
The Ordering Researcher Name	
The Approving Party in the Ordering Institute	
The Approval Term (in Years)	4 Years
The Study Premises	In the institute itself

And _____ _____

Identification Type	ID	Identification No.	
Forename in Hebrew		Surname in Hebrew	
Forename in English		Surname in English	
Institute Name	Shamir Medical Center (Assaf Harofeh)		
Date of birth		Email	
Phone No.		Another Phone	
Department		Faculty	Shamir Medical Center (Assaf Harofeh)
Qualification no. in the Study Institute	MD2031017		

Participants in the Study and their Qualifications

Participant No. 1:

Surname	Forename	ID/Passport No.	Relation to the Study	Qualified
			Study participant	Yes

Qualification

No.	Certification No.	Certification Granting Institute	Animal Type

The Experiment Details

Primary Objective	Promoting health, medicine, and alleviation of suffering Testing or producing materials or items
Secondary Objective	

Summary of Study and the Purpose of Using Animals in the Study

What is the scientific topic under investigation?	The most common method for the treatment of meniscal lesions worldwide remains meniscectomy. An estimated 700,000 to over 1 million arthroscopic partial meniscectomies performed annually in the U.S., associated with estimated annual direct medical costs of $4 billion. The frequency of meniscal sutures is 10-times lower, when compared with meniscectomy. Meniscal substitution with allografts represents an infinitesimal part of the treatment, being applied 600 times less than meniscectomy. The consequence of meniscectomy is well known, however the potential impact on certain sectors of the population with risk factors predisposing them to more rapid OA progression, is significantly underestimated. MEFISTO aims to provide a clear definition of these morphological risk factors and an algorithm for personalized treatment of these patients. Currently there are no guidelines or any predictive factors for the progression of OA of the knee post meniscectomy. The early identification and treatment of high risk patients pre-disposed to OA after meniscectomy is vital. Currently most patients present to the surgeon when OA is already established and it is too late for reconstructive procedures, thus leading to sacrifice of the joint. Moreover, the project will provide clear socio-economic analysis of meniscal substitution in Europe. The ambition of the present project is to provide a meniscal substitute ready for clinical trials that will promote revascularization of the meniscal scaffold in its peripheral zone, while leaving a central avascular zone, mimicking the native meniscal tissue and to transform existing unloading prosthesis into an active drug delivery system, capable of controlling the inflammatory environment in the joint. Extremely innovative technologies including patient specific customized 3D-bioprinting, dendrimer functionalised bio-inks and GFs

	loaded nano/micro-particles will be utilised to achieve this aim. Simultaneous control of the mechanical and inflammatory environment is an innovative concept, which unlocks enormous. possibilities for the development of this system for OA treatment
What is the relevant background to the study?	MEFISTO will develop two novel solutions to treat meniscus loss as a strategy for preventing the onset of an epidemic of post-meniscectomy knee osteoarthritis (OA) in Europe Morphological profiling will identify the population of patients who, after meniscal resection, are at higher risk of early compartment degeneration, providing a personalized approach for the patient. The two different: reconstructive strategies are: i) a controlled vascularized bioactive biodegradable meniscal scaffold, which will regenerate the native meniscus. This strategy will address younger patients with. early osteoarthritic changes ii) a bioactive non-biodegradable meniscal prosthesis, which will act as a mechanical unloading device and a drug delivery system, with the capacity to modulate the inflammatory environment. This strategy will address patients with advanced OA
What is the specific study question in the request and the scientific rationale behind it?	A socio-economic analysis of the efficacy of existing meniscal substitutes will complete the project. This analysis is of vital importance for the European healthcare system, as it will provide a clear understanding of the costs and benefits of current clinical practice and predict the impact of the two new interventions. The technological innovation lies in the development of biologically active functionalized nanobiomaterials that can interact with the surrounding articular tissues. The biodegradable scaffold will promote revascularization in the peripheral zone, while leaving the inner zone avascular, reflecting the native meniscal tissue and functionalization with modulation of inflammation.

	The impact is expected to be significant as so many patients have undergone or will undergo meniscectomy. The interventions developed in MEFISTO will prevent these patients from receiving joint-sacrificing procedures such as metal prosthesis whilst reducing the social burden, associated costs and high levels of morbidity resulting from OA.
What is the proposed use of animals, and why is it suitable to address the study question?	In vivo animal models are essential and instructive to understanding the performance of the scaffolds prior to implantation into patients. These assessments can then be used to develop further iterations to improve scaffold performance and surgical implantation technique before use in a clinical setting. Furthermore, the aim of MEFISTO is to develop a meniscal substitute that translates to the clinic and so this is vital for understanding how the scaffold performs.
What are the anticipated outcomes of this research?	The in vivo animal models will provide the basis for understanding the performance of the prosthesis in a clinical situation and will provide important feedback for improving the meniscal scaffold design and the implantation surgical technique. The expected output of this study is to determine if the designed scaffold, and its implant surgical technique, are suitable for human. implantation or if there are any technical improvements to be made.
Please provide a justification for utilizing animals for this study.	After the initial laboratory proof-of-concept stage, there is a need to progress with tests on large, weight-bearing animals that optimally replicate the physiology of human bone formation, enabling an understanding and examination of these mechanisms.
Were there any phases in the research conducted using alternative methods?	Yes
Details of prior experiments.	Preliminary studies were performed using in vitro models to choose appropriate models for evaluating meniscus substitutes, based on their clinical application.
Were alternatives considered?	Yes

The methodology of searching for alternatives.	Good Search Practice on Animal Alternative-EU
Detail alternative search method	
Results of the search for alternatives.	The selected model cannot be replicated in a lab or through a numerical model as they necessitate the physiological conditions and the tissue's response to the apparatus over time, and tissues will also be taken for histopathology; hence, long-term animal trials are essential.

Animals Required for the Study

No.	Animal	Quantity
1	Sheep	18

Group No. 1			
Animal	Sheep	Breed	
Sex		Quantity	
Age		Age Duration	
Weight		Weight Unit	
Animal source		Other Source	
Genetically modified	No		
The group specific question	To treat partial meniscus loss in a way that prevents an epidemic of post meniscectomy knee OA in sheep model	What is the enrichment provided to the animal and why	Your enrichment is the method in which they are held as a group
Method of Animal Maintenance	Group	Duration of Maintenance	

Animal	Sheep	Species	assaf
Sex	Female	Quantity	18
Age	6	Age Duration	Month
Weight	70	Weight Unit	KG
Animal Source	External Source	Another source	External Source
Genetically modified	No		

Reasoning for Selection and Overview of the Experiment Process

Reason for selecting the species, breed, and gender of the animals:	For the objectives of this study, dissecting large animals capable of bearing weight is essential, and sheep have been selected for their close physiological resemblance to humans. Sheep have meniscal anatomy that is most comparable to humans. The surgical accessibility to the tibia bone in sheep is more convenient compared to other animals like pigs. The bone structure of a pig is shorter than that of a sheep and hence less suitable. Considering the variance in animal weight, a crucial aspect for this study, pigs gain weight more rapidly than sheep. Keeping a consistent weight is vital to avoid alterations in the load on the legs.
Is this study driven by regulatory requirements?	No
Justification for the number of animals used.	The minimum number of animals needed to obtain statistically and biologically valid results will be used. The study will involve 18 sheep, a sufficient number for evaluation and statistical comparison between experimental groups. The quantity per group is determined by literature and the team's prior experience, using statistical data, with 6 animals serving in each group. Group 1 - Meniscectomy – six animals, Group 2 - Bioactive Implant - six animals, Group 3 - Control Group, Non bioactive implant - six animals Total: 18 animals.
Outline of the Procedure on Animals and Their Care	The experiment will be conducted on 18 sheep for a period of up to 3 months. Acclimation and Anaesthesia: After an acclimation period at the farm of at least 5 days, the animals will undergo a clinical examination by the institutional veterinarian to determine their suitability for inclusion in the experiment. Animals that are indeed found suitable according to the veterinarian's clinical examination will be transported on the day of the surgery from the farm to the research unit. The animals will be anesthetized using a mixture of ketamine and xylazine, IM/IV. Once initial anaesthesia is achieved, venflon will be inserted into the ear vein, midazolam will be administered IV as needed, according to the instructions of the institutional veterinarian. An appropriate tube will be inserted into the trachea, the animal will be connected to the anaesthesia machine, and it will be anesthetized with isoflurane. During the procedure, the animal's condition will be monitored: ECG, arterial blood pressure, $ETCO_2$, temperature.

	Procedure: All animals will undergo a meniscectomy procedure. A bone of 2-4 mm thickness within the proximal origin of the medial collateral ligament will be removed from the femoral condyle surface using an oscillating saw to perform a 30° osteotomy and ostectomy to achieve better exposure of the joint and the medial meniscus. 6 animals will serve as control without implantation; remnants of the medial meniscus will be removed along with the bone luwars to create space for the meniscal implant. 6 animals will be implanted with a Bioactive Implant and 6 with a Non-bioactive Implant. The joint will be properly rinsed. The incision will be closed and all facias will be sutured. After the surgery, a sufficient dose of LPS will be injected into the target knee to induce intra-articular inflammation. The purpose of this intervention is to evaluate whether the bioactive implant (loaded with dexamethasone and celecoxib) can reduce intra-articular inflammation. All animals will be monitored for up to 3 months. During the follow-up: In the initial days, animals will have walking restrictions and confined spaces per the instructions of the institutional veterinarian. The institutional veterinarian will conduct a clinical examination once a week during the experiment, focusing on signs of pain in the limbs, inability or difficulty standing on the legs. The clinical health status of the sheep and intra-articular inflammation will be assessed by US and blood tests. All animals will be sacrificed after 3 months with an overdose of KCL IV. The implants and the whole joints will be taken for histological and biochemical evaluations.
Detailing the required follow-up	
Whether anaesthesia materials were used	Yes
Anaesthesia materials	Material Name ; Reason ; Regime ; Dose
Whether pain relievers were used?	Yes
Pain relievers	Material Name ; Reason ; Regime ; Dose
Degree of pain and suffering during and after the experiment	3rd Degree
Conditions for discontinuing a specific animal's participation in the experiment	If one or more of the following occur, during or after experiments, the animal will be euthanized and discontinuation of the experiment will be considered, as per the decision of the institutional veterinarian: If the animal shows signs of pain or distress, which are untreatable with pain relievers. If there are significant changes in their appearance in physiological parameters such as heart rate and breathing or in social behaviour. Any animal showing signs of distress like prolonged lying beyond acceptable, anorexia, aggressive behaviour. Animals should not show signs of self-harm, anorexia, dehydration, overactivity, lying or prolonged lying beyond acceptable, increased vocalization, especially aggressive behaviour, or signs of isolation. An animal that does not feed itself for 48 hours. An

	animal that does not drink by itself for 24 hours. Swelling and/or inflammation and/or infection that are untreatable. A decrease of more than 10% in the animal's body weight during the experiment. If there is injury during the procedure to the oral/nasal cavity that could cause suffering/injury to the animal. In all cases, the decision to discontinue an animal's participation in the experiment and/or to discontinue the experiment is in the hands of the institutional veterinarian.
Specific Criteria for Ceasing Participation	If an animal has a bone injury preventing it from standing or accessing food and water, exhibits signs of leg pain unresponsive to pain relievers, or has leg wounds that are untreatable, leading to an inability to walk or stand, then participation in the experiment may need to be ceased. In any situation, the decision to cease an animal's participation in the experiment and/or to terminate the experiment is at the discretion of the institutional veterinarian.
Has the animal for which permission is sought already been involved in a prior experiment?	No
The previous experiment no.	

The fate of the animal post-experiment	Euthanasia
Method of Euthanasia	Potassium Chloride

Declaration of the Main Researcher

Declarations

Histopathology Evaluation Report - Declaration and Signature

I hereby declare that the histological evaluation of this study was performed and reported based on the OECD principles of Good Laboratory Practice ENV/MC/CHEM (98)17. However, it does not fully comply with GLP regulations and thus is considered a non-GLP study.

The tested items are original materials provided by the Sponsor and analyzed by Patho-Logica Ltd. The evaluation was conducted by a veterinary pathologist expert, license no. 436.

Emmanuel Loeb
Vet. Path
Specialist. Patho-Logica

Date 17/12/2023

0014650-03/05/2024-DGSAF-MDS-P

Ministero della Salute

DIPARTIMENTO DELLA SALUTE UMANA, DELLA SALUTE ANIMALE
E DELL'ECOSISTEMA (ONE HEALTH) E DEI RAPPORTI INTERNAZIONALI
EX DIREZIONE GENERALE DELLA SANITÀ ANIMALE E DEI FARMACI
VETERINARI – UFFICIO 6

Università degli Studi di Bari
pec: universitabari@pec.it
c.a. Prof. Luca LACITIGNOLA
email: luca.lacitignola@uniba.it

e, per conoscenza

ASL BA SIAV C
pec: siavcsud.aslbari@pec.rupar.puglia.it
c.a. Dr. Domenico Roberto CENTOLA
email: domenicoroberto.centola@asl.bari.it
c.a. Dr. Daniele TULLIO
email: daniele.tullio@asl.bari.it

OGGETTO: D.lgs. 26/2014 sulla protezione degli animali utilizzati a fini scientifici.
Trasmissione autorizzazione ai sensi dell'art. 31 del D.lgs. 26/2014.
Autorizzazione **n° 388/2024-PR (Risp. a prot. 30111.29)**

Si trasmette, in allegato, l'autorizzazione in oggetto.

IL DIRETTORE DELL'UFFICIO 6 Ex DGSAF
Dr. Vincenzo Ugo SANTUCCI
Firmato digitalmente da
Vincenzo Ugo Santucci
C = IT

Documento prodotto in originale informatico e firmato digitalmente ai sensi del "Codice dell'Amministrazione Digitale" (d.lgs. n. 82/2005 e ss.mm.)

Referente: G. Aleandri - sperimentazioneanimale@sanita.it

Ministero della Salute

DIPARTIMENTO DELLA SALUTE UMANA, DELLA SALUTE ANIMALE E DELL'ECOSISTEMA
(ONE HEALTH) E DEI RAPPORTI INTERNAZIONALI
EX DIREZIONE GENERALE DELLA SANITÀ ANIMALE E DEI FARMACI VETERINARI
UFFICIO 6

Autorizzazione n. **388/2024-PR**

IL DIRETTORE DELL'UFFICIO 6 Ex DGSAF

Vista la domanda di autorizzazione del progetto di ricerca **"Meniscal functionalized scaffold to prevent knee Osteoarthritis onset after meniscectomy"**, ex articolo 31 del decreto legislativo 4 marzo 2014, n. 26, acquisita con prot. 30111.29 del 02/02/2024 ed integrazione del 29/04/2024, inoltrata dall'**Università degli Studi di Bari, sede legale in Bari, Piazza Umberto, 1**, **Palazzo Ateneo**, per il tramite dell'Organismo preposto al benessere degli animali di cui all'articolo 25 del menzionato d.lgs. n. 26/2014, e finalizzata all'esecuzione di un progetto di ricerca come descritto nella documentazione allegata alla domanda;

Tenuto conto del pagamento della Tariffa D, come previsto dal decreto ministeriale 27 marzo 2019 per le attività contemplate negli articoli 20, 31, 32 e 33 del d.lgs. 4 marzo 2014, n. 26;

Visto l'articolo 31, comma 1, del d.lgs. n. 26/2014, nel quale il Ministero della salute è individuato quale autorità competente al rilascio dell'autorizzazione all'esecuzione di progetti di ricerca che prevedono l'utilizzo di animali a fini scientifici secondo le finalità di cui all'articolo 5, comma 1, in continuità con la precedente normativa di cui al decreto legislativo 27 gennaio 1992, n. 116;

Visti gli articoli 12, 13, 14, 15, 16 e 17 del succitato d.lgs. n. 26/2014, che stabiliscono le modalità di utilizzazione degli animali nelle procedure condotte a fini scientifici;

Visti gli articoli 31, 32, 34 e 35, nonché gli Allegati IV, VI, VII e IX del d.lgs. n. 26/2014, che fissano i requisiti generali per il rilascio di autorizzazione per progetti di ricerca;

Vista la nota n. 17554 del 19/04/2024 con cui l'Istituto Superiore di Sanità ha comunicato l'esito positivo della valutazione tecnico-scientifica sul progetto di ricerca;

Considerato che ricorrono i requisiti stabiliti dal d.lgs. n. 26/2014 per il progetto da autorizzare;

Preso atto che il responsabile del progetto di ricerca, ai sensi dell'articolo 3, comma 1, lettera g) del d.lgs. n. 26/2014, è il **Dr. Alberto CROVACE**;

Considerato che **gli animali saranno stabulati nei locali dello stabilimento utilizzatore del Dipartimento di Medicina di Precisione e Rigenerativa e Area Jonica DiMePRe-J (ex Dipartimento Sezione di Cliniche Veterinarie e P.A. del DETO), Università degli Studi di Bari, Strada Provinciale per Casamassima, Km 3, Valenzano (BA), autorizzato con n. 36/2023-UT del 29/11/2023, ai sensi del D.lgs. 26/2014**;

Visto l'articolo 4, comma 2 e l'articolo 16 del decreto legislativo 30 marzo 2001, n. 165 e successive modifiche, recanti le funzioni dei dirigenti di uffici dirigenziali;

Responsabile del procedimento: Dr. Vincenzo Ugo SANTUCCI
Referente: G. Aleandri - sperimentazioneanimale@sanita.it

This thesis explores the application of advanced biomaterials in two key areas: localized drug delivery and tissue engineering.

In the localized drug delivery section, polymer-coated meniscus prostheses were engineered for sustained anti-inflammatory drug release, aiming to minimize systemic treatment side effects and control joint inflammation by releasing two anti-inflammatory drugs with distinct release kinetics to prevent osteoarthritis progression following meniscectomy.

In the tissue engineering section, thymus organoids were encapsulated within ECM-mimicking hydrogels to study how matrix mechanics influence thymic tissue morphogenesis, providing valuable insights into the development of advanced ex vivo immune system models.